STRUCTURAL RESPONSE of MARINE SANDWICH PANELS to UNIFORM PRESSURE LOADING

by

J. Rowland Huss

B.S. Ocean Engineering, U.S. Naval Academy
(1981)

N00123-89-G-0560

Submitted to the Department of Ocean Engineering
in Partial Fulfillment of the
Requirements for the Degree of

NAVAL ENGINEER

and

MASTER OF SCIENCE IN MATERIALS SCIENCE AND ENGINEERING

at the

MASSACHUSETTS INSTITUTE OF TECHNOLOGY
June, 1990

Signature of Author J. Rowland Huss
Department of Ocean Engineering
May 11, 1990

Certified by Frederick J. McGarry
Professor Frederick J. McGarry
Thesis Supervisor, Department of Materials Science and Engineering

Certified by Tomasz Wierzbicki
Professor Tomasz Wierzbicki
Thesis Reader, Department of Ocean Engineering

Accepted by Thomas W. Eagar
Professor Thomas W. Eagar
Chairman, Materials Science and Engineering Departmental Graduate Committee

Accepted by A. Douglas Carmichael
Professor A. Douglas Carmichael
Chairman, Ocean Engineering Departmental Graduate Committee

STRUCTURAL RESPONSE of MARINE SANDWICH PANELS to UNIFORM PRESSURE LOADING

by

J. Rowland Huss

Submitted to the Department of Ocean Engineering and Department of Materials Science and Engineering on May 11, 1990, in partial fulfillment of the requirements for the Degrees of Naval Engineer and Master of Science in Materials Science and Engineering.

ABSTRACT

The deflection and strain responses of six marine sandwich panels to uniform pressure loading are investigated. Panels are full scale typical of those found in a 40 foot high performance deep-vee monohull. Three combinations of matrix-reinforcement are used in the panel faces: bi-axial (0°-90°) E-glass in a fire retardant vinyl ester resin (DERAKANE® 510A), bi-axial and double bias (±45°) Kevlar in DERAKANE® 510A, and bi-axial and double bias Kevlar with an elastomer modified vinyl ester resin (DERAKANE® 8084). Polyvinyl chloride (PVC) foam AIREX® is the core material. A panel test mechanism applies uniform pressure to panels 90 inches wide by 120 inches long. The central test section is 30 by 60 inches and is isolated by one panel span to simulate in situ boundary conditions. Two pressure loading rates (static and cyclic) are employed allowing examination of viscoelastic effects.

A material and mechanical characterization of the sandwich panel lower faces is conducted. The faces are characterized by specific gravity, reinforcement weight and volume fractions, and void content. The mechanical properties of tensile, compressive, and flexural strengths and moduli, in-plane shear strength, and Poisson's Ratio are determined. Material properties of the panel lower faces are commensurate with those typical of hand lay-up molding processes. The lower specific gravity of Kevlar provides a panel weight saving of 29%. Bias reinforcing in the Kevlar panel faces reduces in-plane mechanical properties and they are lower than the E-glass faces.

A low elastic limit (5.5 psi), pronounced hysteresis, and presence of membrane behavior are evident during static (0.0079 psi/sec.) loading tests. Bias reinforcing lessens the difference between transverse and longitudinal strain components, and reduces the transverse arching effect. The elastomer modified matrix gives a more non-linear response with larger deflections and more permanent deformations.

A larger linear region with steeper slope are present during cyclic (0.684 psi/sec.) testing. Membrane behavior is not evident on a per cycle basis, yet its effect can be seen over successive cycles. The non-linearity and hysteresis diminish with repeated loading. After relatively few cycles, the deflection and strain responses become linear, the rate-normalized bending stiffness lessens, and the overall panel response approaches that recorded during static tests. Thus, the long term response of the panel is closely approximated by static loading conditions.

Thesis Supervisor: Professor Frederick J. McGarry
Title: Professor of Materials Science and Engineering

ACKNOWLEDGEMENTS

I wish to recognize and express my appreciation to the following individuals and groups for their efforts and support in connection with this research:

- Professor Fred McGarry for his support, patience, and understanding. His inspiration and friendship enhanced my academic and professional development.

- John Moalli for his assistance and technical support during the material property tests.

- Jack Germaine for his efforts during development of the panel data acquisition system and for use of the test equipment.

- Zan Miller for his help during construction of the test mechanism and with panel preparation and testing.

- Mike Russell for his support and technical guidance throughout all stages of this project.

- Dr. Ron Reichard for his help during the early stages of the panel test mechanism design. His suggestions and sharing of bladder testing experiences provided a solid foundation for this work.

- Thomas Johannsen (Torin Inc.) for donation of the AIREX® core material.

- NAVSEA PMS 300.4 for financial support.

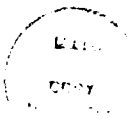

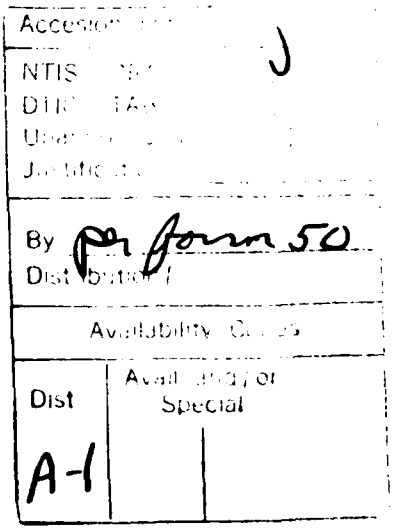

DEDICATION

To one less fortunate, the man for whom I am named.

God Bless You, V. R.

TABLE OF CONTENTS

TABLE OF CONTENTS
(continued)

LIST OF FIGURES

LIST OF FIGURES
(continued)

LIST OF FIGURES
(continued)

LIST OF TABLES

NOMENCLATURE

a	Panel longitudinal dimension, specimen gage length
b	Panel transverse dimension, specimen width
t	Thickness of face layers (uniform), specimen thickness
L	Support span width (3-point flexure test)
P	Load
h	Panel thickness between centers of face layers
h_1	Lower face thickness
h_2	Upper face thickness
E_1	Lower face elastic modulus
E_2	Upper face elastic modulus
E_c	Core elastic modulus
d	Overall panel thickness
u	Deformation in longitudinal direction (x axis)
v	Deformation in transverse direction (y axis)
w	Panel deflection (z axis), specimen deflection
G_c	Shear modulus of core
E_f	Elastic modulus of faces
ν_f, ν	Poisson's Ratio of panel faces
F	Assumed Airy stress function at panel boundary
D	Bending stiffness
p	Uniform pressure load normal to faces
Q_x, Q_y	Shear force per unit length of panel
N_x, N_y, S	Stress resultants per unit length of panel
β	Panel slope in x-direction
γ	Panel slope in y-direction
ϕ	Defined by Equation (5)
ψ	Defined by Equation (6)
∇^2	$\frac{\partial^2}{\partial x^2} + \frac{\partial^2}{\partial y^2}$
q	$\frac{pa^4}{16Eth^3}$, non-dimensional load

1. INTRODUCTION

1.1. OVERVIEW

Composite sandwich panels with fiber reinforced plastic (FRP) faces and low density foam cores are fast becoming the structural material of choice in the marine small craft industry. This is particularly true for high performance applications, where naval architects strive to expand the craft operational envelope by improving the hull structural performance. Most often this is accomplished with a simultaneous reduction in the hull weight. In the commercial sector, the goal in expanding this envelope is typically higher craft speeds with smaller, more efficient power plants. For military applications, the goal is most often a higher payload capacity or combination of the two.

Although many benefits are realized by using sandwich panels, there is a trade-off deriving from the selection of low density foam cores. The tradeoff is the inability to accurately predict the structural response of sandwich panels having such low density, resilient foam cores. Panel prediction techniques for homogeneous isotropic materials are well developed, but those for resilient foam cores are still evolving. Currently, there is an effort in the marine industry to develop more precise methods of predicting the structural response of this type of panel. As with any evolutionary process, validation of new techniques with experimental results is necessary and desirable.

The objective of this research is to develop a realistic method for determining the structural response of marine sandwich panels to uniform pressure loading and to test candidate panels so the data can be used to support the evolution of new panel prediction techniques. The panels are full scale, commensurate with those found in high performance craft having overall lengths ranging from 35 to 50 ft. Within the limits of economic feasibility, the boundary conditions and the application of the pressure load simulate conditions found in the actual craft. Supporting this objective are two additional requirements. First, is a review of panel prediction techniques and their range of applicability. This will help define data collection requirements and methods of presenting

the results. Second, it is necessary to ascertain the material properties of the candidate panels. This will enable direct application of prediction techniques and allow comparison with experimental results.

The research is sponsored by Naval Sea Systems Command (PMS 300.4) for use by the Combat Craft Division (Code 61) of the Naval Sea Combat Systems Engineering Station, Norfolk, VA.

1.2. BACKGROUND

Sandwich panels are well suited for marine applications. The most significant attributes are high strength and high stiffness-to-weight ratios. FRP sandwich panels using E-glass reinforcement are 1.7 times stronger than aluminum and almost 7 times stronger than steel on a per weight basis. Even greater differences exist when comparing stiffness characteristics on a per weight basis. In this case, FRP panels are more than 100 times stiffer than steel and 17 times stiffer than aluminum. [1]

Sandwich panels have several other attributes which make them attractive for marine applications. Some of these include: smooth surface finish for excellent appearance and reduced skin friction drag, good fatigue properties, excellent thermal and acoustic insulation capability, reduced inner structure requirements for more useable volume, superior environmental resistance, and excellent producibility. They are often compared to I-Beams because of their geometry and method of transferring loads. The relatively thin faces, sometimes referred to as skins, perform functions similar to I-beam flanges. A thicker, light weight core, separates the faces and thereby acts like the I-beam web. The loads are transferred in a method similar to I-beams. Tensile and compressive stresses in the faces are accompanied by shear stresses in the core. Inability of the core to absorb these stresses will cause the panel to delaminate so, the bond between the core and

faces becomes an important factor in panel performance. The stiffness of a sandwich panel derives from the distance separating the faces. The core must support the faces to prevent a reduction in the face separation; if the core compresses, a reduction in the moment of inertia will occur which can lead to panel failure. Unlike I-beams in flexure, in sandwich panels the shear deformation plays a larger role and it cannot be neglected. This is particularly true for the resilient foam cores used in the marine industry.

Several authors have pointed out that the core properties influence the performance of a sandwich composite; most recommend that the core have low density, high shear strength and shear stiffness, prevent buckling of the faces, and have good compressive and tensile strength and stiffness perpendicular to the faces in the thickness direction.

1.2.1. Structural Response Prediction Techniques

Techniques which predict the structural response of panels vary in scope and complexity. Earlier work based on classic plate theory is used for predicting finite deflections while more rigorous techniques are developed for predicting large deflections. In recent years, much of the design work for marine panels uses modified composite beam theory due to its simplicity and ease of application. A review of some of these techniques and their applicability to panels with resilient foam cores follows.

1.2.1.1. Panel Methods

In the late 40's and early 50's, considerable effort was directed to deriving sandwich panel deflection prediction techniques. The majority of these refer to the work by Reissner [2] where he derived a system of equations for small deflections of sandwich plates based on a generalization of the classic homogeneous plate equations.[3] Several simplifying assumptions were made by Reissner. These were: stresses in the faces parallel to their

planes were distributed uniformly over the thickness of the face layers; the face-parallel stresses in the core and their effect on the deformation of the composite plate can be neglected; the core only resists the transverse shear and transverse normal stresses; the nonlinear terms could be neglected in all but the most extreme cases of core softness. Reissner arrived at a system of two simultaneous equations by following von Karman's procedure for the homogeneous plate. The solution involved relating the force equilibrium equations with the differential of an Airy's Stress Function:

$$Nx = \frac{\partial^2 F}{\partial y^2} \quad Ny = \frac{\partial^2 F}{\partial x^2} \quad S = -\frac{\partial^2 F}{\partial x\, \partial y} \tag{1}$$

From the stress-strain relations, the first of two simultaneous equations was obtained in the same form as for the homogeneous plate,

$$\nabla^2 \nabla^2 F = 2t\, E_f \left[\left(\frac{\partial^2 w}{\partial x\, \partial y} \right)^2 - \left(\frac{\partial^2 w}{\partial x^2} \right) \left(\frac{\partial^2 w}{\partial y^2} \right) \right] \tag{2}$$

To obtain the second equation, the moment equilibrium equations were introduced into the transverse force equilibrium equation and applied to the stress-strain relations. In the resulting equation, the bending stiffness factor D was introduced,

$$D = \frac{h^2\, t\, E_f}{2(1 - \nu_f^2)} \tag{3}$$

and the second of the two simultaneous equations was derived.

$$D \nabla^2 \nabla^2 w = \left(1 - \frac{h\, t\, E_f}{2(1-\nu_f^2) G_c} \nabla^2 \right) \left(p + \frac{\partial^2 F}{\partial y^2} \frac{\partial^2 w}{\partial x^2} - 2 \frac{\partial^2 F}{\partial x\, \partial y} \frac{\partial^2 w}{\partial x\, \partial y} + \frac{\partial^2 F}{\partial x^2} \frac{\partial^2 w}{\partial y^2} \right) \tag{4}$$

In the case where the core has infinite shear modulus, then Eqn (4) reduces to the form for the homogeneous plate.

The majority of work on sandwich plate deflections which followed Reissner also operated on the assumption that the face-parallel stresses in the core and the face stress variation over the thickness of the face layers were negligible. However, several different solution techniques were developed. Liaw and Little [4] developed the governing equations for the bending of multi-layered sandwich plates by variational methods. They formulated an energy functional with the stresses considered as independent variables and introduced the stress resultants as constraint conditions using Lagrange multipliers. A neutral surface was identified so the equation defining the plate deflection could be obtained in a manner similar to Reissner. The analysis conducted by Ng [5] also employed some of the results developed by Reissner, but it was based on a small parameter perturbation technique. Ng used this method to predict the finite deflection behavior of uniformly loaded clamped circular, elliptical, and rectangular sandwich plates resting on elastic supports. Throughout the analysis, the sandwich plate material was considered to be elastic and the elastic support reaction to be that of the Winkler type, where the reaction is proportional to the deflection.

Energy methods were also used extensively to predict finite deflections of sandwich panels. Thurston [6] used an Lagrangian multiplier technique applied to energy expressions to derive equations for predicting the deflections and buckling loads of rectangular plates clamped on all four edges. In the analysis, he developed an expression for the strain energy of the plate consisting of three parts; the strain energy of the face plates in their own plane, the strain energy from bending of the face plates, and the strain energy of shear in the core. (The strain energy due to transverse shearing in the faces and normal strains in the core were considered negligible and not introduced.) The potential energy expression was developed and included contributions from the energy of the distributed transverse load and the distributed compressive load. Thurston used these expressions applied to the Rayleigh-Ritz method of minimum potential energy to obtain an approximate

solution. He introduced additional simplifying assumptions to reduce the complexity of the solution. The established boundary conditions included setting the shear strain in the faces equal to zero along the panel edges. This assumption was based on the application of the principle of virtual displacements where longitudinal displacements are possible along the edges parallel to the longitudinal axis and that transverse displacements are possible along the edges parallel to the transverse axis. The displacement functions based on symmetric loading included a double cosine series for the vertical displacements, a sine-cosine series for the transverse displacements, and a cosine-sine series for the longitudinal displacements. Since the coefficients of the vertical displacement function are not all independent, Thurston employed the technique of finding an upper and lower bound on the solution. The lower bound was obtained by using the complete set of coefficients but without satisfying all the constraint relations. This method was based on the principle of calculus of variations. The upper bound solution was obtained by satisfying all the constraint relations from setting some of the vertical displacement coefficients to zero.

Since the work of Reissner, considerable effort has been devoted to deriving equations for predicting large deflections of sandwich panels. This effort tried to resolve the disparity between linear solutions and experimental results for plates having deflections greater than the panel thickness. Various methods were used in references [7-11] to develop the governing equations and a corresponding approximate solution. The most thorough of these methods appears to be that provided by Kao, Barron and Hartman [7]. They derived the three governing differential equations using the principle of complementary energy. In their analysis, expressions for the stress resultants were obtained in terms of deflection, a stress function, and auxiliary functions. This allowed evaluation of the plate stresses as well as the deflections. Two of the three governing equations used in the analysis were derived by Reissner (Eqn's 2,4) and similar assumptions were applied.

The third equation was derived from relations between the stress resultants and displacements by introducing two new functions.

$$\phi = \frac{\partial \beta}{\partial x} + \frac{\partial \gamma}{\partial y} \tag{5}$$

$$\psi = \frac{\partial \beta}{\partial y} - \frac{\partial \gamma}{\partial x} \tag{6}$$

Where:

$$\beta = -\frac{\partial w}{\partial x} + \frac{Q_x}{G_c h} \tag{7}$$

$$\gamma = -\frac{\partial w}{\partial y} + \frac{Q_y}{G_c h} \tag{8}$$

Boundary conditions were applied followed by substitution of Eqn's (7) and (8) into Eqn (5) using one of the five equilibrium equations. The Airy Stress function, Eqn (1), was applied to the resulting equation and yielded:

$$\phi = -\nabla^2 w - \frac{1}{G_c h}\left[q + \frac{\partial^2 F}{\partial y^2}\frac{\partial^2 w}{\partial x^2} - 2\frac{\partial^2 F}{\partial x\,\partial y}\frac{\partial^2 w}{\partial x\,\partial y} + \frac{\partial^2 F}{\partial x^2}\frac{\partial^2 w}{\partial y^2}\right] \tag{9}$$

The overall stress resultants were solved for in terms of β and γ using the displacement relations, moment equilibrium equations, and Eqn's (5) and (6). The resulting equations were solved in terms of β and γ, where:

$$\beta = \frac{D}{G_c h}\left[\frac{\partial \phi}{\partial x} + \frac{1-\nu}{2}\frac{\partial \psi}{\partial y}\right] - \frac{\partial w}{\partial x} \tag{10}$$

$$\gamma = \frac{D}{G_c h}\left[\frac{\partial \phi}{\partial y} - \frac{1-\nu}{2}\frac{\partial \psi}{\partial x}\right] - \frac{\partial w}{\partial y} \tag{11}$$

Eqn's (10) and (11) were then introduced into Eqn (6) and simplified to yield the third governing differential equation.

$$\nabla^2 \psi - \frac{2hG_c}{D(1-\nu)} \psi = 0 \tag{12}$$

Several other authors developed predictive techniques for determining large deflections of sandwich panels. Alwan [8] used the method of complementary energy and Lagrangian multipliers to treat plates with orthotropic cores. His technique was similar to Reissner's, but, he accounted for the different elastic properties of the core by introducing bending stiffness factors for both the longitudinal and transverse directions. Kamiya [9] used the method of variational calculus developed by Berger. In his analysis, the deflections were decoupled with the in-plane displacements which disregards the second invariant of the middle plane strains of the plate. Kan and Huang [10] used the governing equations developed by Reissner and applied a power method to approximate the panel deflections. This used ascending powers of the deflection variable for the six characteristic equations. A series of linear differential equations were then obtained by equating like powers of the deflection variable. Nowinski and Ohnabe [11] develop two governing equations in addition to those derived by Reissner and solved the four equations using the variational principles of Lagrange. In their work, they developed methods which account for differences in the elastic properties of the panel faces.

Comparison of experimental and analytic data using the finite deflection panel methods are generally in good agreement for deflections on the order of the panel thickness and for core materials having mechanical properties similar to aluminum honeycomb.[5] As the magnitude of the deflections approach the panel thickness, nonlinear effects dominate and the solution technique breaks down. The extent of the linear region is also severely affected by the properties of the core. When the core shear modulus is

significantly less than the face elastic moduli, the nonlinear terms dominate resulting in a very limited linear region.

Larger deflections can be modeled using reference [7] techniques, but the mechanical properties of the core become even more influential at larger deflections. It also should be noted that the majority of these techniques fail to account for normal strains in the core. In the case of resilient cores, normal strains are present with a reduction in core thickness. If normal displacements in the core are present, a reduction in the panel moment of inertia will occur reducing any benefit from membrane effects.

1.2.1.2. Beam Methods

Deflection prediction techniques based on a variation of sandwich beam theory have been adopted extensively in the marine industry because of their simplicity and ease of application to marine design. Plantema [12] was one of the first to publish many of the relationships governing the bending and buckling of sandwich beams and much of his work has been applied to design techniques in practice today. He derived the basic formulas governing sandwich beam deflections by applying assumptions similar to those applied by Reissner. Plantema believed that the essential difference between sandwich beam analysis and conventional beam theory for bending was that the effect of the shear strains in the core of the sandwich beam could not be omitted. In order to account for these strains, he proposed that the total deflection due to bending was a combination of two components. Thus, the partial deflection from bending and the partial deflection from shear could be superimposed to achieve the total deflection. Plantema used this approach to develop equations for the strain energy produced by moments and shear as a function of their partial deflections. The solution to the total deflection of sandwich beam was obtained by solving for the bending component of deflection using ordinary beam theory and

solving for the shear component of deflection by integration of the shear force diagram. The total deflection was then obtained by adding the two components.

Later, Weissman-Berman [13] expanded the method developed by Plantema to predict the deflection response of FRP sandwich beams with resilient foam cores. In the analysis, Berman calculated the deformations and stresses due to bending and warping using thin walled bars theory. She introduced a core correlation factor to account for the variations in strains from varying equivalent core thicknesses. This was derived from experimental data which illustrated the relationship between foam core beams having the same total skin to core thickness ratio. A skin factor ratio was also introduced, since the shear warping component depends on the face thickness. This was necessary to account for the rather dramatic effect increases in face thickness have on the shear warping component, and thus, an increase in shear stiffness for a similar strain. Weissman-Berman, Petrie and Wang [14] expanded this analysis by presenting two additional approaches to predicting the flexural response of FRP sandwich beams with resilient foam cores. One approach considered the linear foam Airex® as an elastic foundation for the skins of a sandwich beam. Ordinary differential equations were developed to predict the response of the skin on the core, the skin stresses, the shear at the neutral axis, and the total deflection of the beam. The method also introduced a new parameter α.

$$\alpha = 1 - H/R \tag{13}$$

The parameter α was defined as the residual ratio of the energy permanently absorbed (hysteresis) to the capacity of a material to store energy (modulus of resilience). The elastic hysteresis loss (H) was calculated from the area enclosed by stress-strain curve when the load was relaxed and the modulus of resilience (R) was calculated from the area under the linear region of the stress-strain curve. This parameter provided a somewhat better understanding of the dynamic response capabilities of the core.

The second method presented in the analysis was a two-dimensional method which used an extension of the spectrum method for solving Airy's stress function applied to a three-layered beam of finite length. The governing equations were developed as bi-harmonic partial differential equations with the solutions expressed as infinite trigonometric series. This allowed reduction of the partial differential equations to linear differential equations with constant coefficients. Two assumptions were made which reduce the complexity of the solution. The elastic constants and Poisson's Ratio were assumed constant for each layer, and the variation of stress and strain along the vertical axis were assumed to be zero (plane-strain). This method allows prediction of the normal and shear stress distribution in the cross section under the point load in addition to the beam stresses and deflections.

Beam methods have been expanded to take into the account the effect of varying the elastic moduli in the faces and core, and differing face thicknesses.[15] In this case the bending stiffness of a sandwich beam was represented by:

$$D = b\left\{\frac{h_1^3}{3}(E_1-E_c) - \frac{y_0 h_1^2}{2}(E_1-E_c) - \frac{(d-h_2)^3}{3}(E_1-E_c) + y_0\frac{(d-h_2)^2}{2}(E_2-E_c) + E_2 d^2\left(\frac{d}{3} - \frac{y_0}{2}\right)\right\} \qquad (14)$$

and the distance from lower surface to the neutral axis was given by:

$$y_0 = \frac{1}{2}\left|\frac{(d-h_2)^2(E_2-E_c) - h_1^2(E_1-E_c) - E_2 d^2}{(d-h_2)(E_2-E_c) - h_1(E_1-E_c) - E_2 d}\right| \qquad (15)$$

Structural response prediction based on sandwich beam methods compared favorably with three and four point sandwich beam flexure data in the linear-elastic region.[13,14] However, conflict exists when these techniques have been used to predict sandwich panel response. Comparison of sandwich beam and panel deflection test data by Reichard [16,17] indicated that deflections from beam models were significantly higher

than those from similar sandwich panels loaded by uniform pressure, and this was particularly true for panels with bias reinforcing in the faces or having a resilient core material. Additionally, Reichard proposed that the stresses in the cores of sandwich beams were higher than those found in similar sandwich panels, and that the flexural response of the beam was more dependent on the core properties. He attributed this disparity to membrane effects which were present in the panels.

1.2.1.3. Finite Element

The use of finite element methods for modeling sandwich panel response has increased with the development of faster, more capable computers. However use of finite element methods in the small craft industry has been limited because of their relative complexity, expense, and requirement for detailed material property characteristics. Unlike the aircraft industry, there has been only limited information published on finite element modeling of sandwich panel structures, particularly those having resilient foam cores.

Reichard [16,17] modeled the response of sandwich panels to uniform pressure loads using the MSC/NASTRAN Finite Element Structural Analysis Program. Here, a uniform pressure load was applied to the test panels which were assumed to have fixed-end boundary conditions. Finite element predictions based on a pinned edge condition (rotation without in-plane displacement) solution compare favorably to the panel results, while the fixed edge condition predictions underpredict the actual panel response. Reichard concludes that finite element modeling can be used to predict sandwich panel stiffness however, pressure tests should be conducted to determine ultimate panel strength. Other weaknesses noted in finite element modeling include: requirement for accurate laminate material property characteristics, interpretation of the edge constraints for modeling the panel boundary conditions in the actual craft, and the inability to model the through-the-thickness response of resilient foam cores.

Weissman-Berman, Petrie and Wang [14] have also used finite element methods to predict sandwich panel response. In this case however, a small width section of a high aspect ratio, pressure loaded panel was modeled as a point loaded simply supported sandwich beam in flexure. Unlike the MSC/NASTRAN model which uses individual ply laminate properties, the sandwich beam was modeled using three layers. The upper and lower faces were modeled using plane-stress elements and three-dimensional brick elements were used to model the core. Results of three-point sandwich beam flexure tests and finite element predictions showed good correlation in the linear elastic region. Additionally, it was noted that some finite element models do not support explicit specification of the core shear modulus. In [14], the core shear modulus for Airex® was calculated using linear elastic theory with an elastic modulus of 5500 psi and Poisson's Ratio of 0.11 as inputs.

1.2.2. Development of the Panel Test Pressure

Experimental modeling of the pressure loading event imposed on a planing craft operating at high speeds in a random sea is a major undertaking. This is evident when considering that the duration of the pressure impulse is on the order of 40 to 60 msecs. [18], and that the encounter frequency is approximately 1.2 Hz for a craft operating at 50 knots in deep water with sea state 3 surface conditions.[19,20] The project scope and economic constraints do not lend themselves to modeling a dynamic event of this magnitude and complexity. In the spirit of providing results which can be used with existing design methods, it is necessary to formulate a method of testing the candidate panels at an effective pressure load commensurate with that experienced by typical high performance planing craft.

Several methods [18, 21-26] exist which predict the magnitude of the pressure loads imposed on planing craft operating in a seaway. The majority of these methods are

empirically derived using craft characteristics, wave velocity, known or derived craft accelerations, or some combination of these. Load distribution factors and impact area pressure reduction relationships are applied to the derived impact pressure to obtain a mean effective pressure. This mean effective pressure is then used by naval architects to size the structural components dictated by the design area.

The methods of Silvia [22], Heller and Jasper [18], and Allen and Jones [23] are used in this study to determine the mean effective pressure load on a candidate high performance craft. The candidate craft characteristics are provided in Table 1-1. Applying these methods to the craft characteristics results in an impact pressure of 24.7 psi. The load distribution and area pressure reduction factors are then applied to obtain a mean effective pressure. Based on these results and sponsor requirements, a pressure of 10 psi is established as the design test pressure for the candidate panels.

Table 1-1: Characteristics of the Candidate Craft

CHARACTERISTIC	CRAFT
Displacement (lbs.)	18500
Waterline Length (ft.)	32
Chine Beam (ft.)	9
Deadrise Angle (deg.)	24
Draft (ft.)	3
Acceleration (g's)	5

2. EXPERIMENTAL PROCEDURE

2.1. PANEL MATERIALS

Six sandwich panels 90 in. wide by 120 in. long were manufactured by Stolper Marine, Fall River, MA. Two E-glass reinforced sandwich panels and four Kevlar® reinforced sandwich panels were made to marine industry standards. The E-glass reinforced panels and two of the Kevlar reinforced panels have a fire retardant vinyl ester matrix and two of the Kevlar reinforced panels have a non-fire retardant vinyl ester matrix. The panels were hand layed-up and cured at room temperature. Temperature varied from 58° F to 63° F during lay-up. The core was contact molded to the sandwich faces.

2.1.1. Reinforcement

The laminate schedule of the lower faces of panels 1 and 2 include one ply of 1.5 oz. per sq. ft. chopped-strand mat (CSM) and three plies of Vectorply® 1808. The CSM is 1.5 oz. per sq. ft. E-glass produced by PPG Industries, Inc., Pittsburgh, PA. The Vectorply 1808 is an E-glass fabric consisting of two bi-axially (0°-90°) aligned plies of continuous, non-woven fibers stitched to one ply of 0.75 oz. per sq. ft. CSM. The Vertorply 1808 fabric warp and weft weights are 9 oz. per sq. yd. and with stitching yields a total fabric weight of 25 oz. per sq. yd. Vectorply 1808 is produced by Bean Fiberglass Inc., Jaffrey, NH.

The upper face of panels 1 and 2 contain three plies of the 1808 fabric. A 6 in. wide doubler of 1808 is also added to the upper face to reduce local stress concentrations imparted by the panel test mechanism. The doubler is collocated with the test mechanism panel restraining frame. A sectional view of the E-glass reinforced panels less the doubler and core bedding compound is illustrated in Figure 2-1.

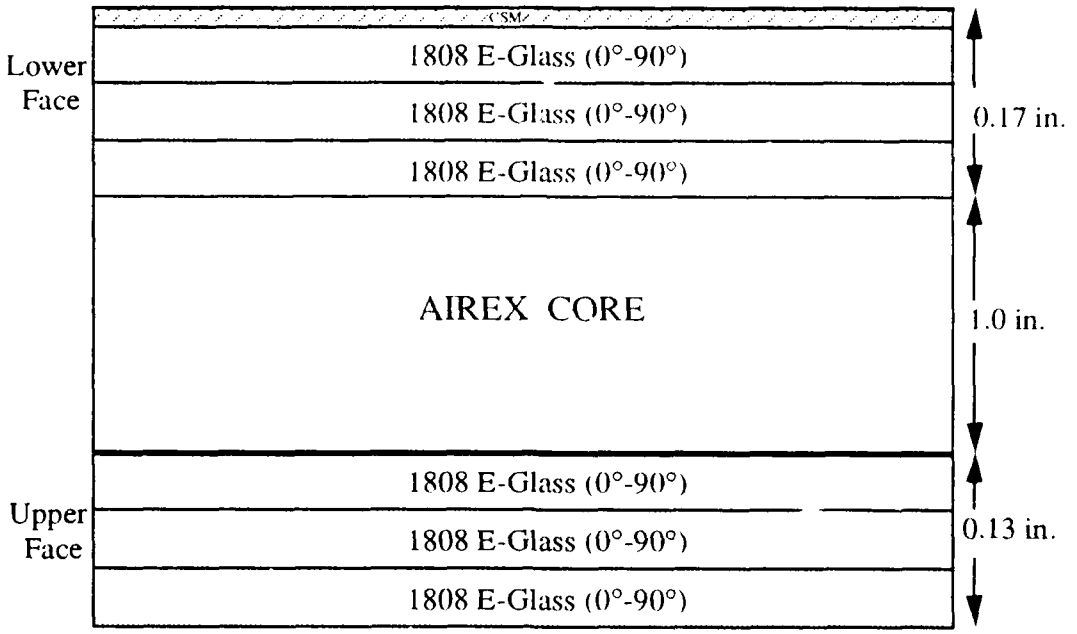

Figure 2-1: Sectional View of E-Glass Reinforced Sandwich Panels (Panels 1 and 2)

Panels 3 through 6 have Kevlar reinforced faces. The laminate schedule of the lower face of these panels includes one ply of 1.5 oz. per sq. ft. CSM followed by two alternating plies of Cofab® 2208 and Knytex® KDB 110. Cofab 2208 is a bi-axial (0°-90°) Kevlar 49 fabric having 3.57 oz. per sq. yd. in the warp and weft directions and a total fabric weight of 8.19 oz. per sq. yd. It is produced by Composite Reinforcements, Tuscaloosa, AL. The Knytex KDB 110 is a double-bias (±45) Kevlar 49 fabric with a total weight of 10.7 oz. per sq. yd. The Knytex® KDB 110 is produced by Knytex-Proform, Sequin, TX.

The upper face of panels 3 through 6 contain two alternating plies of 2208 and KDB 110. The doubler material for panels 3 through 6 is KDB 110. A sectional view of the Kevlar reinforced sandwich panels less the doubler and core bedding compound is shown in Figure 2-2.

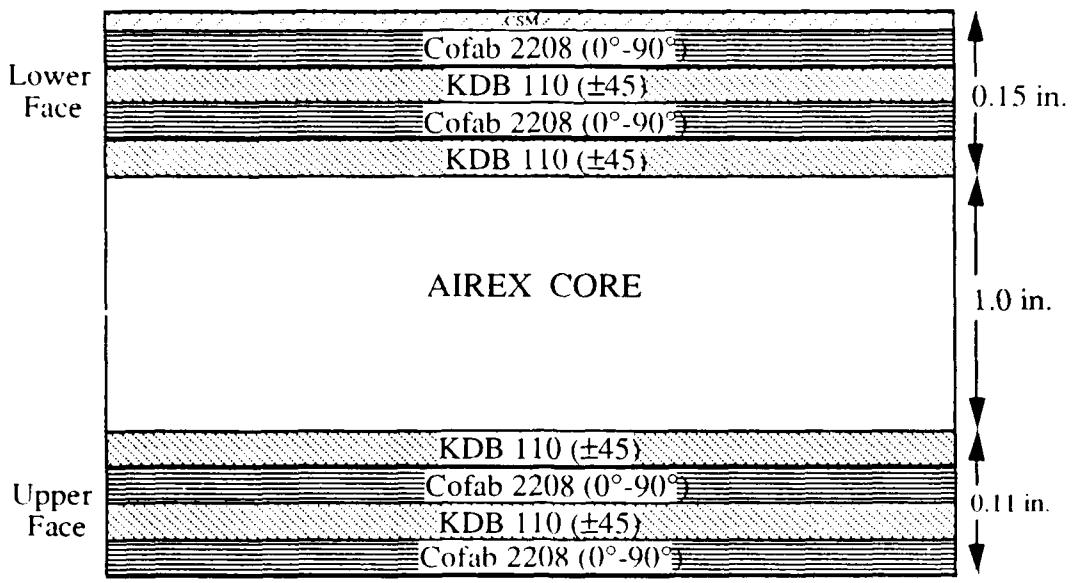

Figure 2-2: Sectional View of Kevlar Reinforced Sandwich Panels (Panels 3 through 6)

2.1.2. Matrix

A brominated vinyl ester resin (Dow DERAKANE® 510A) is used in panels 1 through 4. The DERAKANE 510A panels are promoted with 0.3% cobalt naphthenate solution (CoNap) and catalyzed with 2% methyl ethyl ketone peroxide (MEKP). The CoNap promoter is DMR cobalt 6% produced by Nuodex Inc., Piscataway, NJ. The catalyst is Thermacure® Fast, a 8.8 ± 0.1 % active oxygen MEKP produced by Freeman Chemical Corp., Port Washington, WI.

The matrix in panels 5 and 6 is a high elongation elastomer-modified vinyl ester resin (Dow DERAKANE® 8084). The DERAKANE 8084 panels are promoted with a 0.4% CoNap solution and catalyzed with 3% MEKP.

Room temperature mechanical properties [27] of clear castings of the two resins are provided in Table 2.1.

Table 2-1: Mechanical Properties of Candidate Resins

PROPERTY	DERAKANE 510A	DERAKANE 8084
Tensile Strength (psi)	10-11,000	10-11,000
Tensile Modulus (ksi)	500	460
Elongation (%)	4-5	10-12
Flexural Strength (psi)	16-18,000	16-18,000
Flexural Modulus (ksi)	530	440
Heat Distortion Temp (°F)	220-230	170-180
Barcol Hardness	40	30

2.1.3. Foam Core

A rigid, closed cell, polyvinyl chloride (PVC) foam (AIREX®) is used in the six test panels. The 1 in. thick core is contacted molded to the lower face using a polyester based bedding compound (Core-bond™). The core and bedding compound are produced by Torin Inc., Waldwick, NJ. Mechanical properties of AIREX [28] are provided in Table 2-2.

Table 2-2: Mechanical Properties of AIREX®

PROPERTY	AIREX®
Density (lb./ft.^{3})	5-6
Compressive Strength (psi)	125
Compressive Modulus (psi)	9200
Tensile Strength (psi)	200
Tensile Modulus (psi)	10900
Shear Strength (psi)	170
Shear Modulus (psi)	2900
Flexural Strength (psi)	255
Flexural Modulus (psi)	7558

2.2. PANEL TEST MECHANISM

2.2.1. Panel Test Apparatus

The test apparatus allows uniform pressure loading of full scale sandwich panels typical of those found in high performance craft. Panels 90 in. wide by 120 in. long and up to 1.5 in. thick can be tested in a static or cyclic pressure mode. An actual panel test section of 30 in. width and 60 in. length is isolated by one test section span in both the longitudinal and transverse directions. This isolation allows simulation of boundary conditions similar to those found in the actual craft. Figure 2-3 is a top view of the test mechanism frame illustrating test section isolation.

Data collection for the panel test mechanism allows development of the panel transverse deflected shape and the upper and lower face strain response as a function of the applied pressure load.

2.2.1.1. Panel Test Frame

The panel test mechanism is composed of an upper panel restraining frame and lower bladder support frame contained within a heavy I-beam outer frame. The upper frame is constructed of 6x3x0.25 in. and 6x2x0.25 in. mild steel tubing capped with a 4x3x0.25 in. tubing doubler. The 6x3 tubing is continuous in the longitudinal dimension and the 4x3 tubing is continuous in the transverse dimension. The tubing is welded into a single frame with all interior corners reinforced with a 4 in. lengths of 2x2x0.25 in. angle.

Design of the upper frame is based on a grillage type analysis [29, 30]. In order to decouple the panel deflections from the frame deflections, a longitudinal mid-span deflection limit of 0.25 in. is established for a maximum design load of 50 psi. This restricts frame deflections to at least one order of magnitude less than the anticipated maximum mid-span panel deflections of 2.5 - 2.75 in.

The lower frame is a grillage network of 4x2x0.25 in. steel tubing covered by a 0.25 in. thick steel deck. The 4x2 tubing members are continuous in the longitudinal dimension and located on 15 in. centers. Transverse members are located on 30 in. centers. The lower frame has a 4x2x0.25 tubing doubler located at mid-frame in both the longitudinal and transverse directions

Design of the lower frame is also based on a grillage type analysis. However in this case, the frame is designed to be yield stress limited. A factor of safety of 1.5 is applied to a maximum yield stress of 46 ksi.

The outer frame is constructed of four W18x46 steel I-beams. The beam ends are machined to 45° and joined at the top and bottom with 0.25 in. thick corner plates and 0.75 in. diameter hardened steel bolts. The upper and lower frames fit within the outer frame against the I-beam web and flange. They are secured to the I-beam web with 0.5 in. diameter hardened steel bolts. Two 1x1x0.125 angles are welded to the interior side of the I-beam web. The longitudinally aligned 1x1 angle serves as a guide and supports the panel during installation. A sectional view of the panel test mechanism is shown in Figure 2-4.

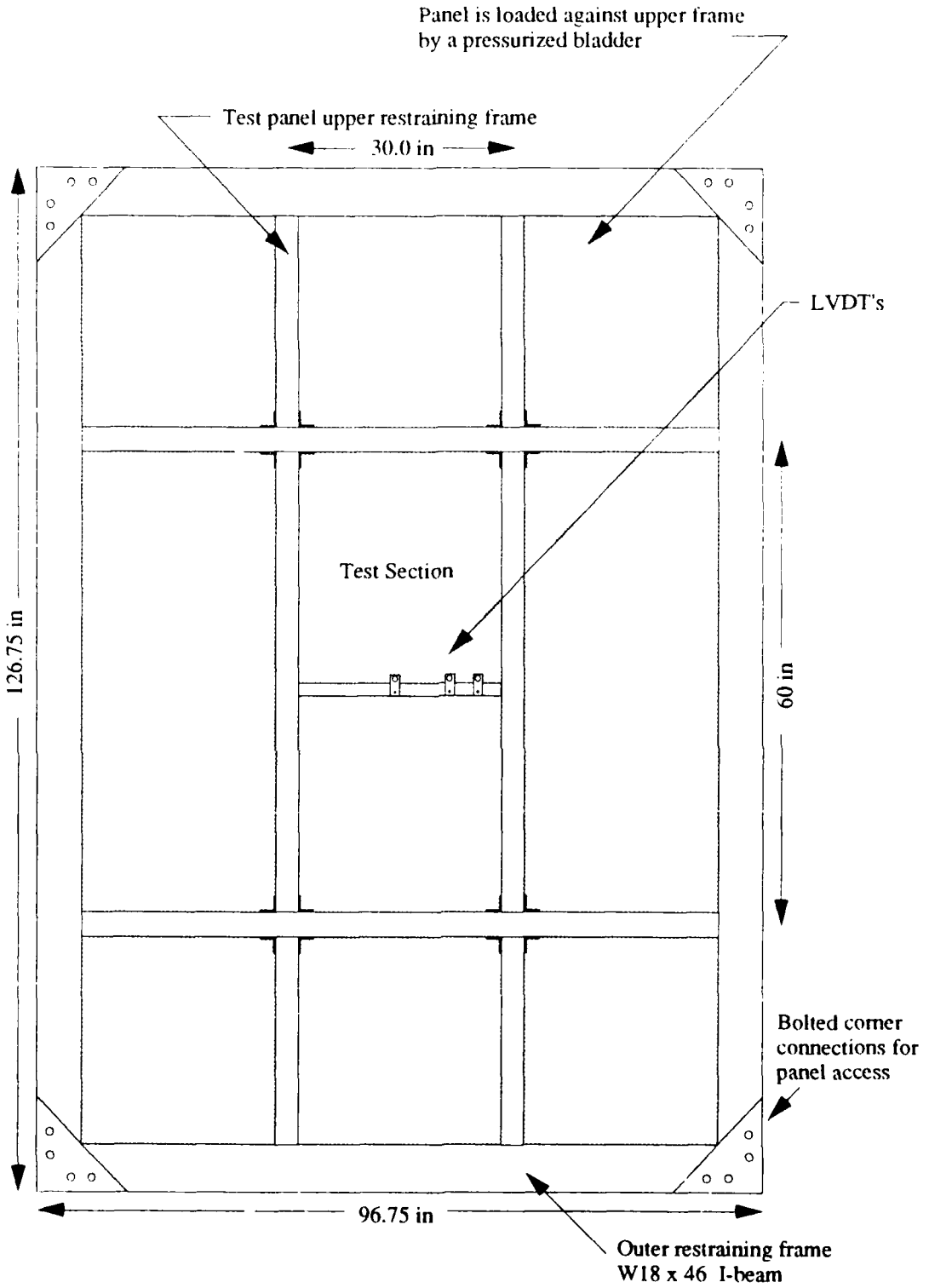

Figure 2-3: Top View of Panel Test Mechanism Frame

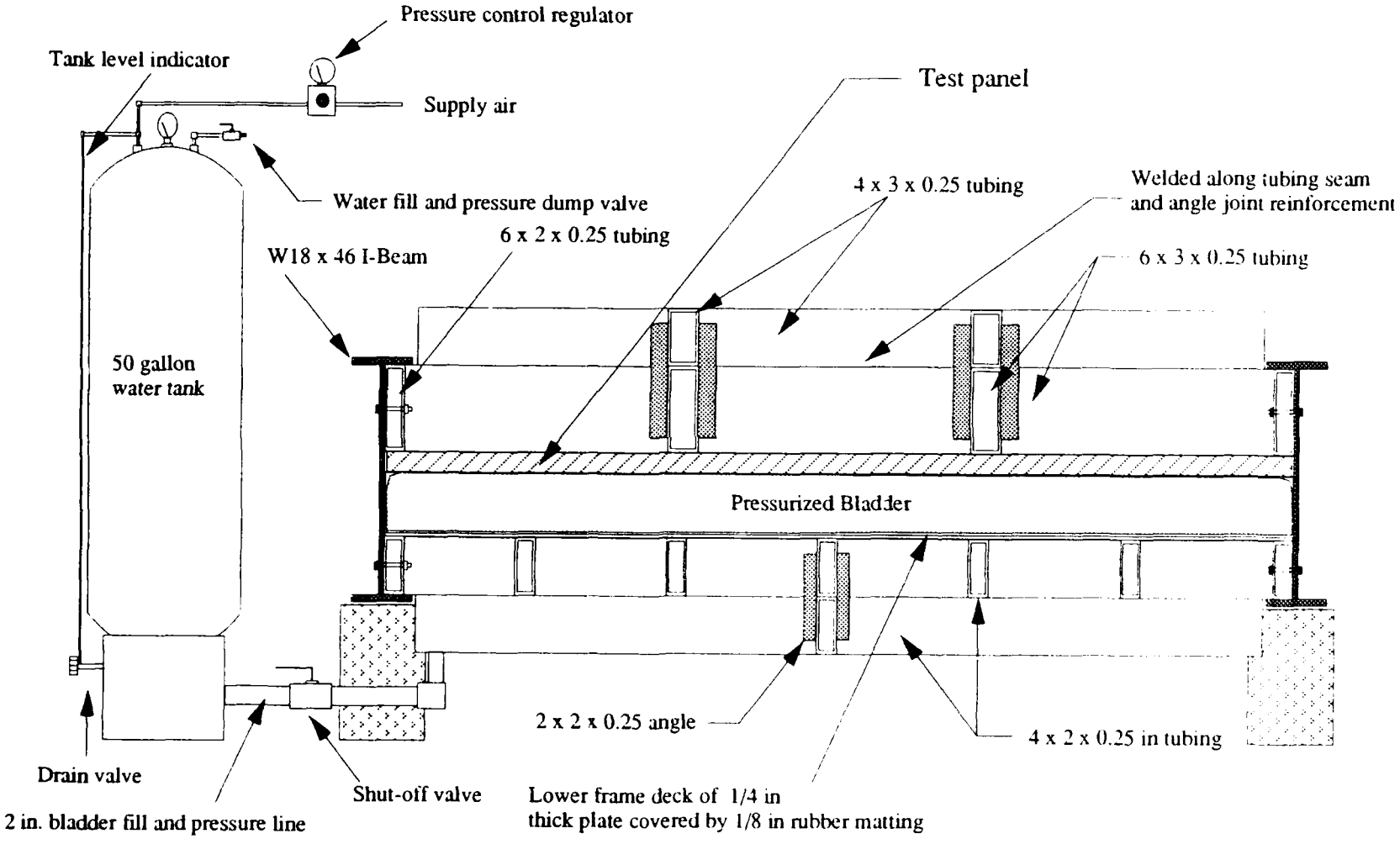

Figure 2-4: Sectional View of Panel Test Mechanism

2.2.1.2. Pressure Control System

Pressure loading is achieved by regulating air pressure to a water storage tank connected to a deformable bladder. The bladder is constrained by the test mechanism frame and panel and provides the means to apply the uniform pressure load. Supply air is available at 90 psi and 12 cu. ft. per min. from the M.I.T. installed system. This is delivered to the water tank by a 0.25 in. diameter pipe and controlled manually by a Kendall® model 10 pressure regulator. The regulator is manufactured by Fairchild Industrial Products Co., Winston-Salem, NC. A 0.25 in. diameter quick action ball valve on the supply air side and a 0.75 in. diameter ball valve on the vent side provides the means to cyclically load the bladder.

The 50 gal. water tank is equipped with a sight level indicator to monitor water level during the filling and pressurizing process. The tank is connected to the bladder with a 2.0 in. diameter pipe that has a quick action 2 in. ball valve in line. The valve allows isolation of the bladder during tank pressurizing and draining. It can also function as an alternative means to control the bladder loading rate.

The bladder is 90 in. wide, 120 in. long and 4.75 in. tall. It is made of a 0.04 in. thick thermoset polyester based, high elongation polyurethane material. The material has a durometer hardness on the Shore A scale of 93. The bladder is equipped with a 2 in. pipe diameter filling orifice and a 0.375 in. diameter bleed line with a petcock valve is located in an upper corner of the bladder to allow venting of trapped air. The bladder is constrained on seven sides by the test mechanism frame, and on the top side by the test panel. It is protected from chaffing by the addition of an 0.125 in. thick rubber lining. The bladder is made by Aero Tec Laboratories Inc., Ramsey, NJ.

2.2.1.3. Data Acquisition

Data acquisition is performed by a Hewlett Packard Model 3497A control unit with strain gage bridge completion assembly (Option 071) and a PC/XT computer using software designed at M.I.T. Panel transverse deflected shape, sandwich panel face strains and bladder pressure are sampled at rate of 300 times per sec. and recorded at a minimum 1 sec. interval. A schematic of the data acquisition is shown in Figure 2-5.

Panel deflected shape is determined from three displacement transducers mounted on a 2 in. steel channel cross-member that is welded to the upper frame. Each transducer is an integrated unit consisting of a linear variable differential transformer, a solid state oscillator, and a phase-sensitive demodulator (LVDT). The LVDT's are produced by Trans-Tek Inc., Ellington, CT. They are mounted at the mid (Model 0245-0000, ± 2.0 in.), quarter (Model 0244-0000, ± 1.0 in.), and eighth (Model 0243-0000, ± 0.5 in.) span positions relative to the center of the longitudinal members of the upper panel restraining frame.

Sandwich panel face strains are measured with FAET 25B-35-S6ET bi-axial 350Ω strain gages produced by BLH Electronics, Canton, MA. Gages are mounted on the upper and lower faces of the sandwich panels using Devcon® epoxy adhesive.

Pressure is measured with a Model AB-50 HP pressure transducer produced by Data Instruments, Lexington, MA. The transducer is a semiconductor strain gage type with an accuracy of ±0.25%.

Separate power power supplies drive the strain gages at approximately 2.0 V_{dc} and the LVDT's and pressure transducer at approximately 5.5 V_{dc}. A digital voltmeter is connected to a distribution terminal to allow monitoring of the power supply input voltages and LVDT's and pressure transducer output voltage.

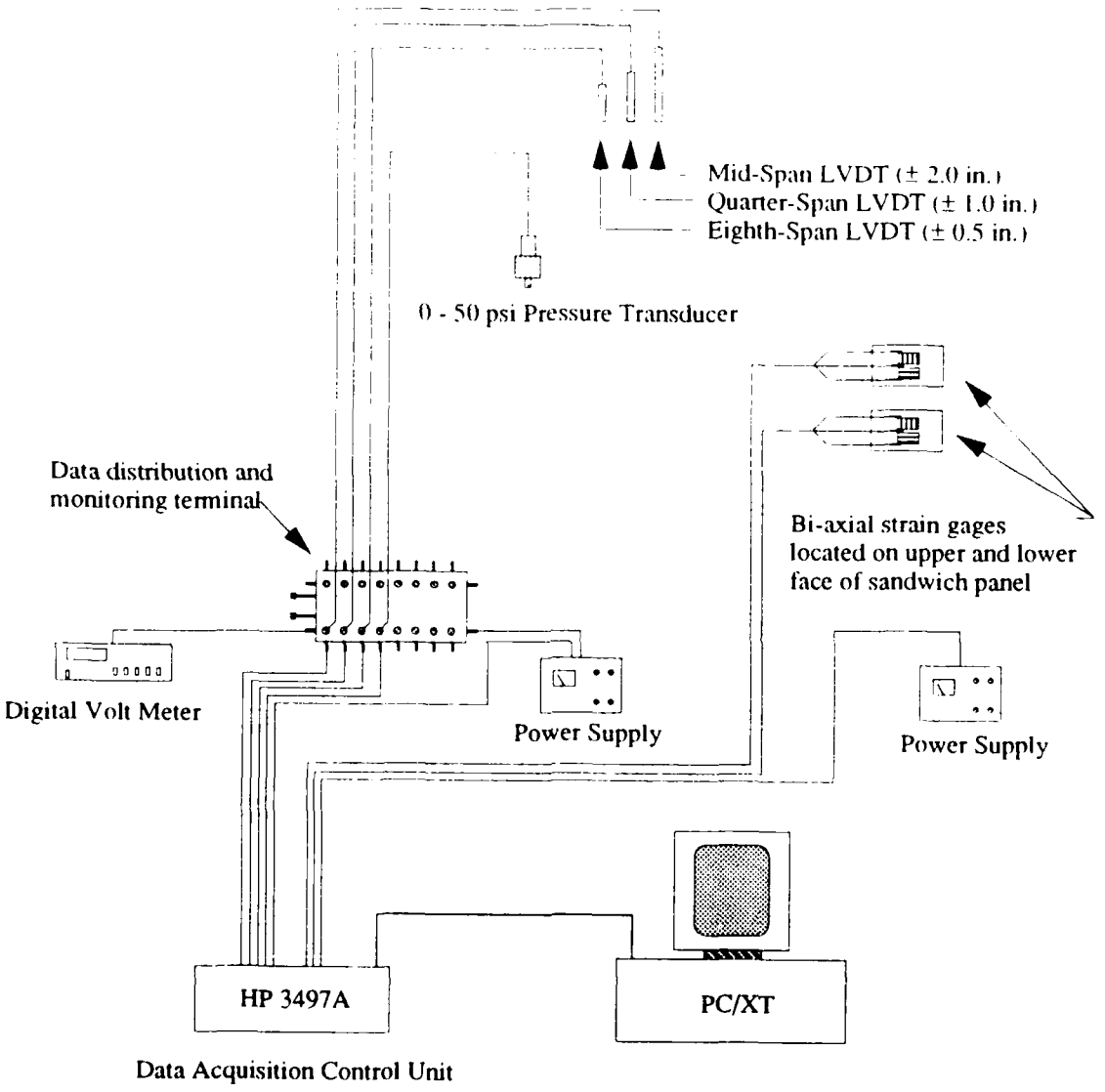

Figure 2-5: Data Acquisition System

2.2.2. Panel Test Procedure

2.2.2.1. Panel Preparation and System Initialization

Detailed panel preparation procedures were necessary prior to installation and testing. The panels were trimmed and squared to nominal dimensions of 90 in. wide by 120 in. long. The edges were sanded and duct tape applied to the transverse ends to prevent chaffing of the bladder. The doubler on the upper panel face was sanded to a uniform height to prevent binding of the panel during loading and to allow uniform loading against the panel restraining frame.

The bi-axial strain gages were aligned and mounted to the upper and lower faces of the panel. Due to a coarse surface on the upper face, a thin layer of polyester filler was necessary prior to strain gage installation. The filler was sanded smooth until the outer ply of fiber reinforcement was exposed. A covering of non-adhereing film and thin rubber matting was used to protect and isolate the strain gages from the bladder on the lower face. A similar covering was used on the upper face to protect the strain gage from the mid-span LVDT probe. Three-lead ribbon wire was soldered to the lower face strain gage and securely taped to the panel surface prior to installation. The upper face strain gage leads were connected after panel installation.

Panel installation required slight elevation of one end of the test mechanism frame to free and allow removal of one of the transverse, outer frame I-beam members. Saw horses cut to the required height were positioned under the panel to allow level entry into the mechanism frame. The panel support guide (1x1x0.125 angle) was cleaned and lubricated with liquid soap to reduce friction and ease panel entry. An even distribution of loading force was necessary to keep the panel aligned with the frame and prevent panel binding. When the panel was within 2 to 3 in. of the opposite end, the lower strain gage leads were routed through an opening in the I-beam web and secured to a terminal

connection. After panel loading, the outer frame I-beam was reattached and the test mechanism frame was lowered to its foundation.

System initialization procedures followed panel loading. The water tank was filled to a height level with the test panel and entrapped air vented by pressurizing the system to 0.5 psi. When the all air was purged from the bladder, the water tank was vented to the atmosphere and the pressure system allowed to stabilize. Power was then applied to the data acquisition system. The LVDT cores were installed and LVDT's aligned to allow initial voltage readings within their linear region. A 24 hour system stabilization and warm-up period was maintained for all tests to eliminate heating transients from the various electronic components. Upon completion of the stabilization period, all data acquisition channels were zeroed.

Then the water tank was filled to ensure that an appropriate water supply was available to support the volume absorbed by the panel deflections. The additional water provided a 22 in. static head and preloaded the panels to 0.8 psi. This allowed initial stressing of the panel test mechanism frame and a constant hydrostatic load on the panel.

2.2.2.2. Pressure Loading Procedures

Two types of pressure loading were used in this study: static and cyclic. The static pressure loading rate was approximately two orders of magnitude slower than the cyclic loading rate. This allows some investigation of the rate sensitivity of this combination of reinforcement, matrix, and core materials.

The static pressure sequence was a 0.5 psi increase over a 30 sec. period with a 30 sec. hold at each 0.5 psi increment. A load sequence to 10.8 psi and back to 0.8 psi took 40 min. The pressure vs. time plots for the static pressure load tests are provided in Appendix E.

The loading rate during the static pressure tests was controlled by manipulating the pressure regulator. Visual feedback from the on-screen pressure reading, a watch, and pressure-time schedule was sufficient to provide repeatability. Depressurization was accomplished by securing the supply air ball valve and purging with the 0.75 in. diameter tank vent valve.

The cyclic pressure test loaded the panels at the maximum rate of the system. Prior to these tests, the bladder was isolated from the water tank by closing the 2 in. ball valve. The pressure regulator was then preset to 30 psi by opening the supply air valve and adjusting the regulator. This procedure was necessary to achieve sufficient flow through the regulator during the cyclic test. The supply air valve was then closed, tank vented to the atmosphere, and bladder isolation valve opened. To initiate a cyclic loading test, the supply air valve was fully opened and pressure allowed to increase to obtain an 10 psi deviation (10.8 psi total pressure). After reaching this pressure, the supply air valve was closed and tank vent valve opened. Multiple cycles were obtained by closing the vent valve after reaching the initial pressure (0.8 psi), and repeating the procedure. System limitation in this configuration was 16 sec. to load from 0.8 to 10.8 psi and 21 sec. to vent to 0.8 psi. Total cycle period was 37 seconds. Pressure vs. time plots for the cyclic load tests are provided in Appendix F.

2.2.3. **Panel Boundary Conditions**

Three types of tests were conducted on the test panels to determine panel boundary conditions. These included; measuring deflections of the panel upper restraining frame, measuring the panel deflections equi-distant from the upper restraining frame members at the panel test section boundary, and measuring the in-plane deflections at the panel test section boundary.

It was necessary to measure the panel upper restraining frame deflections in order to determine the coupling effect between the panel and frame. This was accomplished by attaching dial gages to two, 2 in. channel steel beams placed on top of the panel restraining frame. The beams were simply supported at the ends and their lengths corresponded to those of the longitudinal and transverse frame members. Mid-span deflections as a function of pressure were monitored during testing of panel-1. Frame deflections were less than 0.02 in. for pressure loads to 10 psi while mid-span panel deflections were 0.6 in.

Two additional tests were conducted to determine type of end fixity. At the test section boundary panel deflections were measured to determine if comparable panel rotations were present. A test fixture was made which could be clamped to the upper frame and could measure panel deflections a distance of 4.375 in. from the frame, both inside and outside the test section. This fixture was attached to the frame during the panel static pressure tests at one of four positions and measurements taken at 2.5 psi intervals. These locations corresponded to the mid-span position in the longitudinal and transverse directions. In the panel transverse direction, deflections outside the test section were 6% to 11% more than the corresponding deflection inside the test section. Some inconsistencies between panels were present. These inconsistencies were attributed to non-symmetry in the doubler location and the relative bending stiffness of the panels. At the longitudinal ends of the panel, deflections inside and outside the test section exhibited greater inconsistency between panels. Deflections inside the test section were 5% to 14% larger than deflections outside the test section for panels 1 through 4, while deflections for panels 5 and 6 were 30% to 35% larger inside the test section than outside the test section . Larger panel rotations inside the test section for panels 5 and 6 were attributed to the type of panel response and will be discussed in section 3.2.3.

In addition to panel rotations, it was necessary to determine if in-plane displacements were present at the test section boundary. Fuji Prescale film (pressure sensitive) was placed between the panel and restraining frame during one of the panel tests.

Symmetric pressure distributions with respect to the frame centerline were recorded by the microcapsules of the film and there was no evidence of shear or in-plane displacement.

Interpretation of the results from these tests allows a qualitative and quantitative assessment of the type of boundary conditions imposed by the test mechanism. Upper restraining frame deflections were more than one order of magnitude less than the measured mid-span panel deflections. Therefore, the frame and panel deflection response were effectively decoupled. Similar panel rotations inside and outside the test section, particularly at the mid-longitudinal panel position, and no in-plane displacements at the test section boundaries provides sufficient evidence to conclude that the panel test section has clamped or fixed end conditions.

2.3. MATERIAL PROPERTY TESTING

Material property tests were conducted on the sandwich panels to provide a performance baseline and allow comparative analysis. All specimen were taken from an molded extension of the sandwich panel lower faces. Specimen orientation with respect to the panel differed between the various tests. Specimen were pre-conditioned in accordance with ASTM procedures. This included drying at 100° C for one hour following water polishing and storage at 23° C and 45 (±5%) relative humidity for a minimum of 48 hours.

All mechanical property tests were conducted using an Instron Model 4505 test machine. Data acquisition was performed by an IBM PS2 computer using Instron Corporation, Series IX Automated Materials Testing System software, Ver. 4.06.

2.2.4. Characterization of Sandwich Panel Faces

The specific gravity and density of the sandwich panel lower faces was determined in accordance with ASTM D-792 [31]. Specimens were cut and polished into nominal 0.5 in. width by 0.75 in. length and typically weighed between one and two grams. Specific gravity was determined from the ratio of the specimen dry weight to the difference between the submerged and dry weights.

The reinforcement weight and volume fraction for the E-glass panels was determined by matrix burn-off tests and ASTM D-2584 [32] procedures. A preliminary reinforcement weight and volume fraction for the Kevlar panels was determined by multiplying the specimen area by the fabric weight per unit area and dividing by the specimen weight. The 4 in. width by 6 in. length compressive specimen were used for this calculation. Several unsuccessful attempts at determining fiber weight content were made using matrix digestion techniques in ASTM D-3171 [33] and DUPONT Test Method 724 [34]. Failure of these methods was attributed to the chemical resistance properties of DERAKANE 510A. Matrix digestion did occur using sulfuric acid (H_2SO_4) at elevated

temperatures. However at temperatures near or above 100° C, the H_2SO_4 severely attacked the Kevlar fiber and fiber weight contents were not accurate.

The void content was determined in accordance with ASTM D-2734 [35]. A specific gravity of 2.54 for E-glass and 1.44 for Kevlar was used in the void content calculations.

2.2.5. Tensile Strength and Modulus

The tensile strength and modulus of the sandwich panel lower faces were determined in accordance with ASTM D-3039 [36]. The longitudinal axis of the tensile specimen corresponded with the panel transverse direction. Specimens were cut and polished to a nominal 1.0 in. width by 12 in. length. Grip tabs of 3M Scotchply were cut to a 2 in. length, sanded to a 10° angle of incidence, and attached to the tensile specimen using FM 123 adhesive.

The cross-head rate for all tensile tests was 0.1 in. per min. Data acquisition sample rate was two samples per second.

One specimen from each panel was equipped with a model FAET-25A-12 S6 ES bi-axial strain gage manufactured by BLH Electronics Inc., Canton, MA. Strain gages were used to determine the Poisson's Ratio and validate strain and modulus calculations.

Tensile stress was determined by dividing the load by the minimum cross sectional area in the gage region. Tensile modulus was determined from the linear slope of the Instron load deflection curve by:

$$E = \frac{\nabla P}{\nabla w}\frac{a}{bt} \tag{16}$$

Where:

$\frac{\nabla P}{\nabla w}$ = Linear slope of the load deformation curve

Tensile modulus values based on strain gage data were calculated by dividing the linear slope of the load deformation curve by the specimen cross sectional area and the slope of the longitudinal strain.

The Poisson's Ratio was determined from the linear slope of the longitudinal and transverse strain curves by:

$$\nu = \frac{-\nabla\varepsilon_t}{\nabla\varepsilon_l} \tag{17}$$

where:

$\nabla\varepsilon_t$ = linear slope of the transverse strain
$\nabla\varepsilon_l$ = linear slope of the longitudinal strain

2.2.6. Compressive Strength and Modulus

The compressive strength of the sandwich panel lower faces was determined using the method developed by Byers [37]. The longitudinal axis of the compressive test specimen corresponded to the panel longitudinal axis. This orientation was not consistent with the other tests but necessary because of a limited amount of test material. It was justified from the quasi-orthotropic nature of the laminate Specimens were cut and polished to a nominal 4.0 in. width by 6.0 in. length.

The compressive specimen was placed in a support fixture and loaded in edgewise compression. The crosshead rate for compression testing was 0.1 in. per min.

The compressive stress was determined by dividing the compressive load by the specimen cross sectional area. Compressive strain was calculated by dividing crosshead deflection by the specimen length.

2.2.7. Flexural Strength and Modulus

The flexural strength of the sandwich panel lower faces was determined in accordance with ASTM D-790 [38]. The specimen longitudinal axis corresponded to the sandwich panel transverse direction.

Two series of flexural tests were conducted using specimen of differing geometry. Specimens were cut to facilitate support span-to-depth ratio's of 40:1 and 16:1 for the ASTM three-point bending procedure. This corresponded to specimen sizes of 0.5 in. wide by 9.5 in. long and 0.5 in. wide by 4.0 in. long respectively.

The specimens were placed in a three-point test fixture equipped with support and loading noses having a diameter of 0.5 in. to reduce stress concentrations. Flexural specimen were loaded with crosshead rate of 0.5 in. per min for the 40:1 span-to-depth ratio tests and 0.08 in. per min. for the 16:1 span-to-depth ratio tests. The outer-ply of the sandwich panel lower face was loaded in compression during the 40:1 span-to-depth ratio tests and in tension for the 16:1 span-to-depth ratio tests.

The flexural strength of the specimen was determined from the maximum stress of the fibers in the outermost ply by:

$$\sigma = \frac{3PL}{2bt^2} \tag{18}$$

In the case where the mid-span deflections exceeded 10% of the support span width, the flexural strength was calculated using:

$$\sigma = \frac{3PL}{2bt^2}\left[\, 1 + 6\left(\frac{w}{L}\right)^2 - 4\left(\frac{t}{L}\right)\left(\frac{w}{L}\right)\right] \tag{19}$$

This correction factor was applied to all of the 40:1 span-to-depth ratio test results and to specimens from panels 3 through 6 for the 16:1 span-to-depth ratio tests.

2.2.8. In-Plane Shear Strength

The in-plane shear strength of the sandwich panel lower faces was determined in accordance with ASTM D-3846 [39]. Specimens were cut and polished to a 0.5 in. width by 3.125 in. length. A 0.04 in. transverse notch was machined to one half the specimen depth on opposing sides of the specimen using a water cooled diamond grit-edge blade. These notches were cut to provide a centrally located 0.25 in. longitudinal shear plane.

The in-plane shear specimen was placed in the required support jig with bolts torqued to an approximate 1.0 lbf.-inch. Specimen were loaded in edgewise compression with a cross-head rate of 0.05 in. per minute.

In-plane shear strength was determined by dividing the compressive load by the cross sectional area of the shear plane. In-plane strain was calculated by dividing crosshead deflection by the specimen length.

3. RESULTS and DISCUSSION

3.1. MATERIAL PROPERTIES OF SANDWICH PANEL FACES

Material properties of the sandwich panel lower faces are presented in tabular form for reference and graphically for discussion. Detailed results including load-deformation, stress-strain plots, specimen dimensions, and statistical analysis are provided in the related appendix.

3.1.1. Characterization of Sandwich Panel Faces

The panel lower faces are characterized by specific gravity, reinforcement weight fraction, reinforcement volume fraction, and void content. A summary of the results are provided in Table 3-1. Panel face properties are commensurate with those typical of hand lay-up molding processes. Differences between panels are attributed to the panel constituents.

Table 3-1: Characterization of Sandwich Panel Lower Faces

Panel Number	Specific Gravity	Fiber Weight Content (%)	Fiber Volume Fraction (%)	Void Content (%)
Panel-1	1.635	42.491	27.40	1.44
Panel-2	1.661	43.167	28.39	0.28
Panel-3	1.303	37.597	30.15	8.25
Panel-4	1.377	35.017	29.67	2.52
Panel-5	1.208	42.830	31.84	4.78
Panel-6	1.194	45.388	33.34	6.84

The E-glass/DERAKANE 510A panel faces exhibit specific gravity values 18.7% to 27.5% greater than the Kevlar/DERAKANE 510A panels and 35.3% to 39.1% greater

than the Kevlar/DERAKANE 8084 ones. The higher values are attributed to the specific gravity of E-glass (2.54), as compared to Kevlar (1.44).[40] Differences between the Kevlar panels are attributed to resin type. The specific gravity of DERAKANE 510A is 1.32 and DERAKANE 8084 is 1.09. These values are obtained from clear castings of the cured resins.

The influence of the hand lay-up molding process is evident in the reinforcement weight fraction, volume fraction, and void content results. During this process, E-glass fabric wets-out easily, and entrapped air or voids can be observed visually and removed. This is more difficult for Kevlar due to its poor wetting characteristic and opaque nature.

Burn-off test results for the E-glass panel faces are consistent with marine industry standards. Reinforcement volume fraction values are lower than expected but may be attributed to the loose or open nature of the Vectorply 1808 fabric. Void contents are also within industry standards. Visually the void contents are noticeably lower than for the Kevlar panels.

Quantitative assessment of the characteristics for the Kevlar panels has greater uncertainty since the results of the matrix digestion tests are inconclusive. Reinforcement weight fractions derived from specimen weight and area calculations are consistent, with coefficients of variation less than 3.7%. Weight fraction values for panels 3 and 4 are 5% to 10% less than those for panels 5 and 6. Differences may be related to the wetting-out characteristics of DERAKANE 510A.

Void contents for the Kevlar panels are higher than the E-glass ones. Differences are attributed to manufacturer experience and noted difficulties when working with Kevlar.[41] The distribution of voids varies; visually there is a higher void content along the panel boundaries and outside the panel test section.

3.1.2. Tensile Strength and Modulus

Detailed results for tensile strength, modulus, and Poisson's Ratio tests for the sandwich panel lower faces are available in Appendix A. Table 3-2 summarizes the results which are presented in Figures 3-1 through 3-4. The panels with E-glass reinforced faces have tensile strengths averaging 12% more than the Kevlar ones; these are attributed to the amount of fiber reinforcement in the longitudinal (load) axis. The Kevlar panel faces have 2 plies with ±45° fabric orientation. A reduction in strength occurs with fiber orientations greater than ±10° off the principle axis.[40]

Table 3-2: Tensile Characteristics of Sandwich Panel Lower Faces

Panel Number	Strength (psi)	Modulus (ksi)	Poisson's Ratio
Panel-1	23221	2024.2	0.316
Panel-2	23869	2150.6	0.319
Panel-3	23608	1937.8	0.202
Panel-4	18955	1538.4 *	0.197
Panel-5	20239	1632.7	0.187
Panel-6	20072	1515.7 *	0.237

* Value determined from load deformation analysis

Tensile modulus data based on load-deformation analysis are shown in Figure 3-2 and from a single strain gage measurement in Figure 3-3. Values from load-deformation analysis are lower than the strain gage measured values for the E-glass panel faces. These specimen failed outside the gage region near the tab edge. One surface of the specimens have fiber strands aligned perpendicular (90°) to the longitudinal (load) axis. Between 90° strands a locally reduced cross sectional area exists. This and stress concentrations from the tabs promote tensile failure. The ultimate tensile strength values are not significantly affected while larger displacements are present. These larger displacements provide

reduced modulus values. Subsequent testing using non standard specimen sizes produced similar strength values.

Modulus data for the Kevlar reinforced panels have greater consistency between test methods. This is a result of tensile failures occurring within the gage region. In the case of panels 4 and 6, modulus values derived from load deformation analysis are higher. The strain gage specimen for these panels failed at the gage or close to it. Higher strains are recorded and a lower tensile modulus is derived. Overall lower tensile modulus values for the Kevlar panels are attributed to ply orientation.

Results of the Poisson's Ratio test are illustrated in Figure 3-4. The E-glass panels have higher values but are consistent with other documented results.[40] Lower values for the Kevlar panels are attributed to ply orientation and the greater disparity between the tensile and compressive characteristics of Kevlar.

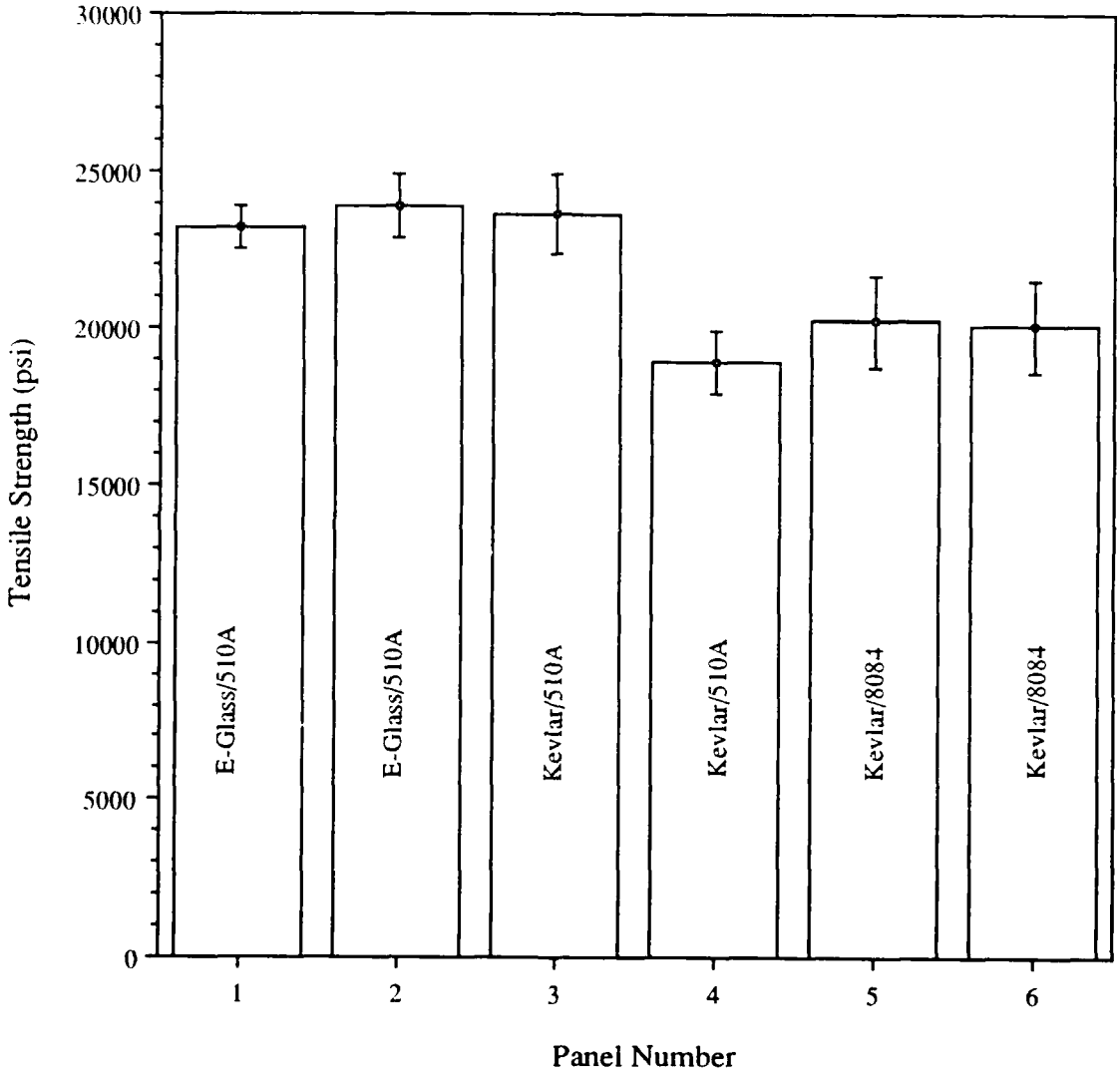

Figure 3-1: Tensile Strength of Sandwich Panel Lower Faces

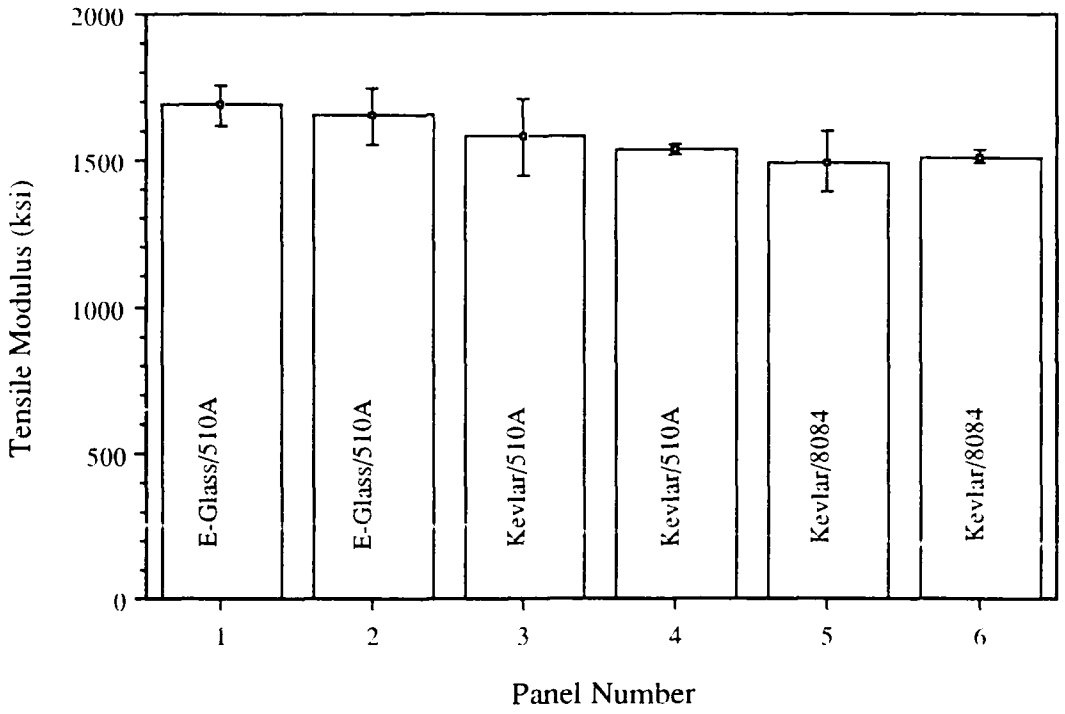

Figure 3-2: Tensile Modulus of Sandwich Panel Lower faces Based on Load Deformation Analysis

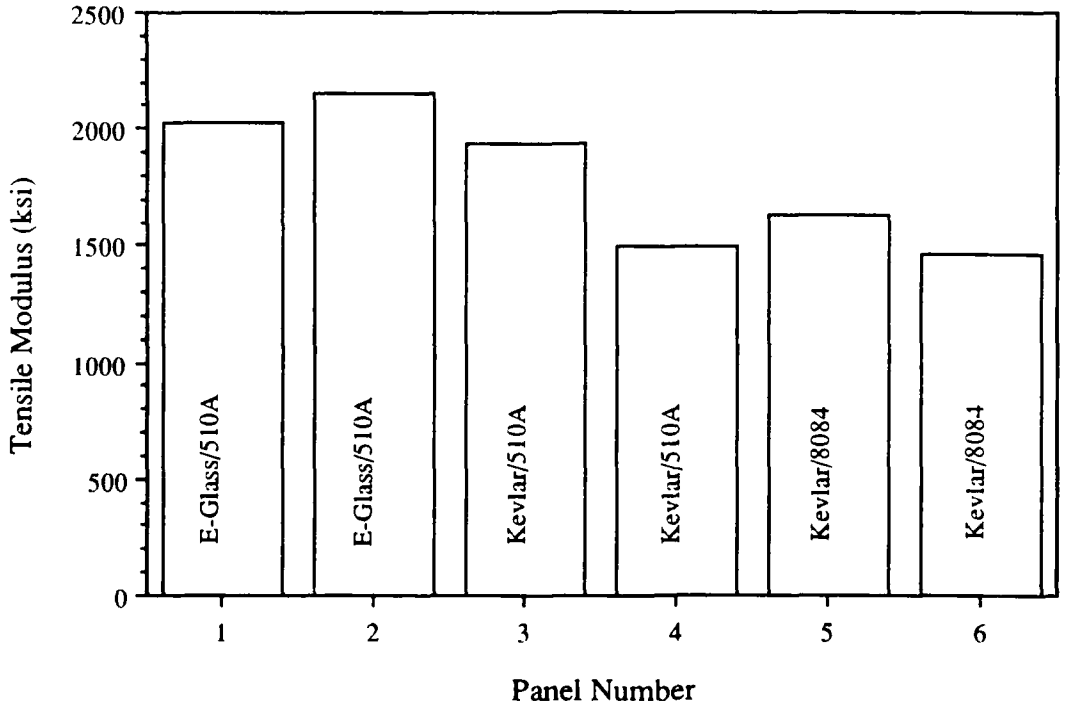

Figure 3-3: Tensile Modulus of Sandwich Panel Lower Faces Based on a Single Strain Gage Measurement

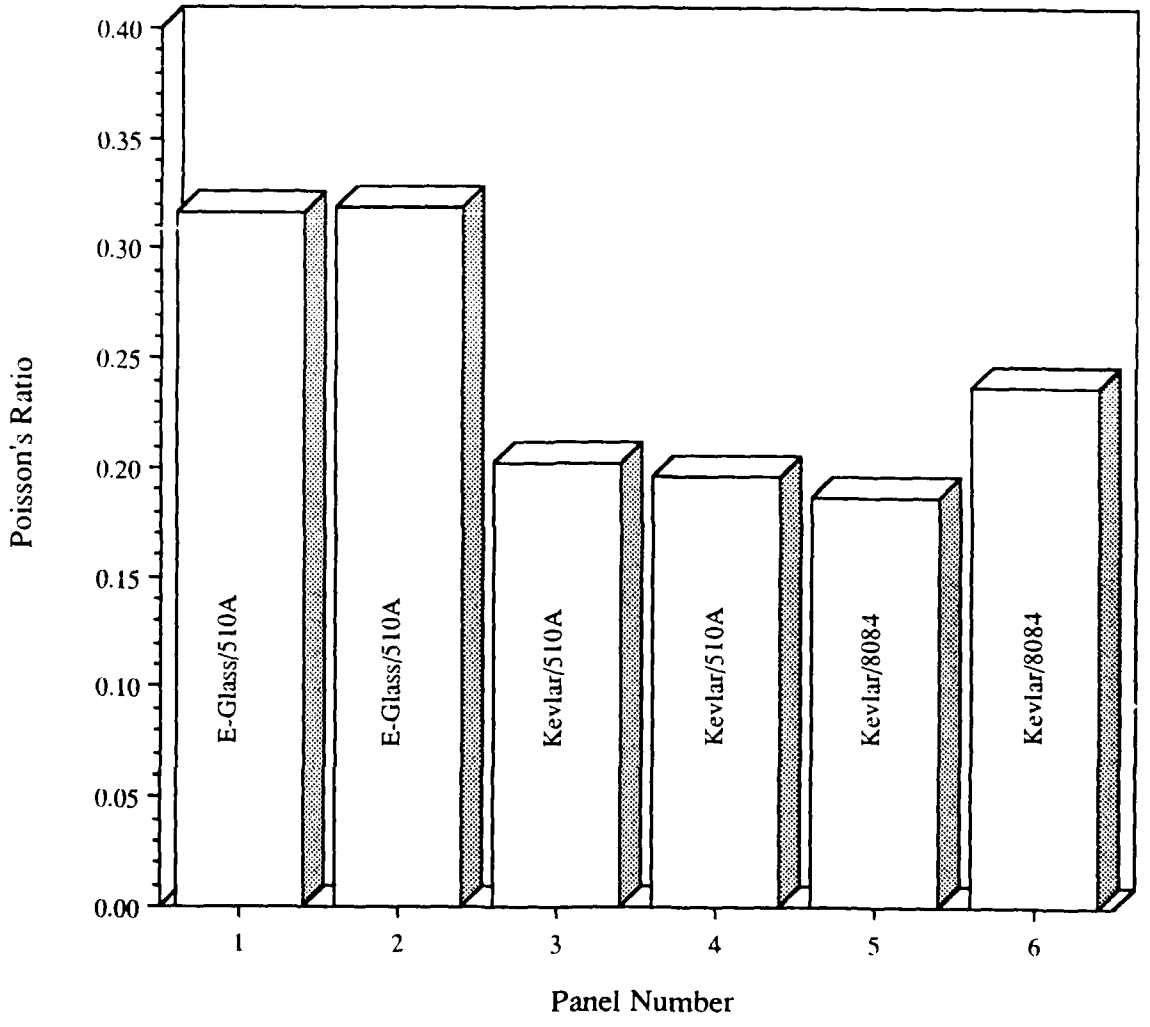

Figure 3-4: Poisson's Ratio of Sandwich Panel Lower Faces based on a Single Bi-axial Strain Gage Measurement

3.1.3. Compressive Strength and Modulus

Detailed compressive strength and modulus data for the sandwich panel lower faces are available in Appendix B. Table 3-3 summarizes the results which are presented in Figures 3-5 and 3-6. The E-glass panel faces have almost twice the compressive strength of the Kevlar ones. They exhibit brittle failure characterized by loud cracking noises and a catastrophic yield. The Kevlar/DERAKANE 510A specimen (panels 3 & 4) have a similar but less pronounced type failure. In contrast, the Kevlar/DERAKANE 8084 faces (panels 5 and 6) exhibit general yielding. This is evident both from the stress-strain curves and from visual observations during testing. Specimen from panels 1 through 4 have a larger change in slope (modulus) near yield than those from panels 5 and 6. Visually, there is less evidence of specimen failure: a reduction in the number of cracks and the specimen remain intact, although deformed. This difference is explained by the properties of the fiber and matrix. When compressed Kevlar fibrilates and the DERAKANE 8084 is a high elongation, elastomer modified resin. The combination produces a high compressive strain-to-failure. The DERAKANE 8084 specimen also show greater scatter: the coefficients of variation are more than double those of the DERAKANE 510A specimens.

Table 3-3: Compressive Characteristics of Sandwich Panel Lower Faces

Panel Number	Strength (psi)	Modulus (ksi)
Panel-1	17564	1146.2
Panel-2	17351	1213.0
Panel-3	8586	774.7
Panel-4	9035	717.5
Panel-5	8055	725.0
Panel-6	9401	726.8

The compressive modulus of the Kevlar panels average 37.6% less than E-glass; the differences are attributed to less fiber reinforcement in the load axis, and a lower fiber compressive modulus for Kevlar. In the linear region, there is little difference between specimens having the DERAKANE 510A or 8084 matrix. Approaching yield, the DERAKANE 8084 specimen (panels 5 & 6) show larger out-of-plane displacements. These suggest a transition from compression loading to combined compression and buckling; the high elongation properties of this matrix may promote the transition. This is a limitation of the test procedure and the modulus data are somewhat uncertain, but the comparison of panel performance is considered valid.

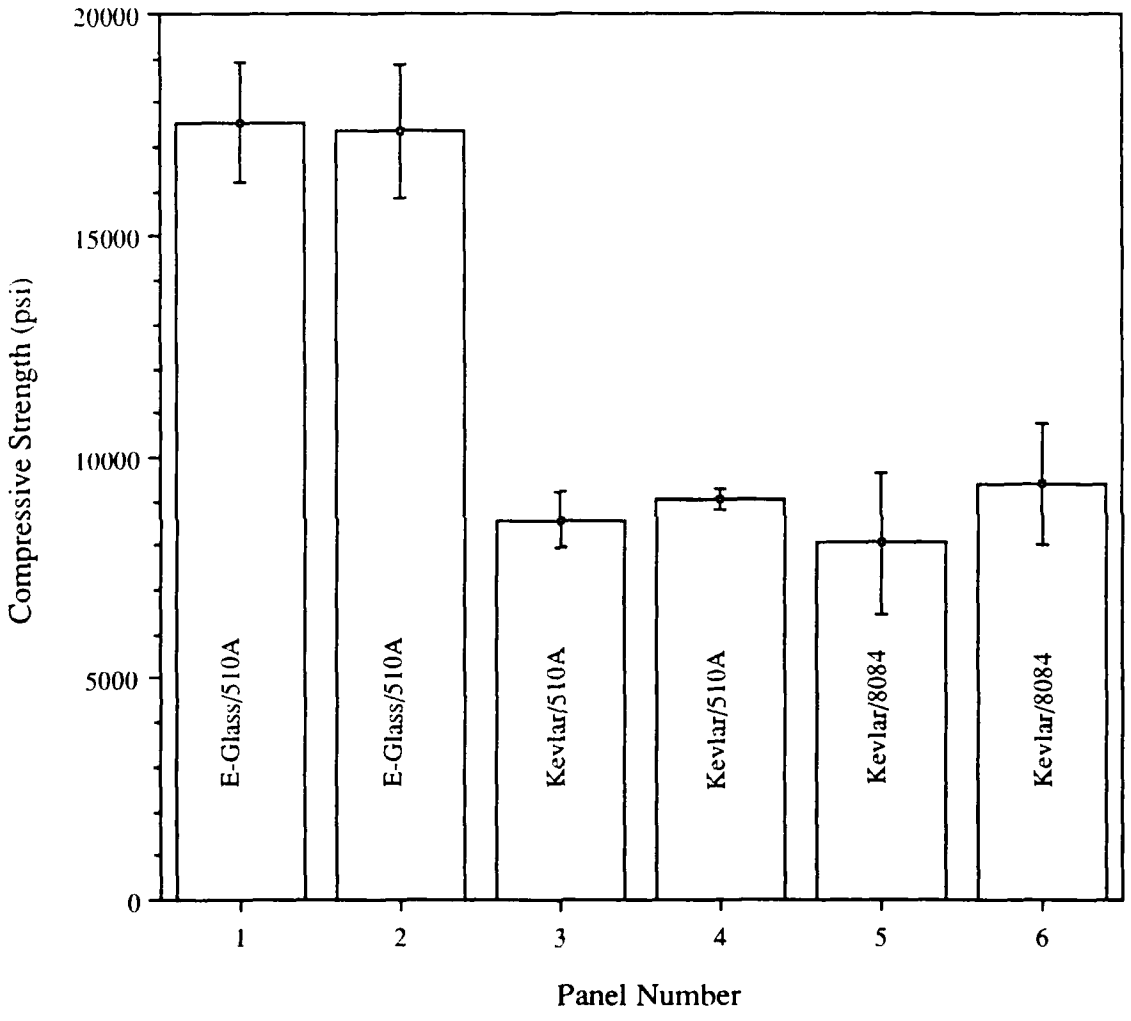

Figure 3-5: Compressive Strength of Sandwich Panel Lower Faces

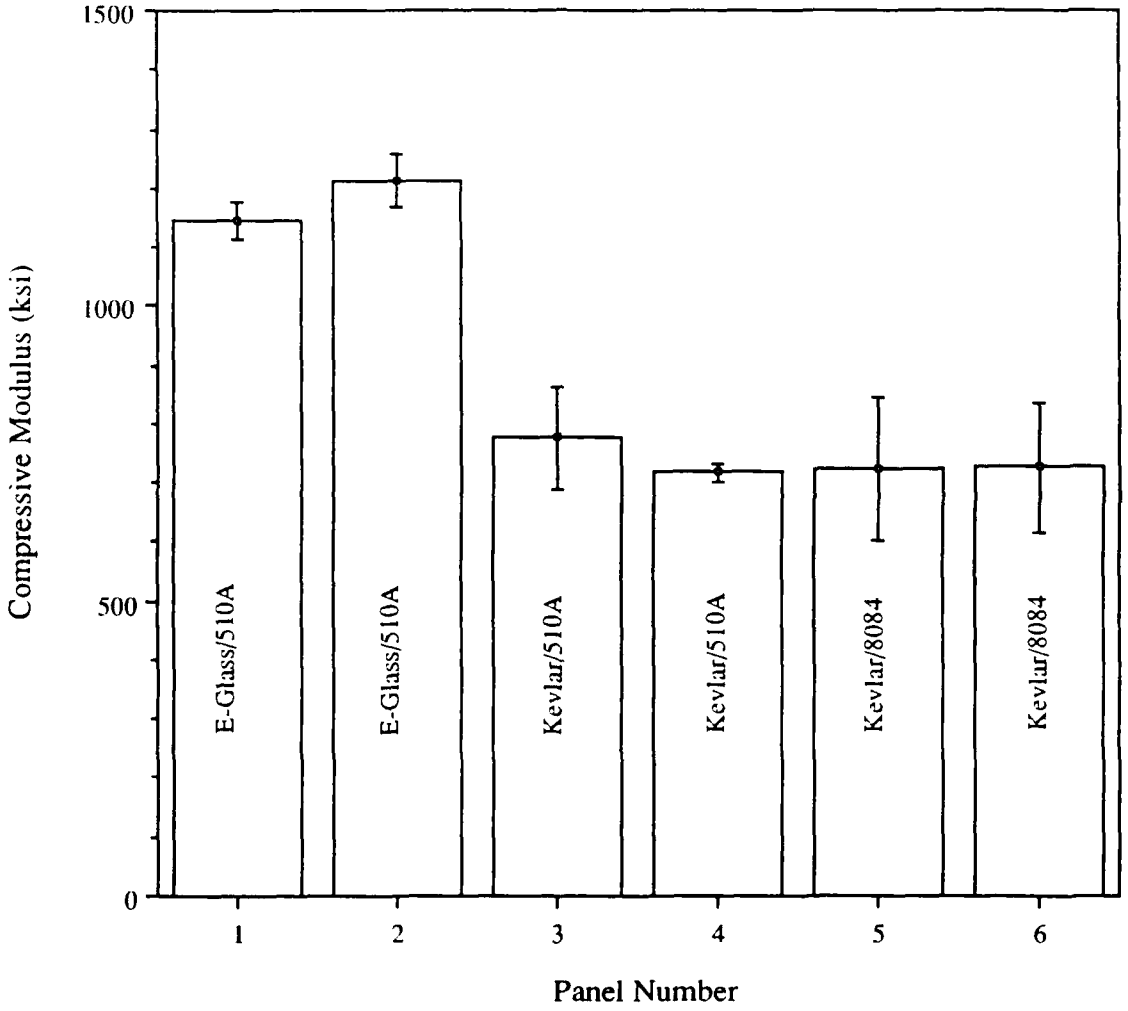

Figure 3-6: Compressive Modulus of Sandwich Panel Lower Faces

3.1.4. Flexural Strength and Modulus

Detailed flexural strength and modulus data for the sandwich panel lower faces are provided in Appendix C. Table 3-4 summarizes the results which are presented in Figures 3-7 through 3-10. With the exception of two cases, the flexural strength and modulus values obtained from method I (40:1 span-to-depth ratio) are higher than those determined from method II (16:1 span-to-depth ratio). Different fracture modes are apparent between methods. In method I, the CSM ply is in compression and the 1808 E-glass 0° ply is in tension (panels 1 and 2). Figures C-1 and C-3 illustrate the initial reduction in load followed by recovery and fracture. The load reduction occurs as compressive failure initiates in the CSM ply. Upon further deflection, the lower 0° ply becomes loaded in tension and fails. There is a more abrupt failure mode for method II specimens (panels 1 and 2) where, the CSM ply is in tension and fails prior to compressive failure of the 1808 0° ply. A 16% higher flexural strength is achieved by loading the E-glass specimen with the continuous ply (0° ply) in tension

Table 3-4: Flexural Characteristics of Sandwich Panel Lower Faces

Panel Number	Strength (psi)	Modulus (ksi)
Panel-1	43286	1554.0*
Panel-2	42851	1687.6
Panel-3	25176	1135.6
Panel-4	23707	1228.3
Panel-5	26283*	1072.0
Panel-6	25000	1154.9

* Obtained from flexure test method II

For panels 3 through 6, the CSM ply is in compression and the Kevlar KDB ±45° ply is in tension during method I tests. Perturbations in the load deformation curve occur near yield as the ±45° strands debond. Total failure is difficult to identify as the specimens

continue to deflect through several loading and unloading cycles; Figures C-5, C-7, C-9, and C-11 illustrate this.

In method II, the CSM ply is in tension and the Kevlar KDB 110 ±45° ply is in compression. The slopes of the load-deflection curves near yield are less with the CSM ply in tension; this is shown in Figures C-6, C-8, C-10, and C-12. The compressive failure mode of Kevlar may contribute to this behavior: as the specimen is loaded, general yielding occurs on the compression face. Only after large deflections are reached is the CSM ply loaded in tension. In several cases, there was no visual evidence when failure occurred. The flexural strengths of the panel lower faces are shown in Figures 3-7 and 3-8. The E-glass panels have flexural strengths averaging 41.9% more than the Kevlar ones. Similarly, the flexural modulus of the E-glass panels average 29% higher than the Kevlar panels. The lower strength and modulus values for the Kevlar panels are caused by the different ply orientation. Differences in performance between the panels of DERAKANE 510A and DERAKENE 8084 resin are not discernable.

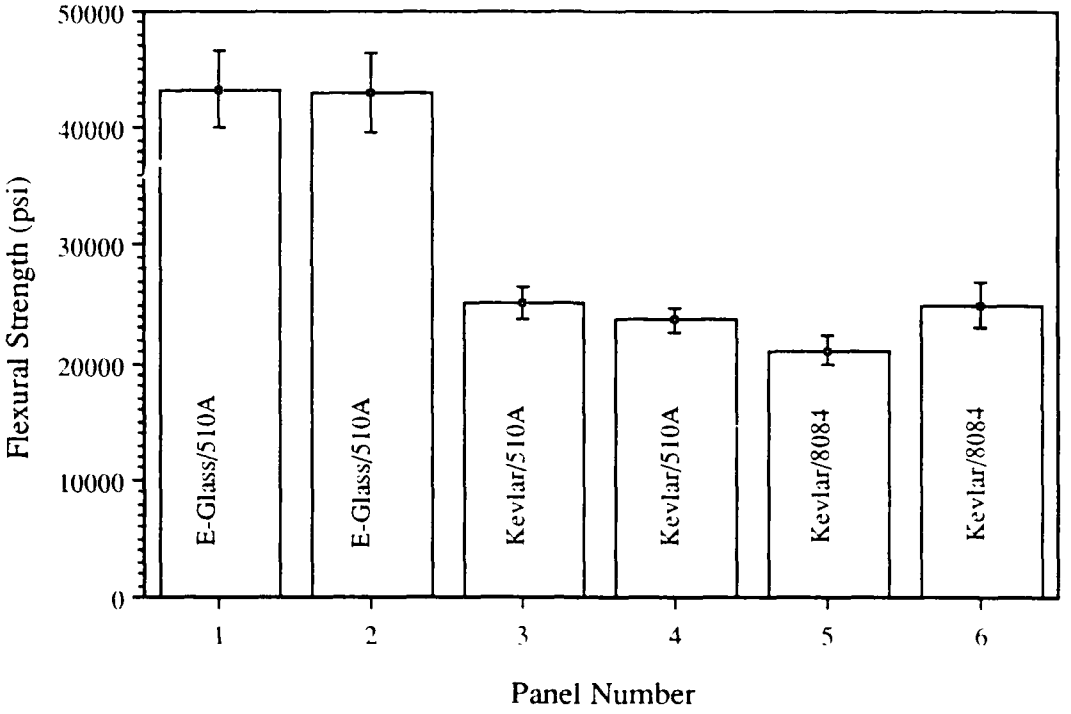

Figure 3-7: Flexural Strength of Sandwich Panel Lower Faces with CSM Ply in Compression and a Support Span-to-Depth Ratio of 40:1

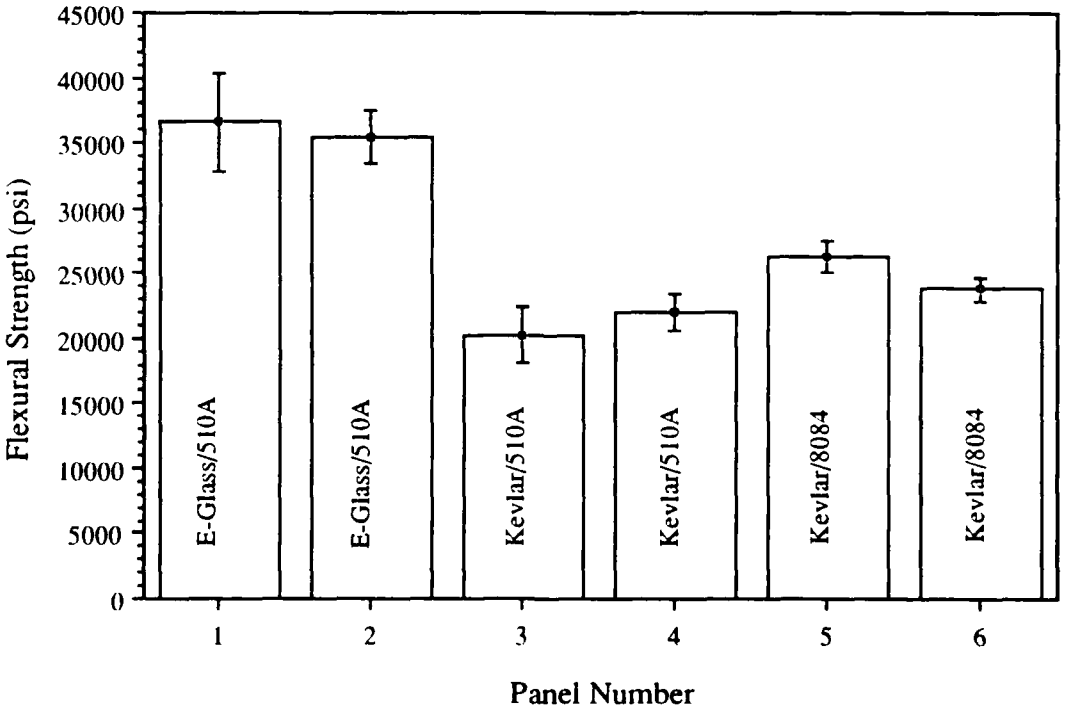

Figure 3-8: Flexural Strength of Sandwich Panel Lower Faces with CSM Ply in Tension and a Support Span-to-Depth Ratio of 16:1

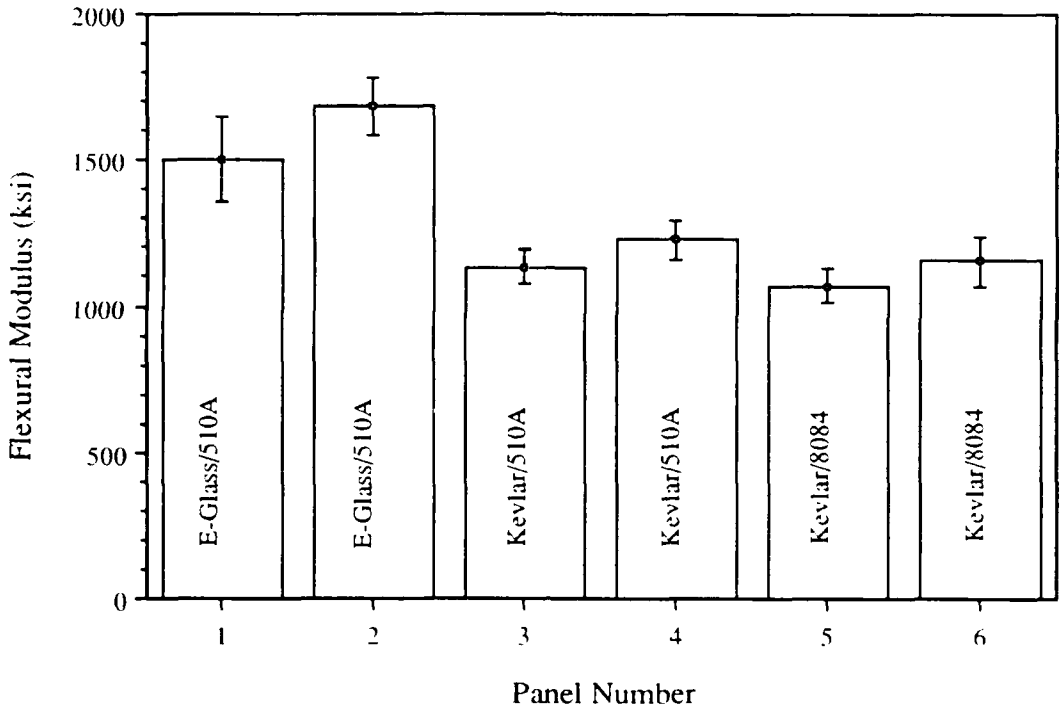

Figure 3-9: Flexural Modulus of Sandwich Panel Lower Faces with CSM Ply in Compression and a Support Span-to-Depth Ratio of 40:1

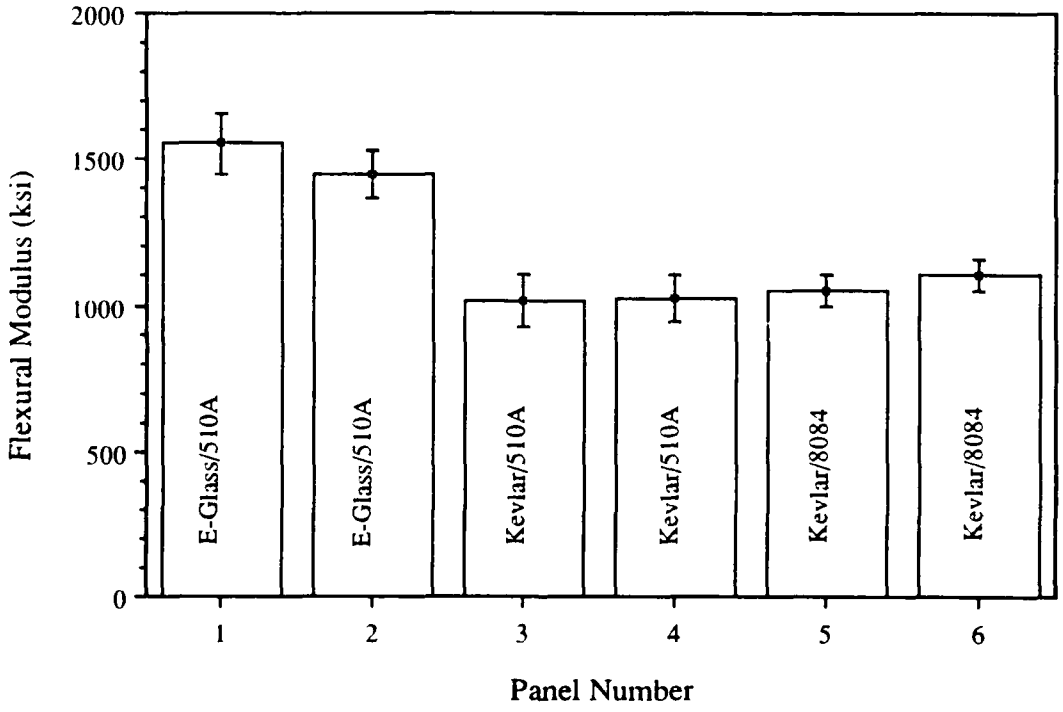

Figure 3-10: Flexural Modulus of Sandwich Panel Lower Faces with CSM Ply in Tension and a Support Span-to-Depth Ratio of 16:1

3.1.5. In-Plane Shear Strength

Detailed in-plane shear strength data for the sandwich panel lower faces are provided in Appendix D. Table 3-5 summarizes the results which are presented in Figure 3-11. In-plane shear strength data provide an assessment of the fiber-matrix bond strength. The E-glass panel faces average 19.1% higher than the Kevlar ones. This suggests the vinyl ester matrix supports E-glass better than Kevlar.

Typically test results are scattered due to inconsistencies in specimen preparation. In this case, the time and expense of machine cutting the specimen and the notches with a water-cooled diamond grit-edge blade are justified. The coefficient of variation for the E-glass panel faces average 3.3%, while those for the Kevlar ones average 8.3%.

Table 3-5: In-plane Shear Strength of Sandwich Panel Lower Faces

Panel Number	Shear Strength (psi)
Panel-1	3648
Panel-2	3767
Panel-3	2942
Panel-4	3234
Panel-5	2739
Panel-6	3080

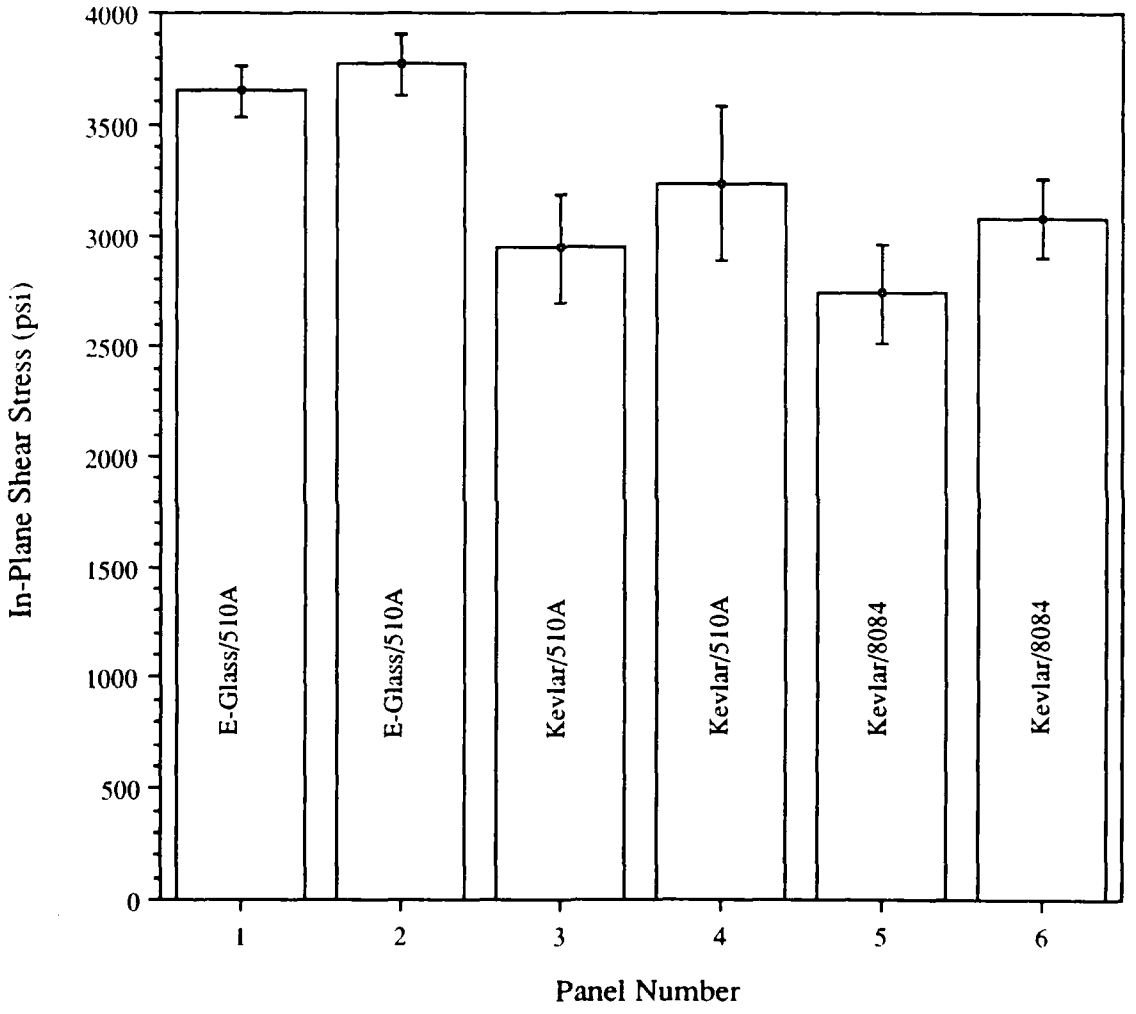

Figure 3-11: In-Plane Shear Strength of Sandwich Panel Lower Faces

3.2. PANEL TESTS

The deflection and strain responses of the panels to static and cyclic pressure loading are presented in sections 3.2.1 and 3.2.2. Detailed results are contained in Appendix E and Appendix F. A comparison of bending stiffness, deflection recovery, tensile and compressive strain rates, and rate dependency are presented in section 3.2.3.

3.2.1. Static Pressure Loading

A description of the static loading sequence is given in section 2.2.2.2. Figures E-1 through E-6 show pressure versus time for the static pressure tests. The static pressure test loading rates average 0.0079 psi/sec. with a coefficient of variation of 6.1%.

3.2.1.1. Deflection Response

The mid, quarter, and eighth-span deflection response of the panels to static pressure loading are shown in Figures 3-12 through 3-17. The deflection recovery after 1 minute and 24 hours are shown on the plots. Some permanent deformations are present in the panels prior to static pressure testing. These result from the cyclic pressure tests. (As a sponsor requirement, the cyclic tests are conducted prior to the static tests to minimize permanent deformations.) Panel deflection behavior is non-linear with pronounced hysteresis. Differences between the two matrix resins are evident. The pressure-deflection curves for panels 1 through 4 (DERAKANE 510A) are shown in Figures 3-12 through 3-15. Two distinct slopes are present. A linear region occurs up to 5.5 psi: this appears to be the first elastic limit. Above 6 psi, there is a finite reduction in slope and the response becomes non-linear.

The deflections of panels 5 and 6 (DERAKANE 8084) are shown in Figures 3-16 and 3-17. These have a smaller linear region with a lower elastic limit (4 psi), larger

deflections at maximum pressure, and more permanent deformation. Above 4 psi, the pressure-deflection shape is similar to panels 1 through 4, however, at approximately 8 psi, a change in slope occurs and the panels become stiffer. This indicates membrane behavior; it coincides with mid-span deflections which approximate the panel thickness.

The transverse deflected shapes of the panels are illustrated in Figures E-7 through E-12. The magnitude of the quarter-span deflections for panels 3 through 6 (Kevlar) are a larger fraction of the mid-span deflections than for panels 1 and 2. This suggests that the Kevlar panels are responding in a different manner; larger quarter-span deflections indicate less of an arching response. The flatter shape is due to the ±45° plies present in the Kevlar reinforced panels; they stiffen the panel diagonal directions.

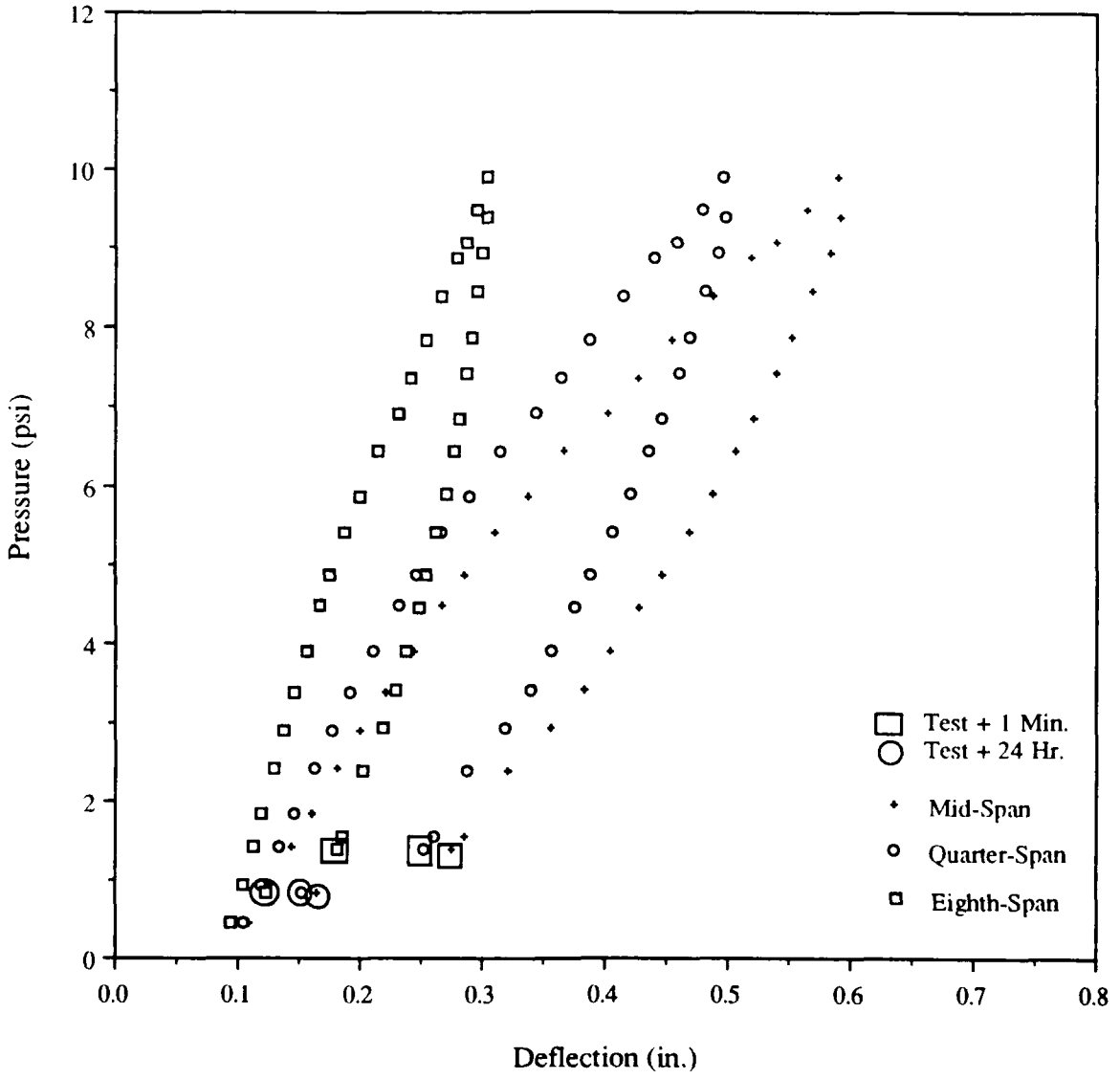

Figure 3-12: Deflection Response of Panel-1 to Static Pressure Loading

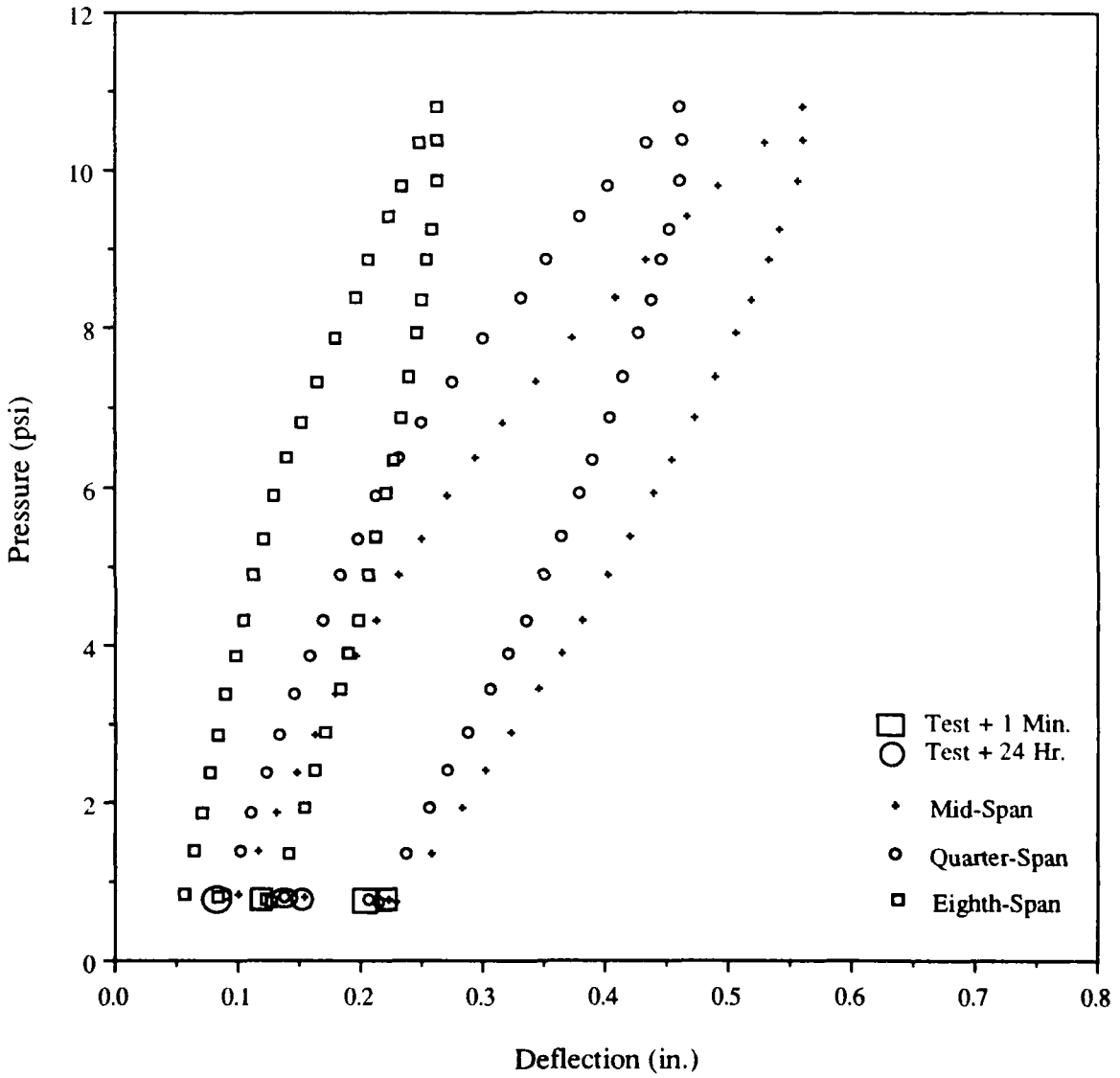

Figure 3-13: Deflection Response of Panel-2 to Static Pressure Loading

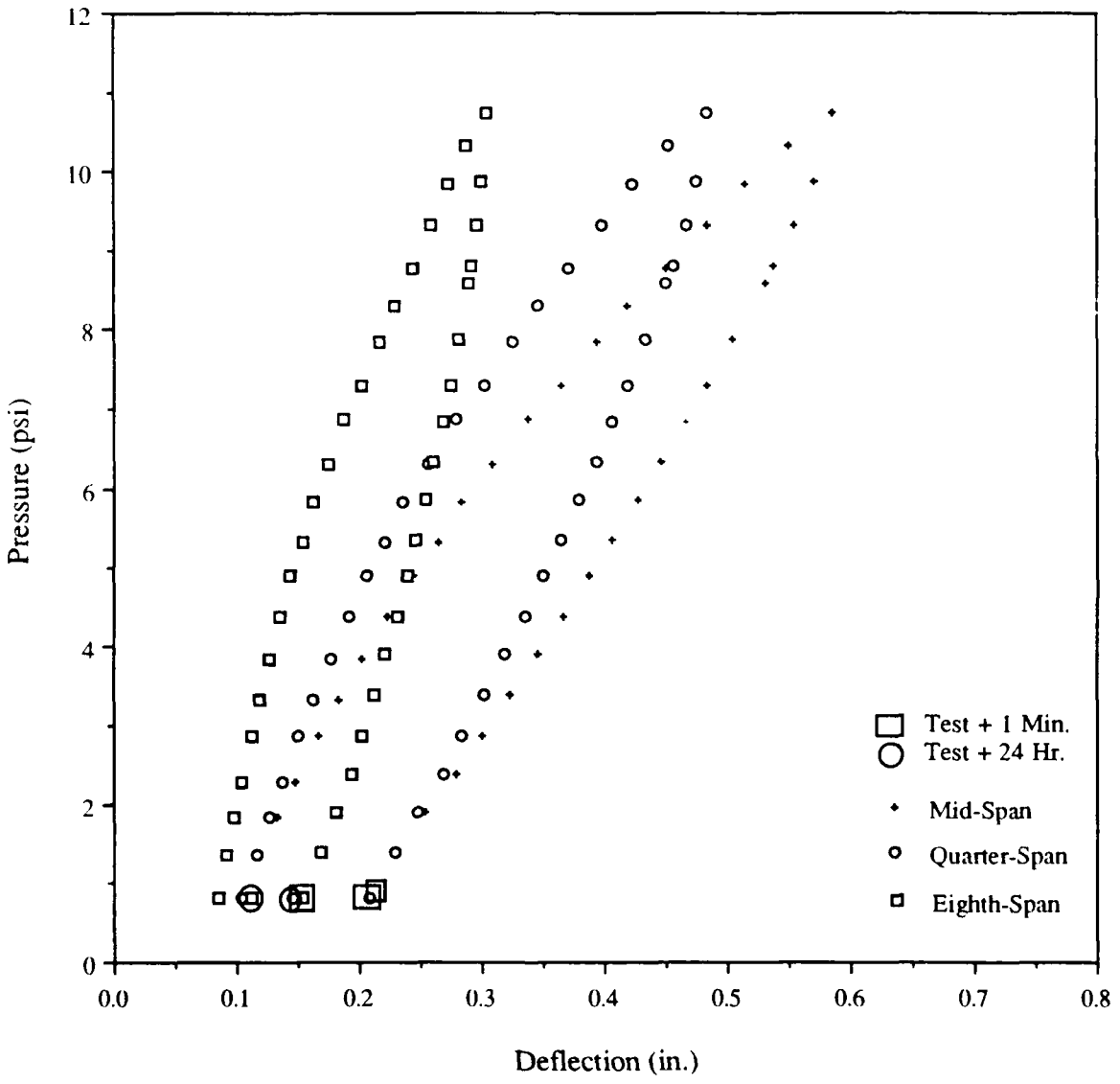

Figure 3-14: Deflection Response of Panel-3 to Static Pressure Loading

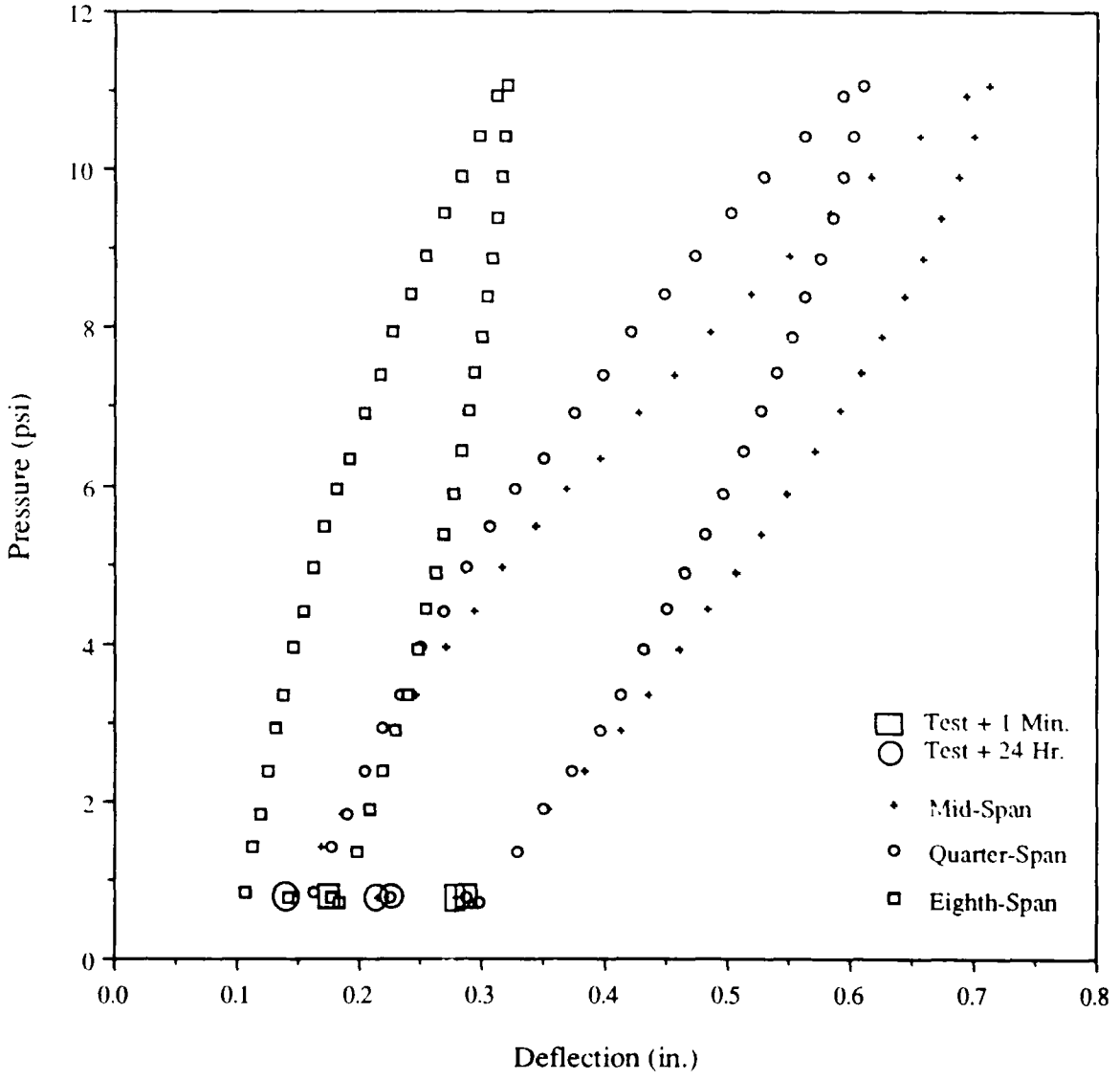

Figure 3-15: Deflection Response of Panel-4 to Static Pressure Loading

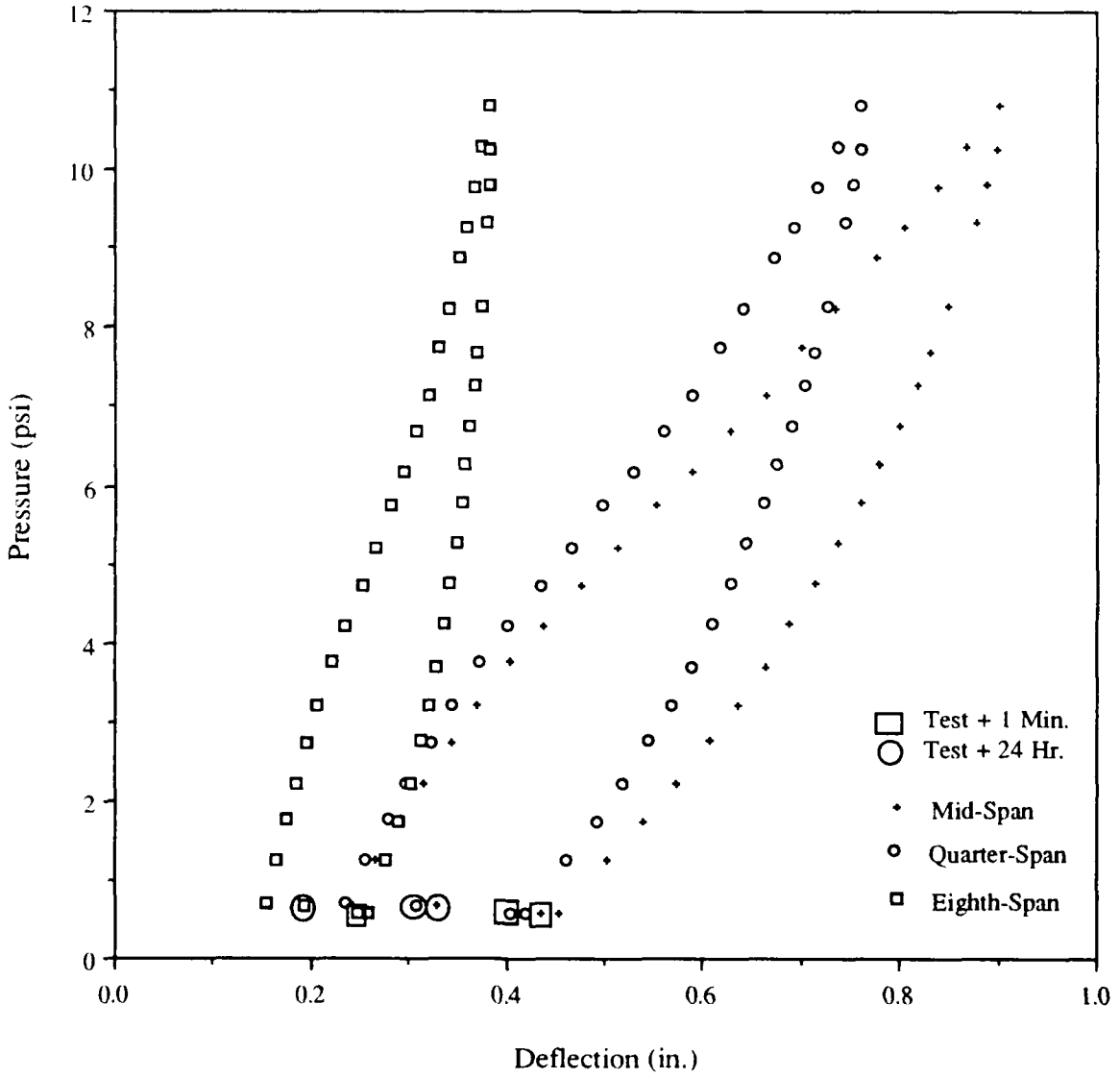

Figure 3-16: Deflection Response of Panel-5 to Static Pressure Loading

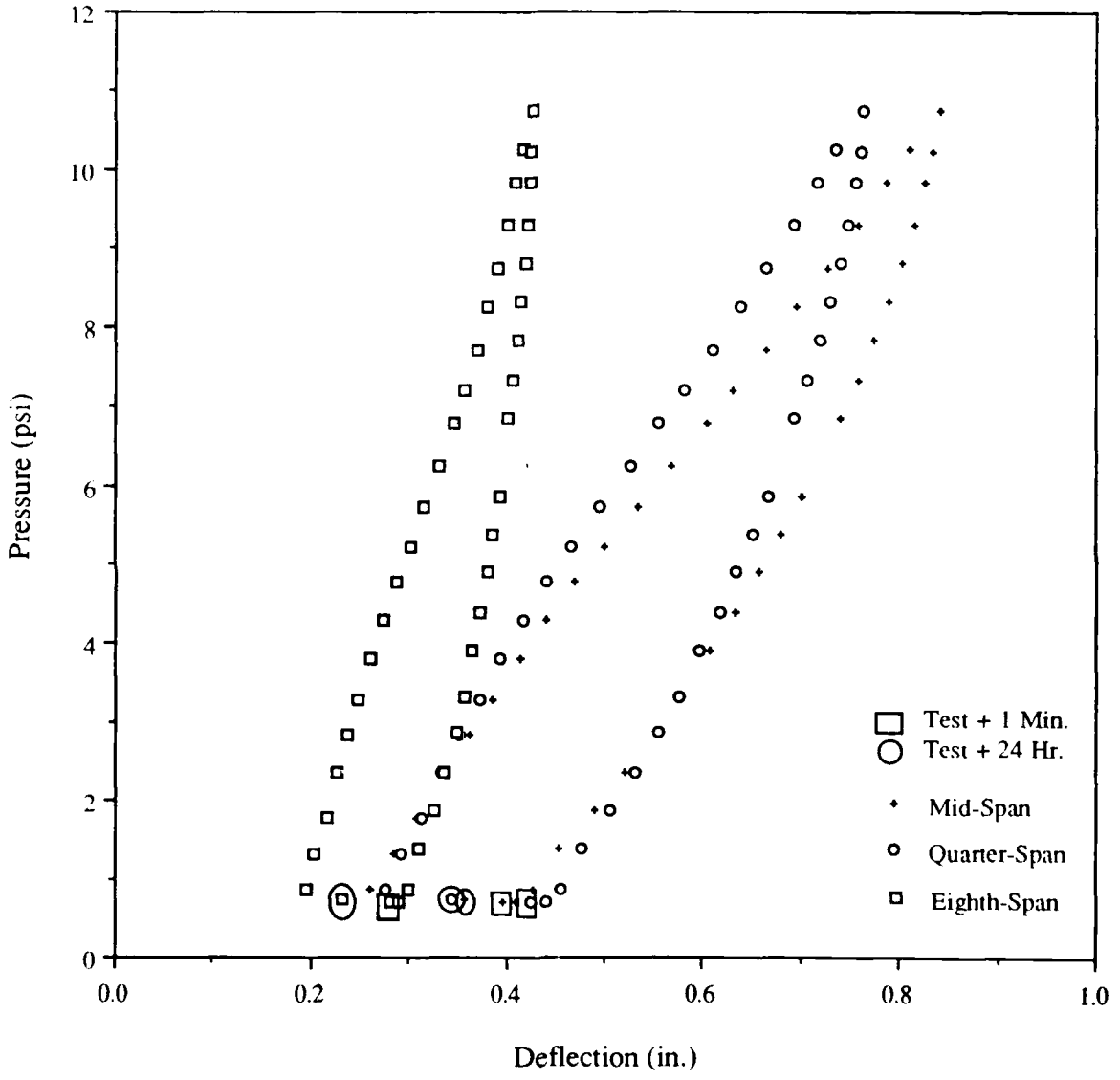

Figure 3-17: Deflection Response of Panel-6 to Static Pressure Loading

3.2.1.2. Strain Response

The longitudinal and transverse strain responses of the upper and lower faces are shown in Figures 3-18 to 3-29. The strain recovery after 1 minute and 24 hours is indicated on the figures. Tensile strains are present on the upper face and compressive strains occur on the lower face.

The behavior of the E-glass panels (1 and 2) are shown in Figures 3-18 to 3-21. The upper face transverse strains at maximum pressure are over 3.5 times greater than the longitudinal strains; the differences between them are attributed to panel aspect ratio. Strain is proportional to curvature: in the transverse axis, curvature is approximately twice that in the longitudinal axis. Hysteresis is dominant in the longitudinal component; there is little or no strain recovery until the pressure is below 5.5 psi. On the lower face of panel-1, the transverse strain at maximum pressure is almost 2.5 times greater than the longitudinal strain and during unloading, it relaxes. A more exaggerated response occurs on the lower face of panel-2; the maximum occurs at approximately 8 psi and it reduces during the remainder of the pressurization cycle. This is attributed to the presence of membrane behavior. As the mid-span deflection approaches the panel thickness, membrane behavior is introduced and the lower face begins a transition to a tensile strain condition. The presence of membrane behavior is not evident in the longitudinal component, however, subsequent testing at higher pressure levels revealed that the longitudinal strains also reach a maximum at approximately 14 - 15 psi and then begin a similar transition to a tensile strain condition.

The strain responses of the Kevlar/DERAKANE 510A panels (3 and 4) are presented in Figures 3-22 to 3-25. These show smaller differences between the transverse and longitudinal components than panels 1 and 2. This behavior is attributed to the presence of bias (±45°) reinforcement: it provides diagonal stiffening which reduces the transverse arching affect. On the lower face, the longitudinal strains are approximately 33% greater than the transverse ones. The transverse strains show evidence of membrane

behavior at about 8 psi, and after unloading they show a residual tensile strain. After a 24 hour period, this recovers to a small compressive condition.

The responses of the Kevlar/DERAKANE 8084 panels (5 and 6) are shown in Figures 3-26 to 3-29. On the upper face of panel-5, the longitudinal strain reaches a maximum at approximately 8 psi and it exhibits less hysteresis than the other panels. In contrast, the longitudinal strain remains near zero in panel-6 and repeated tests with an additional strain gage produced the same results. On the lower face of panel-5, the longitudinal response resembles the transverse responses of panels 2, 3, and 4 by indicating membrane behavior. This may be the result of damage sustained during cyclic testing. The transverse response is also unusual: there is virtually no strain produced during loading. This may reflect an inoperative gage or unknown panel damage. In most respects, the response of panel-6 is similar to that of panels 2, 3, and 4.

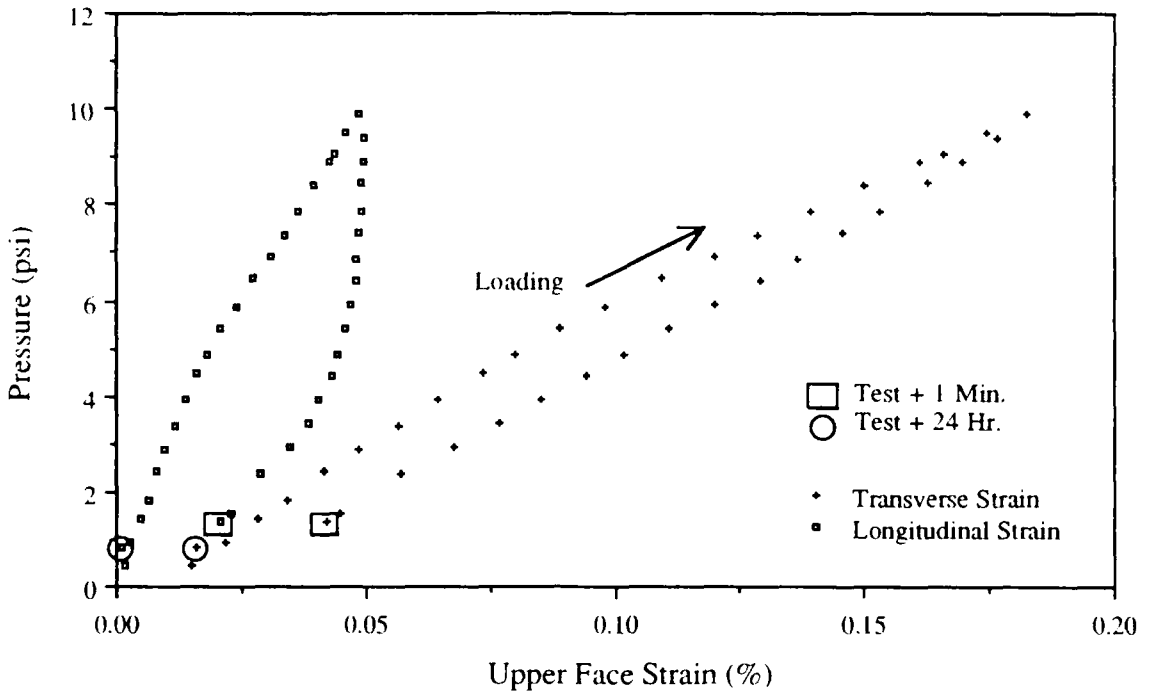

Figure 3-18: Strain Response of Panel-1 Upper Face to Static Pressure Loading

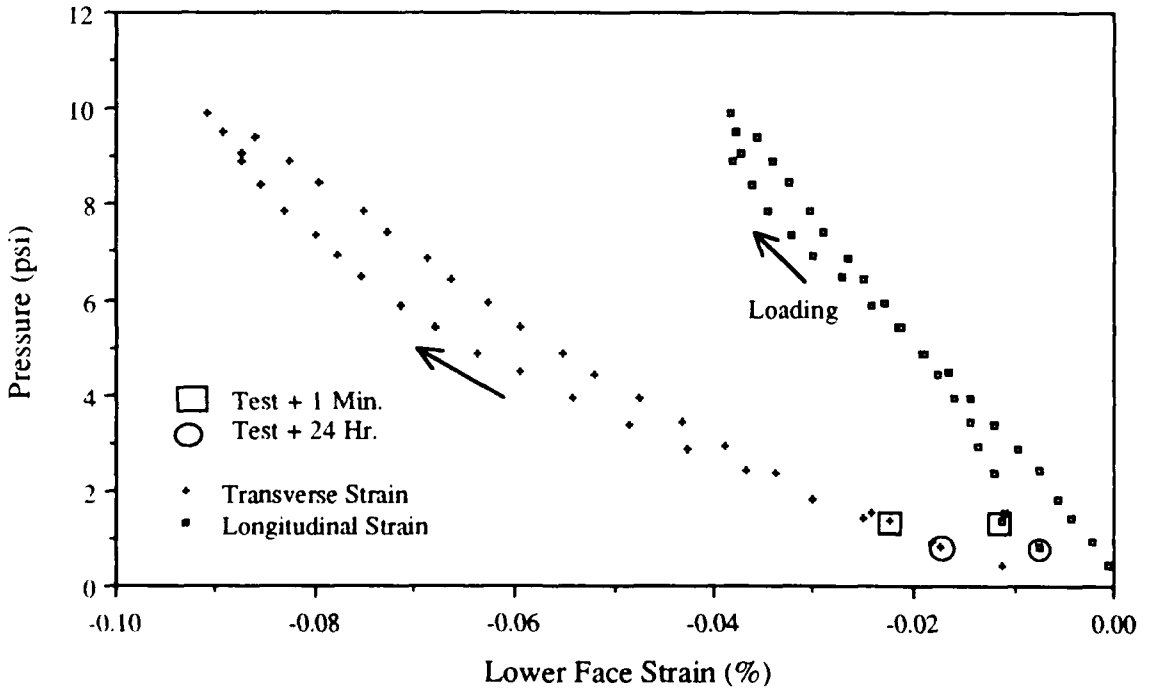

Figure 3-19: Strain Response of Panel-1 Lower Face to Static Pressure Loading

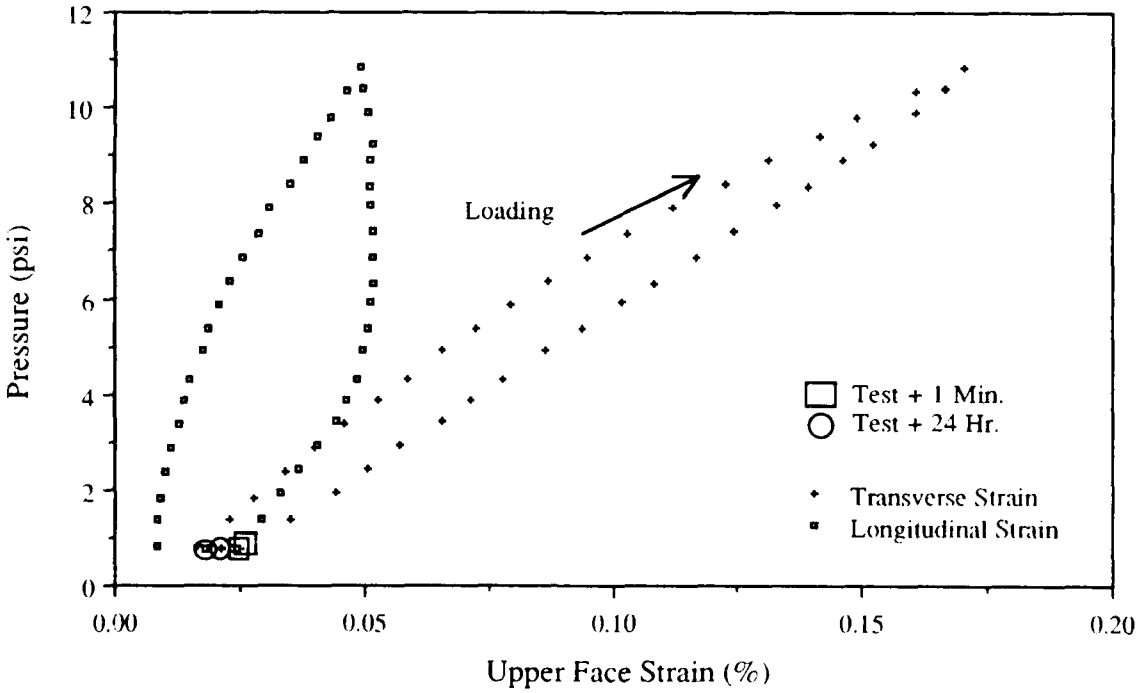

Figure 3-20: Strain Response of Panel-2 Upper Face to Static Pressure Loading

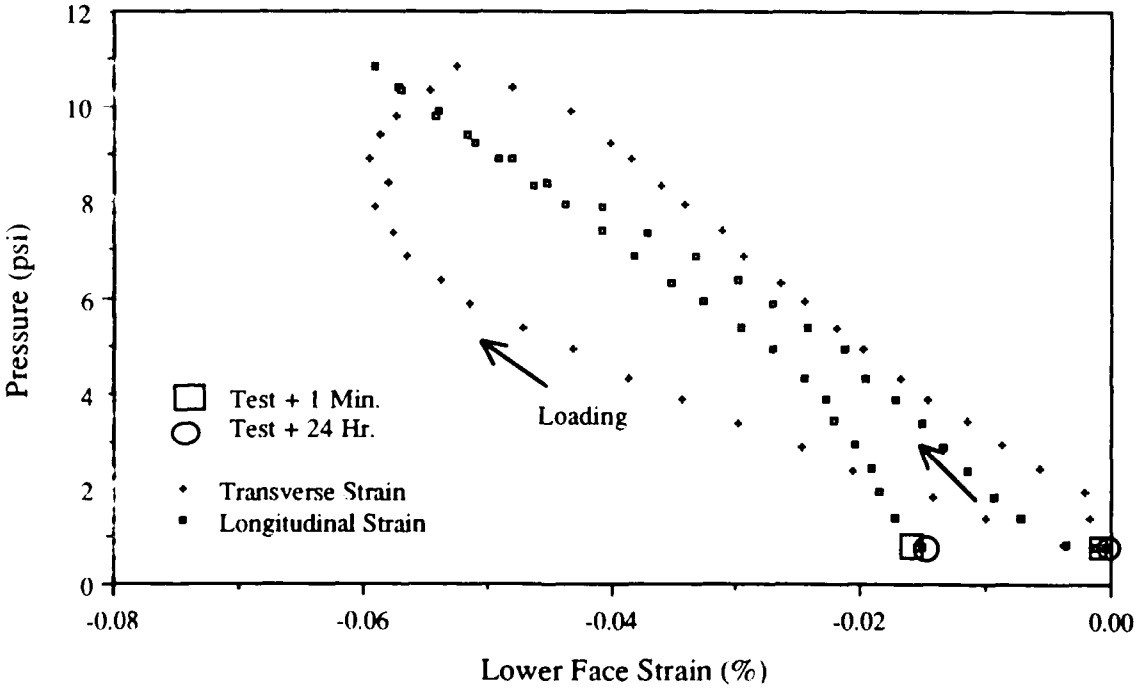

Figure 3-21: Strain Response of Panel-2 Lower Face to Static Pressure Loading

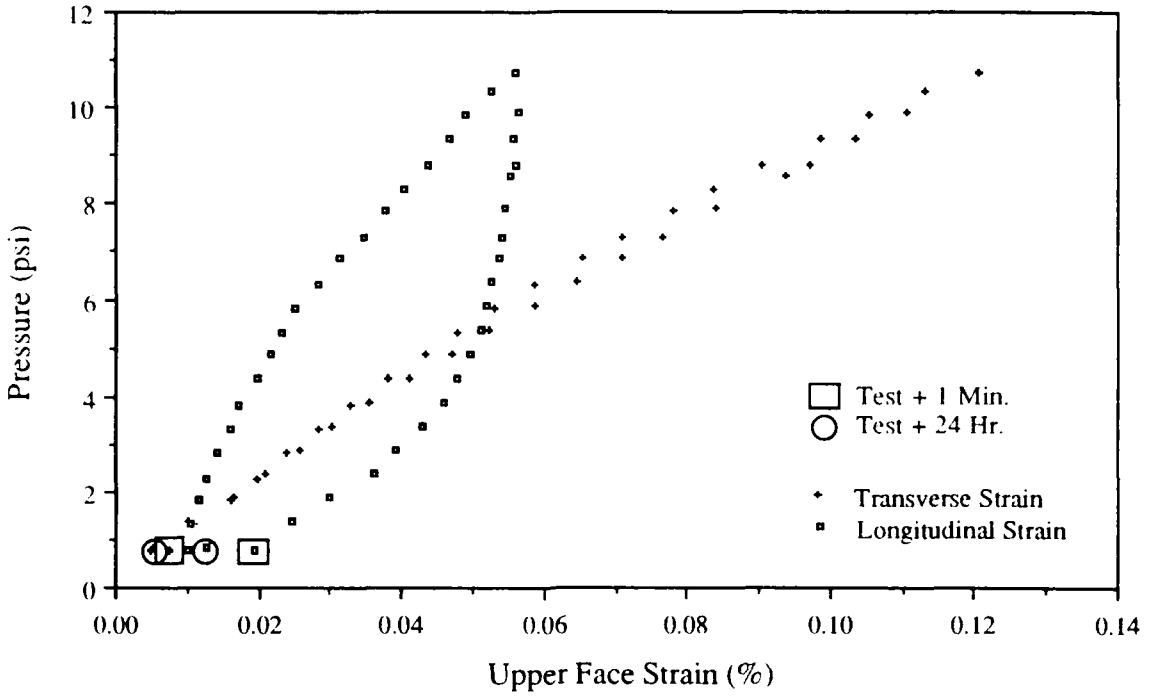

Figure 3-22: Strain Response of Panel-3 Upper Face to Static Pressure Loading

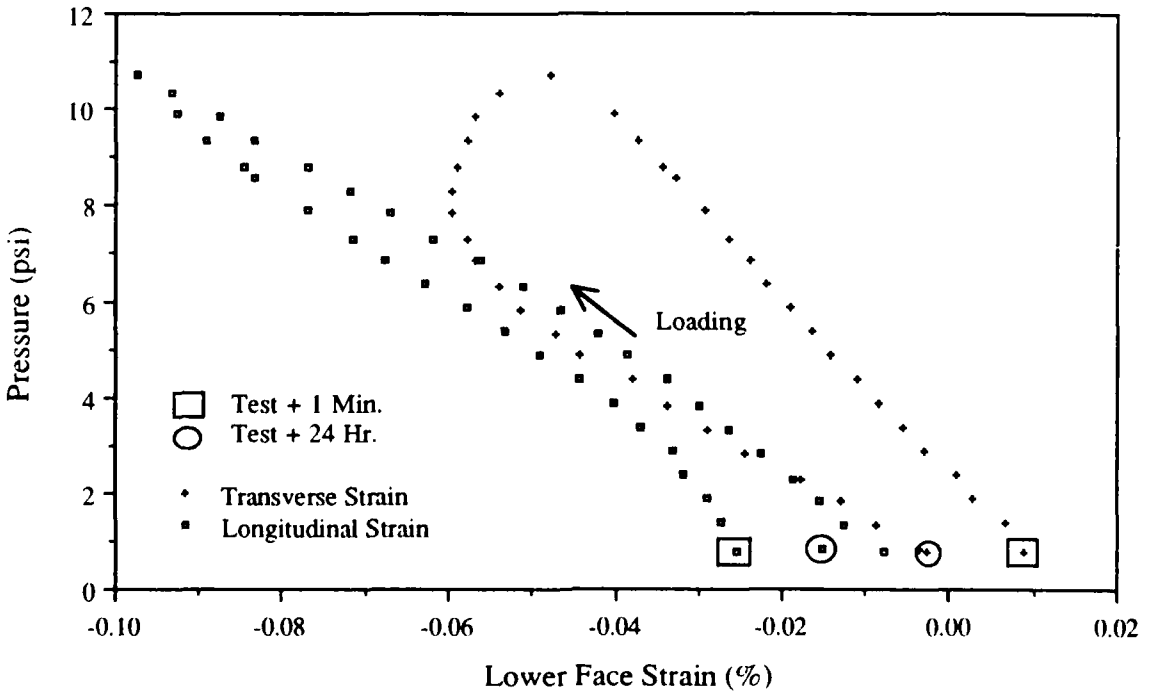

Figure 3-23: Strain Response of Panel-3 Lower Face to Static Pressure Loading

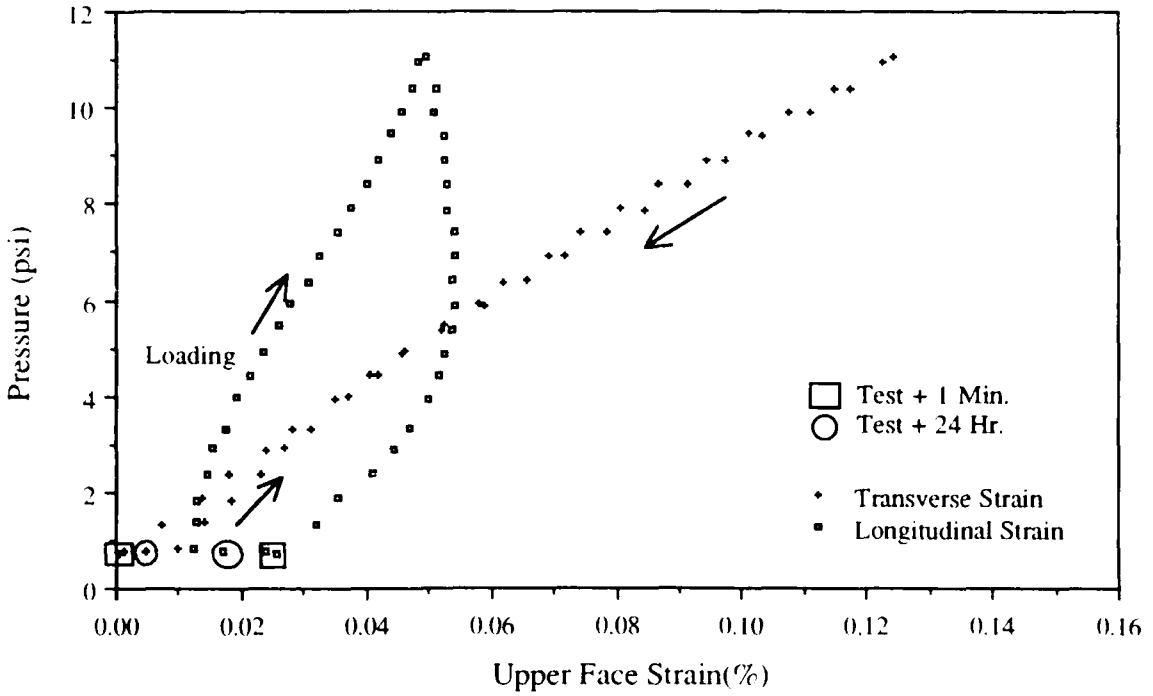

Figure 3-24: Strain Response of Panel-4 Upper Face to Static Pressure Loading

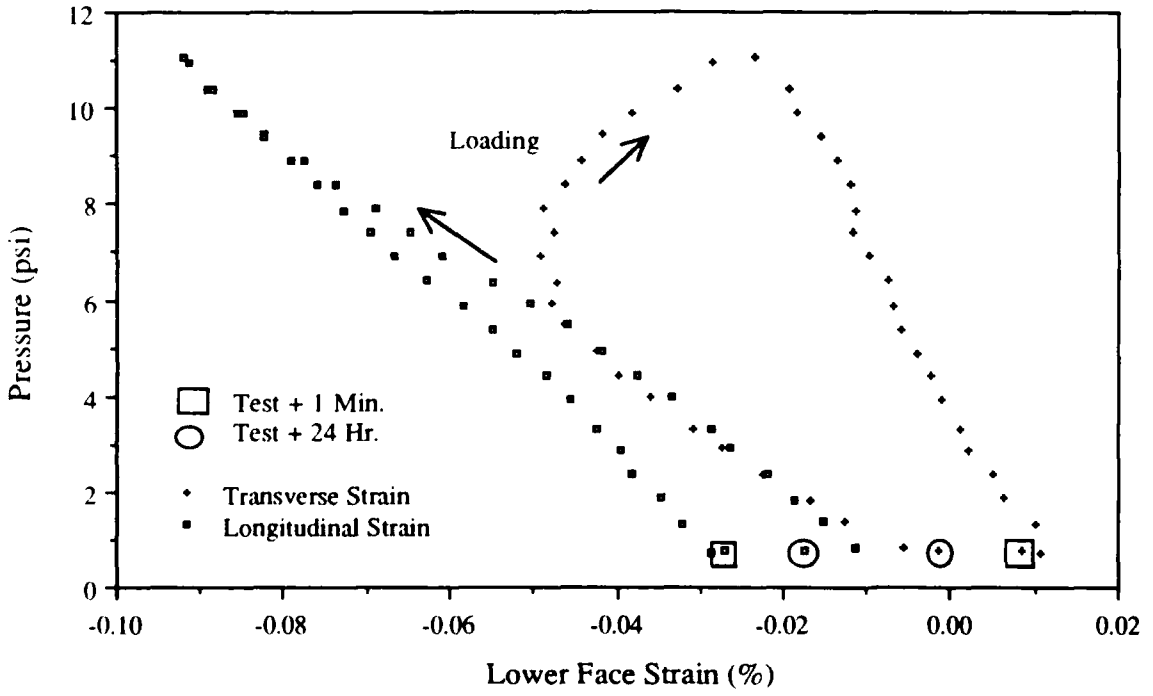

Figure 3-25: Strain Response of Panel-4 Lower Face to Static Pressure Loading

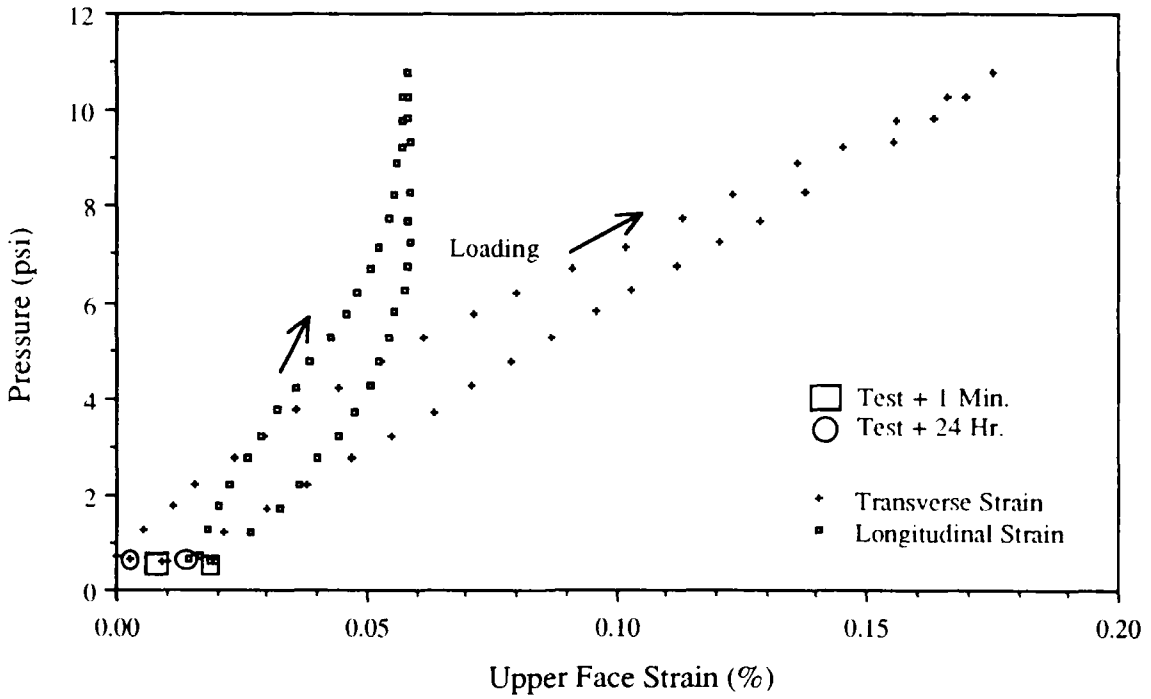

Figure 3-26: Strain Response of Panel-5 Upper Face to Static Pressure Loading

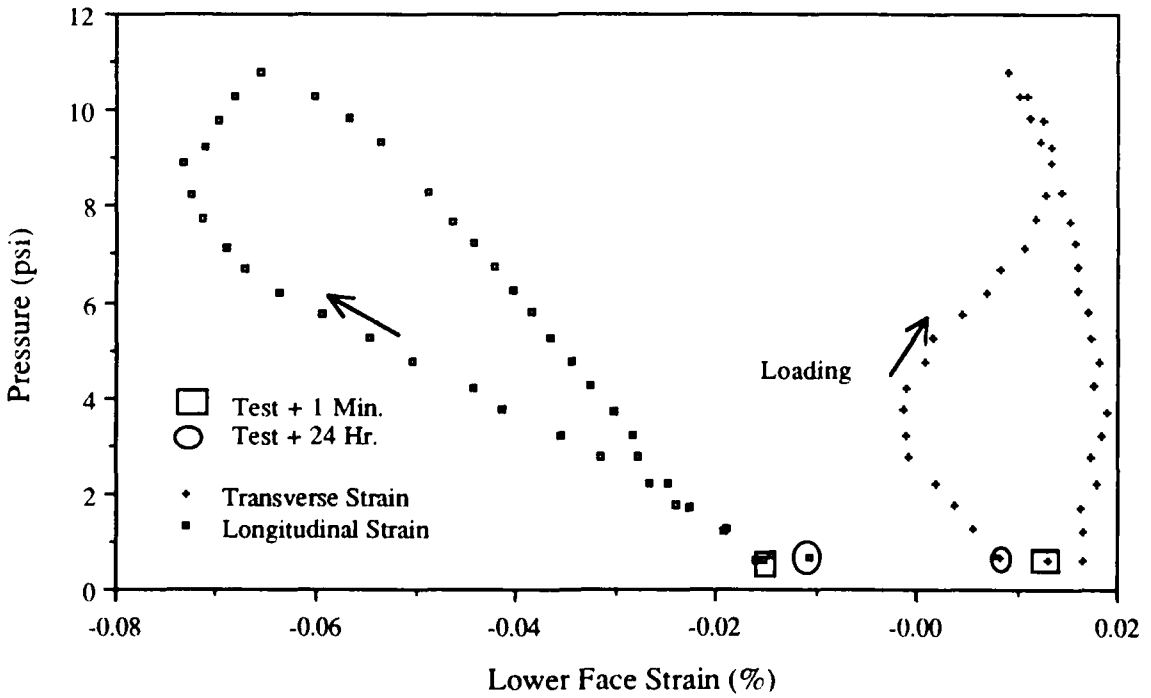

Figure 3-27: Strain Response of Panel-5 Lower Face to Static Pressure Loading

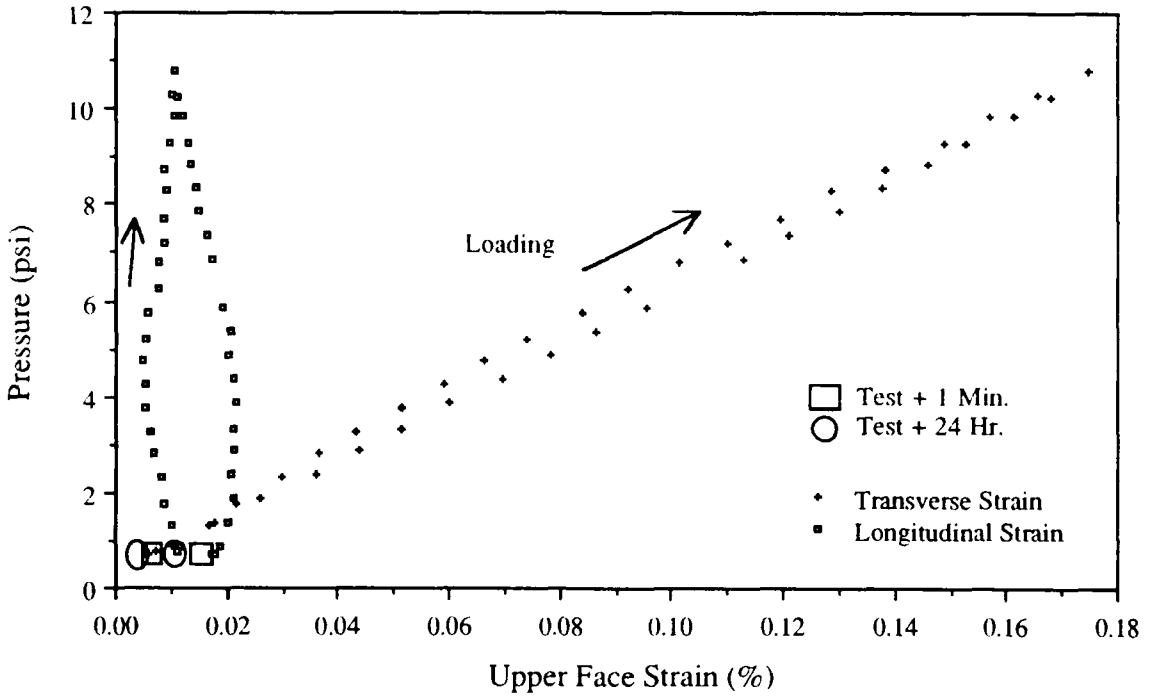

Figure 3-28: Strain Response of Panel-6 Upper Face to Static Pressure Loading

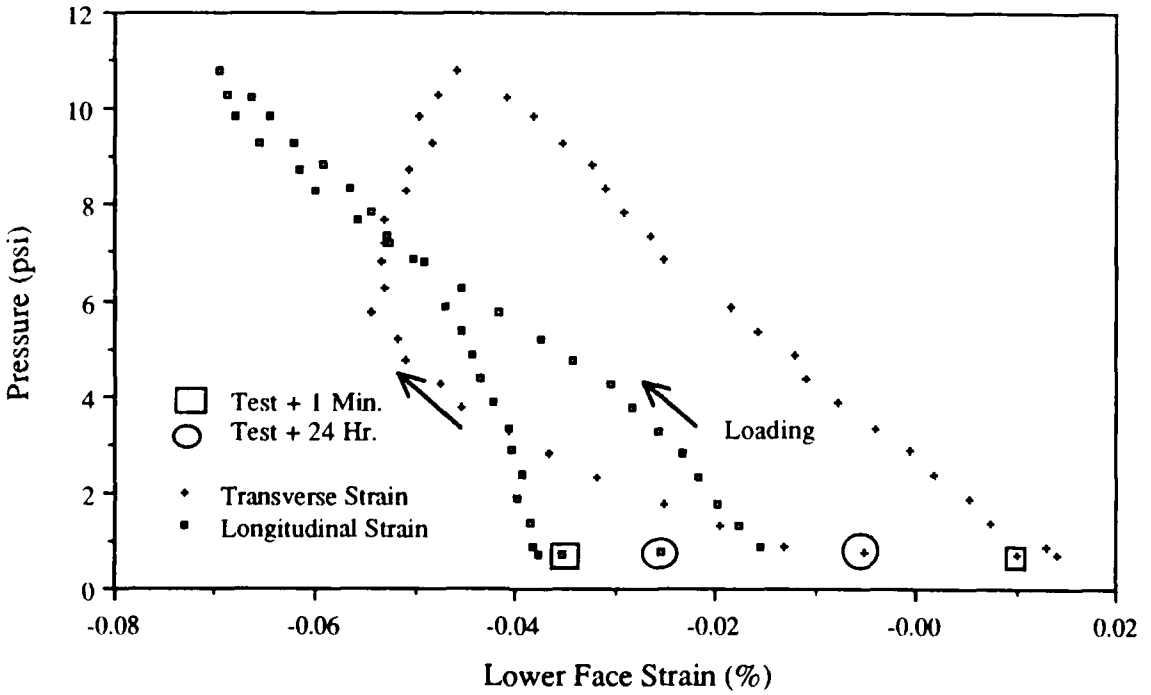

Figure 3-29: Strain Response of Panel-6 Lower Face to Static Pressure Loading

3.2.2. Cyclic Loading

The cyclic pressure loading sequence is described in section 2.2.2.2. Pressure versus time plots are shown in Appendix F. The cyclic loading rates averages 0.684 psi/sec., with a coefficient of variation of 8.5%, in contrast to 0.0079 psi/sec. for the static tests. This difference is intended to explore viscoelastic effects in the behavior of the panels.

3.2.2.1. Deflection Response

The mid-span deflection of the panel is shown in Figures 3-30 to 3-35; only the first and final responses are plotted to enhance clarity. Some similarities between the static and cyclic responses exist. The first cycle response to cyclic testing also can be approximated by two slopes, but in the cyclic case, the linear region has a steeper slope with a higher elastic limit. For panels 1 through 4, the first limit is approximately 7 psi, and for panels 5 and 6, it is 6 psi. Unlike the static tests, the evidence of membrane behavior is not present for panels 5 and 6: their pressure-deflection curves are similar to the other panels. Further, panels 5 and 6 have larger deflections at the maximum pressure, more pronounced hysteresis, and larger deformations at the end of the first load cycle.

All of the panels except one undergo ten cycles. In the final cycle, the response throughout the load range is linear and the hysteresis decreases. In fact, as the cycling progresses, the pressure-deflection plots become more linear and the hysteresis diminishes. Further, the incremental deflection per cycle decreases, so the plastic actions in the panel appear to exercise out.

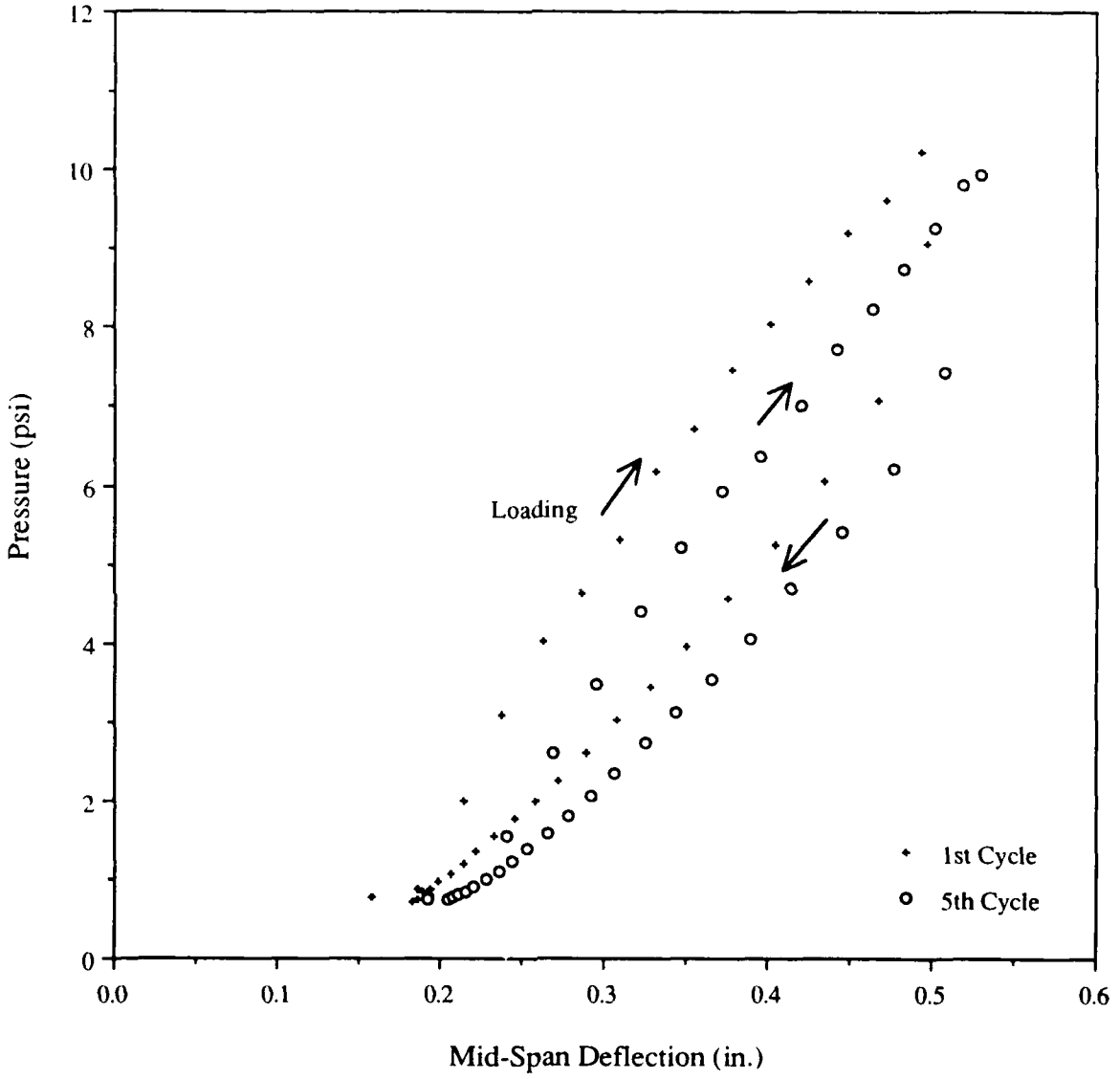

Figure 3-30: Mid-Span Deflection Response of Panel-1 to Cyclic Pressure Loading (Cycles 1 & 5)

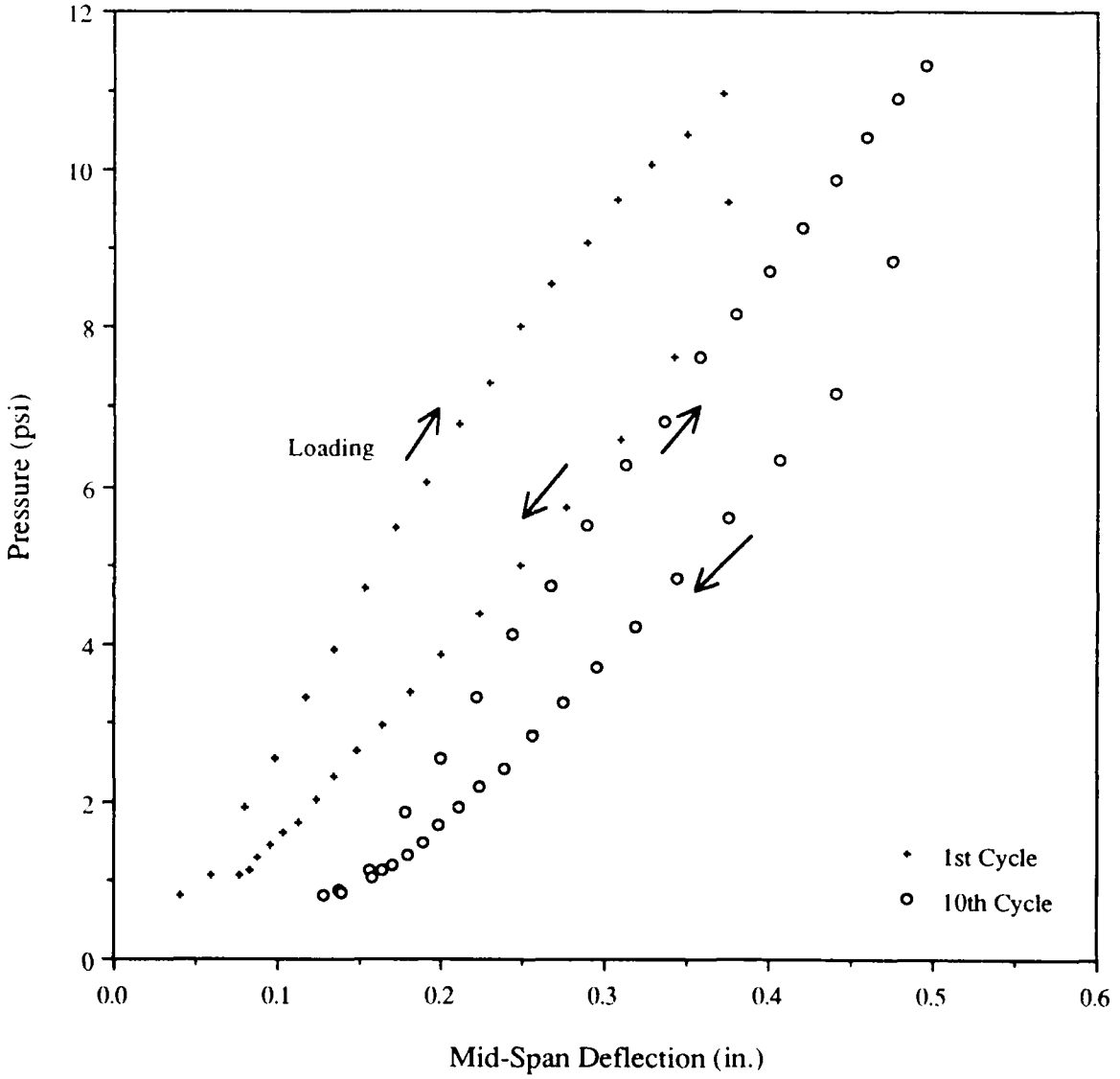

Figure 3-31: Mid-Span Deflection Response of Panel-2 to Cyclic Pressure Loading (Cycles 1 & 10)

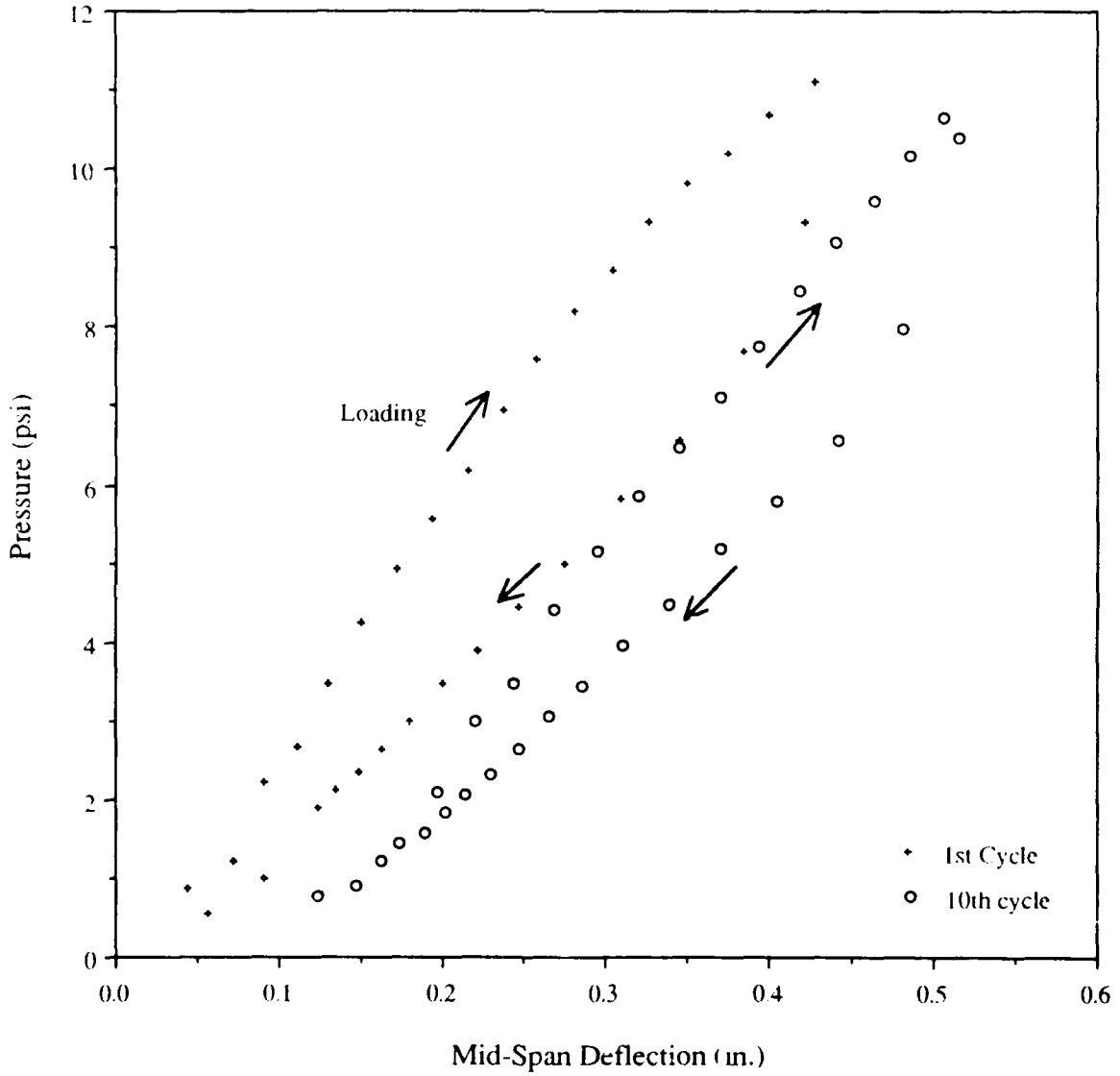

Figure 3-32: Mid-Span Deflection Response of Panel-3 to Cyclic Pressure Loading (Cycles 1 & 10)

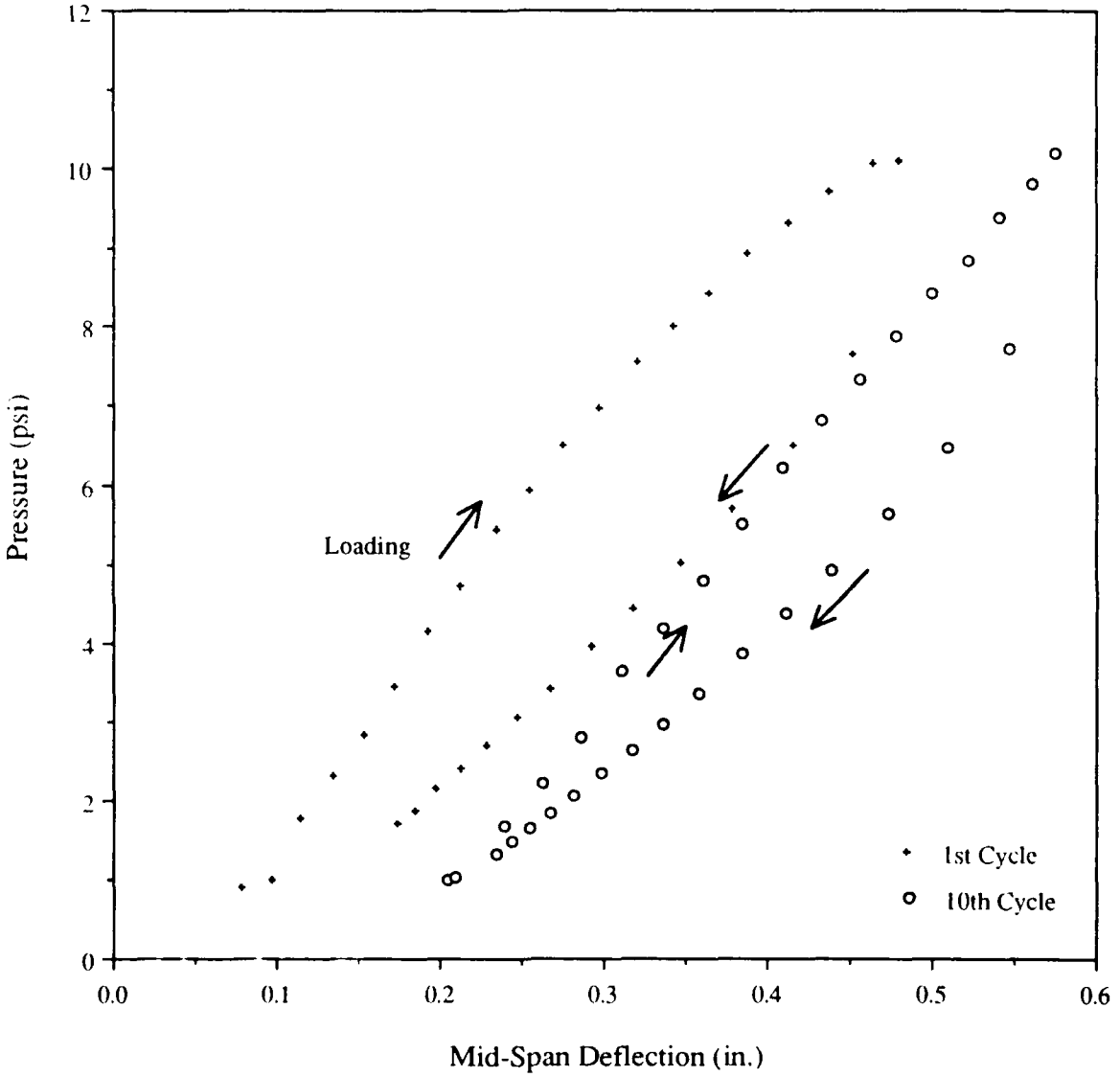

Figure 3-33: Mid-Span Deflection Response of Panel-4 to Cyclic Pressure Loading (Cycles 1 & 10)

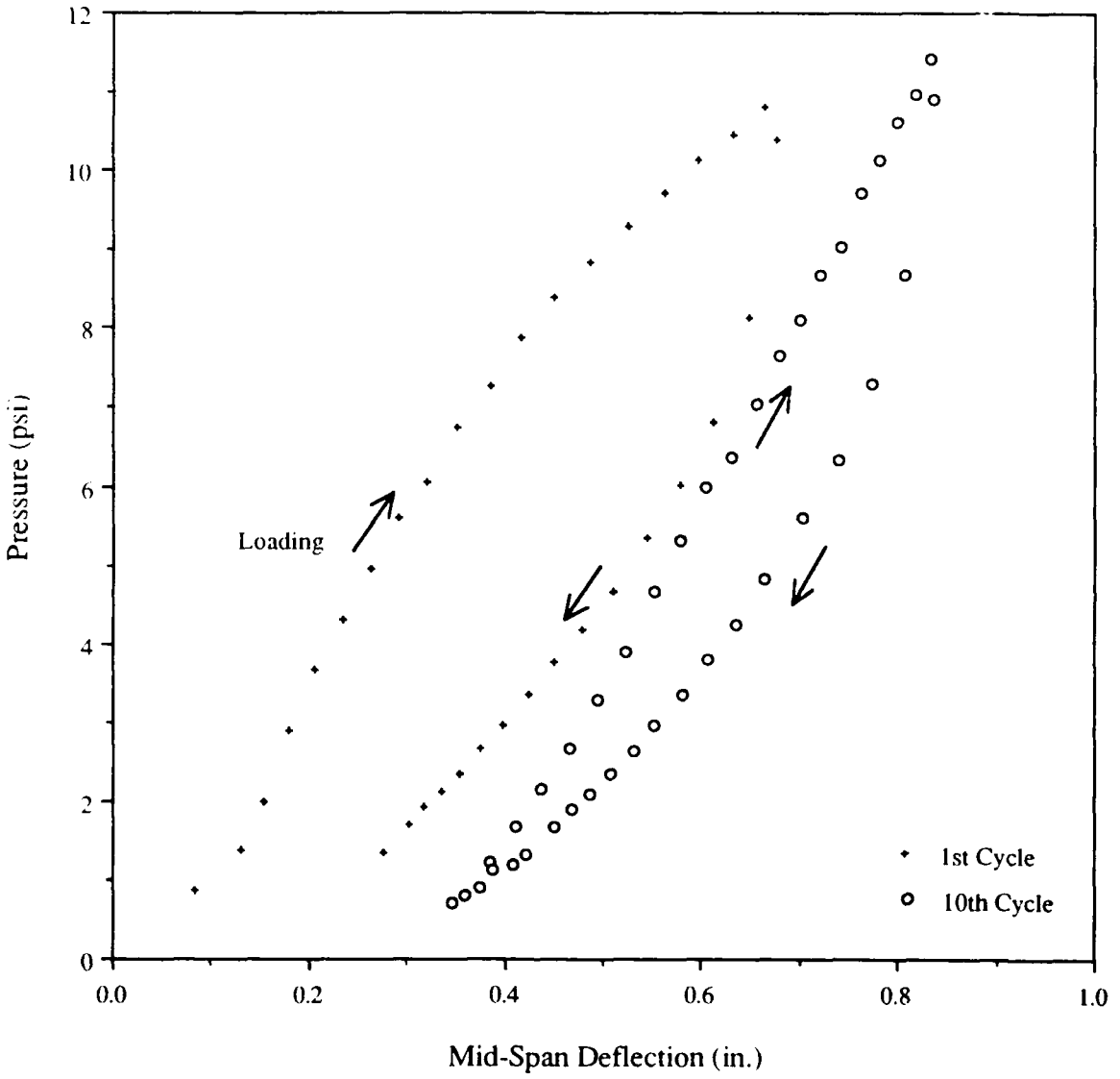

Figure 3-34: Mid-Span Deflection Response of Panel-5 to Cyclic Pressure Loading (Cycles 1 & 10)

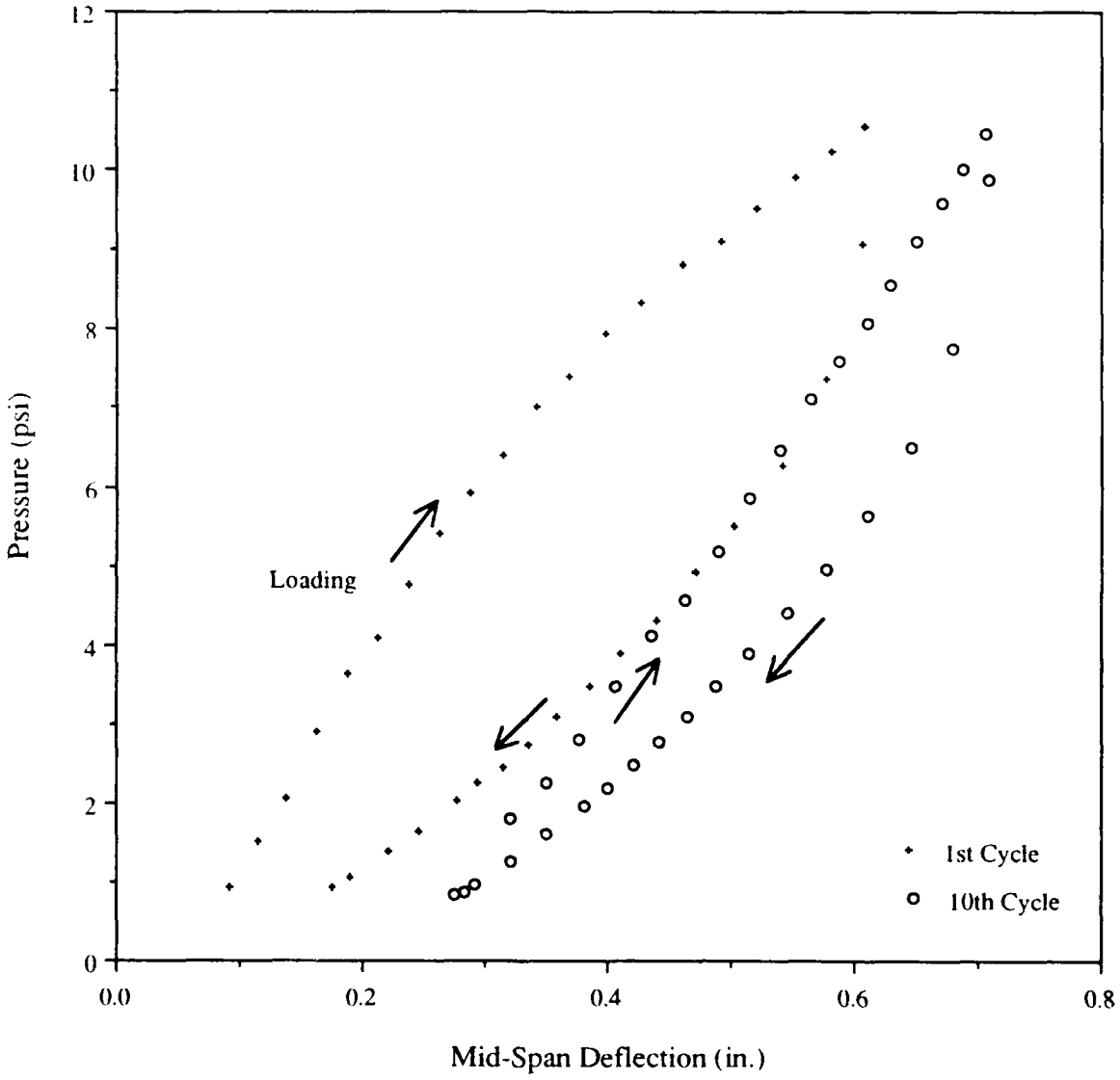

Figure 3-35: Mid-Span Deflection Response of Panel-6 to Cyclic Pressure Loading (Cycles 1 & 10)

3.2.2.2. Strain Response

The strain readings from the upper and lower faces are shown in Figures 3-36 to 3-47; only the first and final readings are presented. (The intermediate cycle data are in Appendix F.)

The behavior of panel-1 is given in Figures 3-36 and 3-37. The upper face exhibits the characteristic looping with pronounced hysteresis in the longitudinal component. Both the transverse and longitudinal strains are linear during loading; the difference between them is similar to that seen in the static case. On the lower face, the cyclic response differs from the static one. Here, the transverse strain does not relax during unloading, but instead, it shows a slight increase as the pressure is reduced. After successive loading cycles, evidence of strain relaxation is present: the maximum transverse strain decreases with each cycle. This indicates the presence of membrane behavior and the slow transition of the lower face to a tensile strain condition. The longitudinal strain is similar to that occurring during static loading: with each successive cycle, the strain increases.

The data from panel-2 are shown in Figures 3-38 and 3-39; the upper face response has the same characteristic shape as panel-1. The lower face behavior also resembles panel-1. Through successive loading cycles, the transverse strain reduces while the longitudinal strain increases; by the tenth cycle, both components of strain have reached approximately the same magnitude at maximum pressure.

The strain responses of panel-3 are shown in Figures 3-40 and 3-41. The upper face behaves similarly to panels 1 and 2 but, the difference between the longitudinal and transverse strains is smaller than on the E-glass panels. This is due to the ±45° reinforcing present in the Kevlar panels. On the lower face, the longitudinal strain is smaller than the transverse in the first cycle. By the tenth cycle, the longitudinal strain has increased and exceeded the transverse. In all cycles very little hysteresis is evident in the transverse component, but the longitudinal strain continues to show considerable hysteresis.

The actions of panel-4 are shown in Figures 3-42 and 3-43; it is very similar to panel-3. One difference is the greater transverse strain relaxation which occurs on the lower face of panel-4; by the tenth cycle, this has reduced 33.7%, compared to 24.8% for panel-3.

Panel-5 data are shown in Figures 3-44 and 3-45. The upper face longitudinal strain curve has a large amount of permanently induced strain: after 10 cycles it is twice that of the previous panels. The difference may be caused by the high elongation of the DERAKANE 8084 resin or by local damage occurring in the first load cycle. The lower face also has several differences from the other panels. The longitudinal first cycle strain is of greater magnitude than the transverse strain and it has a large hysteresis component. By the tenth cycle, the hysteresis has virtually disappeared. The first cycle transverse strain shows evidence of membrane behavior and it recovers as a tensile strain after unloading but later cycles elicit virtually no response. This behavior is present during static loading and it suggests a strain gage failure or local panel damage.

The upper and lower face strain responses of panel-6 are presented in Figures 3-46 and 3-47. Large transverse strains and smaller longitudinal strains occur on the upper face which is in contrast to the other Kevlar panels, where the two strain components differed less. The same response is seen during the static pressure test and as previously mentioned, another strain gage produced similar results. This suggests the presence of local panel damage rather than equipment malfunction. On the lower face, the transverse strain recovers to a tensile condition after 10 cycles and it also exhibits very little hysteresis after the first cycle. The longitudinal strain response is similar to panel-5: during the first cycle, hysteresis effects are dominant. By the tenth cycle, there is no evidence of hysteresis and the response is very linear.

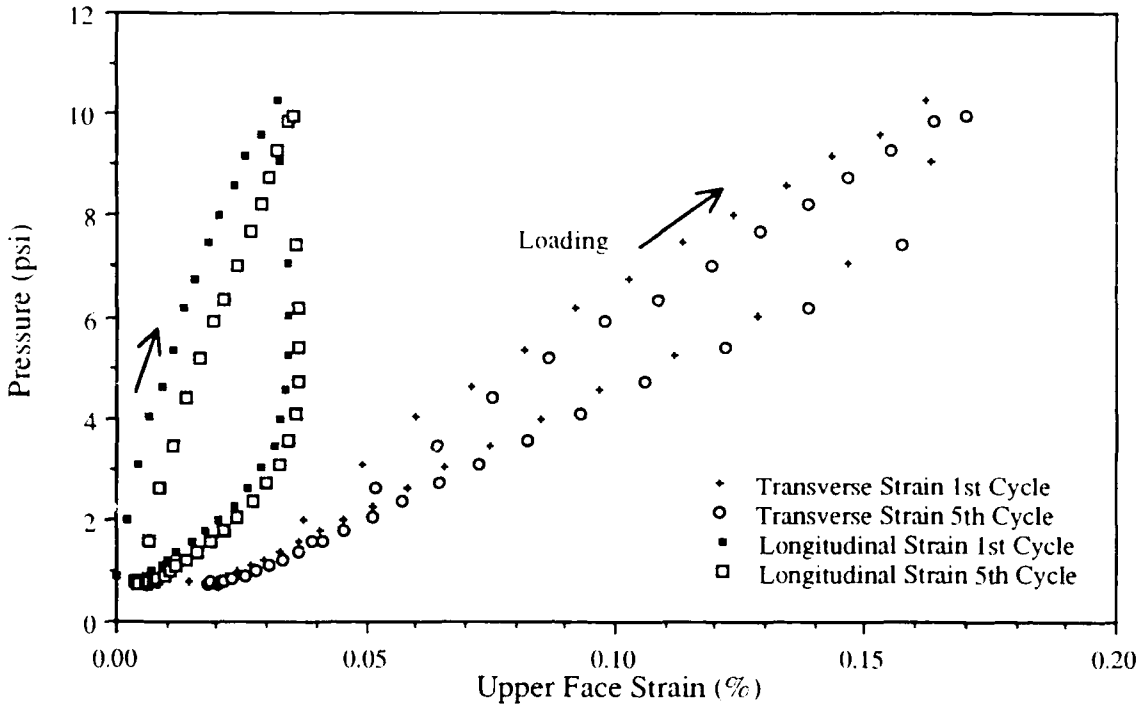

Figure 3-36: Strain Response of Panel-1 Upper Face to Cyclic Pressure Loading (Cycles 1 & 5)

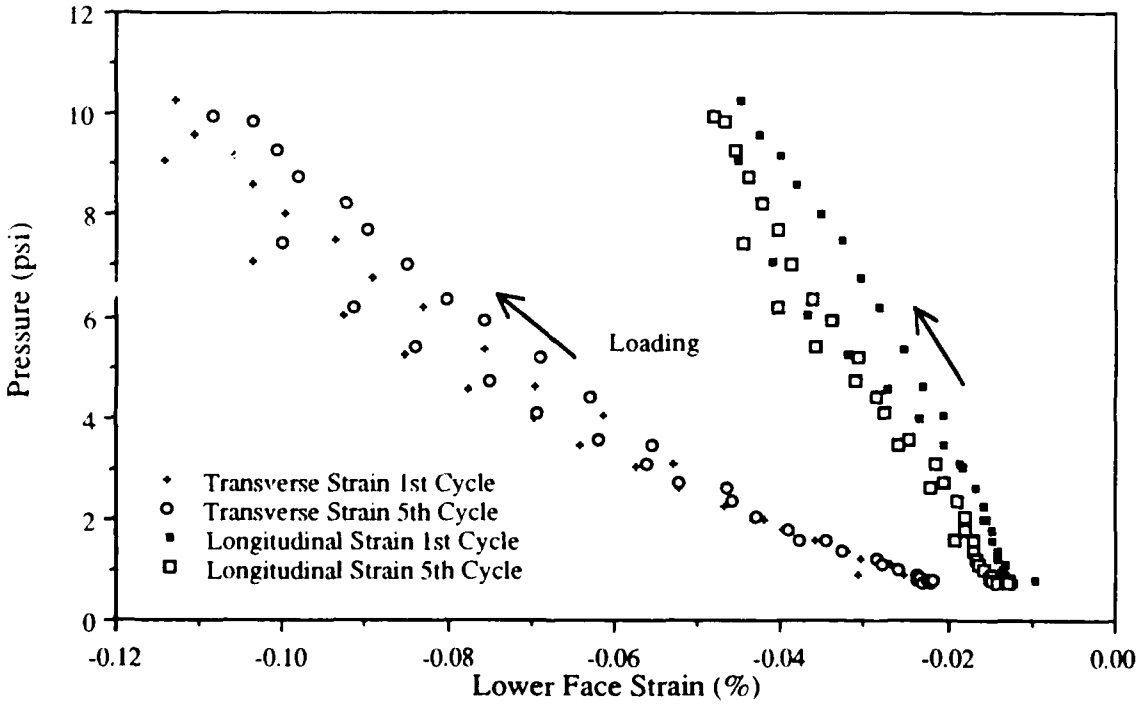

Figure 3-37: Strain Response of Panel-1 Lower Face to Cyclic Pressure Loading (Cycles 1 & 5)

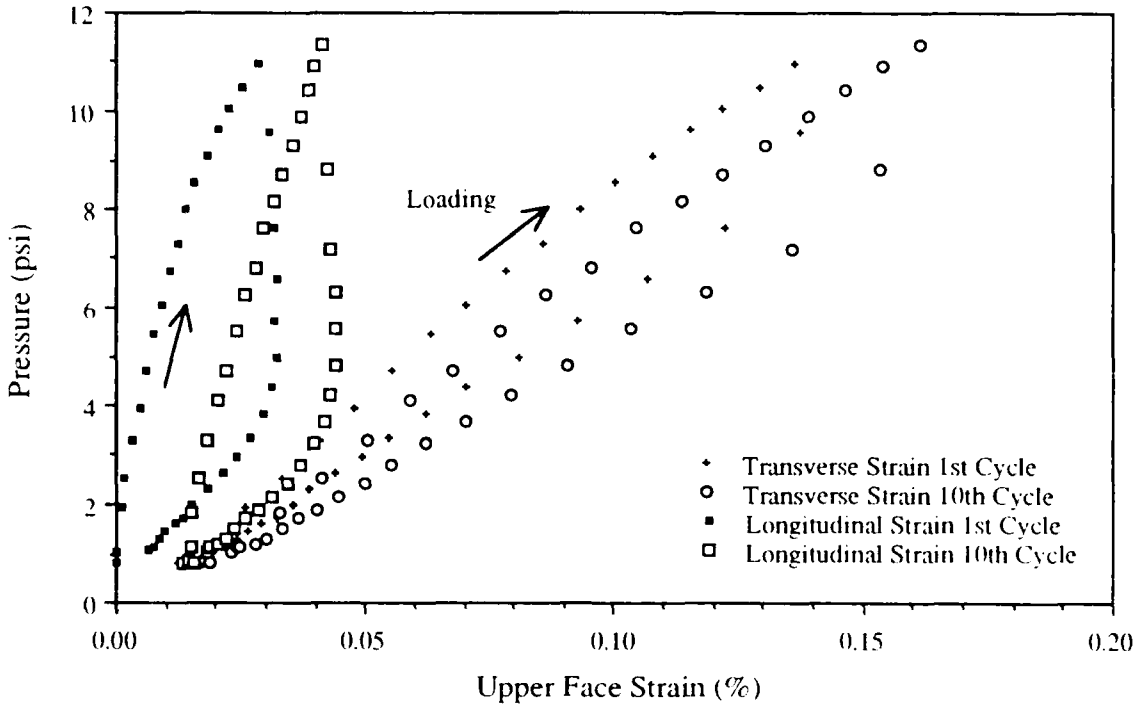

Figure 3-38: Strain Response of Panel-2 Upper Face to Cyclic Pressure Loading (Cycles 1 & 10)

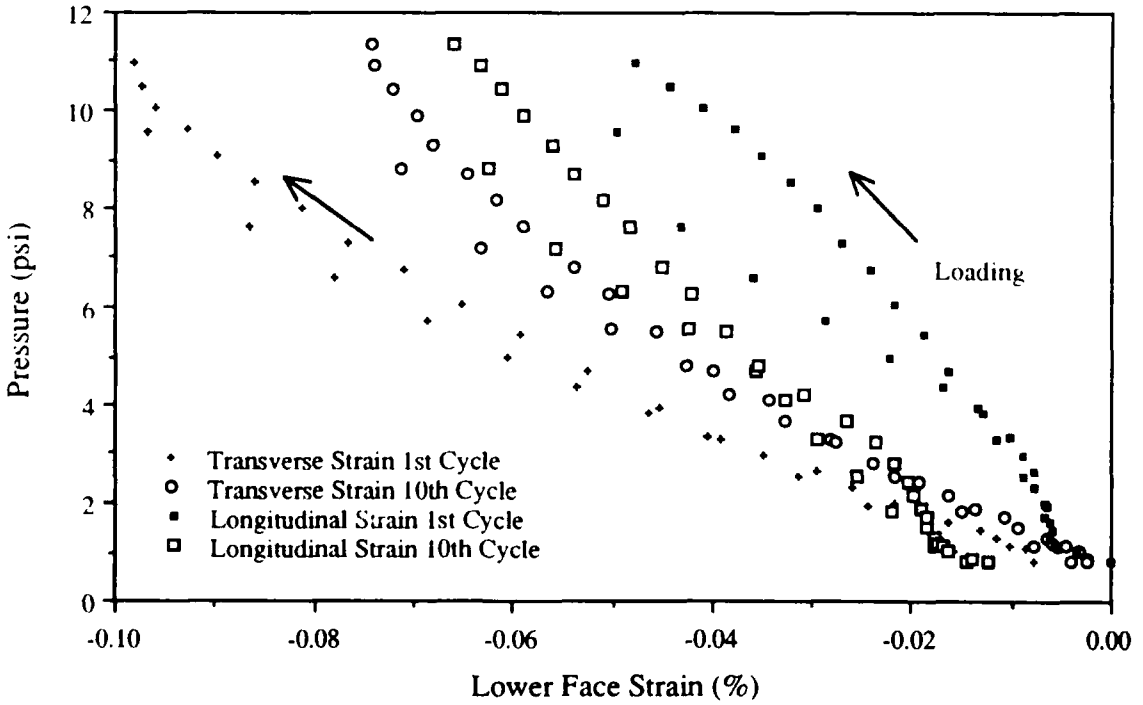

Figure 3-39: Strain Response of Panel-2 Lower Face to Cyclic Pressure Loading (Cycles 1 & 10)

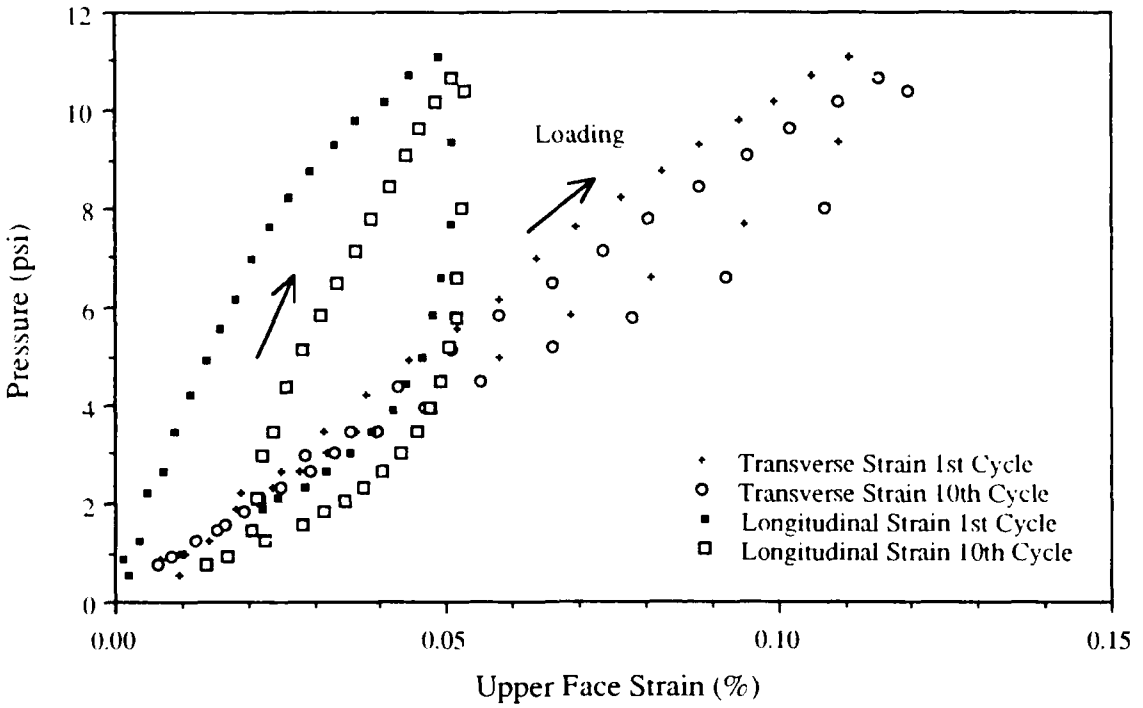

Figure 3-40: Strain Response of Panel-3 Upper Face to Cyclic Pressure Loading (Cycles 1 & 10)

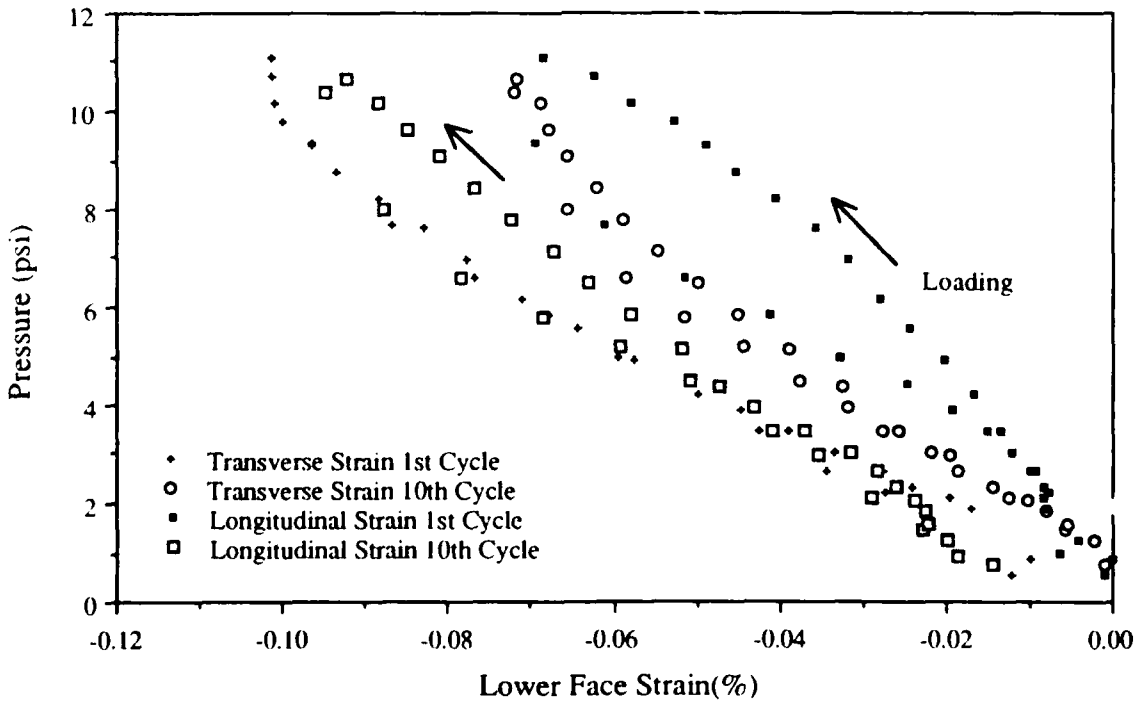

Figure 3-41: Strain Response of Panel-3 Lower Face to Cyclic Pressure Loading (Cycles 1 & 10)

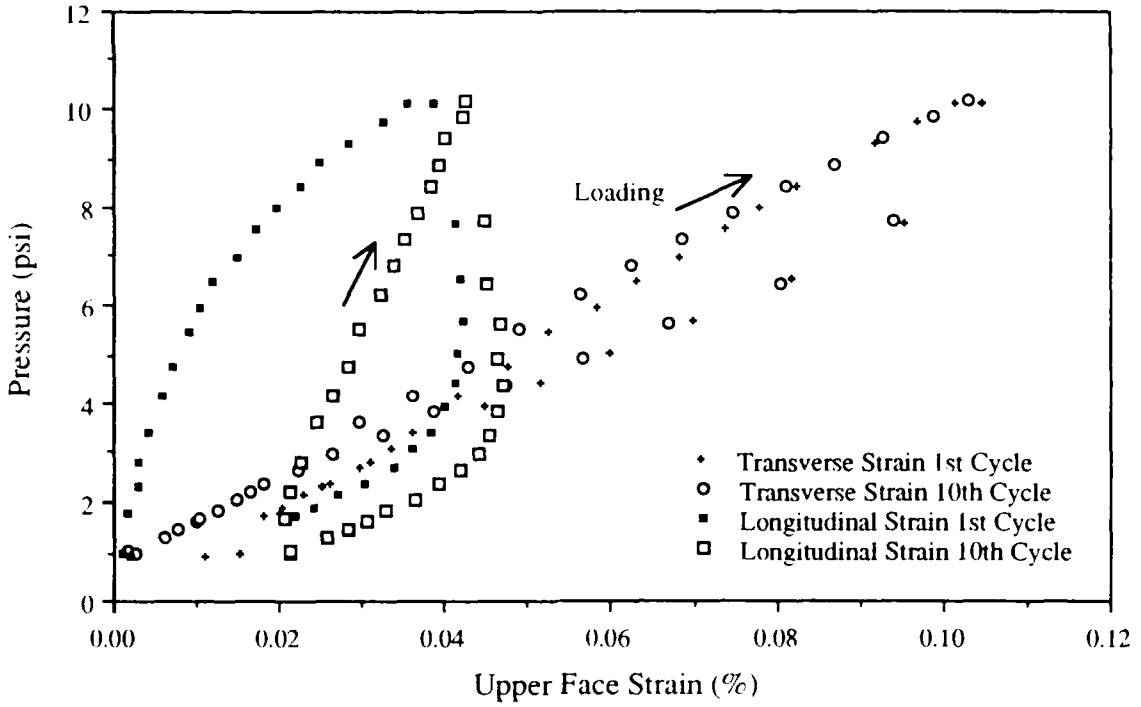

Figure 3-42: Strain Response of Panel-4 Upper Face to Cyclic Pressure Loading (Cycles 1 & 10)

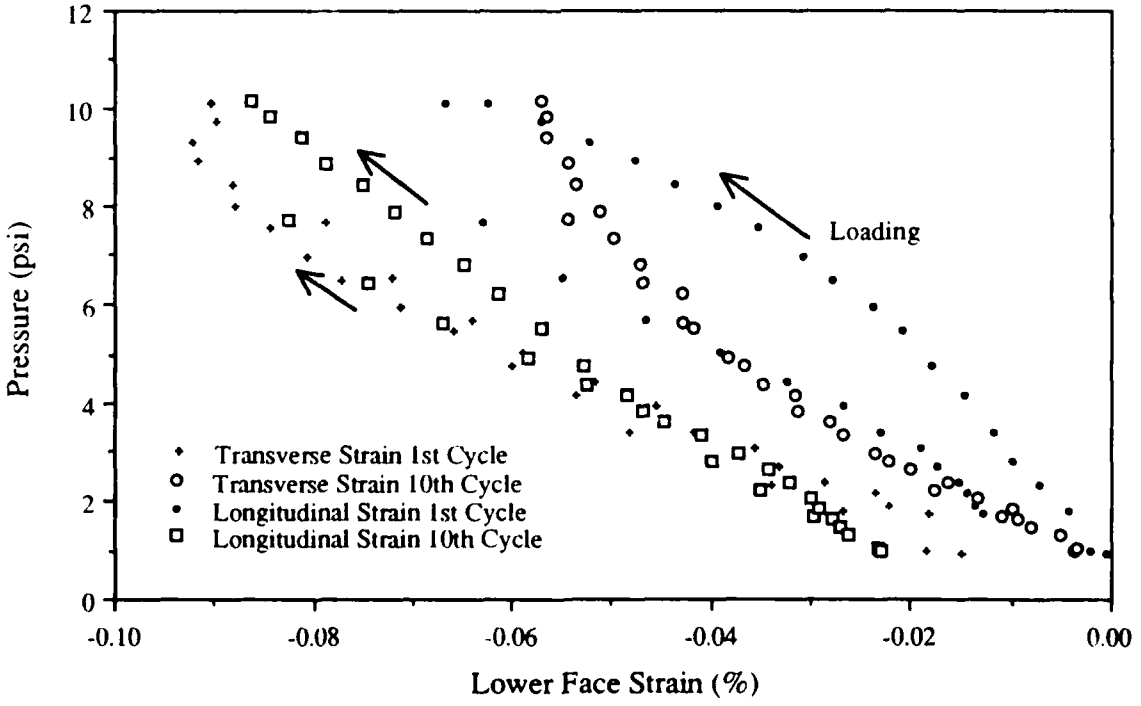

Figure 3-43: Strain Response of Panel-4 Lower Face to Cyclic Pressure Loading (Cycles 1 & 10)

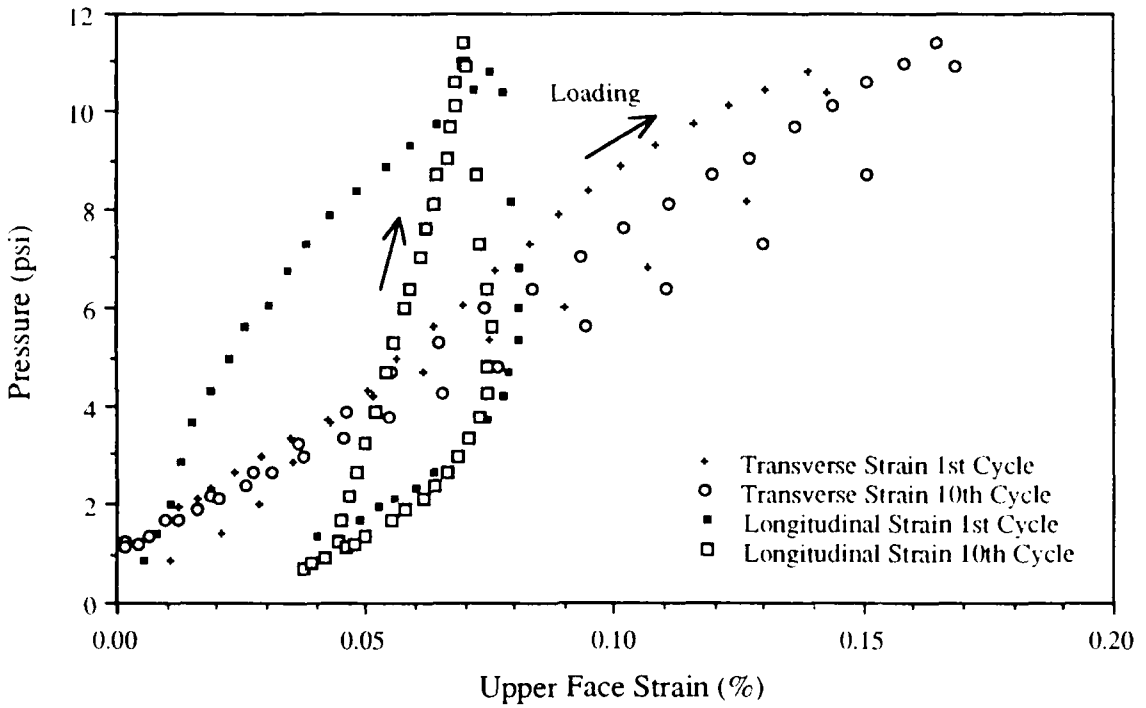

Figure 3-44: Strain Response of Panel-5 Upper Face to Cyclic Pressure Loading (Cycles 1 & 10)

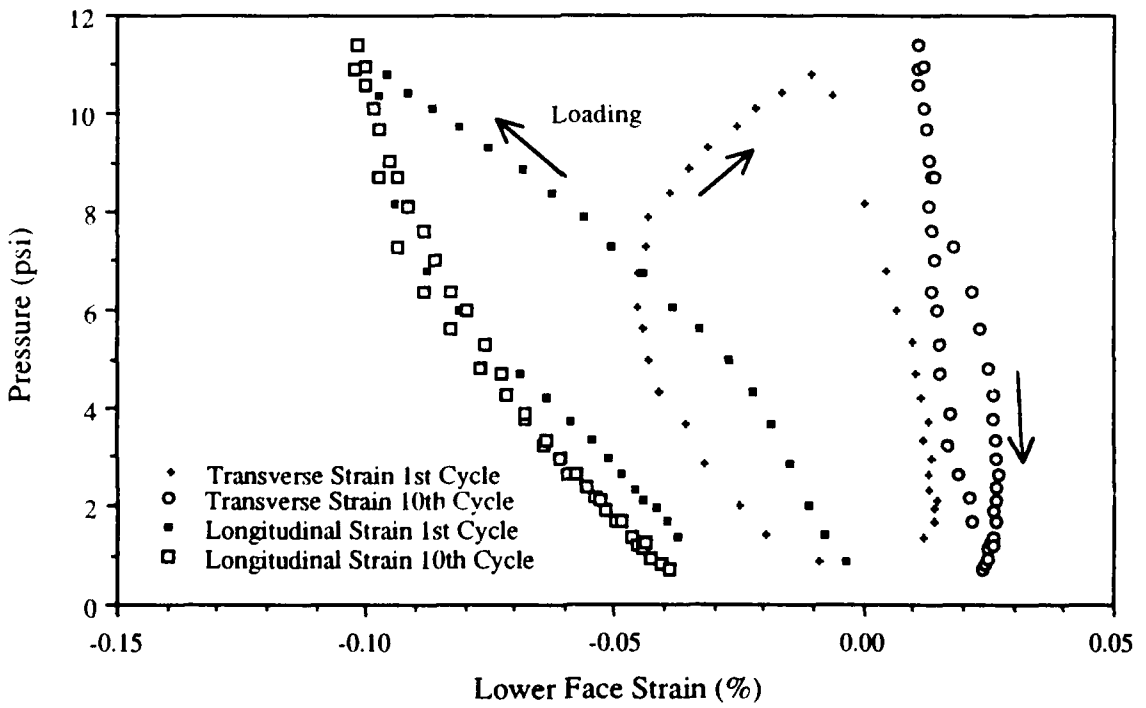

Figure 3-45: Strain Response of Panel-5 Lower Face to Cyclic Pressure Loading (Cycles 1 & 10)

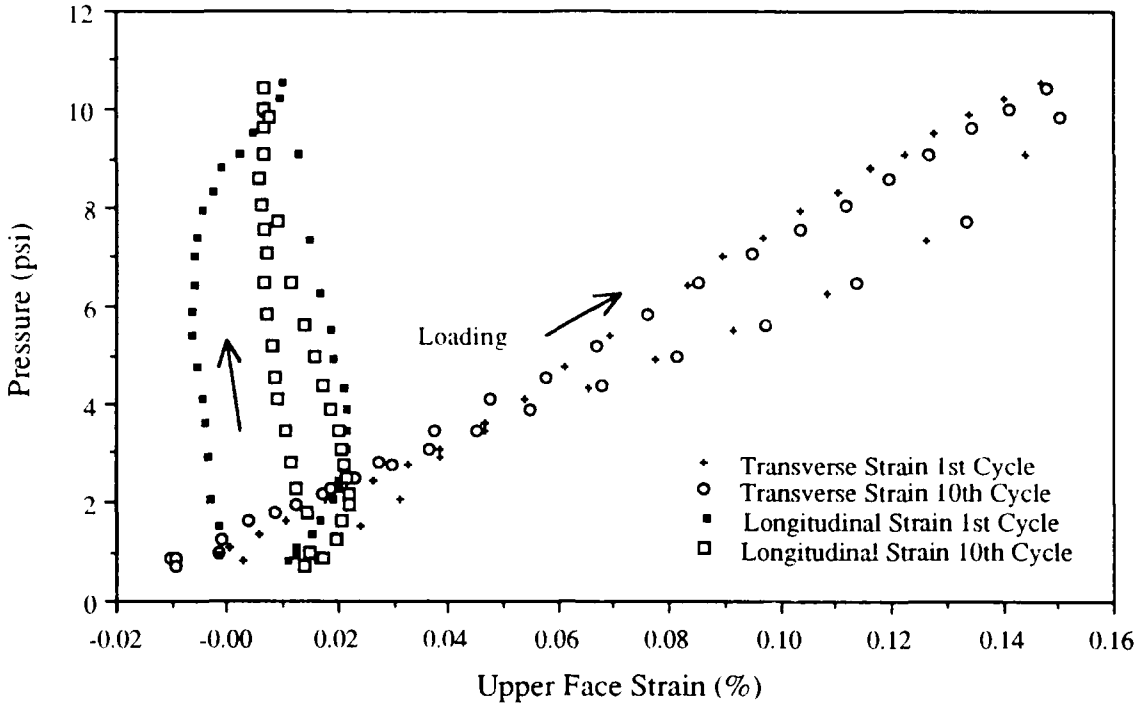

Figure 3-46: Strain Response of Panel-6 Upper Face to Cyclic Pressure Loading (Cycles 1 & 10)

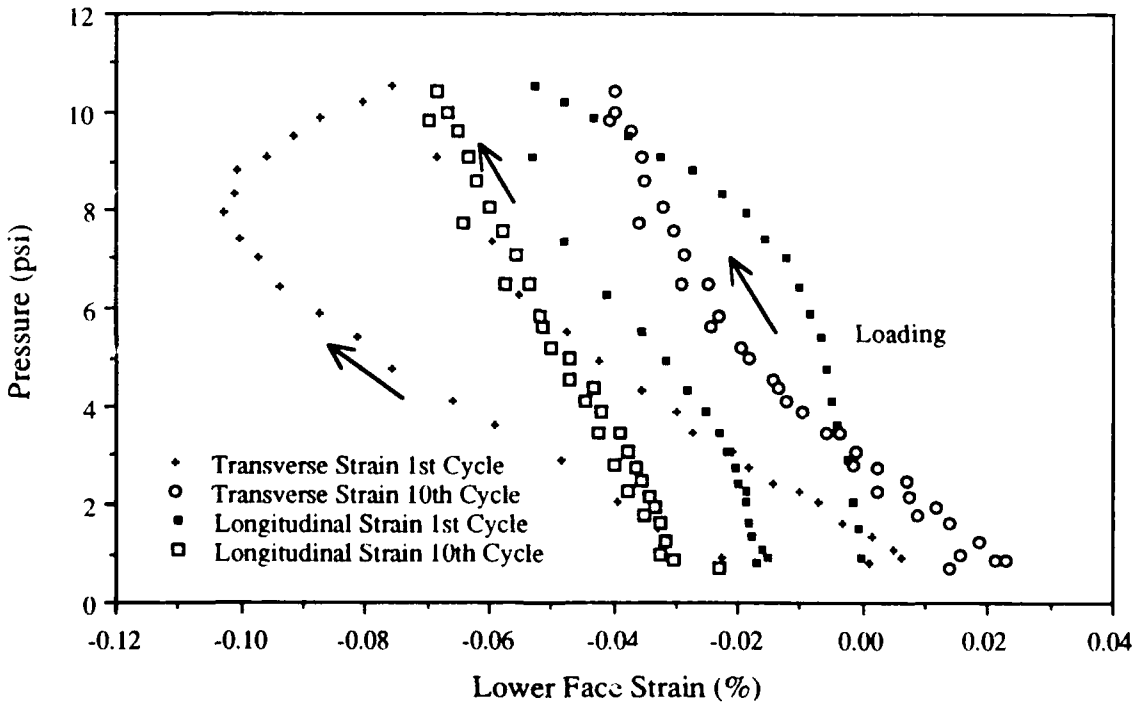

Figure 3-47: Strain Response of Panel-6 Lower Face to Cyclic Pressure Loading (Cycles 1 & 10)

3.2.3. Comparative Panel Performance

There are many characteristics which can be used to compare panel performance; some of these are important to the naval architect because of the severe conditions in a marine environment. Among these are: mid-span deflection and recovery, deflection rate effects, panel bending stiffness, and various other rate responses. Comparisons made on these characteristics are presented in the following sections.

3.2.3.1. Deflection Response

Comparison of the mid-span deflection responses during the load cycle of the static pressure test is illustrated in Figure 3-48. Each deflection is normalized by the panel thickness. The influence of the elongation properties of the matrix are clear: the Kevlar/DERAKANE 8084 panels (5 and 6) have more initial deformation from the cyclic loading tests and greater deflection at test (design) pressure. Using a deflection limit of span/100, panels 5 and 6 are limited to approximately 2.8 psi design pressure while the DERAKANE 510A panels can accommodate about 7 psi.

The mid-span deflection recovery after static pressure testing is shown in Figure 3-49. They average 7.1% for a 1 minute recovery period, and 58.5% for a 24 hour period; little additional recovery occurs thereafter.

The mid-span deflection during the first and final cycles of the cyclic pressure tests are given in Figures 3-50 and 3-51. These provide some indication of the rate sensitivity of the panels and of the effects of repeated loading. In Figure 3-50, the response of panels 5 and 6 is more non-linear, especially at higher loads. They also average 45% more deflection at the maximum test pressure. After cycling, the response becomes linear; see Figure 3-51. Here the deflections of panels 5 and 6 are larger than the DERAKANE 510A panels. Also the disappearance of the non-linear response suggests the core influence is reduced by multiple cycles; the panel faces appear to dominate.

A comparison of the mid-span deflection rates for the different loading conditions is presented in Figure 3-52 where, again the deflection behavior of the Kevlar/DERAKANE 8084 panels is evident: static rates for these average 48.8% higher and cyclic rates average 28.9% higher.

When the loading rate is divided by the deflection rate, a rate dependent bending stiffness is obtained. This is shown in Figure 3-53 where the stiffness increases at the higher rates. The Kevlar/DERAKANE 8084 panels (5 and 6) average 27.8% less stiffness than the other panels.

In Figure 3-54, the bending stiffness at static loading conditions is graphed with that shown during the first cycle of the cyclic pressure test. The slope of the line indicates rate sensitivity: as the rate increases, the panels become stiffer. In contrast, see Figure 3-55: this shows that after repeated loading, the stiffness decreases and approaches that from static loading. This means that the panels should be designed for static load conditions since they exhibit a similar type of response after repeated cycling.

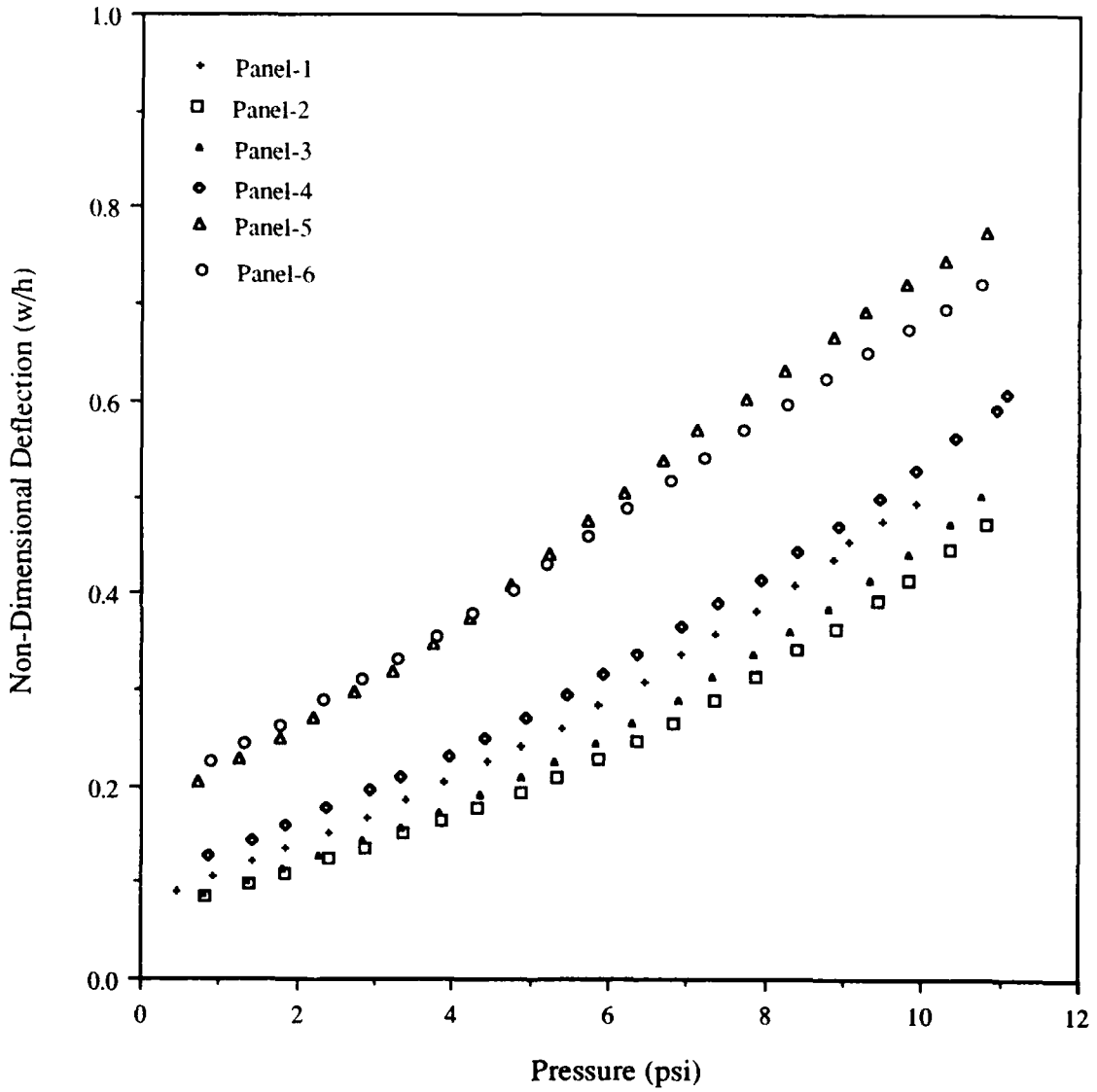

Figure 3-48: Mid-Span Deflection Response of Candidate Panels During Load Cycle of Static Pressure Test

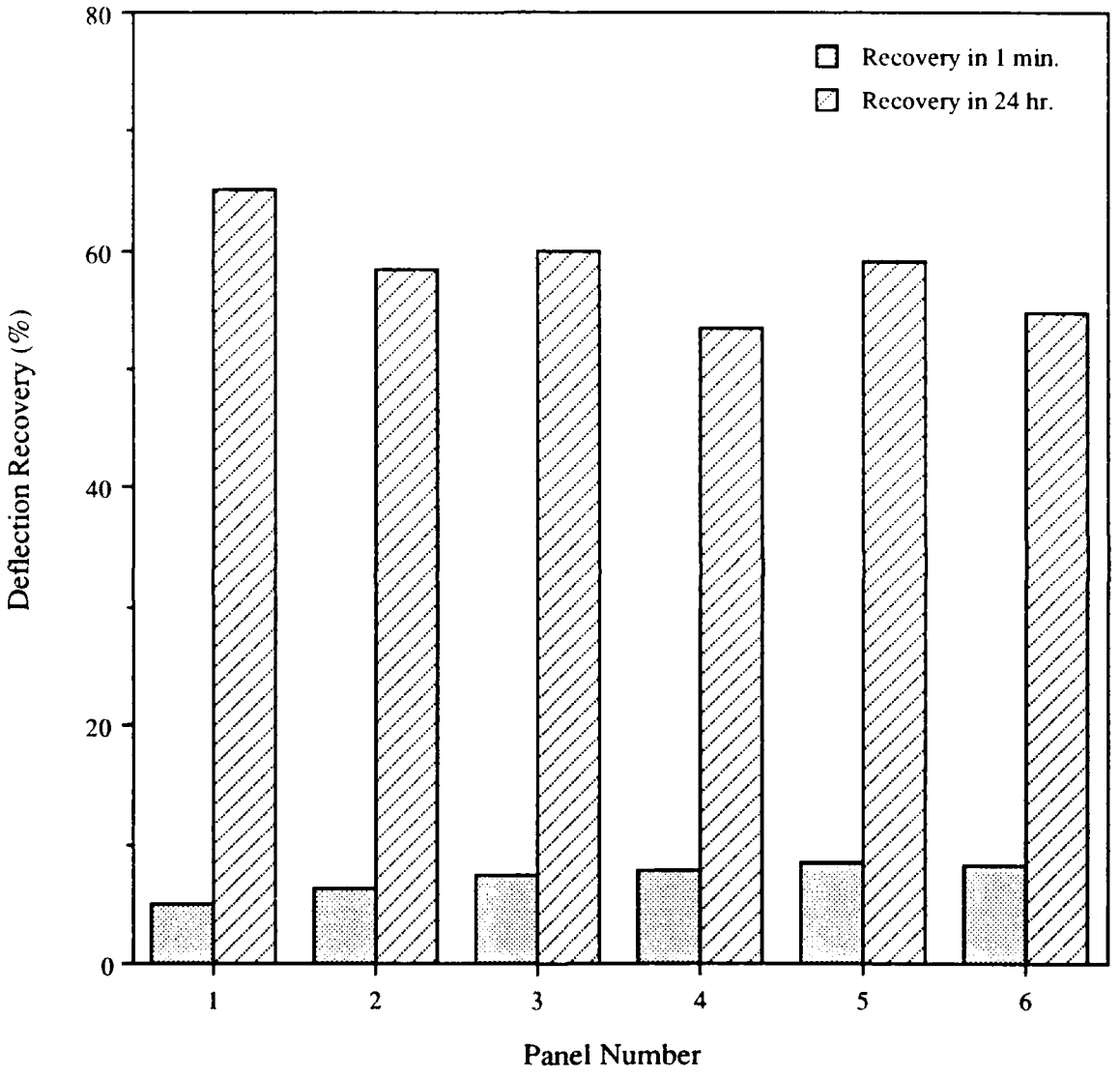

Figure 3-49: Mid-Span Deflection Recovery of Candidate Panels Following Static Pressure Testing

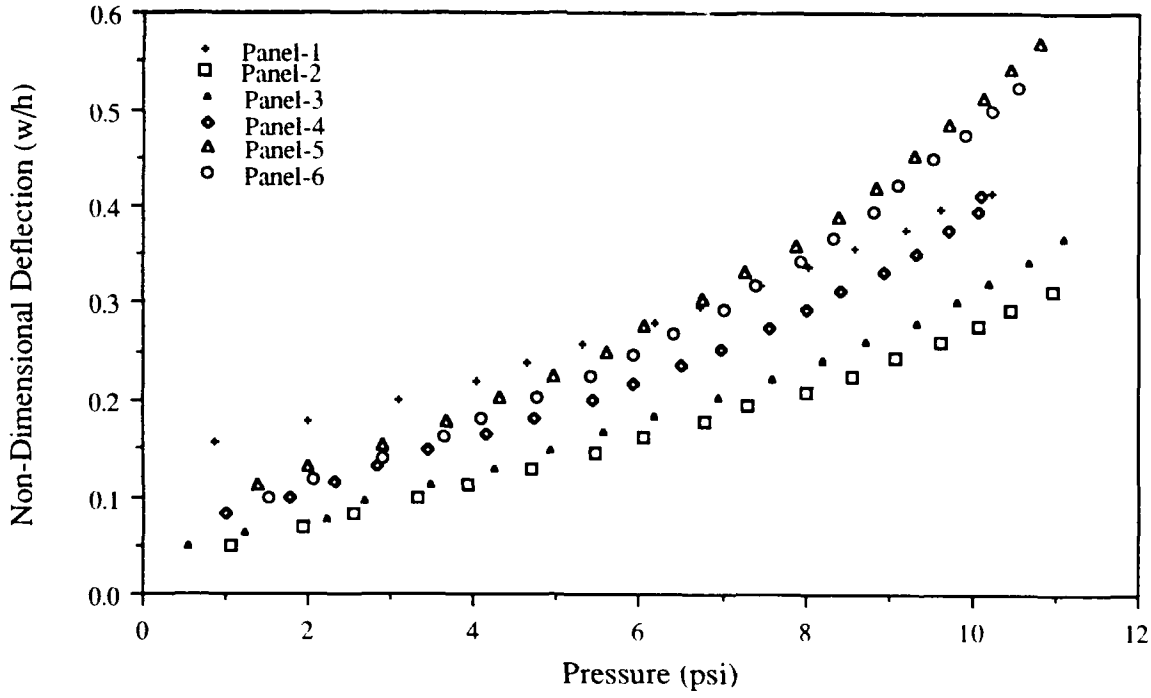

Figure 3-50: Mid-Span Deflection Response of Candidate Panels During Initial Cycle of Cyclic Pressure Test

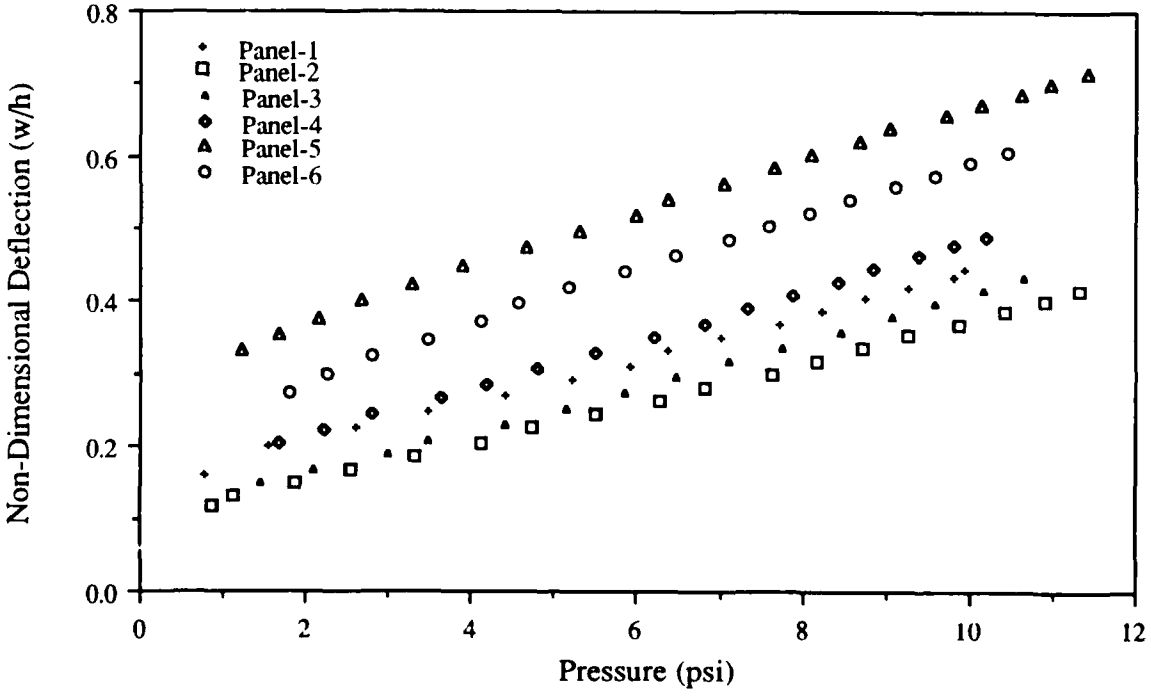

Figure 3-51: Mid-Span Deflection Response of Candidate Panels During Final Cycle of Cyclic Pressure Test

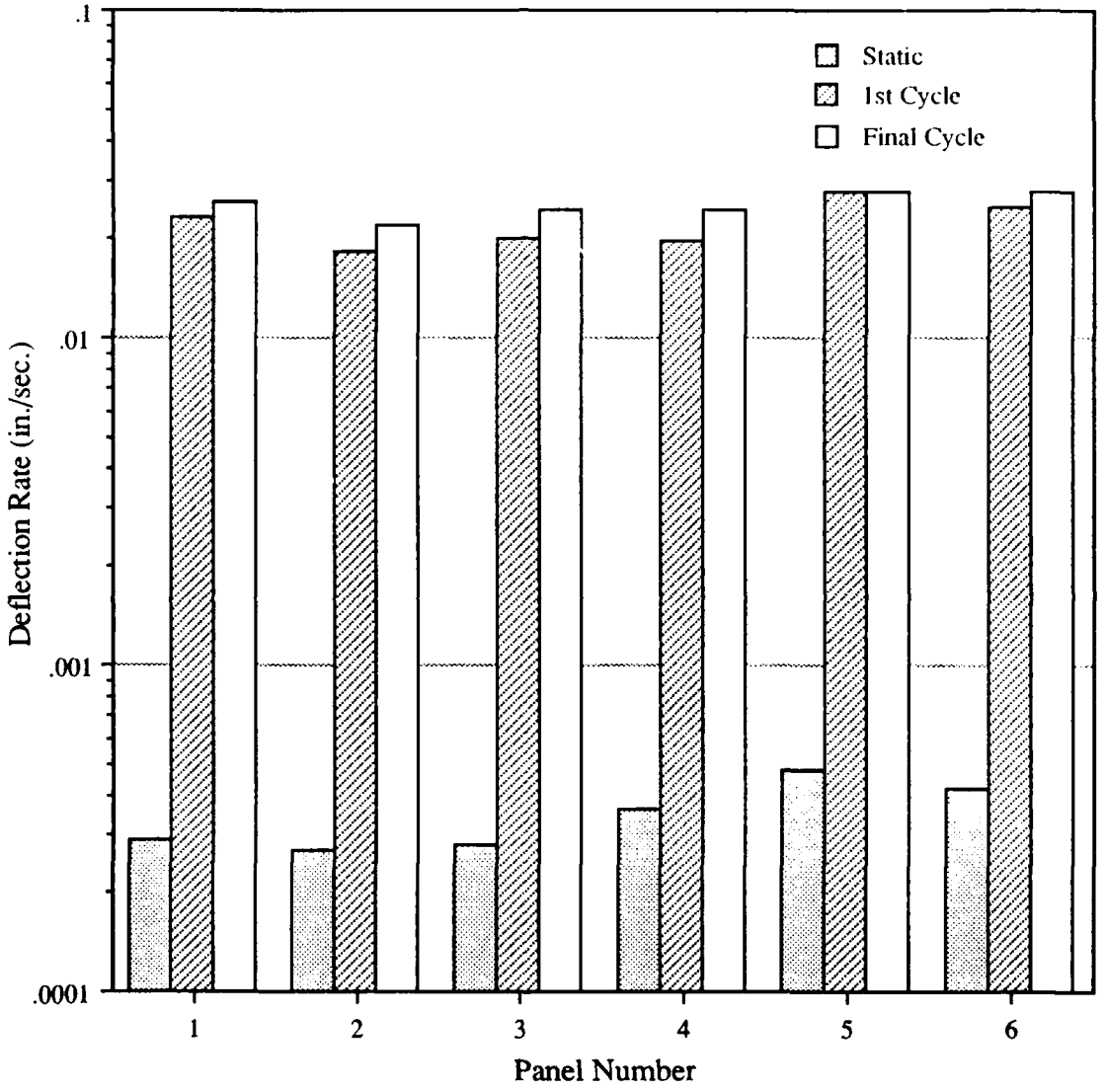

Figure 3-52: Comparison of Panel Mid-Span Deflection Rates for Static and Cyclic Pressure Tests

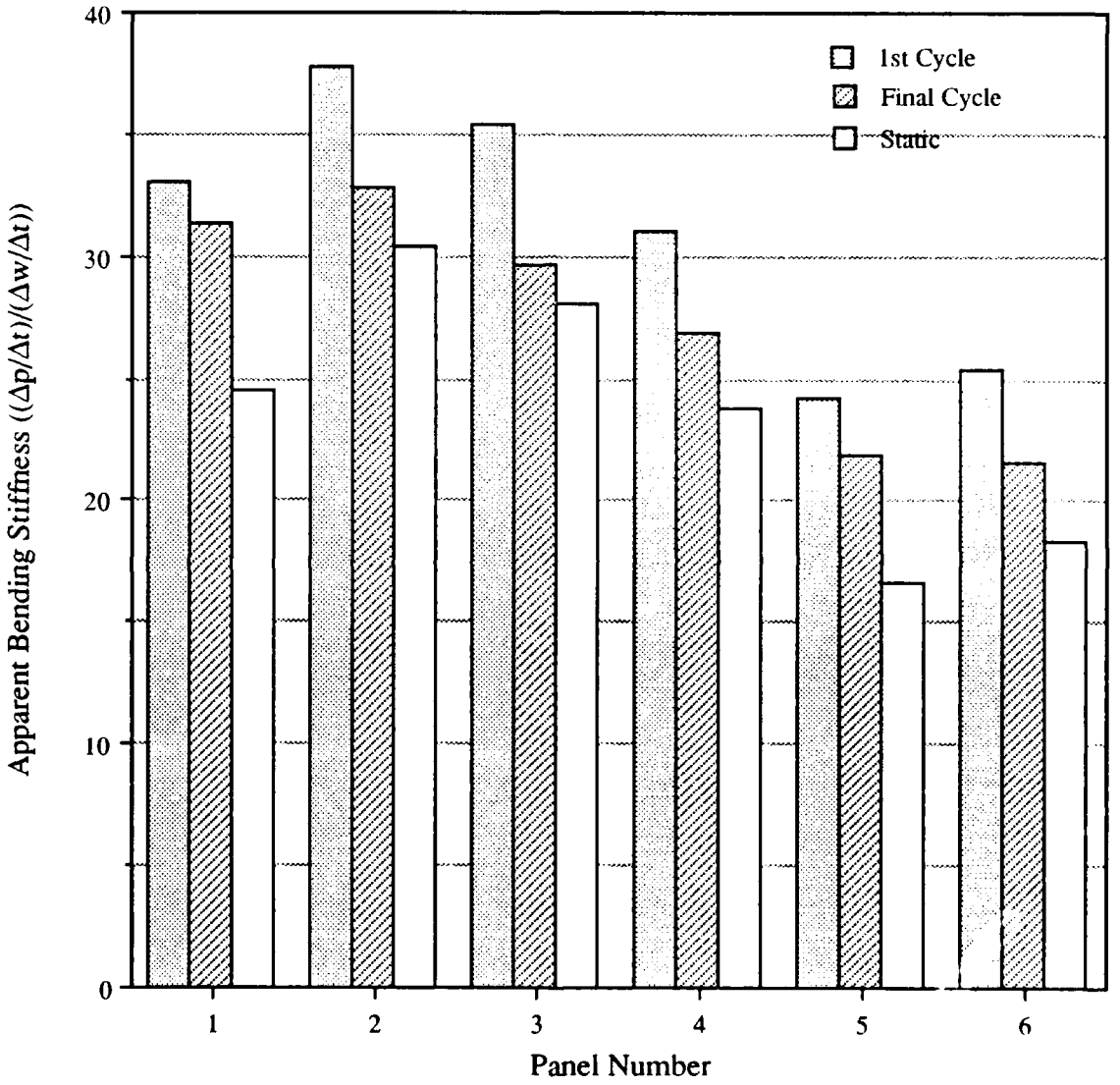

Figure 3-53: Comparison of Rate Normalized Panel Bending Stiffness

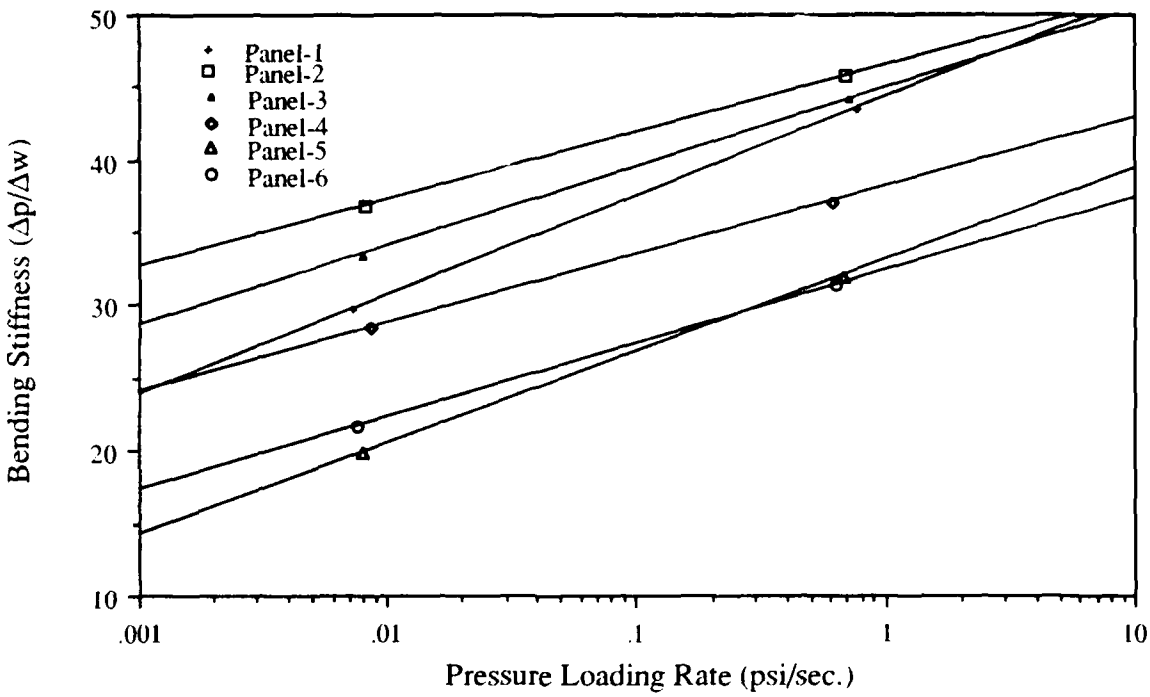

Figure 3-54: Panel Bending Stiffness vs. Pressure Loading Rate for Static and First Cycle Response

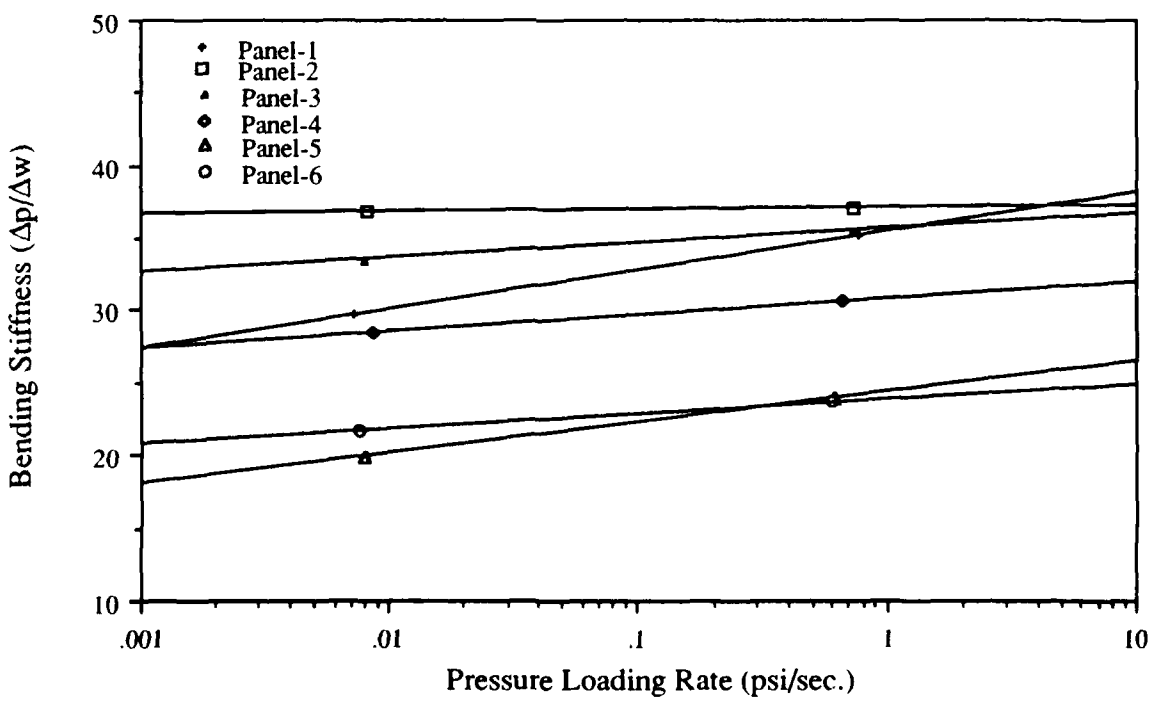

Figure 3-55: Panel Bending Stiffness vs. Pressure Loading Rate for Static and Final Cycle Response

3.2.3.2. Strain Response

Comparison of the upper and lower face strain rates during static pressure testing is presented in Figures 3-56 and 3-57. On the upper face, the transverse rate for the E-glass panels average 13.9 times greater than the Kevlar/DERAKANE 510A panels (3 and 4) and 9.3 times greater than the Kevlar/DERAKANE 8084 panels (5 and 6). The high rates for the E-glass panels are caused by the orthotropic (0°-90°) ply orientation in the faces which contrasts to the bias reinforcing (±45°) in the Kevlar panels. The latter provides diagonal stiffening and a more balanced strain condition. Also, Kevlar has a higher modulus in tension. [40]

On the lower face, the rates are a factor of ten less than the tensile rates, the transverse strain rates are more equal among the panels, and the difference between the transverse and longitudinal rates of the E-glass panels on the upper face are reduced. The lower compressive rates are attributed to a thicker lower face: additional reinforcement (one ply of CSM) is present. The greater consistency between panels is attributed to the response of the constituents: in compression the response is that of the matrix while in tension it is that of the fiber.

In Figures 3-58 and 3-59, the tensile and compressive strain rates during the first cycle are shown . Unlike the static rates, the transverse rates for the Kevlar panels are nearly the same as for the E-glass panels as are also the longitudinal rates. In comparison, only the transverse rate of panel-5 and the longitudinal rate of panel-6 differ from the norms. Both in tension and compression, the longitudinal rate for the Kevlar panels is a smaller percentage of the transverse rate than is the case in the static test.

A comparison of the upper and lower face strain rates during the final cycle of the cyclic tests is shown in Figures 3-60 and 3-61. Here, the transverse tensile strain rates for the Kevlar/DERAKANE 8084 panels (5 and 6) average 40.3% higher than those for the Kevlar/DERAKANE 510A panels (3 and 4). On the lower face, the longitudinal rates for the Kevlar panels are nearly the same as the transverse rates; this is similar to the static

case. It suggests that cycles reduce the differences between the longitudinal and transverse rates, and that the final response of the strain components is the same as produced by static loading.

In Figure 3-62, the upper face transverse tensile strain rates are compared; the E-glass panels are less rate sensitive than the Kevlar ones. The lower face transverse compressive strain rates are compared in Figure 3-63 where the E-glass panels show more rate sensitivity, probably because of the influence of the matrix. In tension the rate insensitive fiber dominates the response. The same may be true with the Kevlar panels: in compression, the more rate sensitive matrix exerts its influence.

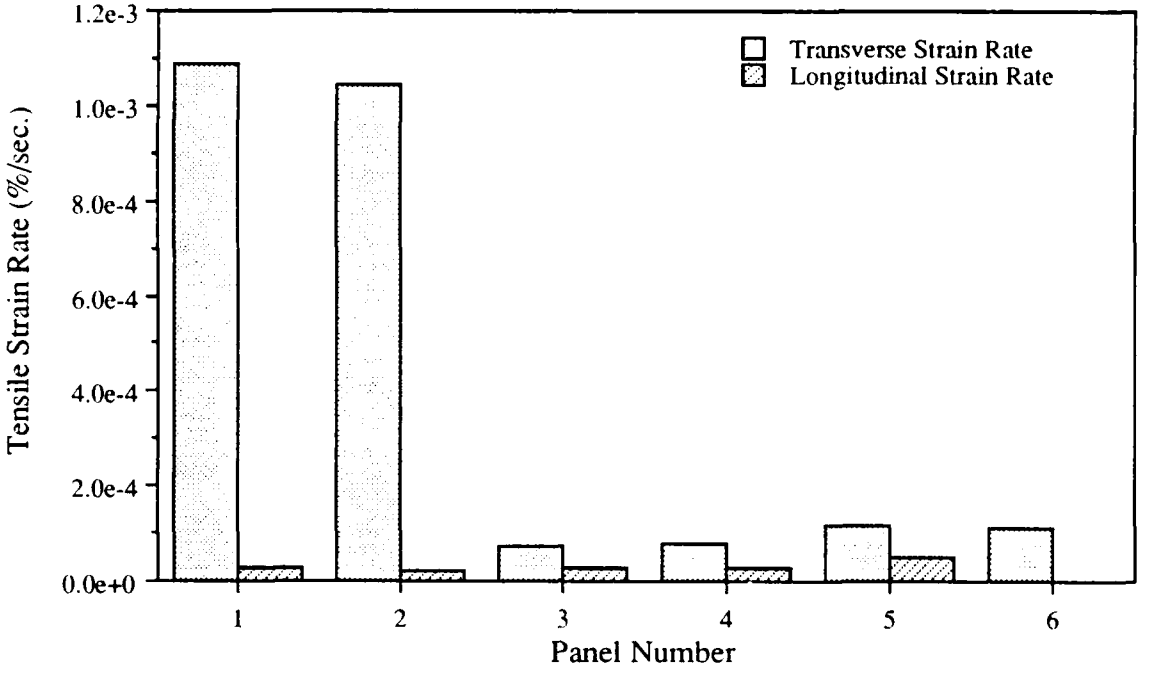

Figure 3-56: Comparison of Panel Upper Face Strain Rates During Static Pressure Test

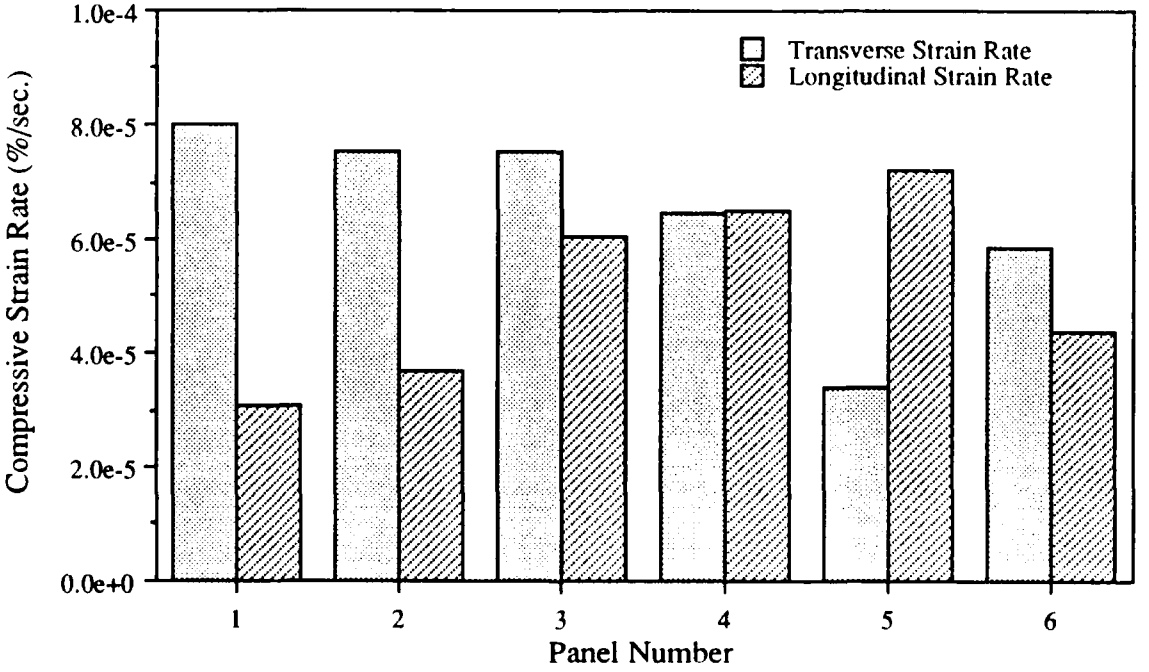

Figure 3-57: Comparison of Panel Lower Face Strain Rates During Static Pressure Test

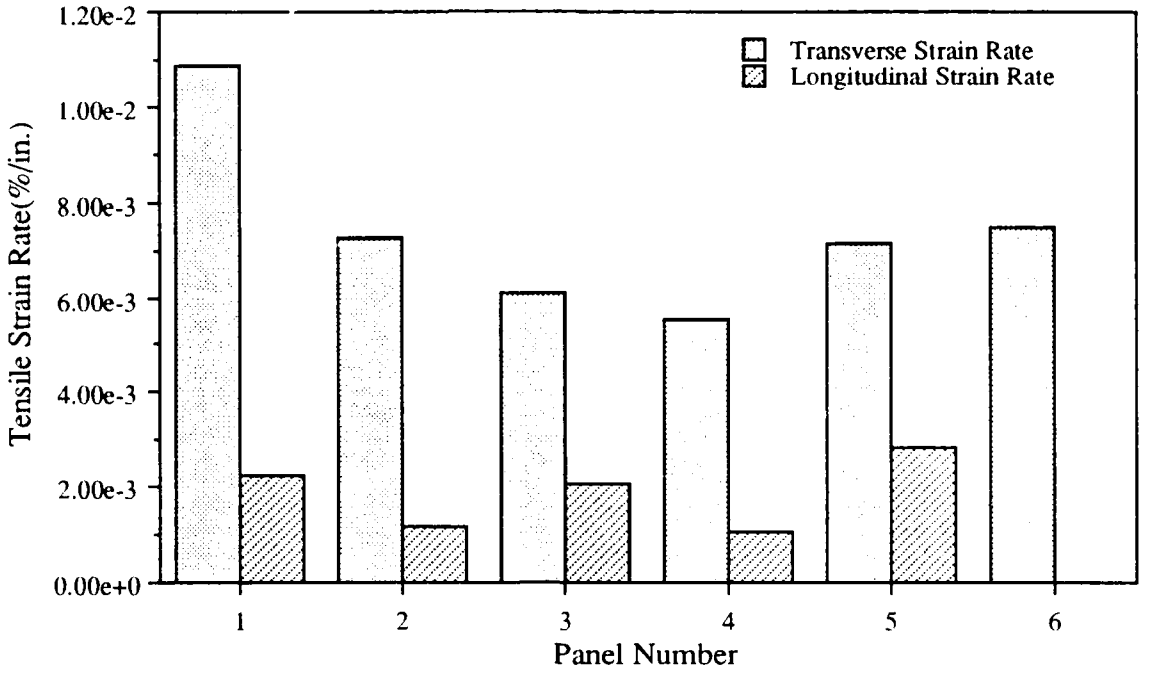

Figure 3-58: Comparison of Panel Upper Face Strain Rates During First Cycle of Cyclic Pressure Test

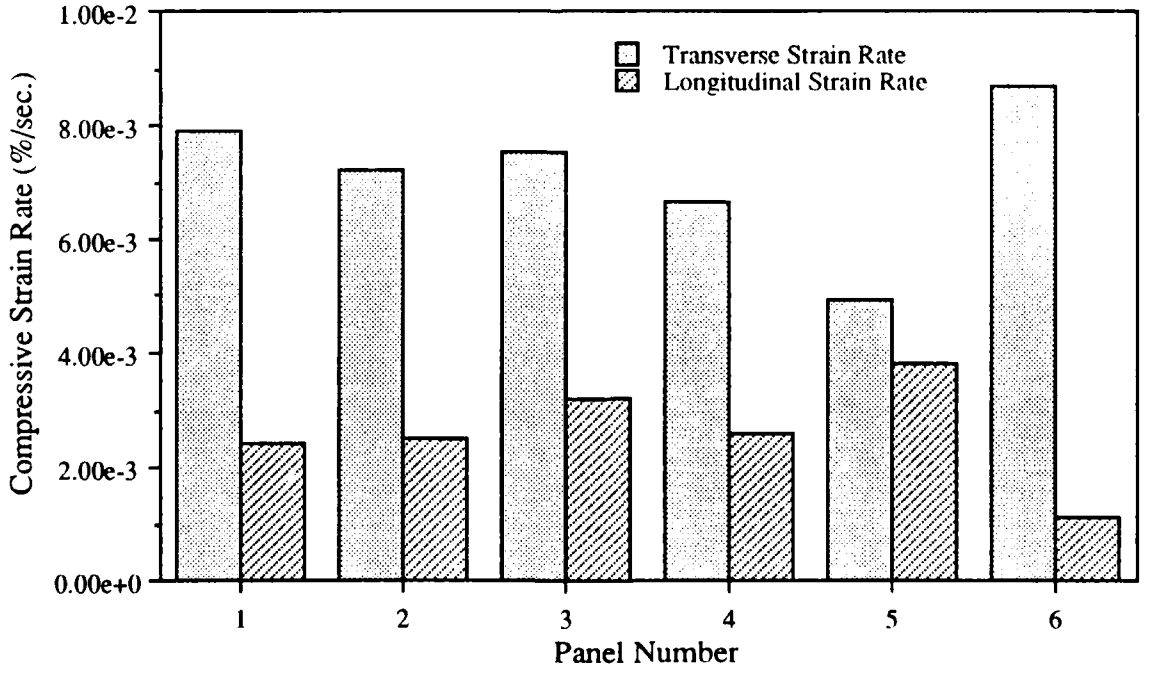

Figure 3-59: Comparison of Panel Lower Face Strain Rates During First Cycle of Cyclic Pressure Test

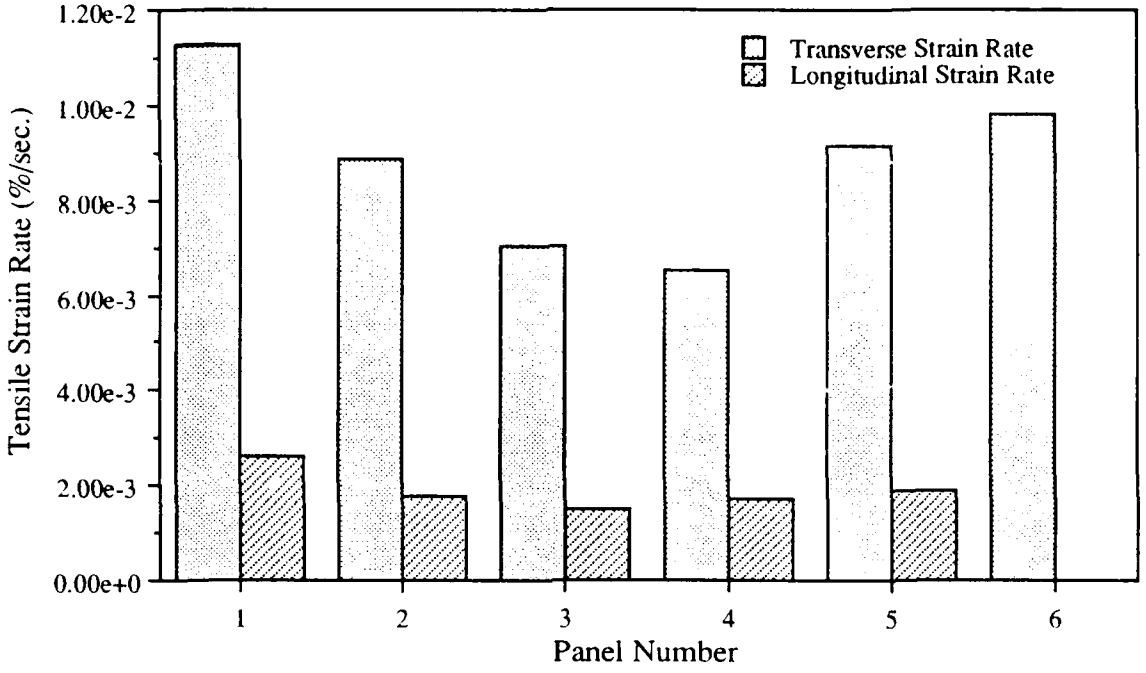

Figure 3-60: Comparison of Panel Upper Face Strain Rates During Final Cycle of Cyclic Pressure Test

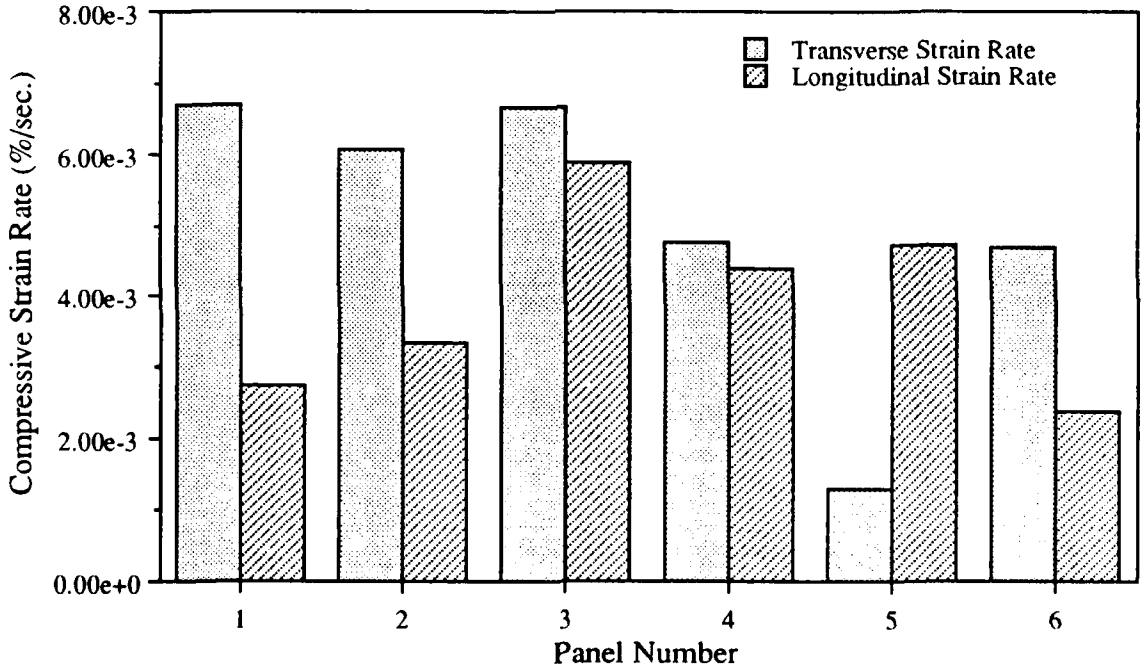

Figure 3-61: Comparison of Panel Lower Face Strain Rates During Final Cycle of Cyclic Pressure Test

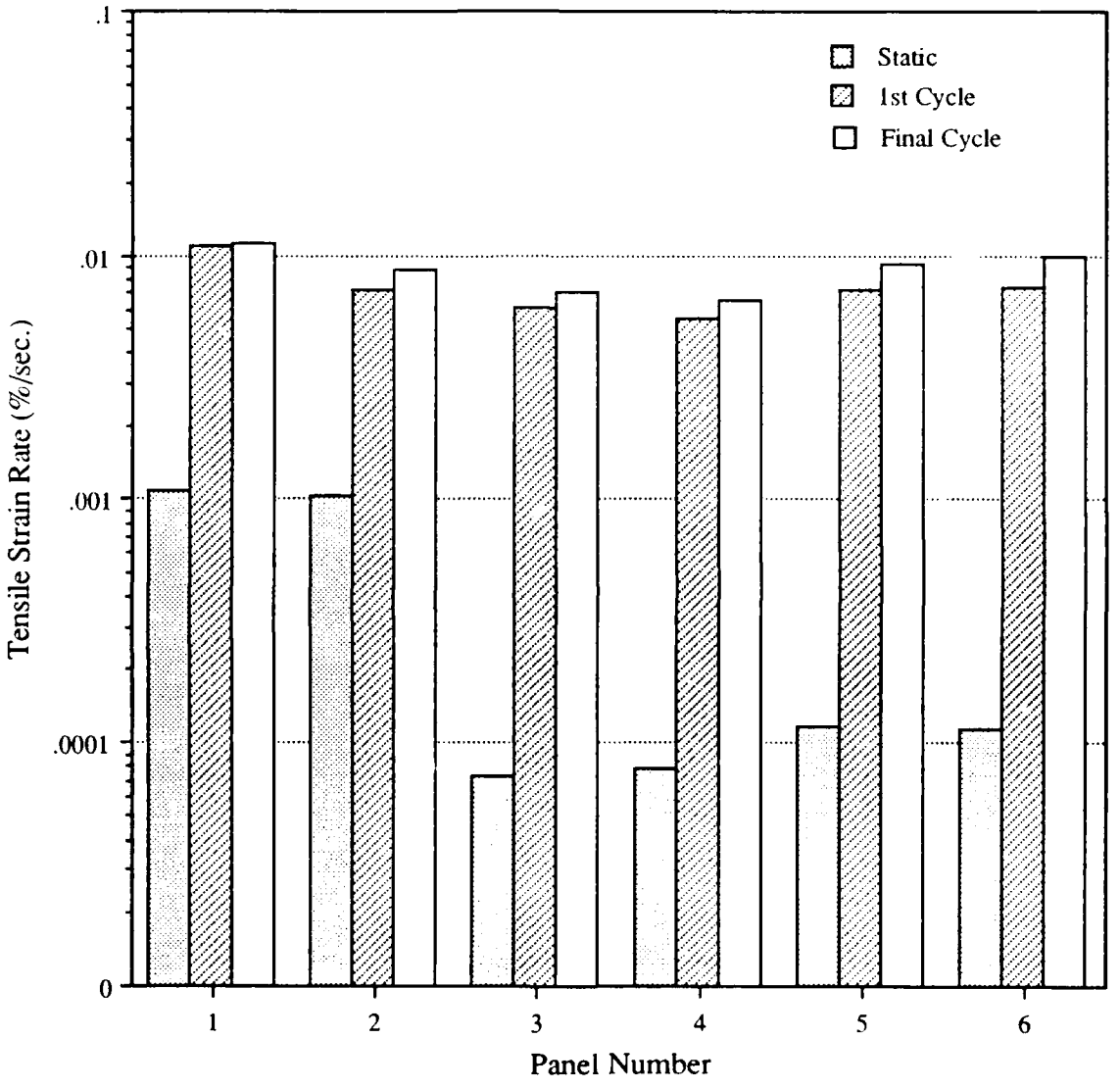

Figure 3-62: Comparison of Panel Upper Face Transverse Strain Rates for Static and Cyclic Pressure Tests

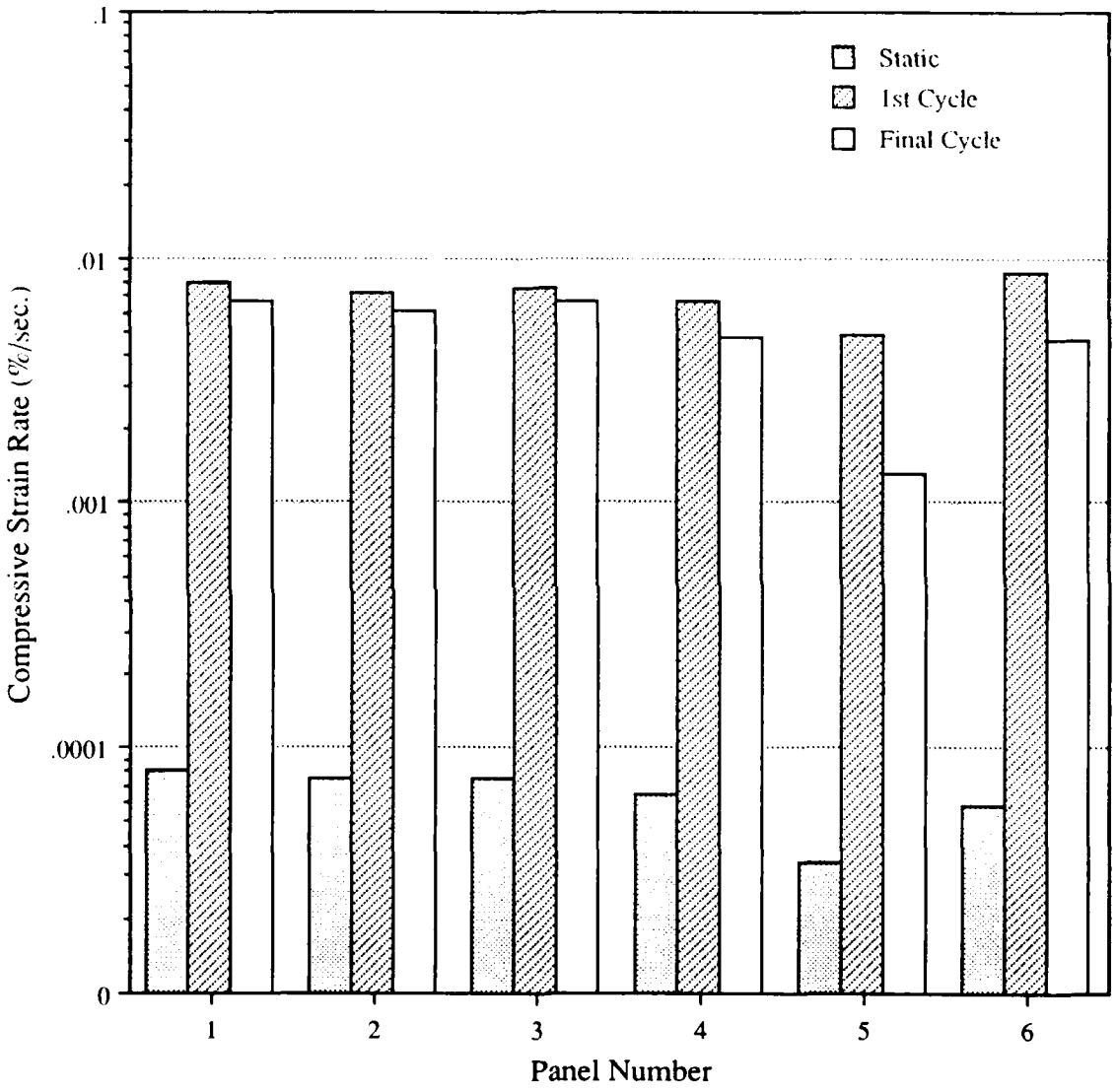

Figure 3-63: Comparison of Panel Lower Face Transverse Strain Rates for Static and Cyclic Pressure Tests

4. SUMMARY and CONCLUSIONS

The objective of the research was to develop a test method for determining the structural response of marine sandwich panels to uniform pressure loads and to test full scale panels so that data could be used for development of more precise prediction techniques. In support of this, the properties of the panel lower faces were measured by ASTM or other recognized methods. Further, the deflection and strain responses of the panels were evaluated for two loading rates.

4.1. MATERIAL PROPERTIES OF SANDWICH PANEL FACES

The panel lower faces were characterized by specific gravity, reinforcement weight fraction, reinforcement volume fraction, and void content. The E-glass faces had a higher specific gravity than the Kevlar ones; this produced a 29% weight saving for the Kevlar sandwich panels. The lower reinforcement volume fraction for E-glass faces was caused by the strand arrangement of the Vectorply 1808 fabric. The Kevlar faces had significantly higher void contents and greater inconsistency in void dispersion than the E-glass ones. This was due to difficulties in working with Kevlar, the experience level of the manufacturer, and limitations of the hand lay-up molding process.

The E-glass skins exhibited 12% greater tensile strength and 20.7% greater tensile modulus than the Kevlar ones. The lower Kevlar values were a result of the bias (±45°) reinforcing present. This bias, plus its lower modulus in compression, also caused the lower Poisson's Ratios in the Kevlar faces.

The E-glass panel faces had twice the compressive strength and 37.6% greater compressive modulus than the Kevlar ones. They failed catastrophically in compression while the Kevlar yielded more globally, which also may have been assisted by the more ductile DERAKANE 8084 resin.

The effect of the bias reinforcing was also evident in the flexural properties of the Kevlar skins: the E-glass faces were 41.9% stronger and 29% stiffer, but the Kevlar specimens never broke completely, whereas the E-glass ones did.

The in-plane shear strengths for the E-glass panel faces were 19.1% greater than the Kevlar ones; this reflected the better adhesion of the glass fibers to the resin.

The effect of the ductile DERAKANE 8084 resin when combined with the Kevlar fibers was remarkable: no catastrophic fractures in compression or flexural tests took place. Instead, a general or global yielding occurred and some, reduced, load capacity remained.

4.2. PANEL TESTS

The six sandwich panels were tested at two loading rates about two orders of magnitude different.

4.2.1. Static Pressure Loading

The pressure-deflection response of each panel was initially linear: this ended at 5.5 psi for the DERAKANE 510A panels (1 through 4) and at 4 psi for the DERAKANE 8084 panels (5 and 6). Beyond, the responses became non-linear. At higher deflections, the 8084 panels showed evidence of membrane behavior, as their mid-span deflections approached the panel thickness. Hysteresis effects were evident during static testing and were prominent in panels 5 and 6. The bias (±45°) reinforcing in the Kevlar panels influenced the transverse deflected shape: it reduced the arching effect and produced a flatter panel response.

The static strain response differed between the three panel types. On the upper face of the E-glass panels (1 and 2), the large difference between the transverse and longitudinal strains was attributed to panel curvature in the transverse axis, and to the orthotropic (0° - 90°) reinforcement orientation. This difference was reduced in the Kevlar panels because of bias (±45°) reinforcing. These differences were not present on the lower faces. It was concluded that the response in compression depended more upon the matrix and was less affected by panel aspect ratio or reinforcing directions. Membrane behavior was evident in the transverse component of strain on the lower face: during loading, the compressive strain went through a maximum, then as the loading increased, it decreased and changed to tension. In subsequent testing at higher pressures, the presence of membrane behavior was also evident in the longitudinal strain component.

Based on the maximum strains observed, the face compressive stress did not exceed 1200 psi for static loading pressures below 11 psi.

The strain response of the Kevlar/DERAKANE 8084 panels (5 and 6) was inconsistent, possibly because of strain gage failure or because of local panel damage that might have occurred during cyclic testing.

4.2.2. Cyclic Pressure Loading

In the cycling loading, the deflection response exhibited a steeper slope and a larger linear region than observed in the static tests. In the first loading cycle, the elastic limit was encountered at 7 psi for the DERAKANE 510A panels (1 through 4) and at 6 psi for the DERAKANE 8084 panels (5 and 6), but in the final cycle the response was linear throughout the pressure range. Apparently the non-linear influence of the core diminished with successive load cycles, and eventually the panel response was controlled by the faces. Two additional observations support this inference: the intermediate cycles showed a progressive reduction in the amount of incremental deflection and the maximum deflections which occurred during the final cycle were less than but approached those recorded during the static test.

The upper face strain curves during cyclic loading were similar in shape to those seen in the static loading case. A progressive increase in strain occurred with successive loading cycles and after the first cycle, the response became linear.

The transverse strain on the lower face showed a more linear response with less hysteresis than during the static tests. Unlike the static case, however, small increases in strain occurred during unloading. The magnitude of the maximum transverse strain diminished with successive loading cycles so membrane behavior was not evident on a individual cycle basis but it was present over multiple cycles. From this, it was concluded that the effects of membrane behavior were rate sensitive.

The longitudinal strain response on the lower face did not show any membrane behavior and a progressive increase in strain occurred with successive cycles.

4.2.3. Panel Performance

The panels were evaluated on the basis of mid-span deflection, deflection recovery, deflection rate effects, rate normalized bending stiffness, and various other aspects of strain rate effects. Recall that the panels were first loaded cyclically and all showed some permanent deformation from this. The Kevlar/DERAKANE 8084 panels (5 and 6) showed the most such deformation, thus when they were later loaded statically their deflections were the greatest. After the cyclic loadings were completed, all panels were allowed to recover from their deformations for at least 24 hours. Then the static loading was applied and another 24 hour recovery period ensued. The average recovery of the six panels was 58.5% of the maximum deflection measured in the static loading phase; while longer recovery times produced further decreases in the panel deformation, the rate of recovery slowed greatly and accurate measurements became difficult.

The cyclic tests provided an insight into the rate dependency of the panels and the effects of repeated loading. Panel bending stiffness increased with increased loading rate. After repeated loading, the stiffness decreased, however, and approached that obtained during static loading; it appeared the core softened when cycled.

The E-glass panels exhibited much higher transverse tensile strain rates than the Kevlar panels and a larger difference between the transverse and longitudinal strain components; the benefit of the bias reinforcing on reducing strains was evident. Generally the Kevlar panels had lower tensile strain rates and the transverse and longitudinal strains were more equal. Differences in the compressive rate sensitivity for the transverse and longitudinal components of the Kevlar panels were evident during the first cycle response to cyclic pressure loading; these were reduced in successive loadings and eventually they approached those obtained during static loading. This was further evidence that the long term cyclic response of the panels approached that of the static loading condition.

The E-glass panels were less tensile strain rate sensitive than the Kevlar panels, yet displayed similar rate sensitivity in compression. The differences between the tensile and

compressive rate sensitivities for the E-glass panels were attributed to characteristics of the fiber and the matrix: in tension, the response was dominated by the non-rate sensitive fiber, while in compression, the rate sensitive matrix had more influence.

5. RECOMMENDATIONS

5.1. MATERIAL PROPERTY TESTING

The determination of reinforcement weight and volume fractions for Kevlar laminates having a vinyl ester matrix is difficult by matrix digestion methods because of the chemical resistance of the matrix. Until a more accurate and reproducible method is developed, consideration should be given to weight and area measurements of the specimens. (This is an alternative way to determine reinforcement weight fractions which can be used in case matrix digestion techniques fail.)

Grip failures in tensile specimens were troublesome and although it is not in accordance with ASTM procedures, a minimum width of 2.0 in. and a specimen aspect ratio of greater than seven should be used for tensile test specimens.[42]

The 4 by 6 in. specimen used in the compression tests bowed and buckled despite clamps on all four edges; this made the definition of compressive failure unclear. A better test procedure is needed. Further, Kevlar based composites are difficult to machine so additional uncertainty arises from this source: poor supporting surfaces. Care must be exercised to minimize this cause of error.

In ASTM D790, a flexural test specimen width of 0.5 in. is recommended for specimens of thickness greater than 0.125 in. but this may not uniformly stress the bias (±45°) plies if they are located in the outer surfaces. A minimum specimen width of 1.0 in. should be used in such cases.

Machining the notches of the in-plane shear specimens with a water cooled, diamond grit-edge blade produces a well defined shear plane; lower standard deviations can be obtained if this procedure is employed.

5.2. PANEL TESTS

Improvements can be made to the panel test mechanism. Control solenoids located at the air inlet and vent outlet to the water tank could be used to regulate system pressure; then the computer can then be used to regulate the pressurization rate by using feedback from the pressure transducer. With such, the test mechanism could be used to investigate fatigue aspects of pressure loaded panels.

A method to measure core compression during pressure loading is needed. This would clarify the origins of membrane behavior in the bent panels.

Future work with this panel test mechanism should include:

(1). Investigation of high stress low cycle fatigue and low stress high cycle fatigue of panels with the same construction.

(2). Panels with identical skins but different cores should be studied, to assess the effects arising from the core.

(3). More strain gages on both faces near the panel test section boundary should be used to clarify the boundary effects on panel deflections and strains.

(4). Local impact damage could influence panel behavior; tests should be done to explore this area.

6. REFERENCES

1. Reichard, Ronnal P., "Materials Selection for Boats and Ships", *Proceedings from the Second International Conference on Marine Applications of Composite Materials*, March 21-23, 1988, Florida Institute of Technology, Melbourne, Florida.

2. Reissner, Eric, "Finite Deflections of Sandwich Plates", *Journal of the Aeronautical Sciences*, Vol. 15, July, 1948, pp. 435-440.

3. Timoshenko, S., Theory of Plates and Shells, McGraw-Hill Book Company, Inc., New York, 1940.

4. Liaw, Boen-Dar, and Little, Robert W., "Theory of Bending Multilayer Sandwich Plates", *AIAA Journal*, Vol. 5, No. 2, February, 1967, pp. 301-304.

5. Ng, S. F., "Finite Deflection of Sandwich Panels Resting on Elastic Supports", *Aeronautical Journal*, Vol. 78, April, 1974, pp. 147-150.

6. Thurston, G. A., "Bending and Buckling of Clamped Sandwich Plates", *Journal of Aeronautical Sciences*, Vol. 24, June, 1957, pp. 407-411.

7. Kao, J., Guzman-Barron, L., and Hartman, A. J., "Large Deflections of Rectangular Sandwich Plates", *International Journal of Solids and Structures*, Vol. 10, 1974, pp. 587-601.

8. Alman, A. M., "Large Deflection of Sandwich Plates with Orthotropic Cores", *AIAA Journal*, Vol. 2, No. 1, 1964, pp. 1820-1822.

9. Kamiya, N., "Governing Equations for Large Deflections of Sandwich Plates", *AIAA Journal*, Vol. 14, February, 1976, pp. 250-253.

10. Kan, Han-Pin, and Huang, Ju-Chin, "Large Deflection of Rectangular Sandwich Plates", *AIAA Journal*, Vol. 5, No. 9, October, 1967, pp. 1706-1708.

11. Nowinski, J. L., and Ohnabe, H., "Fundamental Equations for Large Deflections of Sandwich Plates with Orthotropic Core and Faces", *Proceedings from the Tenth International Symposium on Space Technology and Science*, September 3-8, 1973, Tokyo, Japan.

12. Plantema, F. F., Sandwich Construction; The Bending and Buckling of Sandwich Beams, Plates and Shells, John Wiley & Sons, Inc., New York, 1966.

13. Weissman-Berman, Deborah, "A Preliminary Design Method for FRP Sandwich-Cored Panels", The Society of Naval Architects and Marine Engineers, Star Symposium, Norfolk, VA, May 21-24, 1985.

14. Weissman-Berman, D., Petrie, G.L., and Wang, M., "Flexural Response of Foam-Cored FRP Sandwich Panels", New York Metropolitan Section, The Society of Naval Architects and Marine Engineers, November, 1988.

15. Prabhakaran, P. M. and Sendlein, L. S., "Design of Four-Point Flexure Sandwich Beams", *Proceedings from the Second International Conference on Marine Applications of Composite Materials*, March 21-23, 1988, Florida Institute of Technology, Melbourne, Florida.

16. Reichard, R. P., "The Design of FRP Sandwich Panels for Ships and Boat Hulls", *First International Conference on Sandwich Construction*, June, 1989, The Royal Institute of Technology, Stockholm, Sweden.

17. Reichard, R. P. and Robinson, R., "The Response of RP Sandwich Panels to Pressure Loading", *Society of Plastics Industry 44th Annual Conference*, February, 1989, Dallas, Texas.

18. Heller, S. R. and Jasper, N. H., "On the Structural Design of Planing Craft", Quarterly Transactions, Royal Institution of Naval Architects, July, 1960.

19. Newman, J. N., Marine Hydrodynamics, MIT Press, Cambridge, MA, 1977.

20. Lewis, Edward V., editor, Principles of Naval Architecture (Second Revision), The Society of Naval Architects and Marine Engineers, Jersey City, NJ, 1989.

21. Stiles, H. R., "Planing Hull Structure", New York Metropolitan Section, The Society of Naval Architects and Marine Engineers, January, 1974.

22. Silvia, P. A., "Structural Design of Planning Craft - A State of the Art Survey", Chesapeake Section, The Society of Naval Architects and Marine Engineers, March, 1978.

23. Allen, R. A. and Jones, R. R., "Considerations on the Structural Design of High Performance Marine Vehicles", New York Metropolitan Section, The Society of Naval Architects and Marine Engineers, January, 1977.

24. Danahy, P. J., "Adequate Strength for Small High-Speed Vessels", *Marine Technology*, January, 1968.

25. Spencer, J. S., "Structural Design of Aluminum Crewboats", *Marine Technology*, July, 1975.

26. Heller, S. R. and Clark, D. J., "The Outlook for Lighter Structures in High-Performance Marine Vehicles", *Marine Technology*, October, 1974.

27. "DERAKANE® Resins Technical Product Information", DOW Chemical Co.,Plastics Group, Midland, Michigan, January, 1989.

28. AIREX® Technical Data Sheet, Torin Inc., Waldwick, New Jersey.

29. Edkins, J. N., "The Computer-Aided Design of Flat Rectangular Grillages", Masters Thesis, Massachusetts Institute of Technology, Department of Ocean Engineering, May, 1980.

30. Chang, Pin-Yu, "A Simple Method for Elastic Analysis of Grillages", *Journal of Ship Research*, June, 1968, pp. 153-159.

31. "Specific Gravity and Density of Plastics by Displacement", ASTM D792-86, *1989 Annual Book of ASTM Standards*, Vol. 8.01, American Society for Testing and Materials, Philadelphia, PA, 1989, pp. 299-302.

32. "Ignition Loss of Cured Reinforced Resins", ASTM D2584-68 (Reapproved 1985), *1989 Annual Book of ASTM Standards*, Vol. 8.02, American Society for Testing and Materials, Philadelphia, PA, 1989, pp. 352-353.

33. "Fiber Content of Resin-Matrix Composites by Matrix Digestion", ASTM D3171-76(Reapproved 1982), *1989 Annual Book of ASTM Standards*, Vol. 15.03, American Society for Testing and Materials, Philadelphia, PA, 1989, pp. 122-124.

34. Kaufman, J. A., "Test Method 724, Fiber Content of Composites", E.I. Dupont De Nemours & Co., Inc., Textile Fibers Department, Wilmington, Delaware, April, 1989.

35. "Void Content of Reinforced Plastics", ASTM D2734-70 (Reapproved 1985), *1989 Annual Book of ASTM Standards*, Vol. 8.02, American Society for Testing and Materials, Philadelphia, PA, 1989, pp. 386-388.

36. "Tensile Properties of Fiber-Resin Composites", ASTM D3039-76 (Reapproved 1989), *1989 Annual Book of ASTM Standards*, Vol. 15.03, American Society for Testing and Materials, Philadelphia, PA, 1989, pp. 117-121.

37. Byers, B. A., *Behavior of Damaged Graphite/Epoxy Laminates Under Compression Loading*, Technical Report CR 159293, National Aeronautics and Space Administration, August, 1980.

38. "Flexural Properties of Unreinforced and Reinforced Plastics and Electrical Insulating Materials", ASTM D790-86, *1989 Annual Book of ASTM Standards*, Vol. 8.01, American Society for Testing and Materials, Philadelphia, PA, 1989, pp. 280-289.

39. "In-Plane Shear Strength of Reinforced Plastics", ASTM D3846-79 (Reapproved 1985), *1989 Annual Book of ASTM Standards*, Vol. 8.03, American Society for Testing and Materials, Philadelphia, PA, 1989, pp. 195-197.

40. Lubin, G., editor, Handbook of Composites, Van Nostrand Reinhold Co. Inc., New York, 1982.

41. Goldfarb, P. M., "Investigation of Kevlar and Glass Reinforced Plastic Materials for Naval Structural Applications", David W. Taylor Naval Ship Research and Development Center, Report DTNSRDC/SME-81/49, Bethesda, MD, September, 1981.

42. Antonio, B. K., "Material and Mechanical Characterizations for Braided Composite Pressure Vessels", Naval Engineers Thesis, Massachusetts Institute of Technology, Cambridge, MA, May, 1990.

APPENDIX A

TENSILE CHARACTERISTICS OF TEST PANEL LOWER FACES

Table A-1: Panel-1 Tensile Specimen Dimensions

Specimen ID	Width (in)	Thickness (in)
Panel 1-1	1.01	0.164
Panel 1-2	0.99	0.171
Panel 1-3	1.002	0.171
Panel 1-4	0.989	0.169
Panel 1-5	1.003	0.166

Table A-2: Panel-1 Tensile Test Data

Specimen ID	Maximum Load (lbs)	Maximum Stress (psi)	Max Load Deflection (in)	Maximum Strain (%)	Tensile Modulus (ksi)	Energy to Break (in-lbs)
Panel 1-1	3779	22815	0.22351	2.35	1668.06	460.1
Panel 1-2	3922.6	23171	0.21272	2.24	1696.35	474.4
Panel 1-3	4102.4	23943	0.24908	2.62	1617.27	571.5
Panel 1-4	3727.1	22299	0.23069	2.43	1796.43	487.2
Panel 1-5	3975.2	23875	0.23438	2.47	1668.03	525.9

Table A-3: Panel-1 Tensile Test Data Statistics

Statistic	Maximum Load (lbs)	Maximum Stress (psi)	Max Load Deflection (in)	Maximum Strain (%)	Tensile Modulus (ksi)	Energy to Break (in-lbs)
Mean	3901	23221	0.230076	2.42	1689.23	503.82
SDEV	151	701	0.013458	0.14	66.37	45.06
CVAR	3.88	3.02	5.85	5.85	3.93	8.94
Minimum	3727	22299	0.21272	2.24	1617.27	460.1
Maximum	4102	23943	0.24908	2.62	1796.43	571.5

SDEV - Standard Deviation
CVAR - Coefficient of Variation (%)

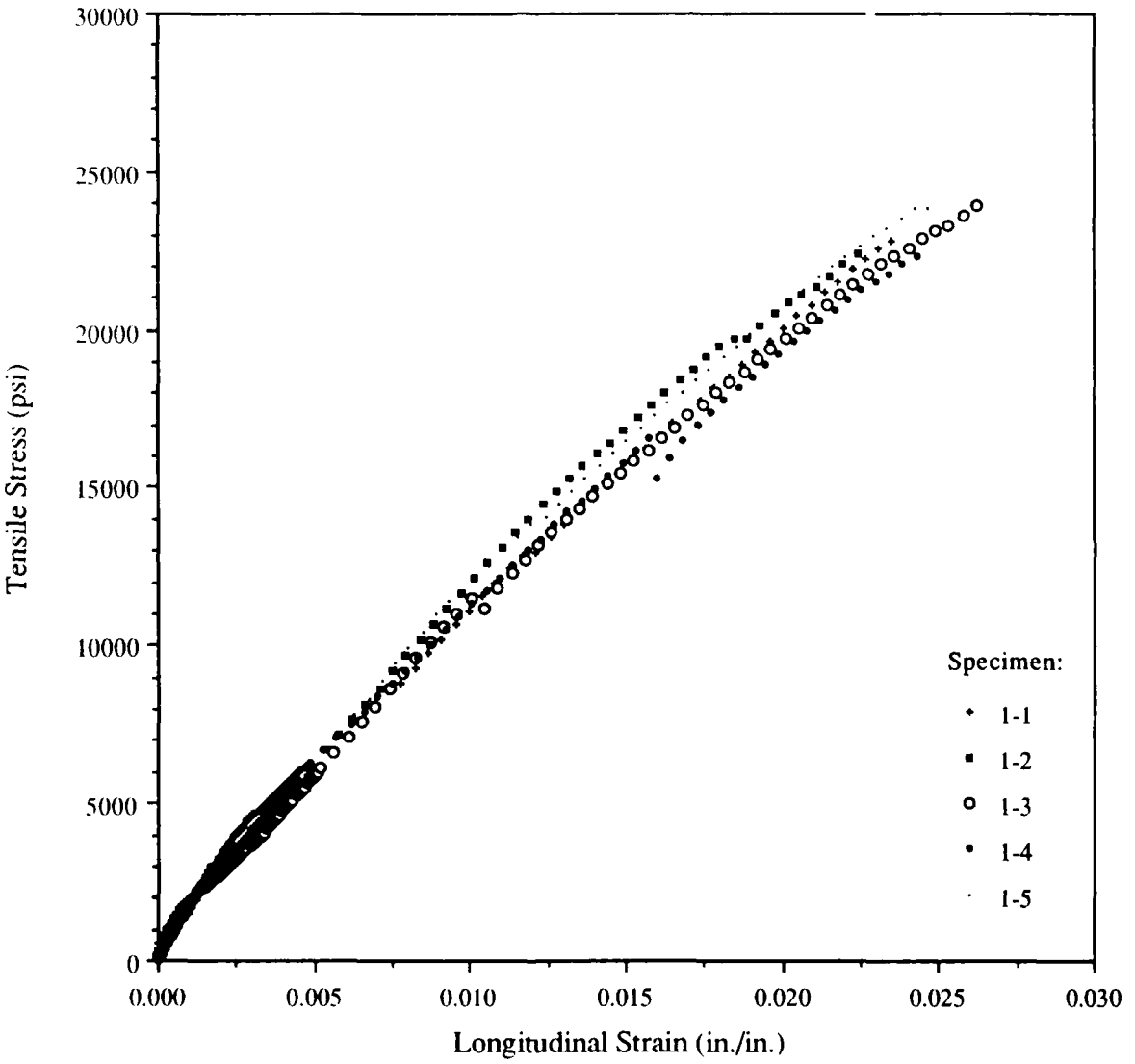

Figure A-1: Tensile Stress vs. Strain for Panel-1 (E-Glass/DERAKANE® 510A) Lower Face Based on Load Deformation Analysis

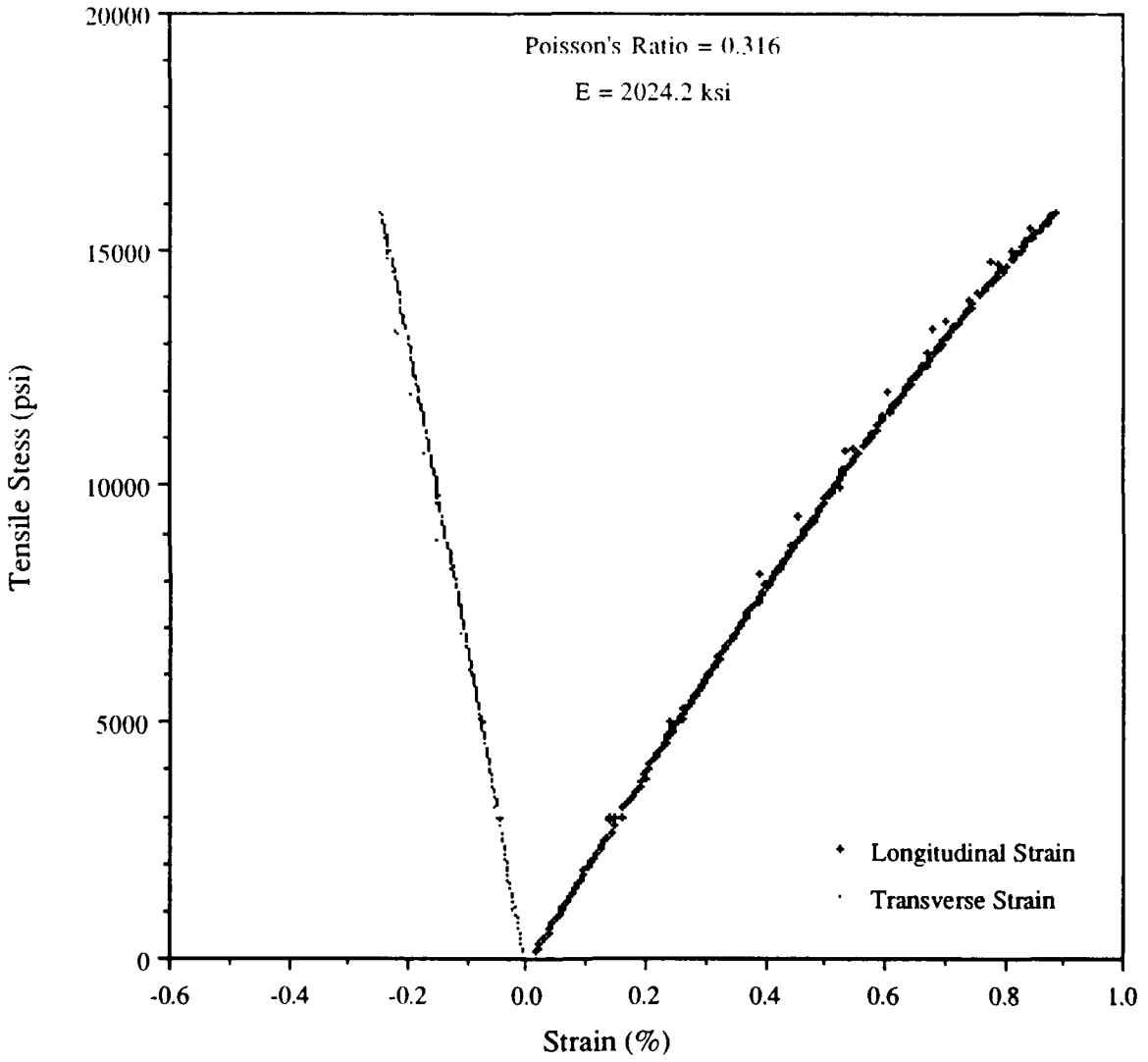

Figure A-2: Tensile Stress vs. Strain for Panel Specimen 1-4 Based on Bi-axial Strain Gage Measurements

Table A-4: Panel-2 Tensile Specimen Dimensions

Specimen ID	Width (in)	Thickness (in)
Panel 2-1	0.995	0.157
Panel 2-2	0.994	0.161
Panel 2-3	0.975	0.171
Panel 2-4	0.996	0.162
Panel 2-5	0.972	0.172

Table A-5: Panel-2 Tensile Test Data

Specimen ID	Maximum Load (lbs)	Maximum Stress (psi)	Max Load Deflection (in)	Maximum Strain (%)	Tensile Modulus (ksi)	Energy to Break (in-lbs)
Panel 2-1	3730.7	23882	0.21962	2.31	1776.24	467.4
Panel 2-2	3871.7	24193	0.25028	2.63	1575.18	500
Panel 2-3	3970	23812	0.1831	3.33	1630.06	439.1
Panel 2-4	4047.8	25087	0.26019	2.74	1555.19	559.4
Panel 2-5	3740.1	22371	0.2345	2.47	1728.69	512.9

Table A-6: Panel-2 Tensile Test Data Statistics

Statistic	Maximum Load (lbs)	Maximum Stress (psi)	Max Load Deflection (in)	Maximum Strain (%)	Tensile Modulus (ksi)	Energy to Break (in-lbs)
Mean	3872	23869	0.229538	2.70	1653.07	495.76
SDEV	140	979	0.030205	0.39	96.26	45.76
CVAR	3.60	4.10	13.16	14.43	5.82	9.23
Minimum	3731	22371	0.1831	2.31	1555.19	439.1
Maximum	4048	25087	0.26019	3.33	1776.24	559.4

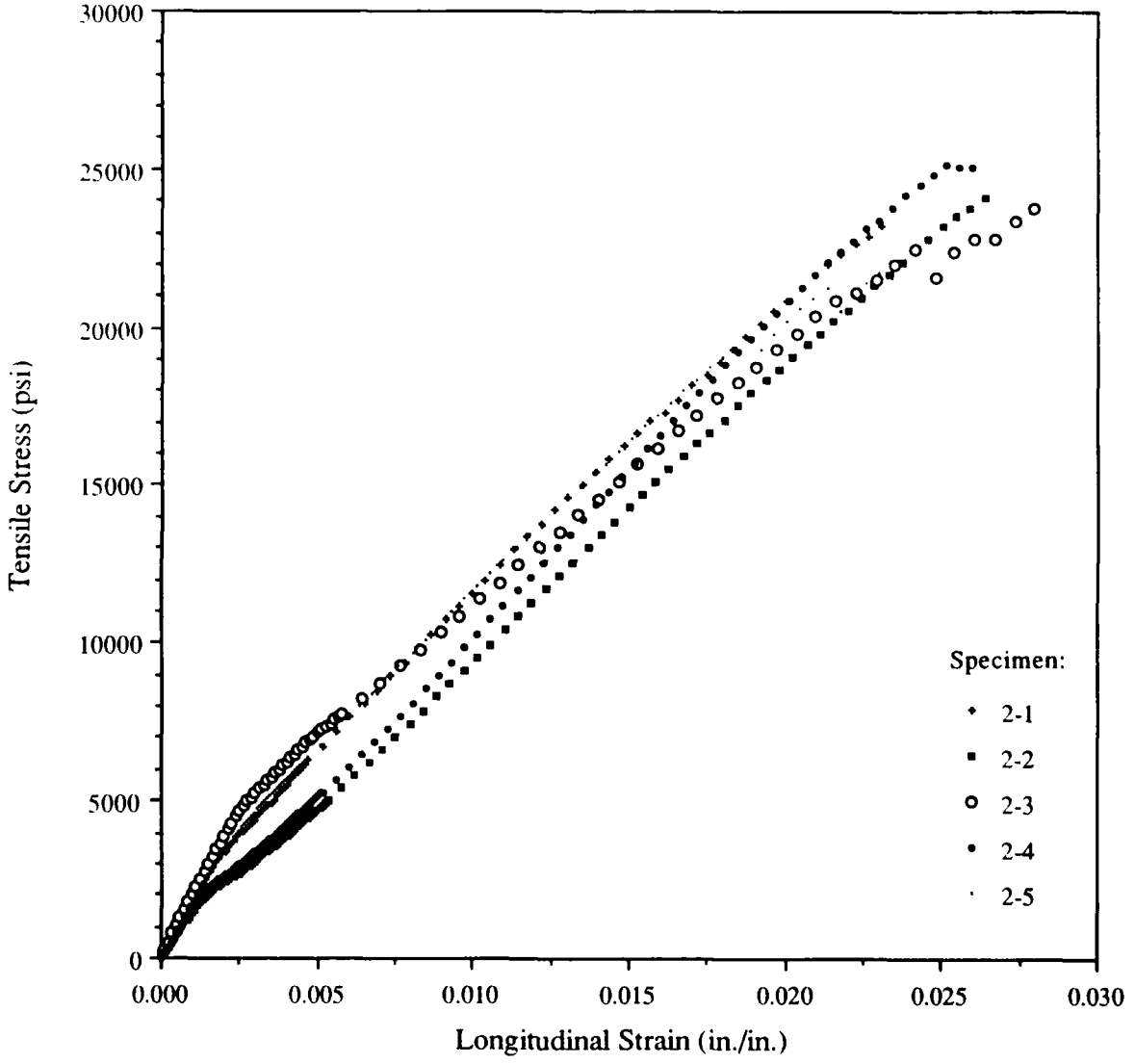

Figure A-3: Tensile Stress vs. Strain for Panel-2 (E-Glass/DERAKANE® 510A) Lower Face Based on Load Deformation Analysis

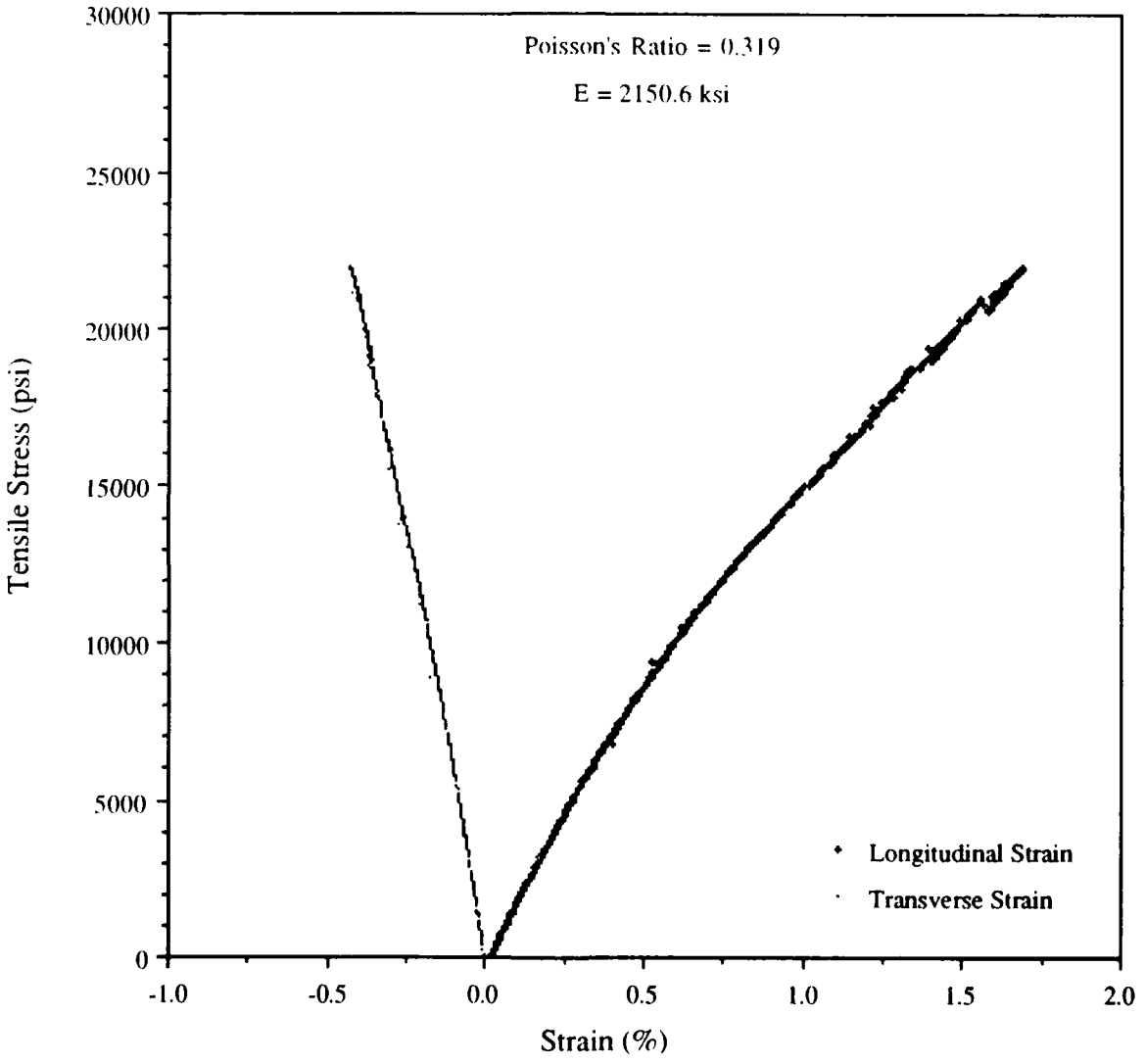

Figure A-4: Tensile Stress vs. Strain for Panel Specimen 2-5 Based on Bi-axial Strain Gage Measurements

Table A-7: Panel-3 Tensile Specimen Dimensions

Specimen ID	Width (in)	Thickness (in)
Panel 3-1	0.999	0.145
Panel 3-2	0.997	0.142
Panel 3-3	0.996	0.144
Panel 3-4	0.998	0.146
Panel 3-5	0.999	0.138

Table A-8: Panel-3 Tensile Test Data

Specimen ID	Maximum Load (lbs)	Maximum Stress (psi)	Max Load Deflection (in)	Maximum Strain (%)	Tensile Modulus (ksi)	Energy to Break (in-lbs)
Panel 3-1	3578	24701	0.32187	3.39	1592.55	636.2
Panel 3-2	3297.8	23294	0.34841	3.67	1453.38	641.4
Panel 3-3	3464	24152	0.33358	3.51	1462.45	631.2
Panel 3-4	3143.7	21575	0.19876	2.09	1628.93	362.3
Panel 3-5	3352.6	24319	0.2537	2.67	1773.80	470.4

Table A-9: Panel-3 Tensile Test Data Statistics

Statistic	Maximum Load (lbs)	Maximum Stress (psi)	Max Load Deflection (in)	Maximum Strain (%)	Tensile Modulus (ksi)	Energy to Break (in-lbs)
Mean	3367	23608	0.291264	3.07	1582.22	548.3
SDEV	165	1248	0.063169	0.66	132.23	126.42
CVAR	4.90	5.28	21.69	21.69	8.36	23.06
Minimum	3144	21575	0.19876	2.09	1453.38	362.3
Maximum	3578	24701	0.34841	3.67	1773.80	641.4

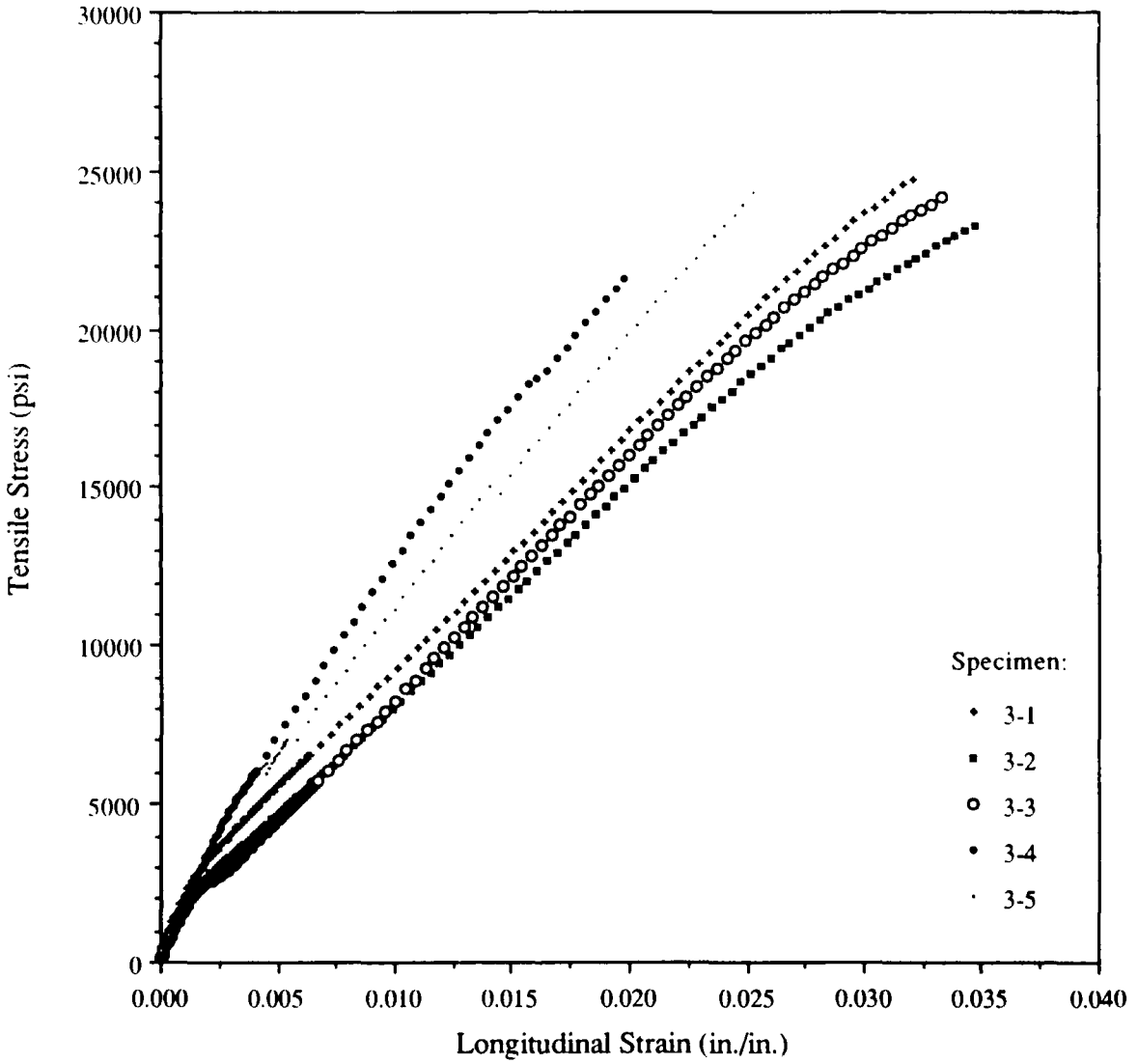

Figure A-5: Tensile Stress vs. Strain for Panel-3 (Kevlar/DERAKANE® 510A) Lower Face Based on Load Deformation Analysis

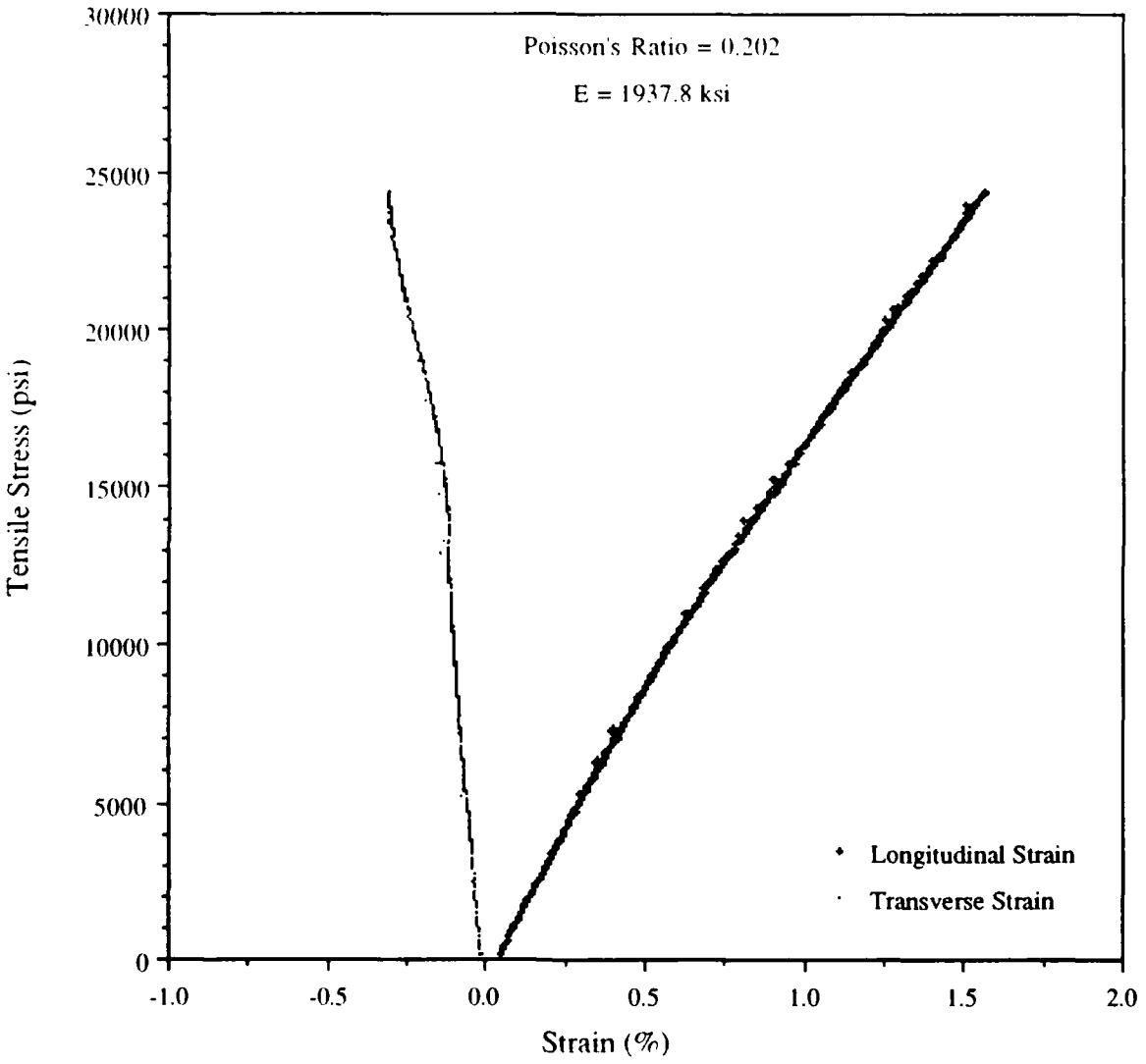

Figure A-6: Tensile Stress VS. Strain for Panel Specimen 3-5 Based on Bi-axial Strain Gage Measurements

Table A-10: Panel-4 Tensile Specimen Dimensions

Specimen ID	Width (in)	Thickness (in)
Panel 4-1	0.992	0.145
Panel 4-2	0.998	0.149
Panel 4-3	0.996	0.147
Panel 4-4	0.998	0.148
Panel 4-5	0.996	0.149

Table A-11: Panel-4 Tensile Test Data

Specimen ID	Maximum Load (lbs)	Maximum Stress (psi)	Max Load Deflection (in)	Maximum Strain (%)	Tensile Modulus (ksi)	Energy to Break (in-lbs)
Panel 4-1	2567.6	17850	0.17707	1.86	1521.62	251.7
Panel 4-2	2747.2	18475	0.19608	2.06	1534.74	299.7
Panel 4-3	2752.7	18801	0.19805	2.08	1553.75	326.6
Panel 4-4	3028.5	20504	0.20305	2.14	1566.91	338.1
Panel 4-5	2841	19144	0.19039	2.00	1514.90	311.5

Table A-12: Panel-4 Tensile Test Data Statistics

Statistic	Maximum Load (lbs)	Maximum Stress (psi)	Max Load Deflection (in)	Maximum Strain (%)	Tensile Modulus (ksi)	Energy to Break (in-lbs)
Mean	2787	18955	0.192928	2.03	1538.38	305.52
SDEV	167	989	0.009957	0.10	21.77	33.44
CVAR	6.01	5.22	5.16	5.16	1.41	10.94
Minimum	2568	17850	0.17707	1.86	1514.90	251.7
Maximum	3029	20504	0.20305	2.14	1566.91	338.1

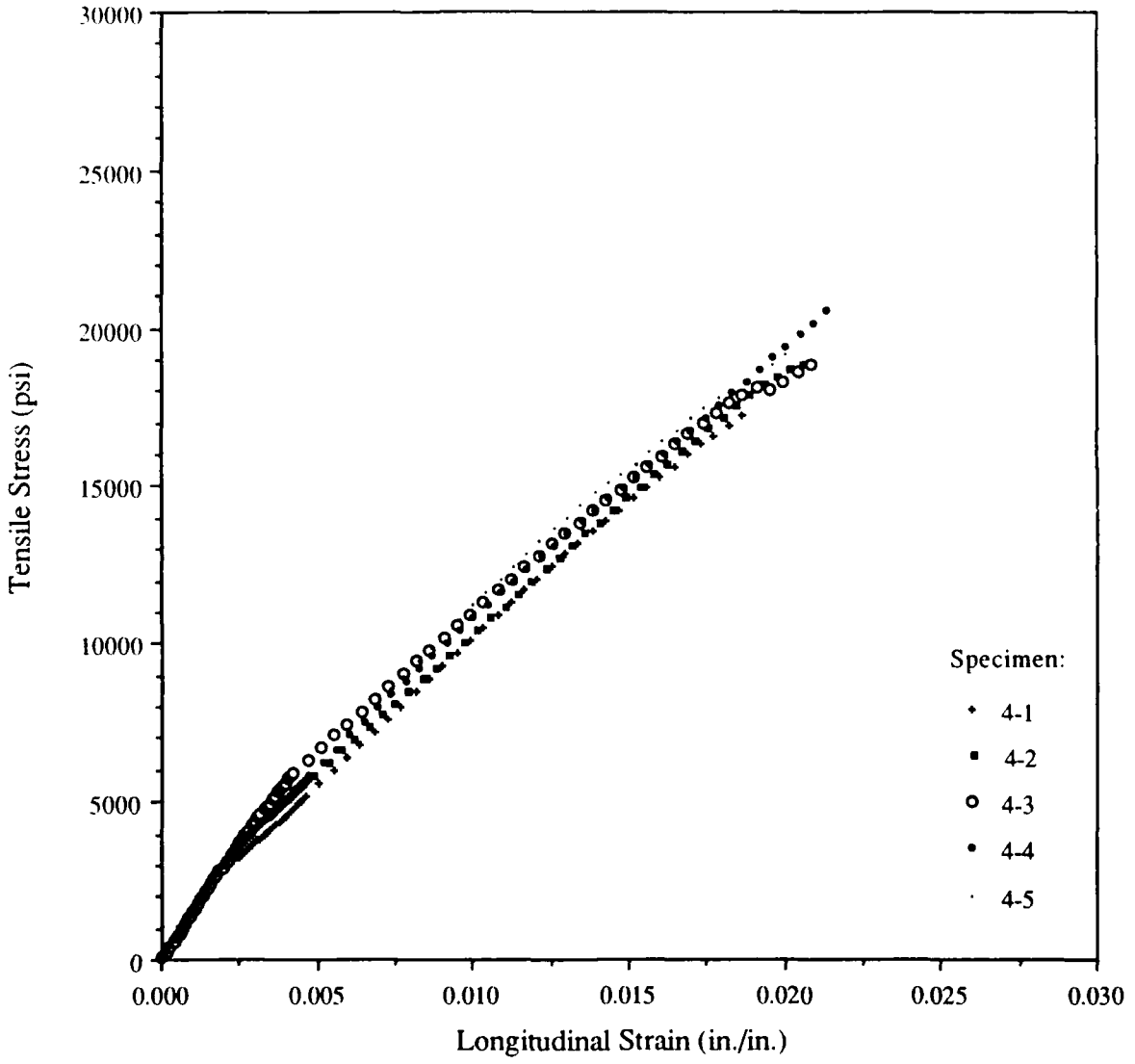

Figure A-7: Tensile Stress vs. Strain for Panel-4 (Kevlar/DERAKANE® 510A) Lower Face Based on Load Deformation Analysis

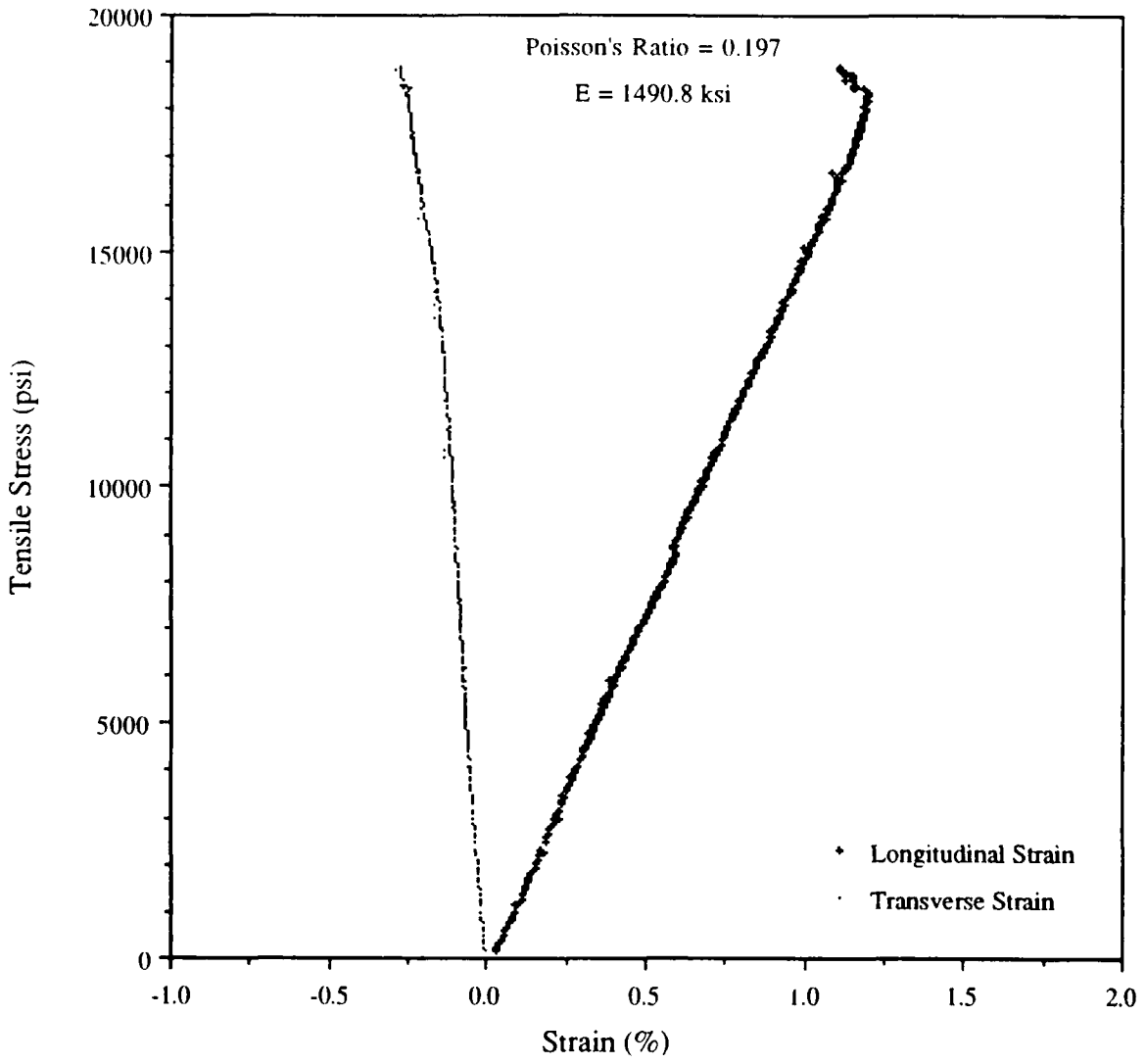

Figure A-8: Tensile Stress VS. Strain for Panel Specimen 4-1 Based on Bi-axial Strain Gage Measurements

Table A-13: Panel-5 Tensile Specimen Dimensions

Specimen ID	Width (in)	Thickness (in)
Panel 5-1	1.01	0.137
Panel 5-2	0.996	0.149
Panel 5-3	1.01	0.14
Panel 5-4	1.007	0.155
Panel 5-5	1.002	0.152

Table A-14: Panel-5 Tensile Test Data

Specimen ID	Maximum Load (lbs)	Maximum Stress (psi)	Max Load Deflection (in)	Maximum Strain (%)	Tensile Modulus (ksi)	Energy to Break (in-lbs)
Panel 5-1	2907.2	21010	0.20865	2.20	1578.76	344.5
Panel 5-2	3041.9	20497	0.168	3.05	1446.64	295.4
Panel 5-3	3120.2	22066	0.23111	2.43	1630.45	414.3
Panel 5-4	2976.4	19069	0.22284	2.35	1391.60	375.7
Panel 5-5	2825.5	18552	0.23617	2.49	1432.51	376.8

Table A-15: Panel-5 Tensile Test Data Statistics

Statistic	Maximum Load (lbs)	Maximum Stress (psi)	Max Load Deflection (in)	Maximum Strain (%)	Tensile Modulus (ksi)	Energy to Break (in-lbs)
Mean	2974	20239	0.213354	2.50	1495.99	361.34
SDEV	115	1433	0.027409	0.33	102.83	44.39
CVAR	3.85	7.08	12.85	13.07	6.87	12.28
Minimum	2826	18552	0.168	2.20	1391.60	295.4
Maximum	3120	22066	0.23617	3.05	1630.45	414.3

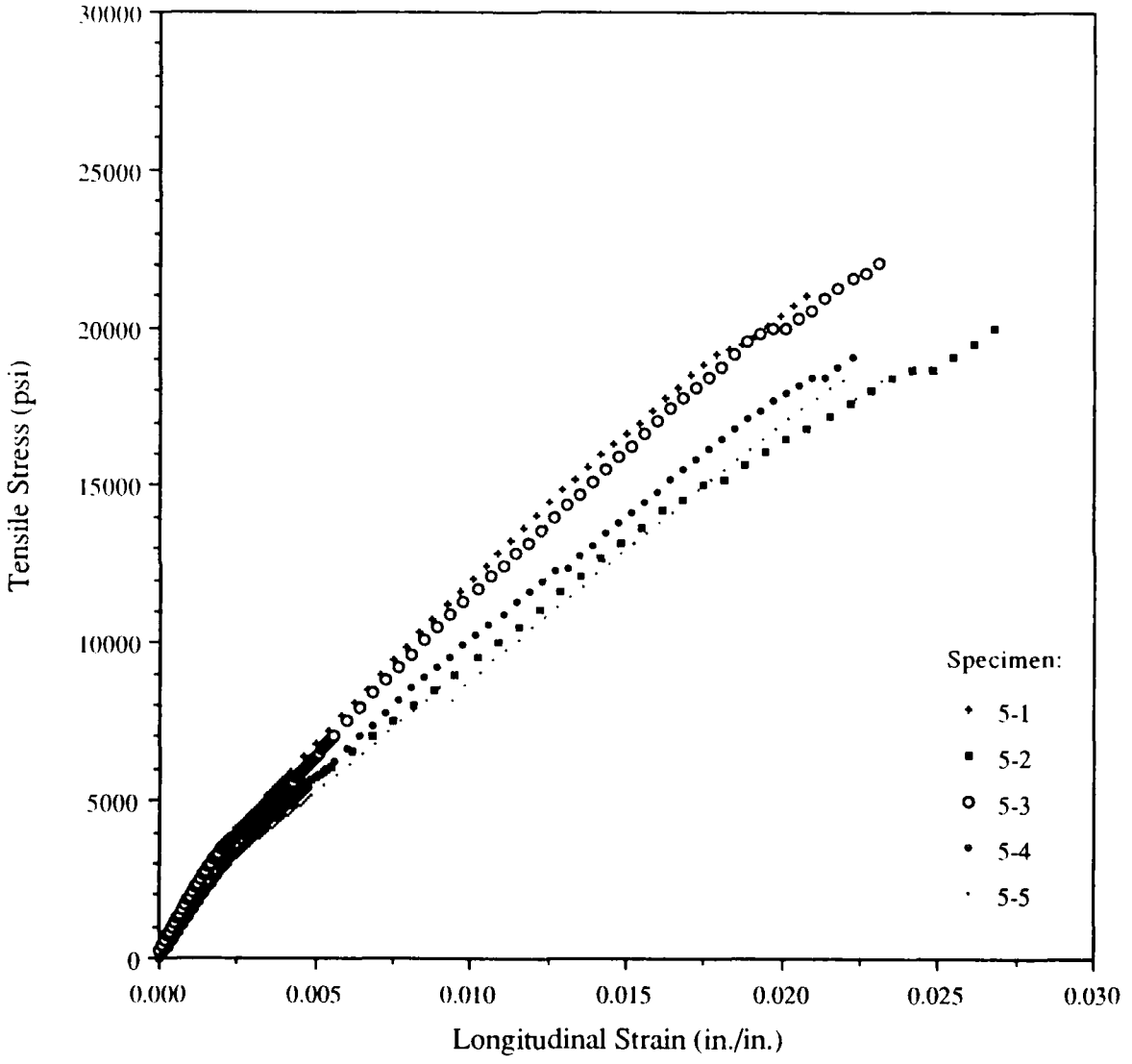

Figure A-9: Tensile Stress vs. Strain for Panel-5 (Kevlar/DERAKANE® 8084) Lower Face Based on Load Deformation Analysis

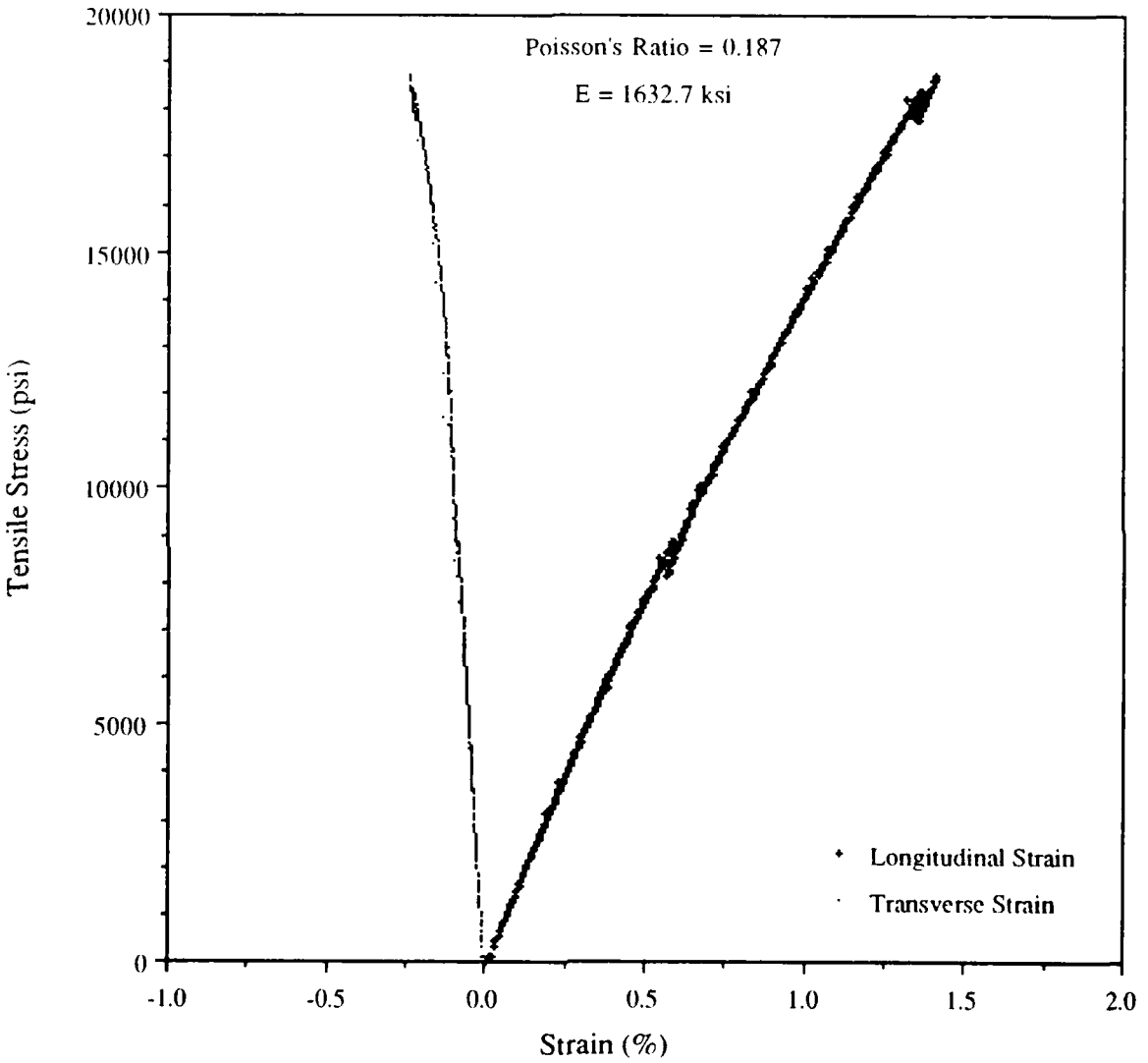

Figure A-10: Tensile Stress vs. Strain for Panel Specimen 5-1 Based on Bi-axial Strain Gage Measurements

Table A-16: Panel-6 Tensile Specimen Dimensions

Specimen ID	Width (in)	Thickness (in)
Panel 6-1	1.01	0.148
Panel 6-2	1.001	0.153
Panel 6-3	1.017	0.148
Panel 6-4	1.015	0.141
Panel 6-5	1.01	0.151

Table A-17: Panel-6 Tensile Test Data

Specimen ID	Maximum Load (lbs)	Maximum Stress (psi)	Max Load Deflection (in)	Maximum Strain (%)	Tensile Modulus (ksi)	Energy to Break (in-lbs)
Panel 6-1	2942.9	19688	0.20205	2.13	1525.16	332.1
Panel 6-2	2929.3	19127	0.21819	2.30	1494.66	356.4
Panel 6-3	3011.5	20008	0.20696	2.18	1503.05	353.3
Panel 6-4	3231.5	22580	0.21385	2.25	1555.15	382.6
Panel 6-5	2891.2	18957	0.20857	2.20	1500.22	335.3

Table A-18: Panel-6 Tensile Test Data Statistics

Statistic	Maximum Load (lbs)	Maximum Stress (psi)	Max Load Deflection (in)	Maximum Strain (%)	Tensile Modulus (ksi)	Energy to Break (in-lbs)
Mean	3001	20072	0.209924	2.21	1515.65	351.94
SDEV	136	1464	0.006252	0.07	24.94	20.20
CVAR	4.53	7.30	2.98	2.98	1.65	5.74
Minimum	2891	18957	0.20205	2.13	1494.66	332.1
Maximum	3232	22580	0.21819	2.30	1555.15	382.6

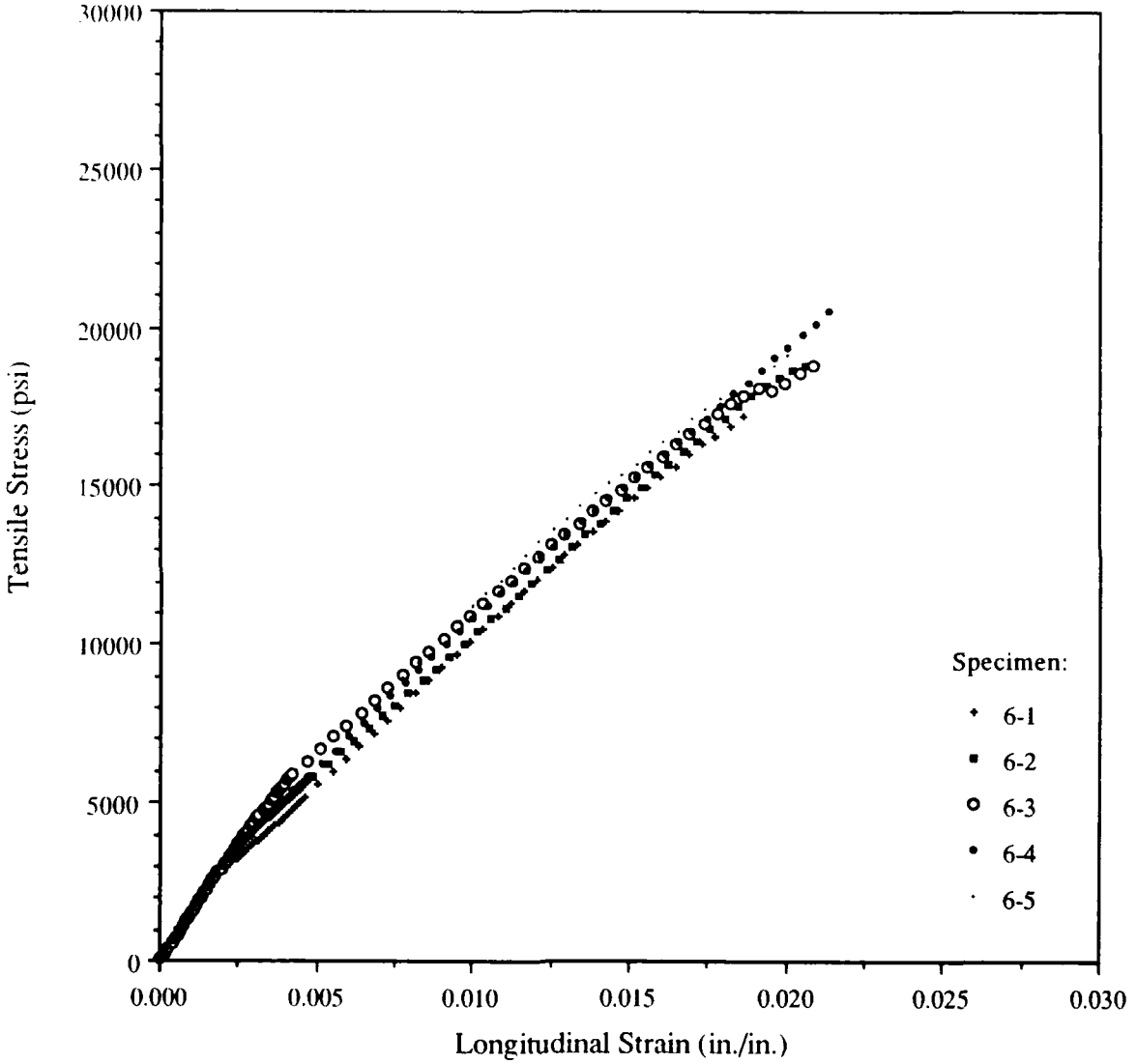

Figure A-11: Tensile Stress vs. Strain for Panel-6 (Kevlar/DERAKANE® 8084) Lower Face Based on Load Deformation Analysis

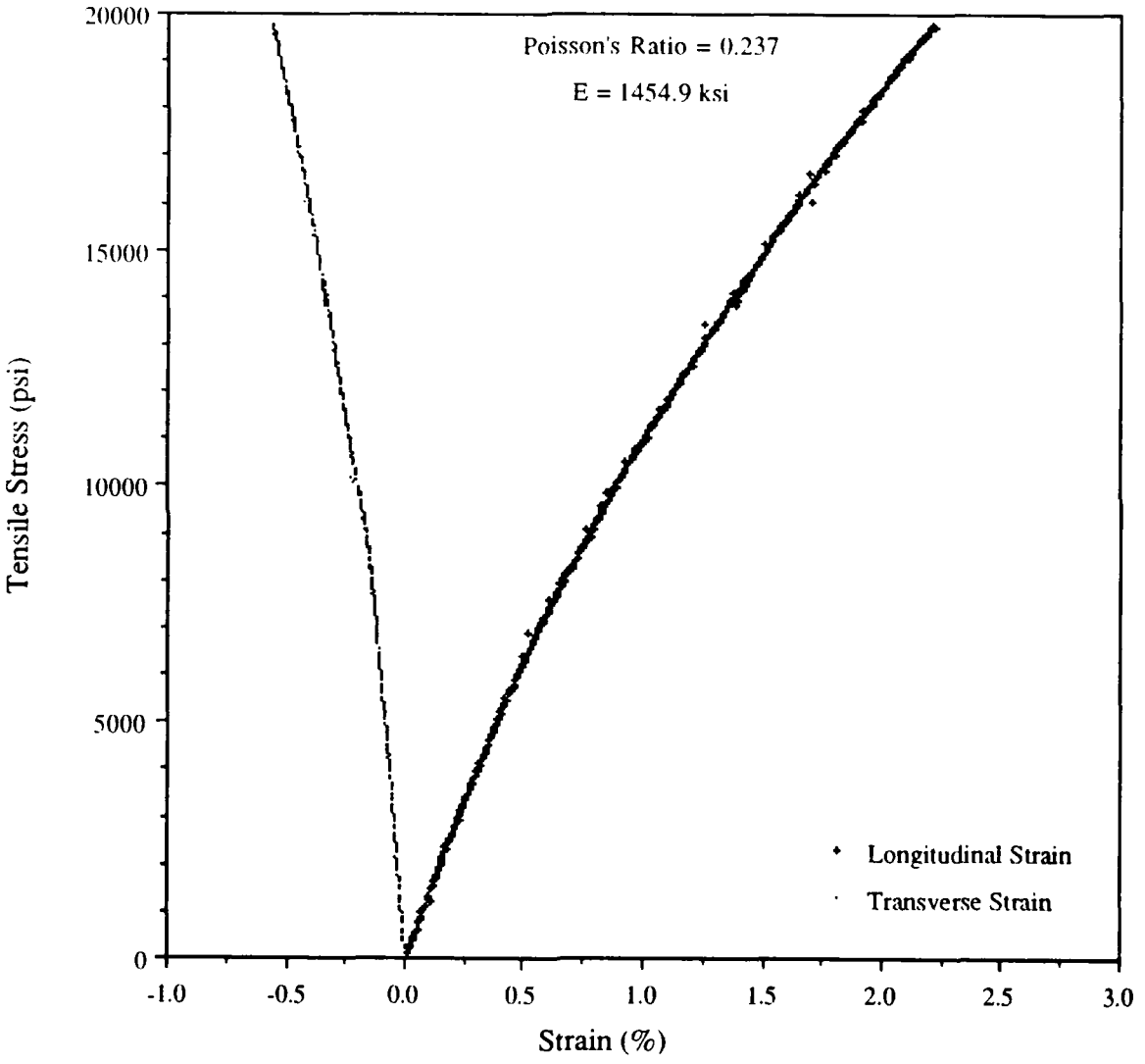

Figure A-12: Tensile Stress vs. Strain for Panel Specimen 6-2 Based on Bi-axial Strain Gage Measurements

APPENDIX B

COMPRESSIVE CHARACTERISTICS OF TEST PANEL LOWER FACES

Table B-1: Panel-1 Compressive Specimen Dimensions

Specimen ID	Width (in)	Thickness (in)
Panel 1-1	3.989	0.171
Panel 1-2	3.981	0.171
Panel 1-3	3.968	0.168
Panel 1-4	3.972	0.172
Panel 1-5	3.966	0.168

Table B-2: Panel-1 Compressive Test Data

Specimen ID	Maximum Load (lbs)	Maximum Stress (psi)	Max Load Deflection (in)	Maximum Strain (%)	Elastic Modulus (ksi)	Energy to Break (in-lbs)
Panel 1-1	12010	17607	0.133	2.42	1152	794.9
Panel 1-2	11324	16635	0.14275	2.60	1107	813.6
Panel 1-3	11277	16917	0.12442	2.26	1125	581.9
Panel 1-4	13562	19851	0.12902	2.35	1193	847.7
Panel 1-5	11201	16811	0.135	2.45	1154	771.8

Table B-3: Panel-1 Compressive Test Data Statistics

Statistic	Maximum Load (lbs)	Maximum Stress (psi)	Max Load Deflection (in)	Maximum Strain (%)	Elastic Modulus (ksi)	Energy to Break (in-lbs)
Mean	11875	17564	0.132838	2.42	1146.2	761.98
SDEV	997	1331	0.006863	0.12	32.68	104.43
CVAR	8.4	7.58	5.17	5.17	2.85	13.7
Minimum	11201	16635	0.12442	2.26	1107	581.9
Maximum	13562	19851	0.14275	2.60	1193	847.7

SDEV - Standard Deviation
CVAR - Coefficient of Variation (%)

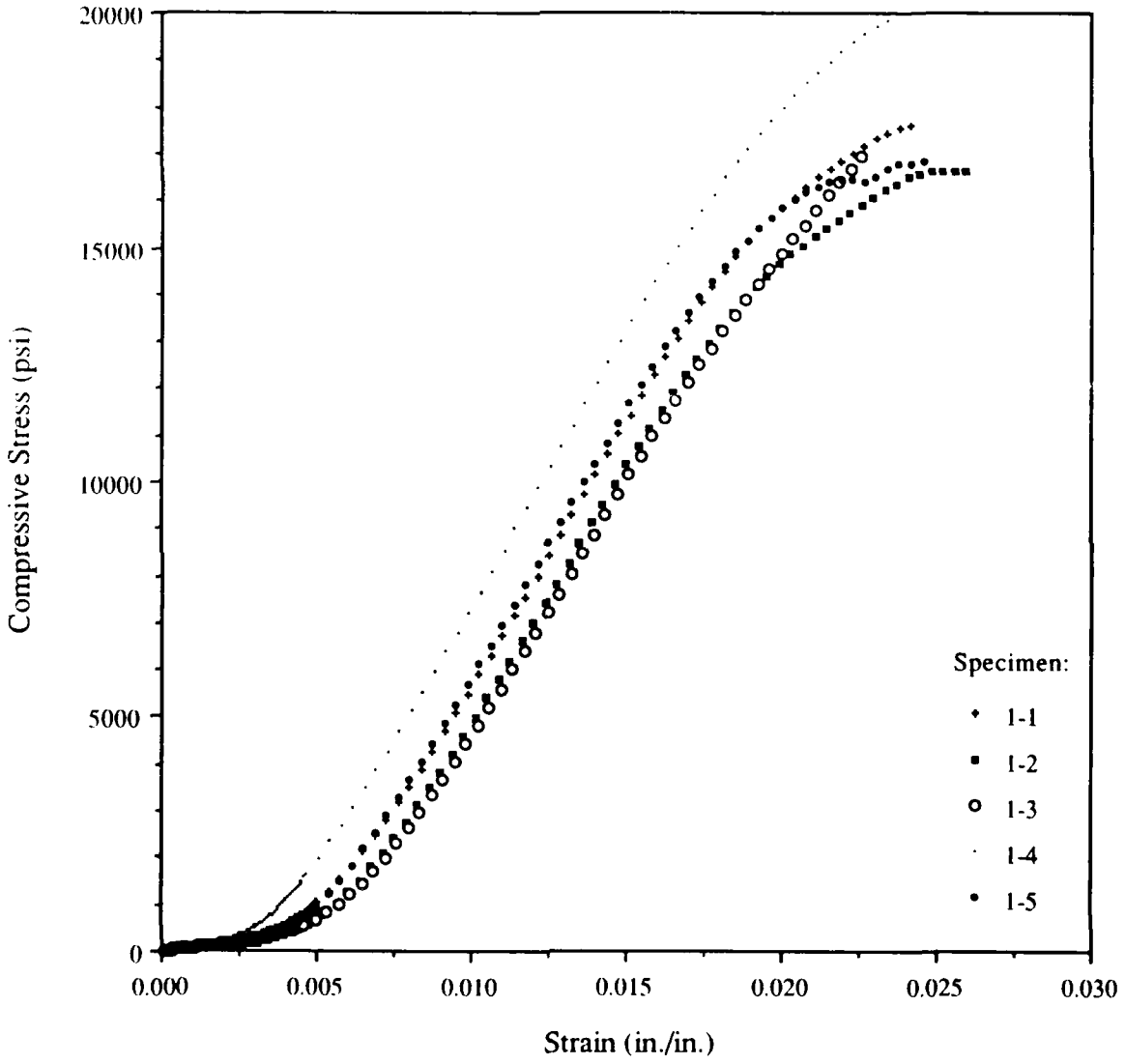

Figure B-1: Compressive Stress vs. Strain for Panel-1 Lower Face (E-Glass/DERAKANE® 510A)

Table B-4: Panel-2 Compressive Specimen Dimensions

Specimen ID	Width (in)	Thickness (in)
Panel 2-1	4.001	0.168
Panel 2-2	4.002	0.159
Panel 2-3	3.998	0.171
Panel 2-4	4.008	0.173
Panel 2-5	4.009	0.166

Table B-5: Panel-2 Compressive Test Data

Specimen ID	Maximum Load (lbs)	Maximum Stress (psi)	Max Load Deflection (in)	Maximum Strain (%)	Elastic Modulus (ksi)	Energy to Break (in-lbs)
Panel 2-1	12869	19146	0.13169	2.39	1230	821.1
Panel 2-2	11878	18667	0.13494	2.45	1272	870.7
Panel 2-3	10849	15869	0.11794	2.14	1213	657.6
Panel 2-4	11065	15958	0.12268	2.23	1143	760.2
Panel 2-5	11389	17114	0.11946	2.17	1207	803.7

Table B-6: Panel-2 Compressive Test Data Statistics

Statistic	Maximum Load (lbs)	Maximum Stress (psi)	Max Load Deflection (in)	Maximum Strain (%)	Elastic Modulus (ksi)	Energy to Break (in-lbs)
Mean	11610	17351	0.125342	2.28	1213	782.66
SDEV	803	1512	0.007565	0.14	46.65	80.34
CVAR	6.92	8.71	6.04	6.04	3.85	10.26
Minimum	10849	15869	0.11794	2.14	1143	657.6
Maximum	12869	19146	0.13494	2.45	1272	870.7

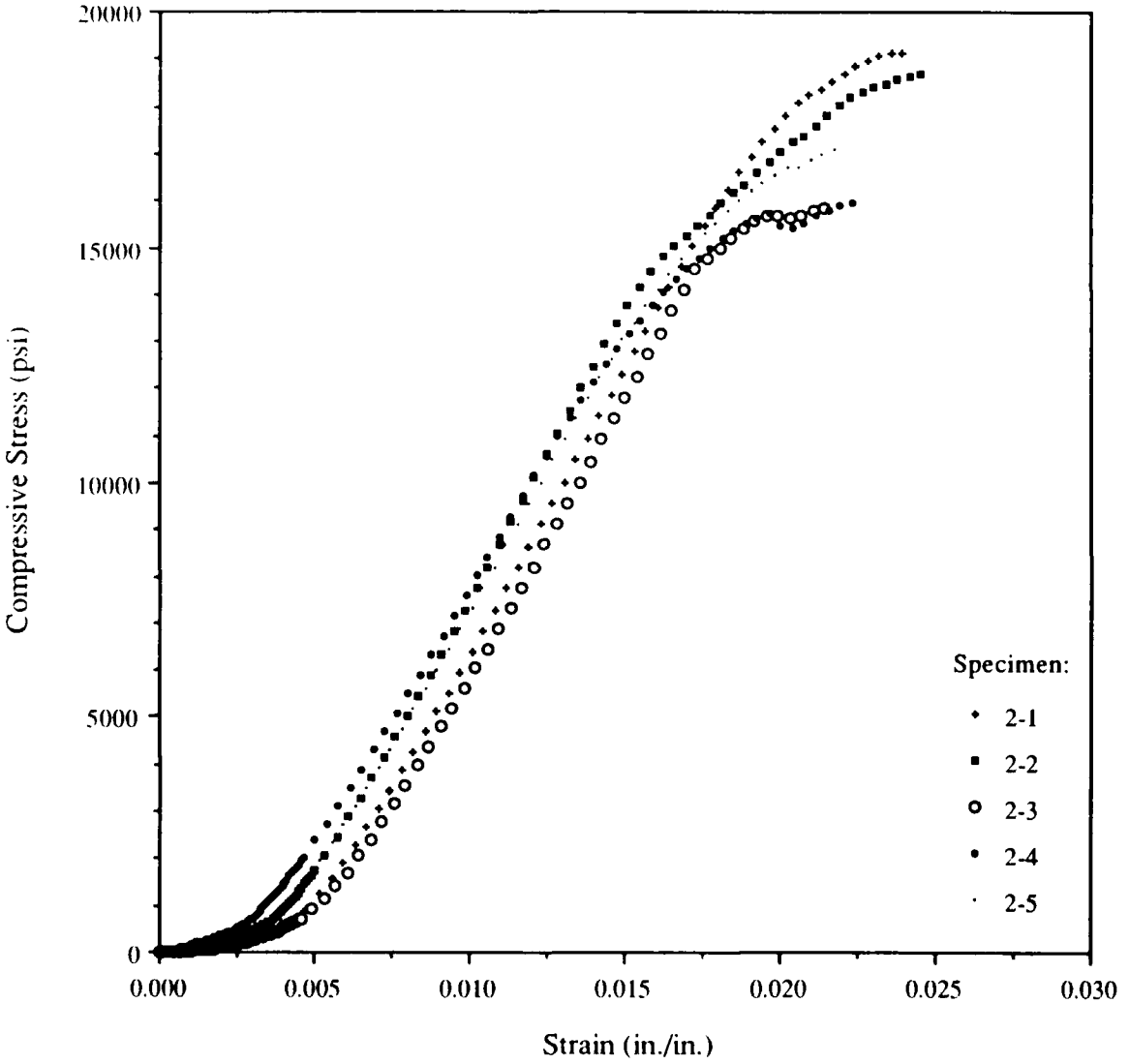

Figure B-2: Compressive Stress vs. Strain for Panel-2 Lower Face (E-Glass/DERAKANE® 510A)

Table B-7: Panel-3 Compressive Specimen Dimensions

Specimen ID	Width (in)	Thickness (in)
Panel 3-1	4.003	0.147
Panel 3-2	3.971	0.138
Panel 3-3	3.949	0.134
Panel 3-4	3.934	0.141
Panel 3-5	3.994	0.147

Table B-8: Panel-3 Compressive Test Data

Specimen ID	Maximum Load (lbs)	Maximum Stress (psi)	Max Load Deflection (in)	Maximum Strain (%)	Elastic Modulus (ksi)	Energy to Break (in-lbs)
Panel 3-1	4755.6	8082	0.11624	2.11	641.5	413.1
Panel 3-2	4934.1	9004	0.13157	2.39	823.1	330.7
Panel 3-3	4564.5	8626	0.11213	2.04	868.2	383.4
Panel 3-4	5174.6	9329	0.11743	2.14	805.8	328.5
Panel 3-5	4631.5	7889	0.1411	2.57	735	361

Table B-9: Panel-3 Compressive Test Data Statistics

Statistic	Maximum Load (lbs)	Maximum Stress (psi)	Max Load Deflection (in)	Maximum Strain (%)	Elastic Modulus (ksi)	Energy to Break (in-lbs)
Mean	4812	8586	0.123694	2.25	774.72	363.34
SDEV	247	606	0.012181	0.22	88.56	35.93
CVAR	5.13	7.06	9.85	9.85	11.43	9.89
Minimum	4565	7889	0.11213	2.04	641.5	328.5
Maximum	5175	9329	0.1411	2.57	868.2	413.1

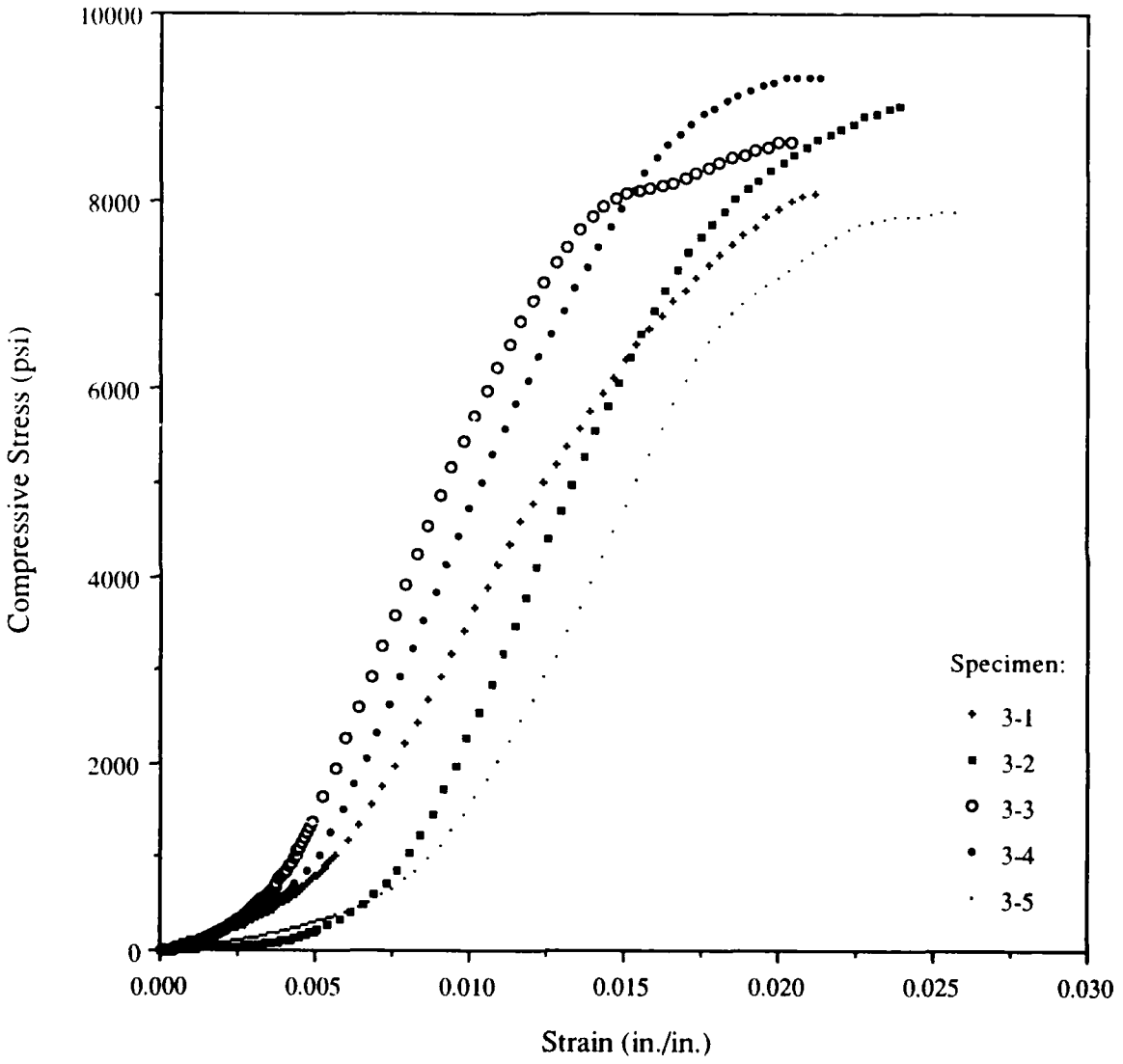

Figure B-3: Compressive Stress vs. Strain for Panel-3 Lower Face (Kevlar/DERAKANE® 510A)

Table B-10: Panel-4 Compressive Specimen Dimensions

Specimen ID	Width (in)	Thickness (in)
Panel 4-1	3.978	0.156
Panel 4-2	3.98	0.146
Panel 4-3	4.002	0.143
Panel 4-4	3.973	0.153
Panel 4-5	3.978	0.139

Table B-11: Panel-4 Compressive Test Data

Specimen ID	Maximum Load (lbs)	Maximum Stress (psi)	Max Load Deflection (in)	Maximum Strain (%)	Elastic Modulus (ksi)	Energy to Break (in-lbs)
Panel 4-1	5637.2	9084	0.1291	2.35	699.7	477.8
Panel 4-2	5148.8	8861	0.13448	2.45	729.6	391.3
Panel 4-3	5276.2	9220	0.13453	2.45	722.9	402.5
Panel 4-4	5286.3	8696	0.12874	2.34	701.9	435.4
Panel 4-5	5151.6	9317	0.13624	2.48	733.3	405.3

Table B-12: Panel-4 Compressive Test Data Statistics

Statistic	Maximum Load (lbs)	Maximum Stress (psi)	Max Load Deflection (in)	Maximum Strain (%)	Elastic Modulus (ksi)	Energy to Break (in-lbs)
Mean	5300	9035	0.132618	2.41	717.48	422.46
SDEV	200	255	0.003452	0.06	15.70	34.98
CVAR	3.77	2.83	2.60	2.60	2.19	8.28
Minimum	5149	8696	0.12874	2.34	699.7	391.3
Maximum	5637	9317	0.13624	2.48	733.3	477.8

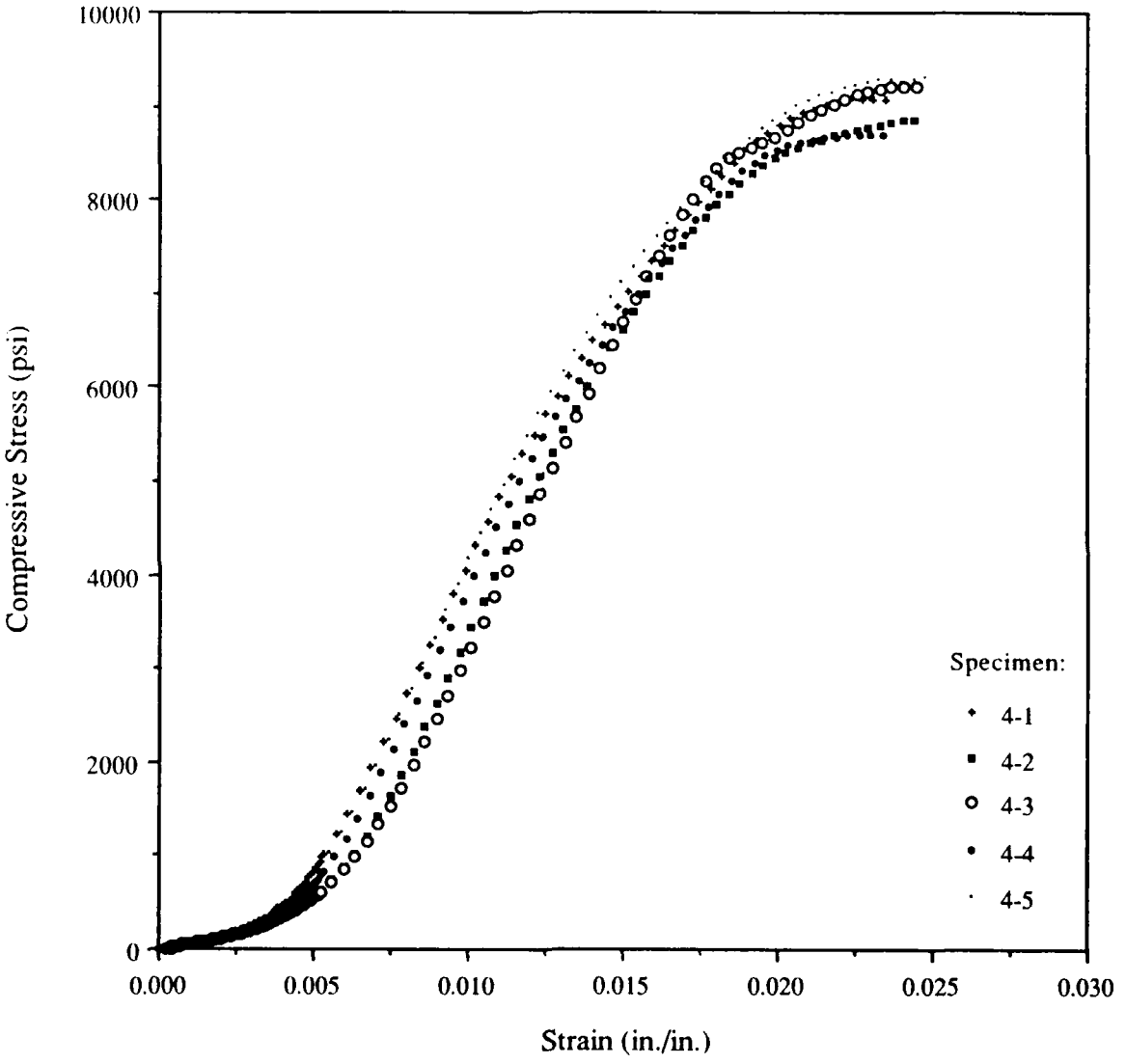

Figure B-4: Compressive Stress vs. Strain for Panel-4 Lower Face (Kevlar/DERAKANE® 510A)

Table B-13: Panel-5 Compressive Specimen Dimensions

Specimen ID	Width (in)	Thickness (in)
Panel 5-1	3.97	0.138
Panel 5-2	3.954	0.139
Panel 5-3	3.964	0.143
Panel 5-4	3.975	0.133
Panel 5-5	3.971	0.146

Table B-14: Panel-5 Compressive Test Data

Specimen ID	Maximum Load (lbs)	Maximum Stress (psi)	Max Load Deflection (in)	Maximum Strain (%)	Elastic Modulus (ksi)	Energy to Break (in-lbs)
Panel 5-1*	3518.4	6422	0.10282	1.87	627.7	180.9
Panel 5-2*	3399.5	6185	0.10928	1.99	640.3	154.4
Panel 5-3	4184.3	7382	0.13203	2.40	660.7	338.9
Panel 5-4	3643.1	6891	0.13845	2.52	648.8	336.2
Panel 5-5	5735.7	9893	0.099926	1.82	864.7	336.5

Table B-15: Panel-5 Compressive Test Data Statistics

Statistic	Maximum Load (lbs)	Maximum Stress (psi)	Max Load Deflection (in)	Maximum Strain (%)	Elastic Modulus (ksi)	Energy to Break (in-lbs)
Mean	4521	8055	0.123469	2.24	725	337.20
SDEV	1086	1610	0.020640	0.38	121.36	1.48
CVAR	24.03	19.99	16.72	16.72	16.75	0.44
Minimum	3643	6891	0.099926	1.82	648.8	336
Maximum	5736	9893	0.13845	2.52	864.7	339

* Specimen 5-1 and 5-2 not counted in statistics due to local buckling at top of test fixture.

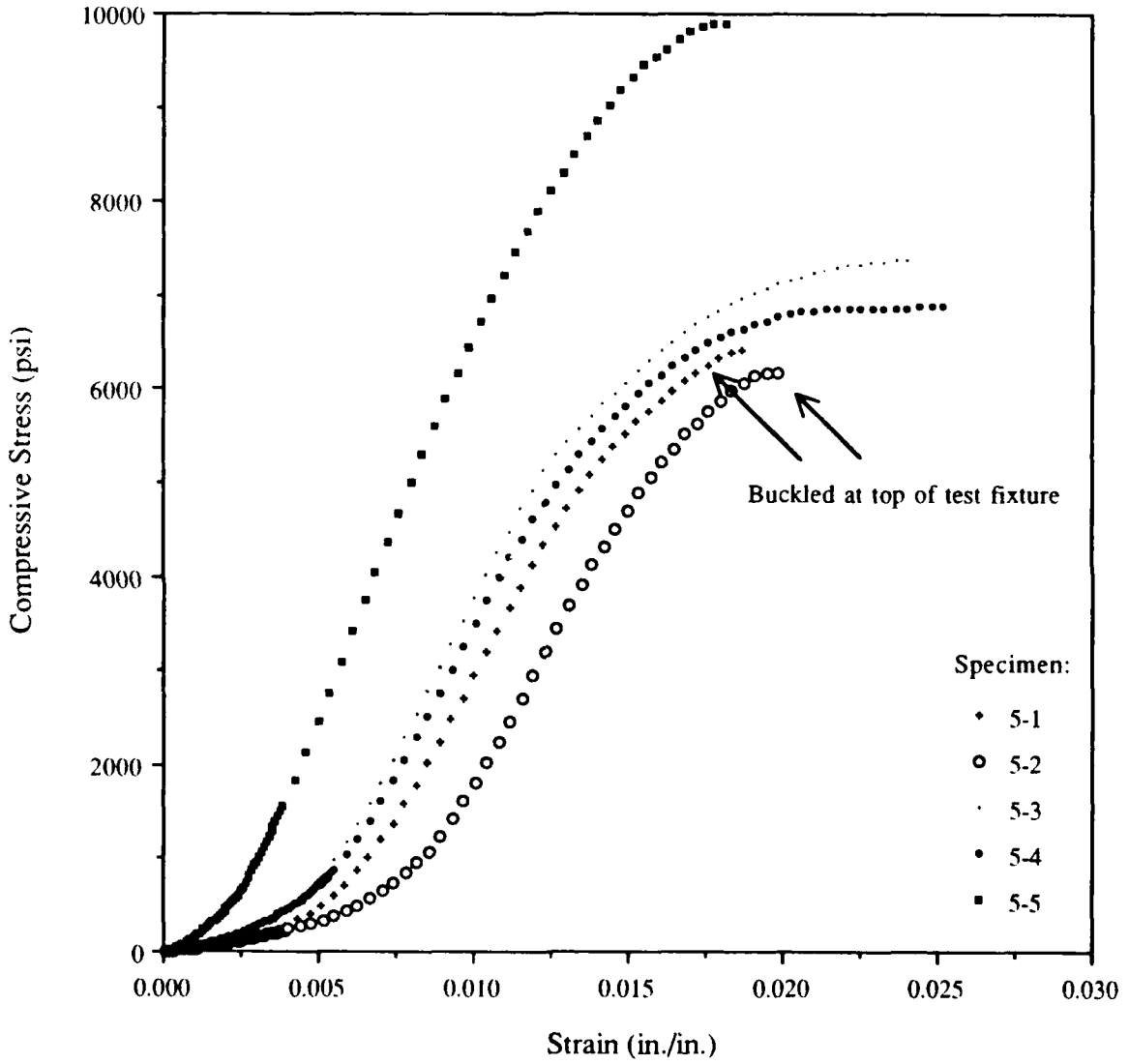

Figure B-5: Compressive Stress vs. Strain for Panel-5 Lower Face (Kevlar/DERAKANE® 8084)

Table B-16: Panel-6 Compressive Specimen Dimensions

Specimen ID	Width (in)	Thickness (in)
Panel 6-1	3.966	0.144
Panel 6-2	3.958	0.14
Panel 6-3	3.97	0.137
Panel 6-4	3.976	0.147
Panel 6-5	3.98	0.148

Table B-17: Panel-6 Compressive Test Data

Specimen ID	Maximum Load (lbs)	Maximum Stress (psi)	Max Load Deflection (in)	Maximum Strain (%)	Elastic Modulus (ksi)	Energy to Break (in-lbs)
Panel 6-1	4968.5	8700	0.16542	3.01	628.4	454.8
Panel 6-2	5429.9	9799	0.16711	3.04	897.1	462.7
Panel 6-3*	3555.4	6537	0.11086	2.02	666.3	275
Panel 6-4	5655.7	9677	0.18062	3.28	648.3	546.2
Panel 6-5	5553.9	9429	0.1473	2.68	733.3	536.6

Table B-18: Panel-6 Compressive Test Data Statistics

Statistic	Maximum Load (lbs)	Maximum Stress (psi)	Max Load Deflection (in)	Maximum Strain (%)	Elastic Modulus (ksi)	Energy to Break (in-lbs)
Mean	5402	9401	0.165113	3.00	726.78	500.075
SDEV	867	1350	0.027002	0.49	109.33	108.90
CVAR	16.04	14.36	16.35	16.35	15.04	21.78
Minimum	4969	8700	0.1473	2.68	628.4	454.8
Maximum	5656	9799	0.18062	3.28	897.1	546.2

* Specimen 6-3 not counted in statistics due to local buckling at top of test fixture.

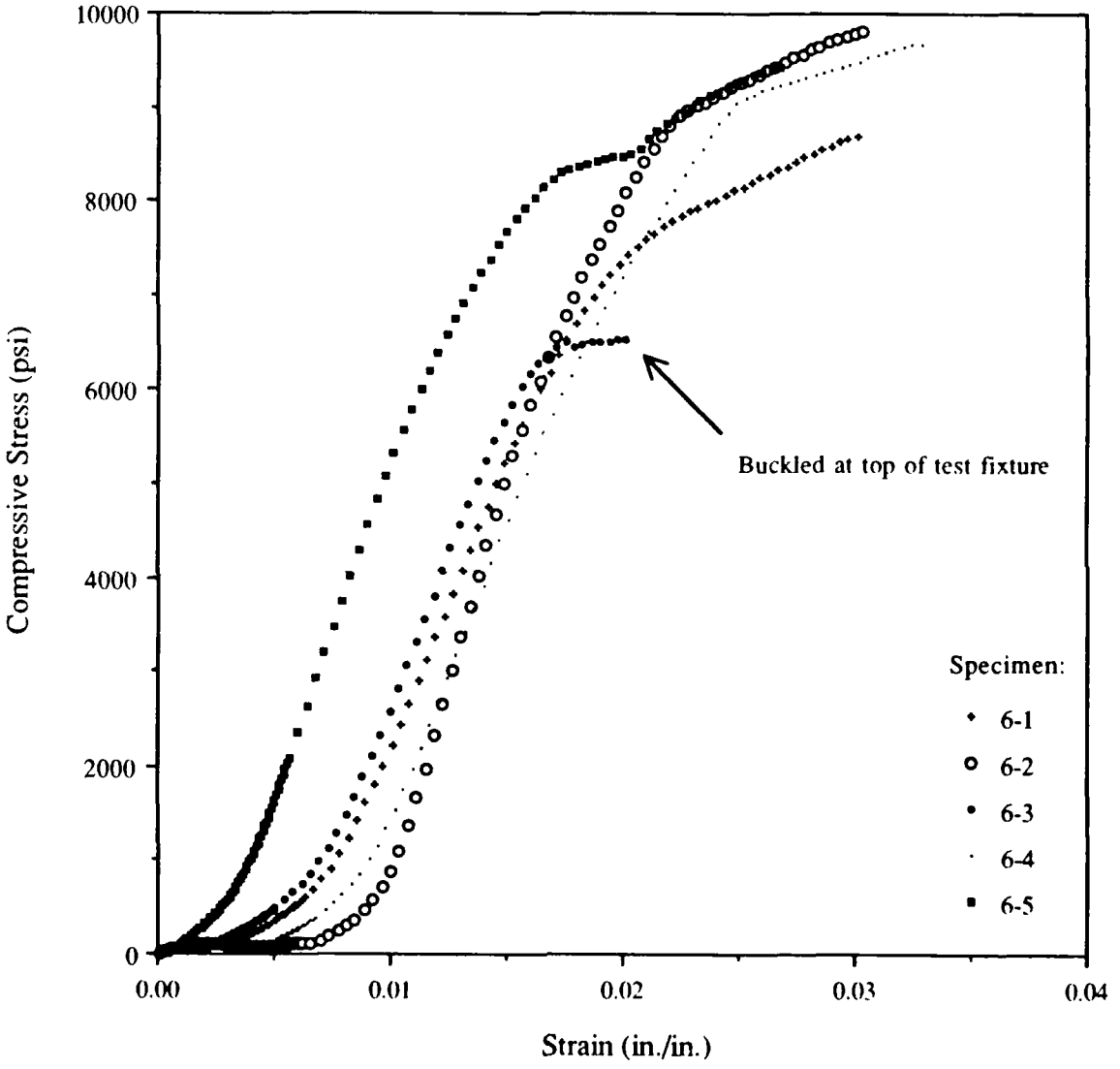

Figure B-6: Compressive Stress vs. Strain for Panel-6 Lower Face (Kevlar/DERAKANE® 8084)

APPENDIX C

FLEXURAL CHARACTERISTICS OF TEST PANEL LOWER FACES

Table C-1: Panel-1 Flexural Specimen Dimensions (Method I)

Specimen ID	Width (in)	Thickness (in)
Panel 1-1	0.494	0.169
Panel 1-2	0.494	0.169
Panel 1-3	0.499	0.166
Panel 1-4	0.504	0.171
Panel 1-5	0.503	0.165

Table C-2: Panel-1 Flexural Test Data (Method I)

Specimen ID	Maximum Load (lbs)	Maximum Stress (psi)	Max Load Deflection (in)	Maximum Strain (%)	Linear Slope (lb/in)	Flexural Modulus (ksi)
Panel 1-1	59.968	45694	1.1382	3.21	73.66	1668
Panel 1-2	60.789	46499	1.1509	3.24	69.72	1579
Panel 1-3	54.933	43858	1.2051	3.33	64.80	1533
Panel 1-4	53.247	42234	1.3972	3.98	59.88	1283
Panel 1-5	48.488	38145	1.1436	3.14	61.15	1461

Table C-3: Panel-1 Flexural Test Data Statistics (Method I)

Statistic	Maximum Load (lbs)	Maximum Stress (psi)	Max Load Deflection (in)	Maximum Strain (%)	Linear Slope (lb/in)	Flexural Modulus (ksi)
Mean	55.49	43286	1.207	3.38	65.84	1504.90
SDEV	5.06	3316	0.109636	0.34	5.80	144.89
CVAR	9.12	7.66	9.08	10.13	8.81	9.63
Minimum	48.488	38145	1.1382	3.14	59.88	1283
Maximum	60.789	46499	1.3972	3.98	73.66	1668

SDEV - Standard Deviation
CVAR - Coefficient of Variation (%)

Table C-4: Panel-1 Flexural Specimen Dimensions (Method II)

Specimen ID	Width (in)	Thickness (in)
Panel 1-1	0.568	0.179
Panel 1-2	0.553	0.176
Panel 1-3	0.502	0.173
Panel 1-4	0.513	0.171
Panel 1-5	0.525	0.173

Table C-5: Panel-1 Flexural Test Data (Method II)

Specimen ID	Maximum Load (lbs)	Maximum Stress (psi)	Max Load Deflection (in)	Maximum Strain (%)	Linear Slope (lb/in)	Flexural Modulus (ksi)
Panel 1-1	147.42	36451	0.22954	1.37	668.02	1384
Panel 1-2	128.85	33849	0.20753	1.22	684.69	1533
Panel 1-3	118.44	35474	0.20597	1.19	636.60	1653
Panel 1-4	143.03	42907	0.27191	1.55	618.32	1627
Panel 1-5	119.02	34086	0.21415	1.23	633.23	1572

Table C-6: Panel-1 Flexural Test Data Statistics (Method II)

Statistic	Maximum Load (lbs)	Maximum Stress (psi)	Max Load Deflection (in)	Maximum Strain (%)	Linear Slope (lb/in)	Flexural Modulus (ksi)
Mean	131.35	36554	0.22582	1.31	648.17	1553.97
SDEV	13.41	3706	0.027399	0.15	27.28	105.84
CVAR	10.21	10.14	12.13	11.45	4.21	6.81
Minimum	118.44	33849	0.20597	1.19	618.32	1384
Maximum	147.42	42907	0.27191	1.55	684.69	1653

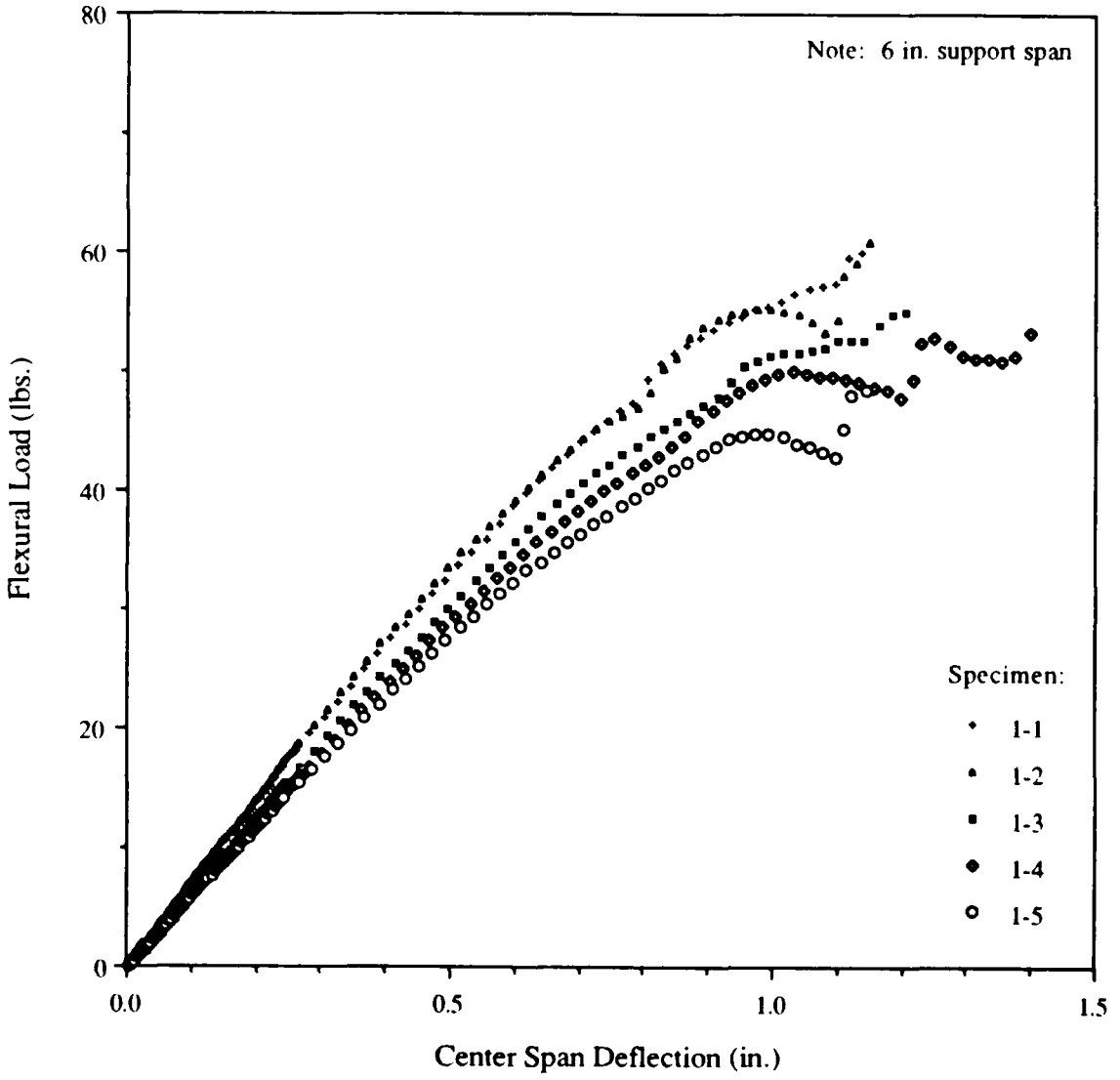

Figure C-1: Flexural Load vs. Center Span Deflection for Panel-1 Lower Face with CSM Ply in Compression and 1808 E-Glass 0° Ply in Tension

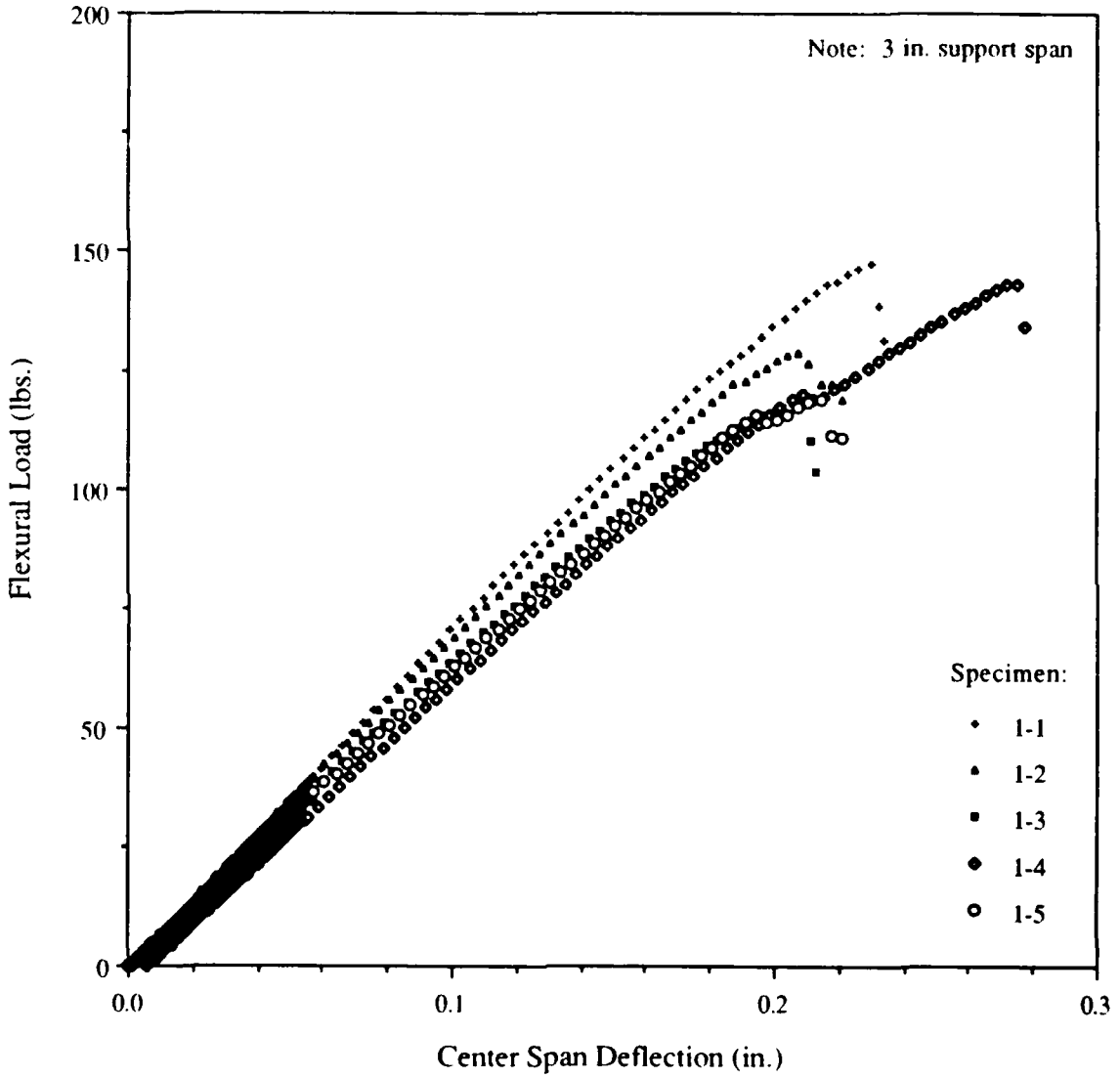

Figure C-2: Flexural Load vs. Center Span Deflection for Panel-1 Lower Face with CSM Ply in Tension and 1808 E-Glass 0° Ply in Compression

Table C-7: Panel-2 Flexural Specimen Dimensions (Method I)

Specimen ID	Width (in)	Thickness (in)
Panel 2-1	0.506	0.158
Panel 2-2	0.505	0.159
Panel 2-3	0.506	0.154
Panel 2-4	0.51	0.157
Panel 2-5	0.504	0.158

Table C-8: Panel-2 Flexural Test Data (Method I)

Specimen ID	Maximum Load (lbs)	Maximum Stress (psi)	Max Load Deflection (in)	Maximum Strain (%)	Linear Slope (lb/in)	Flexural Modulus (ksi)
Panel 2-1	45.13	37125	1.0172	2.68	60.72	1643
Panel 2-2	52.756	44993	1.1762	3.12	60.96	1622
Panel 2-3	48.456	43480	1.1382	2.92	54.96	1606
Panel 2-4	51.134	42788	1.0601	2.77	62.87	1720
Panel 2-5	53.403	45867	1.1513	3.03	68.01	1847

Table C-9: Panel-2 Flexural Test Data Statistics (Method I)

Statistic	Maximum Load (lbs)	Maximum Stress (psi)	Max Load Deflection (in)	Maximum Strain (%)	Linear Slope (lb/in)	Flexural Modulus (ksi)
Mean	50.18	42851	1.1086	2.90	61.50	1687.61
SDEV	3.41	3423	0.067036	0.18	4.69	99.54
CVAR	6.79	7.99	6.05	6.20	7.62	5.90
Minimum	45.13	37125	1.0172	2.68	54.96	1606
Maximum	53.403	45867	1.1762	3.12	68.01	1847

Table C-10: Panel-2 Flexural Specimen Dimensions (Method II)

Specimen ID	Width (in)	Thickness (in)
Panel 2-1	0.497	0.178
Panel 2-2	0.529	0.178
Panel 2-3	0.538	0.179
Panel 2-4	0.518	0.171
Panel 2-5	0.524	0.169

Table C-11: Panel-2 Flexural Test Data (Method II)

Specimen ID	Maximum Load (lbs)	Maximum Stress (psi)	Max Load Deflection (in)	Maximum Strain (%)	Linear Slope (lb/in)	Flexural Modulus (ksi)
Panel 2-1	134.91	38553	0.26526	1.57	617.17	1486
Panel 2-2	126.48	33958	0.21329	1.27	611.31	1383
Panel 2-3	132.41	34566	0.25807	1.54	611.72	1338
Panel 2-4	113.83	33818	0.22353	1.27	579.98	1511
Panel 2-5	120.58	36256	0.24471	1.38	568.12	1516

Table C-12: Panel-2 Flexural Test Data Statistics (Method II)

Statistic	Maximum Load (lbs)	Maximum Stress (psi)	Max Load Deflection (in)	Maximum Strain (%)	Linear Slope (lb/in)	Flexural Modulus (ksi)
Mean	125.64	35430	0.240972	1.41	597.66	1447.03
SDEV	8.62	1997	0.022174	0.14	22.08	81.26
CVAR	6.86	5.64	9.20	10.30	3.69	5.62
Minimum	113.83	33818	0.21329	1.27	568.12	1338
Maximum	134.91	38553	0.26526	1.57	617.17	1516

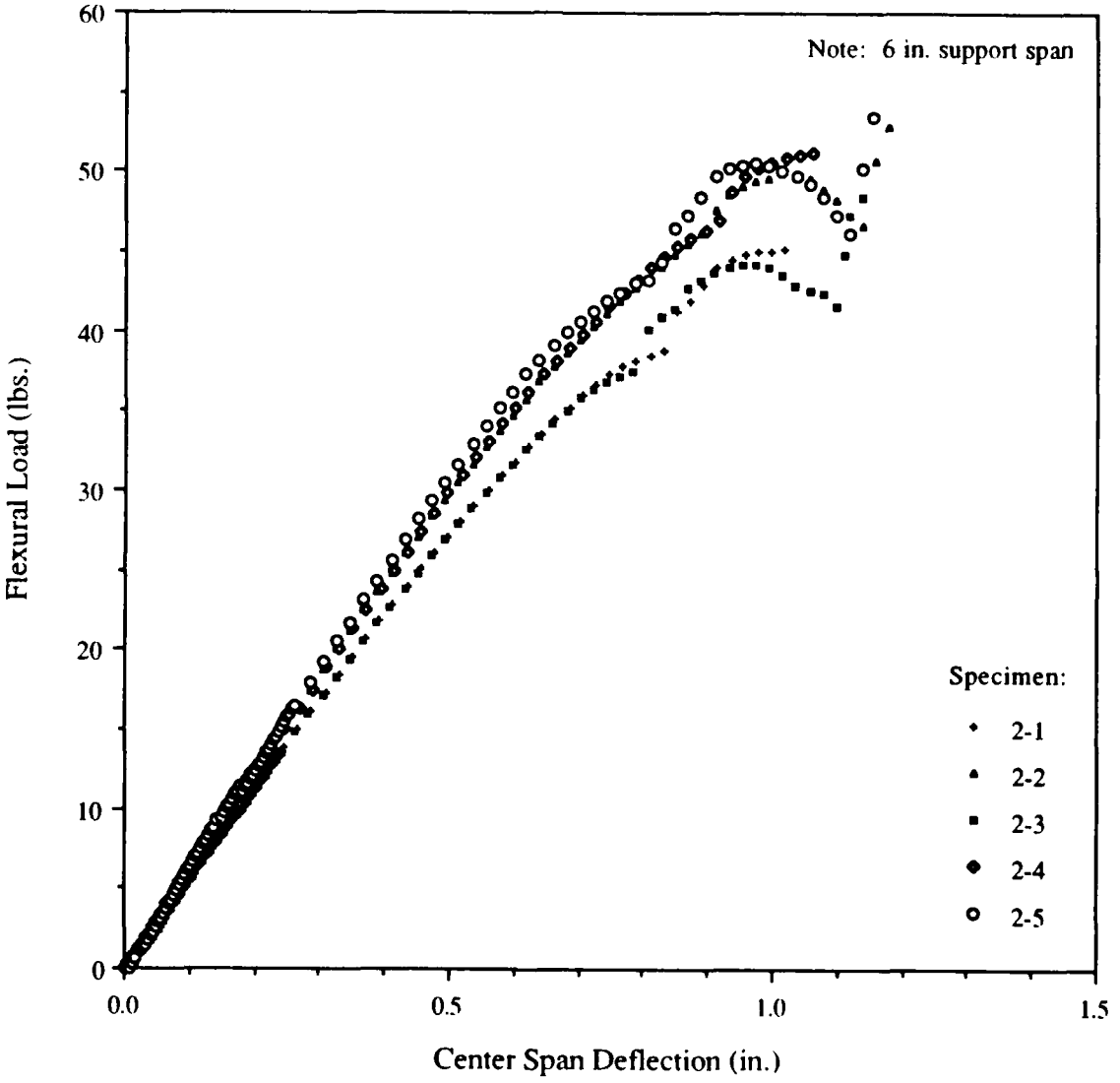

Figure C-3: Flexural Load vs. Center Span Deflection for Panel-2 Lower Face with CSM Ply in Compression and 1808 E-Glass 0° Ply in Tension

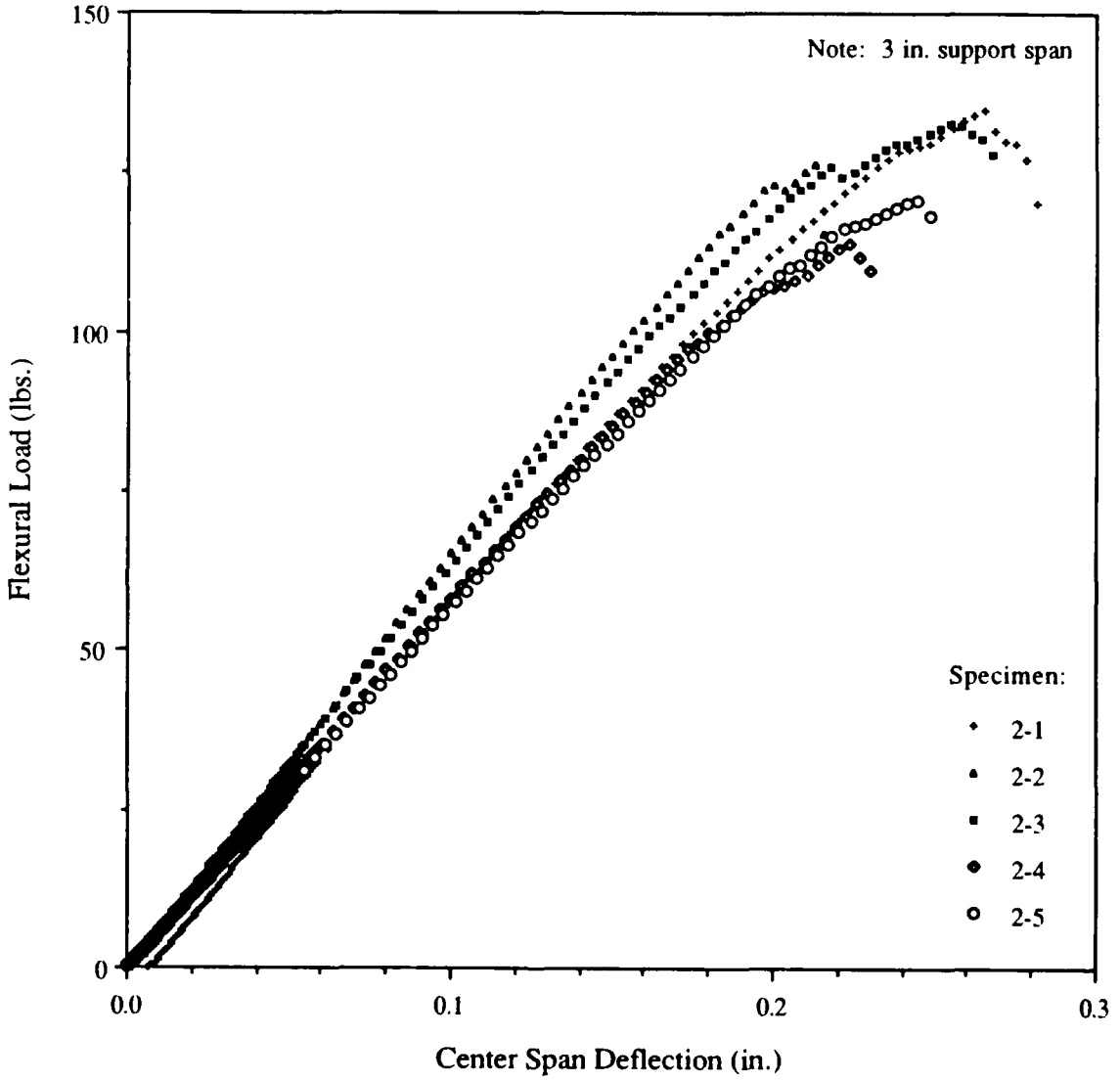

Figure C-4: Flexural Load vs. Center Span Deflection for Panel-2 Lower Face with CSM Ply in Tension and 1808 E-Glass 0° Ply in Compression

Table C-13: Panel-3 Flexural Specimen Dimensions (Method I)

Specimen ID	Width (in)	Thickness (in)
Panel 3-1	0.517	0.146
Panel 3-2	0.519	0.146
Panel 3-3	0.513	0.146
Panel 3-4	0.513	0.146
Panel 3-5	0.514	0.147

Table C-14: Panel-3 Flexural Test Data (Method I)

Specimen ID	Maximum Load (lbs)	Maximum Stress (psi)	Max Load Deflection (in)	Maximum Strain (%)	Linear Slope (lb/in)	Flexural Modulus (ksi)
Panel 3-1	25.956	25040	1.0927	2.66	35.40	1188
Panel 3-2	23.875	22946	1.0931	2.66	32.43	1084
Panel 3-3	24.928	25784	1.2907	3.14	33.66	1138
Panel 3-4	25.907	26065	1.2049	2.93	35.23	1192
Panel 3-5	26.224	26043	1.2135	2.97	32.53	1076

Table C-15: Panel-3 Flexural Test Data Statistics (Method I)

Statistic	Maximum Load (lbs)	Maximum Stress (psi)	Max Load Deflection (in)	Maximum Strain (%)	Linear Slope (lb/in)	Flexural Modulus (ksi)
Mean	25.38	25176	1.17898	2.87	33.85	1135.61
SDEV	0.97	1314	0.085388	0.21	1.42	54.97
CVAR	3.84	5.22	7.24	7.31	4.20	4.84
Minimum	23.875	22946	1.0927	2.66	32.43	1076
Maximum	26.224	26065	1.2907	3.14	35.40	1192

Table C-16: Panel-3 Flexural Specimen Dimensions (Method II)

Specimen ID	Width (in)	Thickness (in)
Panel 3-1	0.517	0.131
Panel 3-2	0.518	0.133
Panel 3-3	0.503	0.133
Panel 3-4	0.512	0.134
Panel 3-5	0.511	0.134

Table C-17: Panel-3 Flexural Test Data (Method II)

Specimen ID	Maximum Load (lbs)	Maximum Stress (psi)	Max Load Deflection (in)	Maximum Strain (%)	Linear Slope (lb/in)	Flexural Modulus (ksi)
Panel 3-1	34.148	18893	0.4153	3.63	162.95	946
Panel 3-2	40.354	21497	0.40354	3.58	187.53	1039
Panel 3-3	42.434	23499	0.4243	3.76	203.22	1159
Panel 3-4	36.021	19162	0.40829	3.65	175.02	959
Panel 3-5	34.032	18222	0.4184	3.74	173.00	950

Table C-18: Panel-3 Flexural Test Data Statistics (Method II)

Statistic	Maximum Load (lbs)	Maximum Stress (psi)	Max Load Deflection (in)	Maximum Strain (%)	Linear Slope (lb/in)	Flexural Modulus (ksi)
Mean	37.40	20255	0.413966	3.67	180.34	1010.59
SDEV	3.80	2194	0.008203	0.08	15.49	91.32
CVAR	10.17	10.83	1.98	2.11	8.59	9.04
Minimum	34.032	18222	0.40354	3.58	162.95	946
Maximum	42.434	23499	0.4243	3.76	203.22	1159

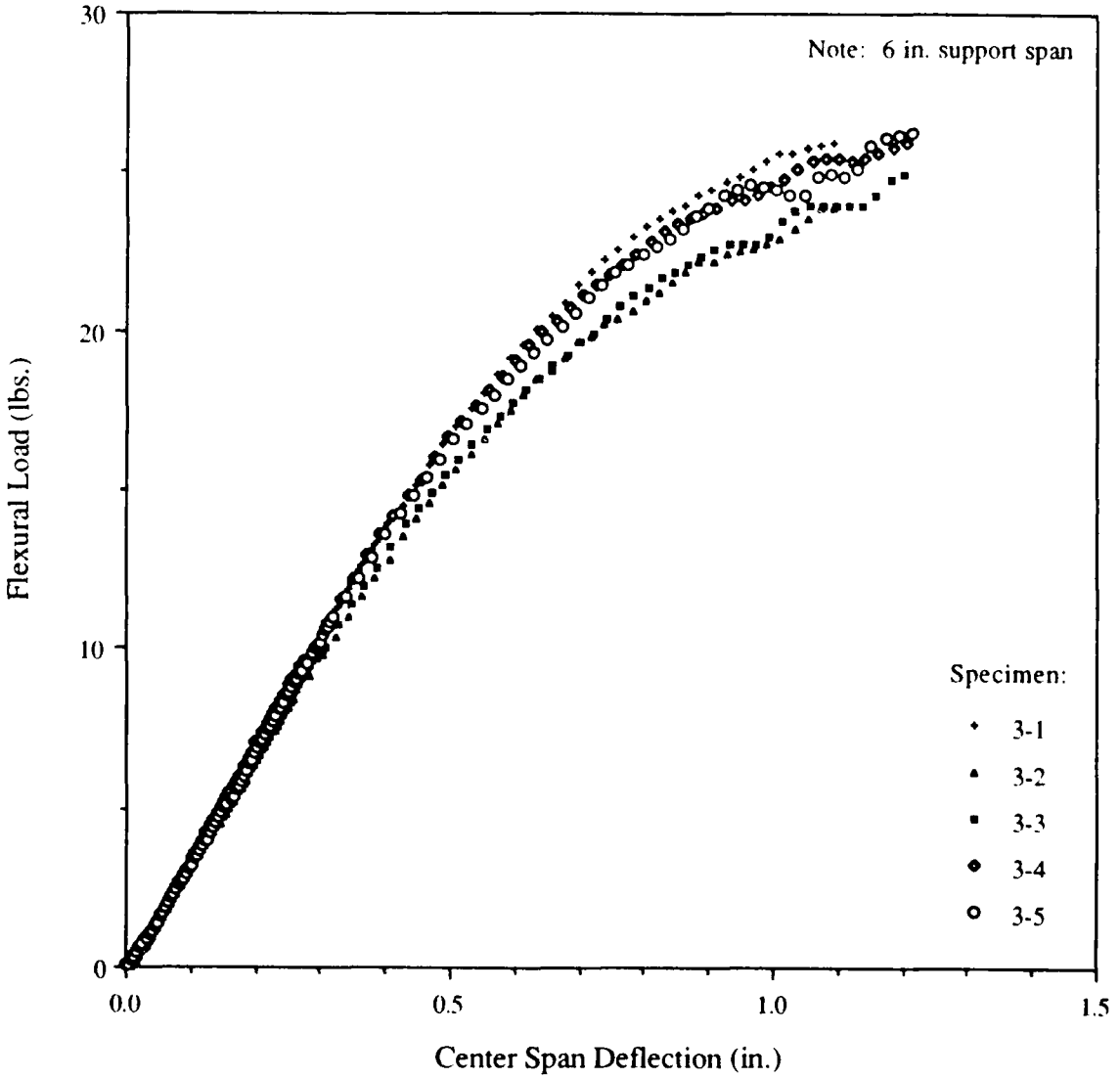

Figure C-5: Flexural Load vs. Center Span Deflection for Panel-3 Lower Face with CSM Ply in Compression and Kevlar KDB 110 45° Ply in Tension

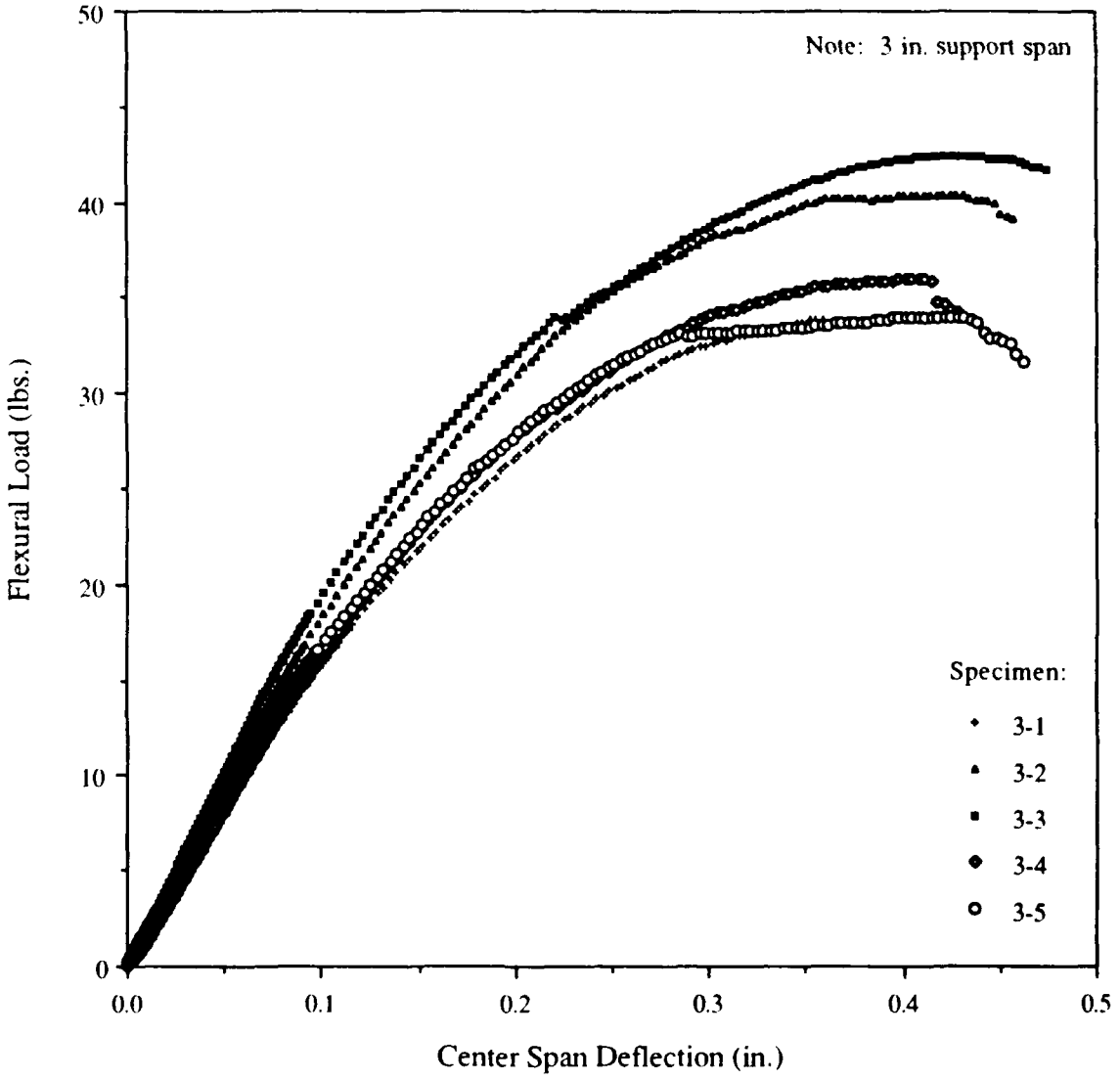

Figure C-6: Flexural Load vs. Center Span Deflection for Panel-3 Lower Face with CSM Ply in Tension and Kevlar KDB 110 45° Ply in Compression

Table C-19: Panel-4 Flexural Specimen Dimensions (Method I)

Specimen ID	Width (in)	Thickness (in)
Panel 4-1	0.515	0.148
Panel 4-2	0.519	0.142
Panel 4-3	0.515	0.146
Panel 4-4	0.515	0.146
Panel 4-5	0.518	0.143

Table C-20: Panel-4 Flexural Test Data (Method I)

Specimen ID	Maximum Load (lbs)	Maximum Stress (psi)	Max Load Deflection (in)	Maximum Strain (%)	Linear Slope (lb/in)	Flexural Modulus (ksi)
Panel 4-1	23.736	22150	1.0594	2.61	35.40	1145
Panel 4-2	23.909	24439	1.1121	2.63	34.38	1249
Panel 4-3	24.735	23865	1.0799	2.63	35.20	1186
Panel 4-4	24.433	23341	1.0455	2.54	36.79	1240
Panel 4-5	24.308	24739	1.1382	2.71	37.08	1322

Table C-21: Panel-4 Flexural Test Data Statistics (Method I)

Statistic	Maximum Load (lbs)	Maximum Stress (psi)	Max Load Deflection (in)	Maximum Strain (%)	Linear Slope (lb/in)	Flexural Modulus (ksi)
Mean	24.22	23707	1.08702	2.63	35.77	1228.32
SDEV	0.40	1023	0.038032	0.06	1.13	67.18
CVAR	1.66	4.32	3.50	2.29	3.17	5.47
Minimum	23.736	22150	1.0455	2.54	34.38	1145
Maximum	24.735	24739	1.1382	2.71	37.08	1322

Table C-22: Panel-4 Flexural Specimen Dimensions (Method II)

Specimen ID	Width (in)	Thickness (in)
Panel 4-1	0.531	0.153
Panel 4-2	0.526	0.155
Panel 4-3	0.533	0.153
Panel 4-4	0.527	0.153
Panel 4-5	0.52	0.156

Table C-23: Panel-4 Flexural Test Data (Method II)

Specimen ID	Maximum Load (lbs)	Maximum Stress (psi)	Max Load Deflection (in)	Maximum Strain (%)	Linear Slope (lb/in)	Flexural Modulus (ksi)
Panel 4-1	62.142	23592	0.326	3.33	307.62	1092
Panel 4-2	55.398	20455	0.29264	3.02	274.56	946
Panel 4-3	58.389	22021	0.3177	3.24	302.35	1069
Panel 4-4	54.236	20732	0.32399	3.30	260.47	931
Panel 4-5	62.03	23033	0.31471	3.27	320.33	1095

Table C-24: Panel-4 Flexural Test Data Statistics (Method II)

Statistic	Maximum Load (lbs)	Maximum Stress (psi)	Max Load Deflection (in)	Maximum Strain (%)	Linear Slope (lb/in)	Flexural Modulus (ksi)
Mean	58.44	21967	0.315008	3.23	293.07	1026.76
SDEV	3.66	1377	0.013315	0.12	24.73	81.08
CVAR	6.26	6.27	4.23	3.76	8.44	7.90
Minimum	54.236	20455	0.29264	3.02	260.47	931
Maximum	62.142	23592	0.326	3.33	320.33	1095

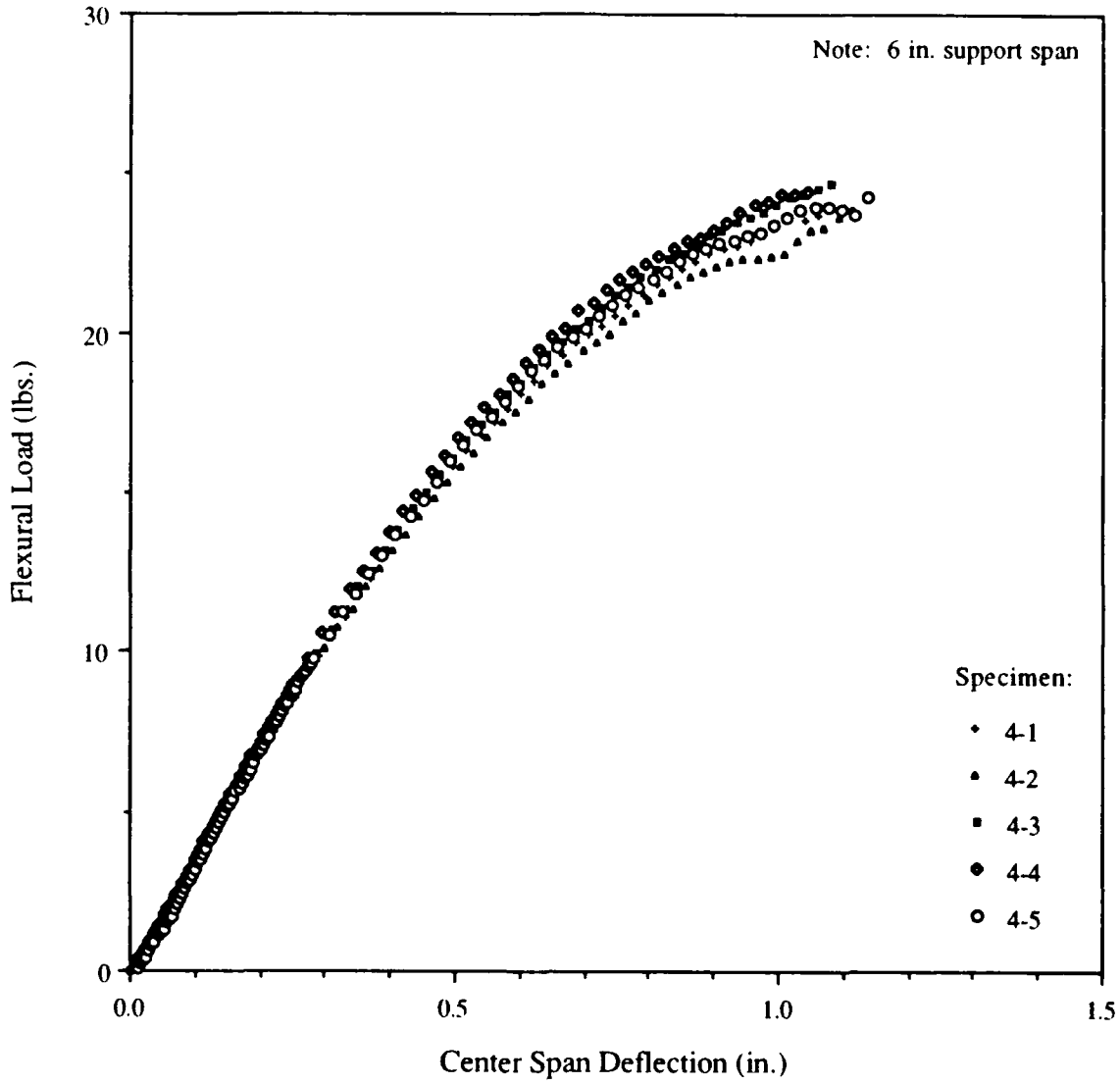

Figure C-7: Flexural Load vs. Center Span Deflection for Panel-4 Lower Face with CSM Ply in Compression and Kevlar KDB 110 45° Ply in Tension

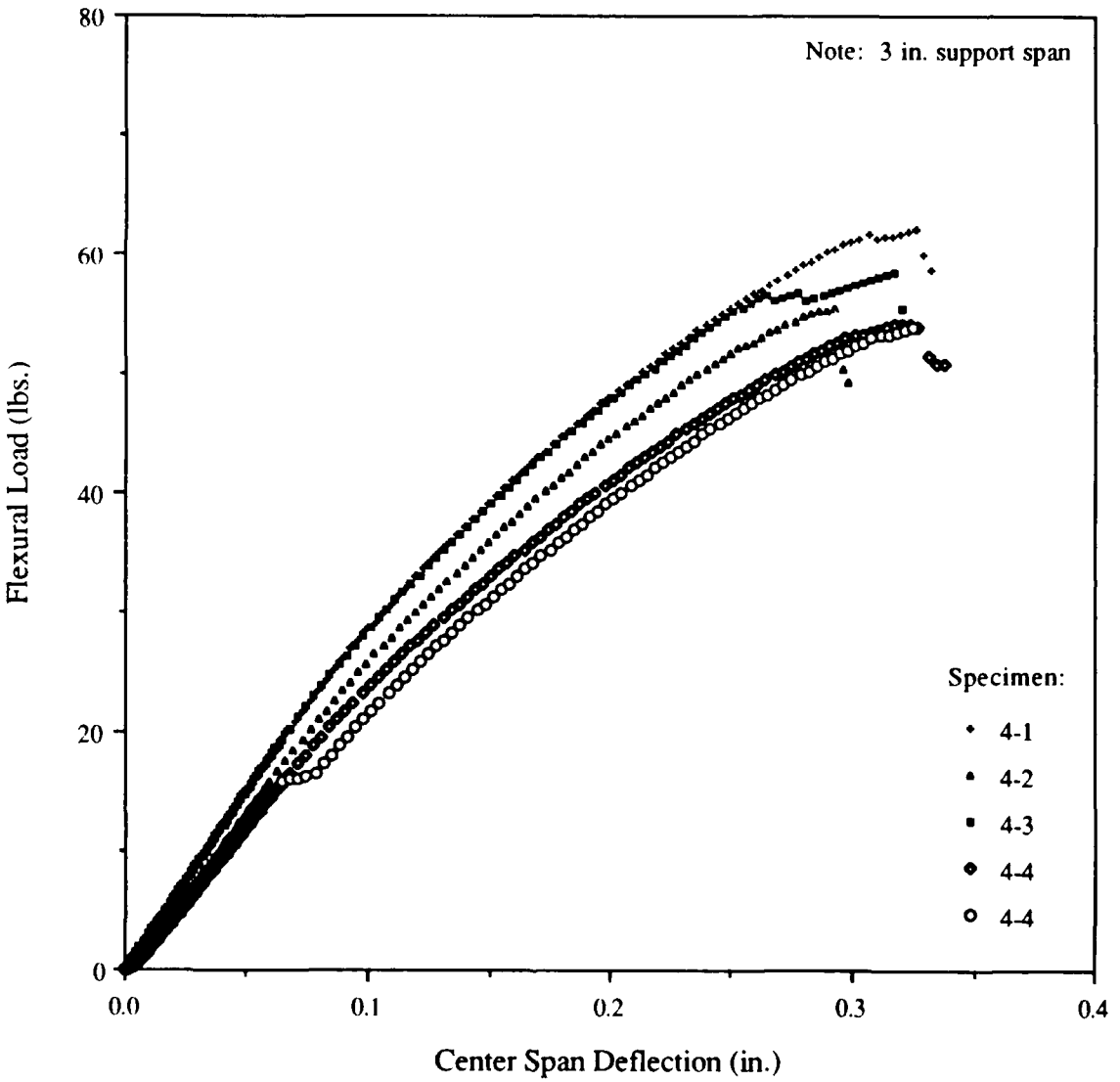

Figure C-8: Flexural Load vs. Center Span Deflection for Panel-4 Lower Face with CSM Ply in Tension and Kevlar KDB 110 45° Ply in Compression

Table C-25: Panel-5 Flexural Specimen Dimensions (Method I)

Specimen ID	Width (in)	Thickness (in)
Panel 5-1	0.521	0.144
Panel 5-2	0.519	0.143
Panel 5-3	0.521	0.139
Panel 5-4	0.52	0.141
Panel 5-5	0.515	0.145

Table C-26: Panel-5 Flexural Test Data (Method I)

Specimen ID	Maximum Load (lbs)	Maximum Stress (psi)	Max Load Deflection (in)	Maximum Strain (%)	Linear Slope (lb/in)	Flexural Modulus (ksi)
Panel 5-1	21.226	20545	1.0347	2.48	30.36	1054
Panel 5-2	21.687	21193	1.005	2.40	32.43	1154
Panel 5-3	19.527	22186	1.3218	3.06	26.52	1024
Panel 5-4	19.501	19430	0.9794	2.30	29.71	1101
Panel 5-5	21.954	22298	1.2034	2.91	29.89	1028

Table C-27: Panel-5 Flexural Test Data Statistics (Method I)

Statistic	Maximum Load (lbs)	Maximum Stress (psi)	Max Load Deflection (in)	Maximum Strain (%)	Linear Slope (lb/in)	Flexural Modulus (ksi)
Mean	20.78	21131	1.10886	2.63	29.78	1071.98
SDEV	1.18	1195	0.147756	0.33	2.12	55.07
CVAR	5.70	5.66	13.33	12.73	7.12	5.14
Minimum	19.501	19430	0.9794	2.30	26.52	1024
Maximum	21.954	22298	1.3218	3.06	32.43	1154

Table C-28: Panel-5 Flexural Specimen Dimensions (Method II)

Specimen ID	Width (in)	Thickness (in)
Panel 5-1	0.532	0.137
Panel 5-2	0.521	0.136
Panel 5-3	0.514	0.129
Panel 5-4	0.519	0.136
Panel 5-5	0.519	0.137

Table C-29: Panel-5 Flexural Test Data (Method II)

Specimen ID	Maximum Load (lbs)	Maximum Stress (psi)	Max Load Deflection (in)	Maximum Strain (%)	Linear Slope (lb/in)	Flexural Modulus (ksi)
Panel 5-1	49.301	25227	0.49863	4.55	208.50	1029
Panel 5-2	48.259	25367	0.48182	4.37	194.89	1004
Panel 5-3	46.58	28282	0.52571	4.52	187.73	1148
Panel 5-4	48.936	25807	0.48066	4.36	199.85	1033
Panel 5-5	50.293	26731	0.52304	4.78	206.04	1042

Table C-30: Panel-5 Flexural Test Data Statistics (Method II)

Statistic	Maximum Load (lbs)	Maximum Stress (psi)	Max Load Deflection (in)	Maximum Strain (%)	Linear Slope (lb/in)	Flexural Modulus (ksi)
Mean	48.67	26283	0.501972	4.52	199.40	1051.29
SDEV	1.38	1263	0.021673	0.17	8.42	56.14
CVAR	2.84	4.80	4.32	3.78	4.22	5.34
Minimum	46.58	25227	0.48066	4.36	187.73	1004
Maximum	50.293	28282	0.52571	4.78	208.50	1148

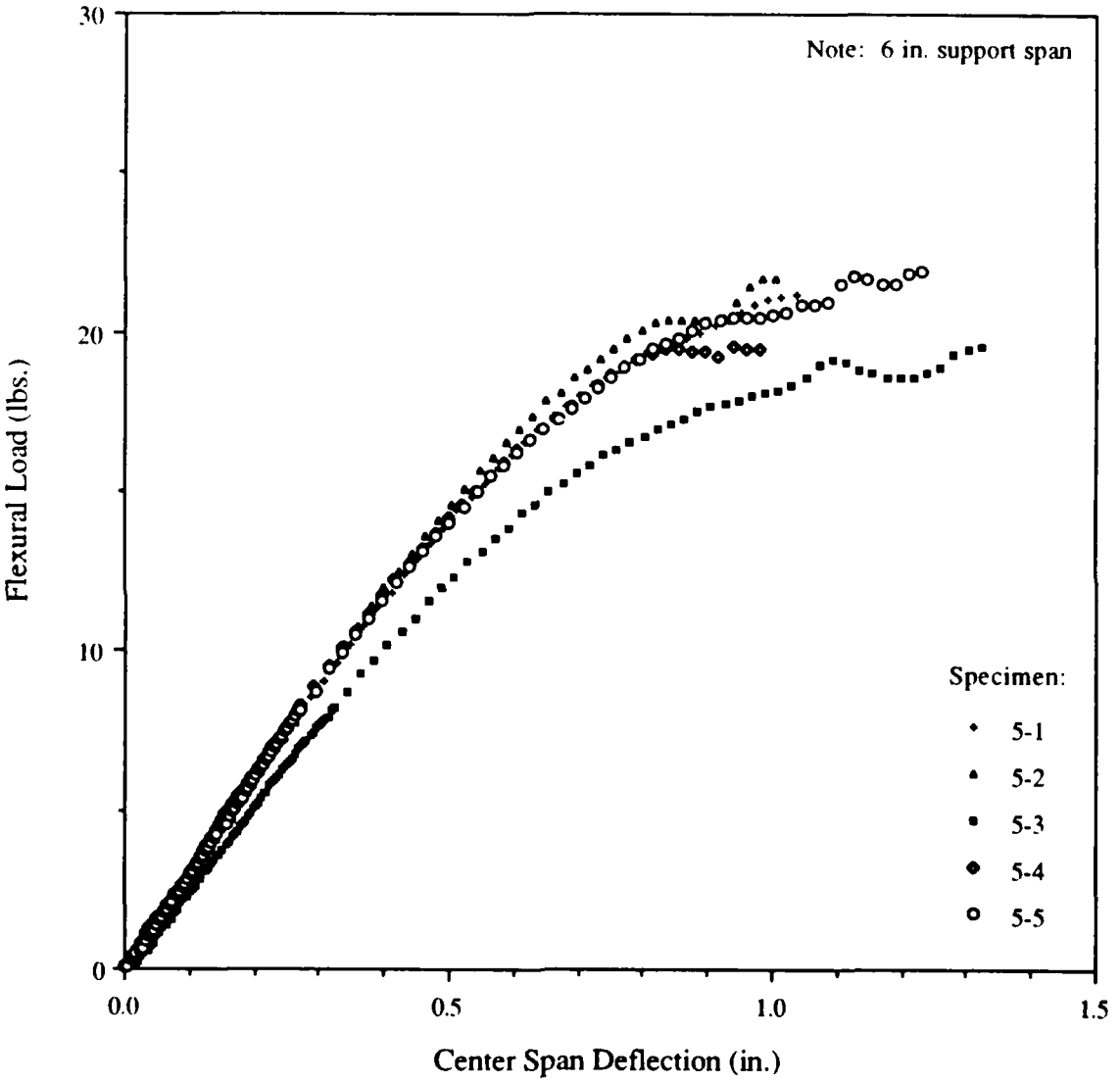

Figure C-9: Flexural Load vs. Center Span Deflection for Panel-5 Lower Face with CSM Ply in Compression and Kevlar KDB 110 45° Ply in Tension

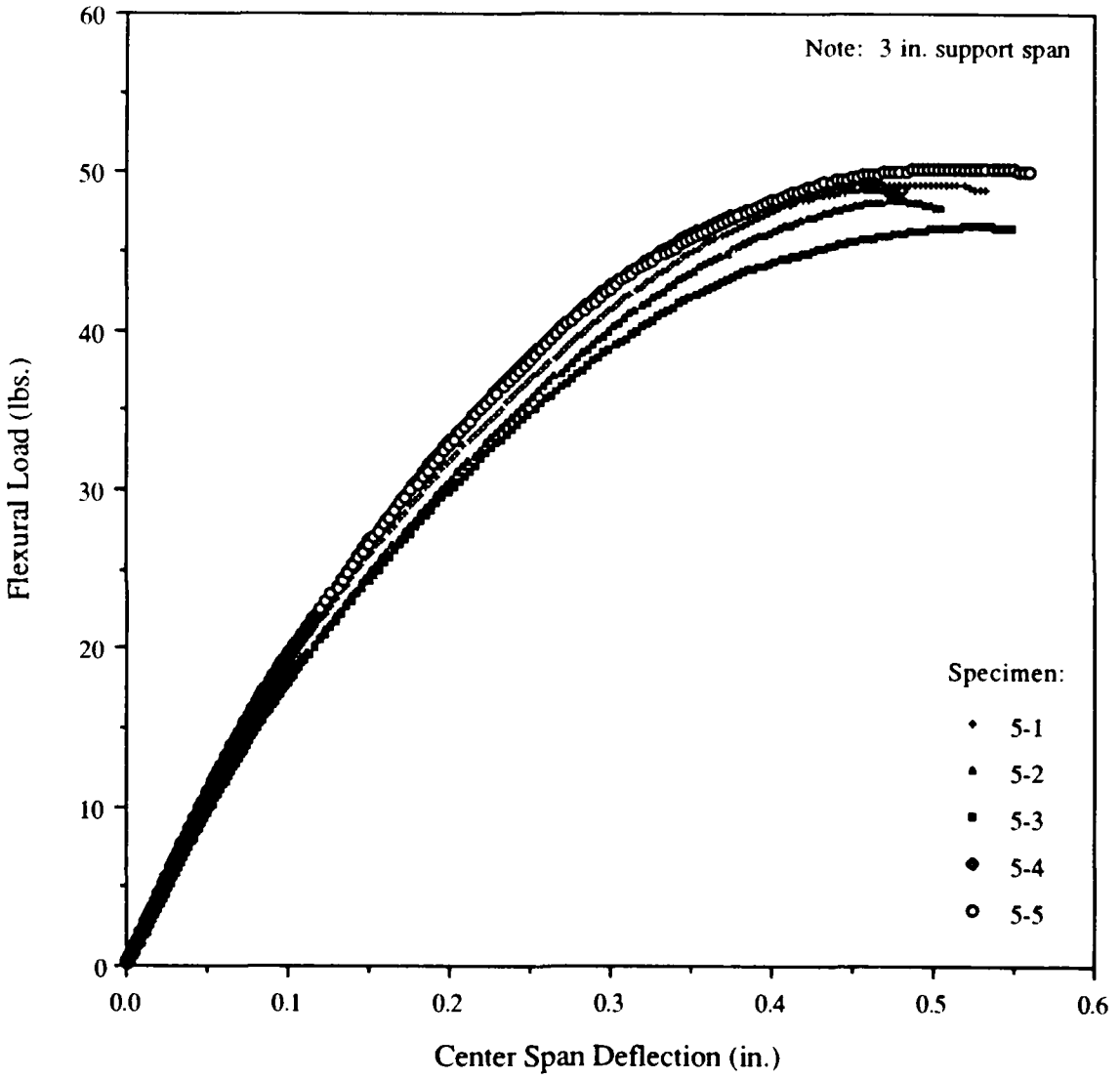

Figure C-10: Flexural Load vs. Center Span Deflection for Panel-5 Lower Face with CSM Ply in Tension and Kevlar KDB 110 45° Ply in Compression

Table C-31: Panel-6 Flexural Specimen Dimensions (Method I)

Specimen ID	Width (in)	Thickness (in)
Panel 6-1	0.509	0.145
Panel 6-2	0.513	0.146
Panel 6-3	0.515	0.139
Panel 6-4	0.516	0.143
Panel 6-5	0.516	0.143

Table C-32: Panel-6 Flexural Test Data (Method I)

Specimen ID	Maximum Load (lbs)	Maximum Stress (psi)	Max Load Deflection (in)	Maximum Strain (%)	Linear Slope (lb/in)	Flexural Modulus (ksi)
Panel 6-1	24.392	25378	1.2422	3.00	34.70	1207
Panel 6-2	23.833	24304	1.2472	3.03	31.08	1051
Panel 6-3	24.188	27613	1.3013	3.01	31.90	1245
Panel 6-4	23.504	25397	1.3139	3.13	30.19	1081
Panel 6-5	22.22	22308	1.0794	2.57	33.26	1190

Table C-33: Panel-6 Flexural Test Data Statistics (Method I)

Statistic	Maximum Load (lbs)	Maximum Stress (psi)	Max Load Deflection (in)	Maximum Strain (%)	Linear Slope (lb/in)	Flexural Modulus (ksi)
Mean	23.63	25000	1.2368	2.95	32.22	1154.94
SDEV	0.86	1928	0.093564	0.22	1.78	84.36
CVAR	3.63	7.71	7.56	7.37	5.53	7.30
Minimum	22.22	22308	1.0794	2.57	30 '9	1051
Maximum	24.392	27613	1.3139	3.13	34.70	1245

Table C-34: Panel-6 Flexural Specimen Dimensions (Method II)

Specimen ID	Width (in)	Thickness (in)
Panel 6-1	0.512	0.136
Panel 6-2	0.527	0.135
Panel 6-3	0.511	0.133
Panel 6-4	0.526	0.133
Panel 6-5	0.521	0.137

Table C-35: Panel-6 Flexural Test Data (Method II)

Specimen ID	Maximum Load (lbs)	Maximum Stress (psi)	Max Load Deflection (in)	Maximum Strain (%)	Linear Slope (lb/in)	Flexural Modulus (ksi)
Panel 6-1	43.792	22900	0.43621	3.95	194.92	1022
Panel 6-2	48.197	25042	0.4518	4.07	217.29	1131
Panel 6-3	42.439	23134	0.4243	3.76	205.83	1156
Panel 6-4	45.431	23941	0.4136	3.67	200.55	1094
Panel 6-5	46.373	23643	0.45054	4.11	222.82	1123

Table C-36: Panel-6 Flexural Test Data Statistics (Method II)

Statistic	Maximum Load (lbs)	Maximum Stress (psi)	Max Load Deflection (in)	Maximum Strain (%)	Linear Slope (lb/in)	Flexural Modulus (ksi)
Mean	45.25	23732	0.43529	3.91	208.28	1105.01
SDEV	2.24	839	0.016562	0.19	11.58	51.59
CVAR	4.94	3.54	3.80	4.93	5.56	4.67
Minimum	42.439	22900	0.4136	3.67	194.92	1022
Maximum	48.197	25042	0.4518	4.11	222.82	1156

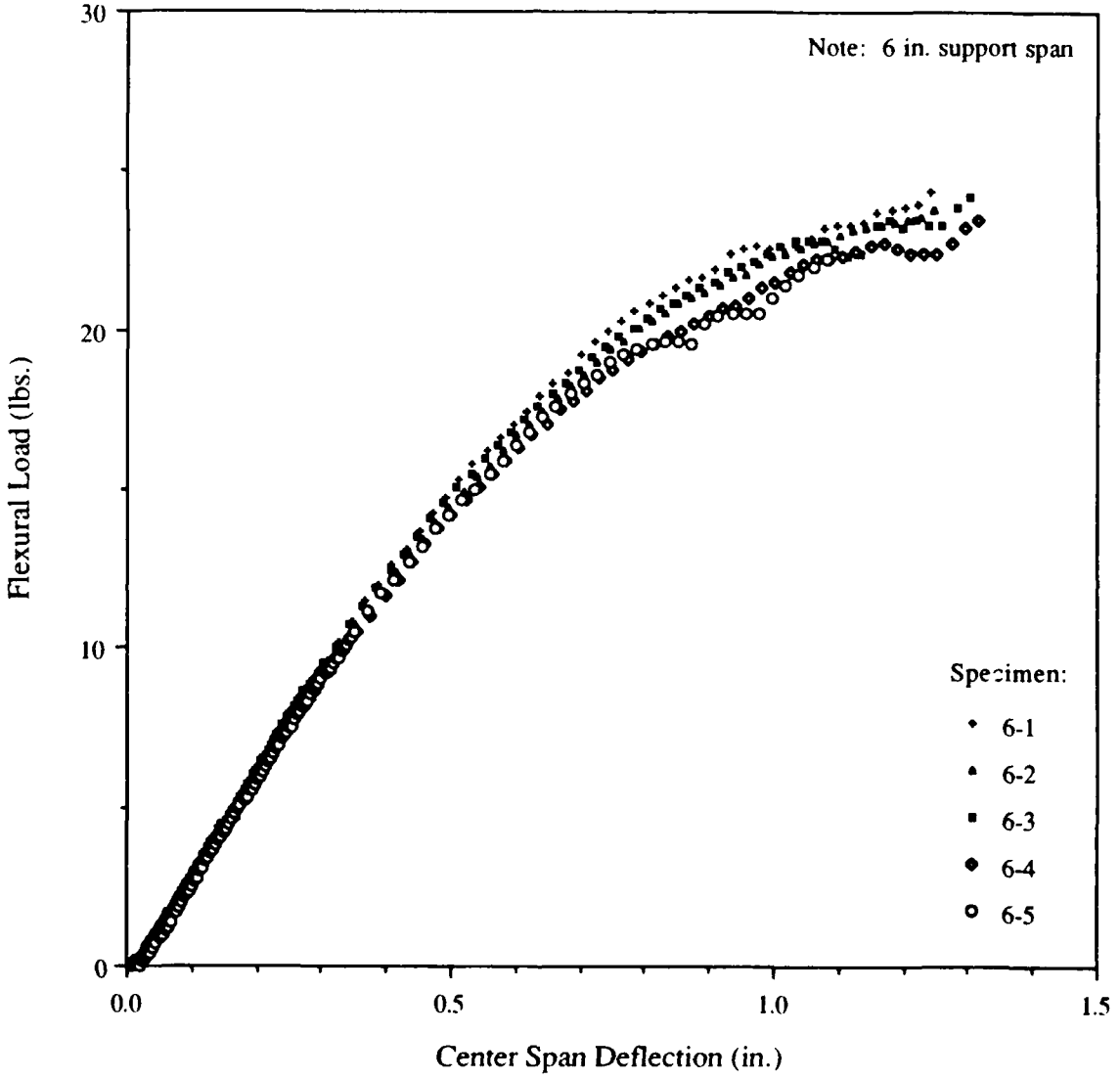

Figure C-11: Flexural Load vs. Center Span Deflection for Panel-6 Lower Face with CSM Ply in Compression and Kevlar KDB 110 45° Ply in Tension

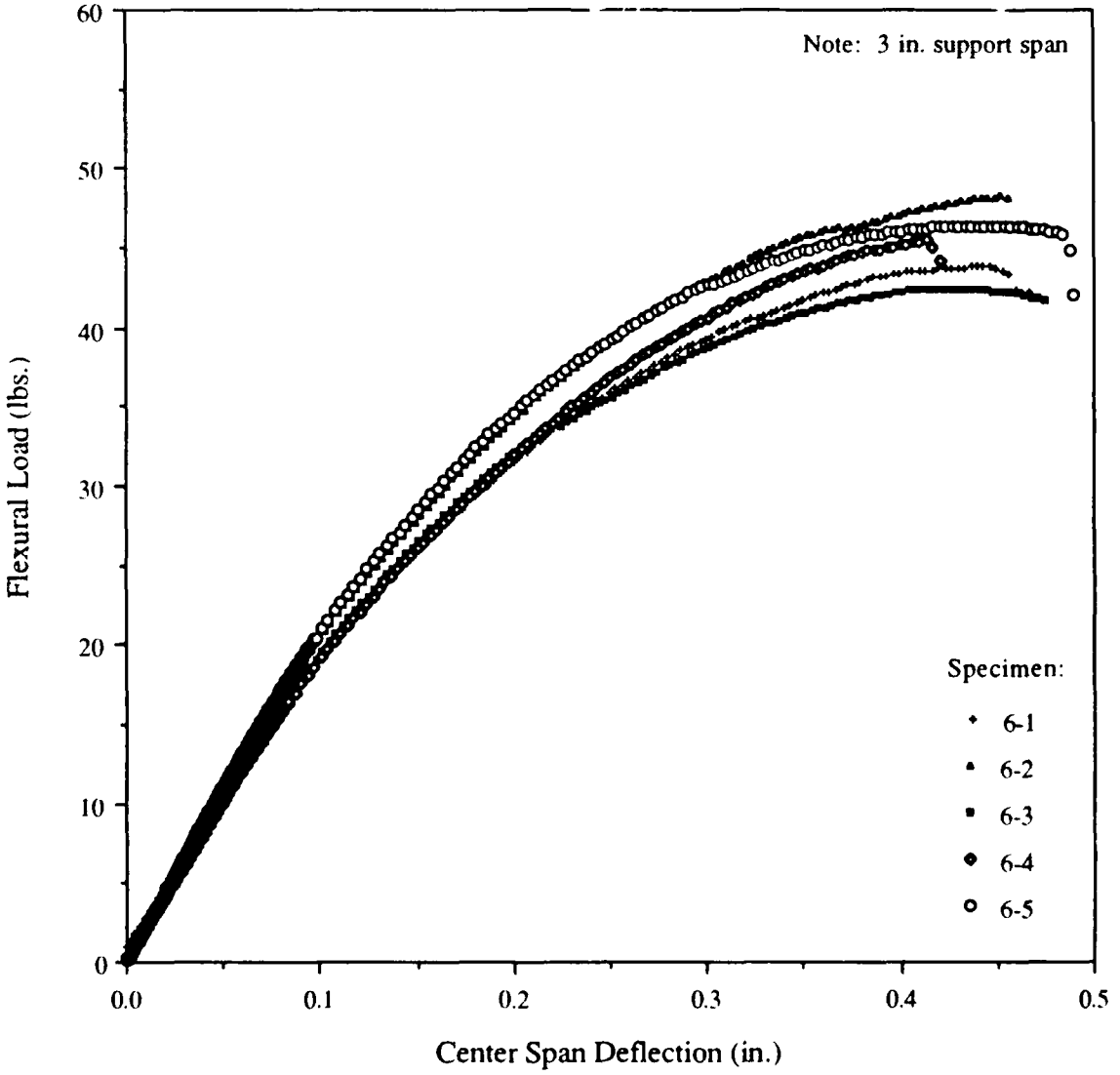

Figure C-12: Flexural Load vs. Center Span Deflection for Panel-6 Lower Face with CSM Ply in Tension and Kevlar KDB 110 45° Ply in Compression

APPENDIX D

IN-PLANE SHEAR CHARACTERISTICS OF TEST PANEL LOWER FACES

Table D-1: Panel-1 In-Plane Shear Specimen Dimensions

Specimen ID	Width (in)	Length (in)
Panel 1-1	0.515	0.255
Panel 1-2	0.514	0.255
Panel 1-3	0.514	0.257
Panel 1-4	0.513	0.257
Panel 1-5	0.51	0.24

Table D-2: Panel-1 In-Plane Shear Test Data

Specimen ID	Maximum Load (lbs)	Shear Stress (psi)	Max Load Deflection (in)	Shear Strain (%)	Energy to Break (in-lbs)
Panel 1-1	473.01	3602	0.03126	0.98	5.643
Panel 1-2	480.07	3663	0.031328	0.98	6.264
Panel 1-3	504.28	3817	0.029192	0.91	6.549
Panel 1-4	481.12	3649	0.03028	0.95	5.815
Panel 1-5	429.43	3508	0.03422	1.07	6.729

Table D-3: Panel-1 In-Plane Shear Test Data Statistics

Statistic	Maximum Load (lbs)	Shear Stress (psi)	Max Load Deflection (in)	Shear Strain (%)	Energy to Break (in-lbs)
Mean	474	3648	0.031256	0.98	6.2
SDEV	27	112	0.001871	0.06	0.46
CVAR	5.77	3.08	5.99	5.95	7.50
Minimum	429.43	3508	0.029192	0.91	5.643
Maximum	504	3817	0.03422	1.07	6.729

SDEV - Standard Deviation
CVAR - Coefficient of Variation (%)

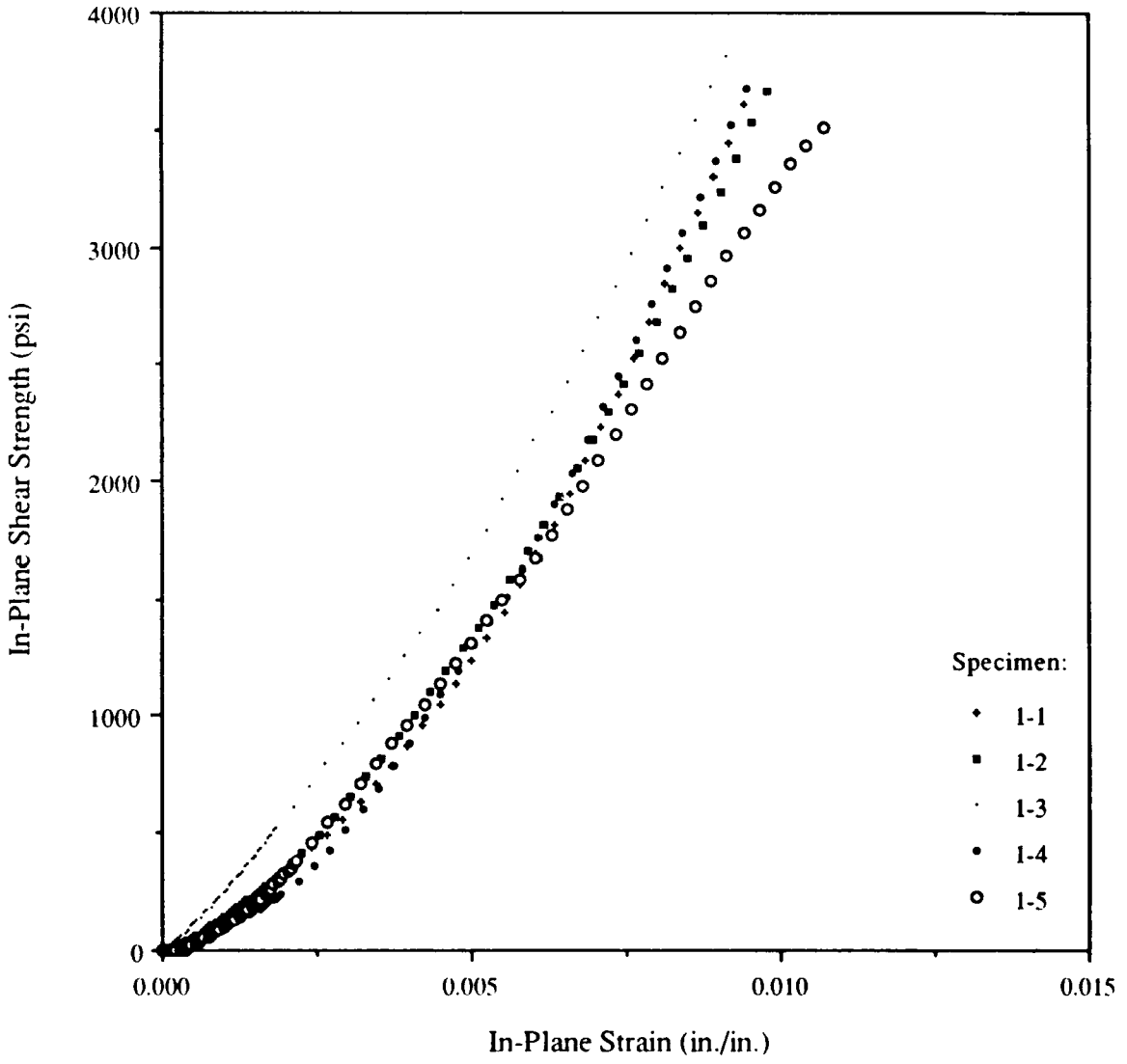

Figure D-1: In-Plane Shear Strength vs. Strain for Panel-1 Lower Face (E-Glass/DERAKANE® 510A)

Table D-4: Panel-2 In-Plane Shear Specimen Dimensions

Specimen ID	Width (in)	Length (in)
Panel 2-1	0.515	0.242
Panel 2-2	0.513	0.24
Panel 2-3	0.515	0.239
Panel 2-4	0.512	0.24
Panel 2-5	0.514	0.237

Table D-5: Panel-2 In-Plane Shear Test Data

Specimen ID	Maximum Load (lbs)	Shear Stress (psi)	Max Load Deflection (in)	Shear Strain (%)	Energy to Break (in-lbs)
Panel 2-1	480.15	3853	0.039326	1.22	6.658
Panel 2-2	478.35	3885	0.041364	1.28	7.075
Panel 2-3	447.95	3639	0.031131	0.97	5.671
Panel 2-4	441.94	3597	0.041422	1.28	8.398
Panel 2-5	470.15	3859	0.041458	1.28	6.788

Table D-6: Panel-2 In-Plane Shear Test Data Statistics

Statistic	Maximum Load (lbs)	Shear Stress (psi)	Max Load Deflection (in)	Shear Strain (%)	Energy to Break (in-lbs)
Mean	464	3767	0.038940	1.21	6.918
SDEV	18	137	0.004458	0.14	0.98
CVAR	3.81	3.64	11.45	11.44	14.19
Minimum	441.94	3597	0.031131	0.97	5.671
Maximum	480	3885	0.041458	1.28	8.398

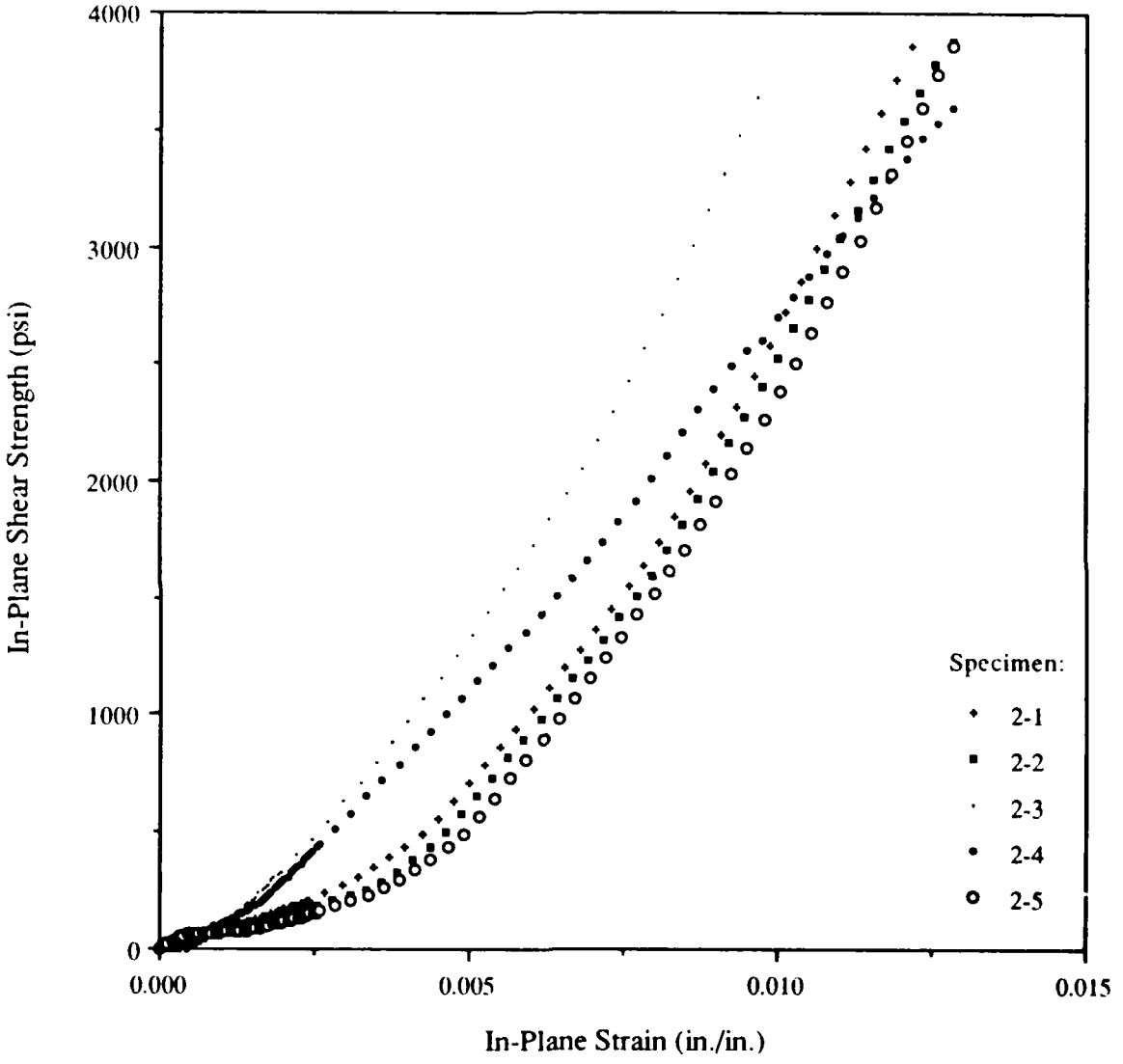

Figure B-2: In-Plane Shear Strength vs. Strain for Panel-2 Lower Face (E-Glass/DERAKANE® 510A)

Table D-7: Panel-3 In-Plane Shear Specimen Dimensions

Specimen ID	Width (in)	Length (in)
Panel 3-1	0.509	0.232
Panel 3-2	0.511	0.256
Panel 3-3	0.51	0.259
Panel 3-4	0.511	0.243
Panel 3-5	0.507	0.229

Table D-8: Panel-3 In-Plane Shear Test Data

Specimen ID	Maximum Load (lbs)	Shear Stress (psi)	Max Load Deflection (in)	Shear Strain (%)	Energy to Break (in-lbs)
Panel 3-1	314.37	2662	0.039654	1.24	5.527
Panel 3-2	399.58	3055	0.050216	1.57	9.272
Panel 3-3	384.26	2909	0.048641	1.52	11.44
Panel 3-4	410.33	3305	0.050869	1.59	11.09
Panel 3-5	323.02	2782	0.053394	1.67	9.767

Table D-9: Panel-3 In-Plane Shear Test Data Statistics

Statistic	Maximum Load (lbs)	Shear Stress (psi)	Max Load Deflection (in)	Shear Strain (%)	Energy to Break (in-lbs)
Mean	366	2942	0.048555	1.52	9.4192
SDEV	45	249	0.005262	0.17	2.35
CVAR	12.16	8.48	10.84	10.88	24.99
Minimum	314.37	2662	0.039654	1.24	5.527
Maximum	410	3305	0.053394	1.67	11.44

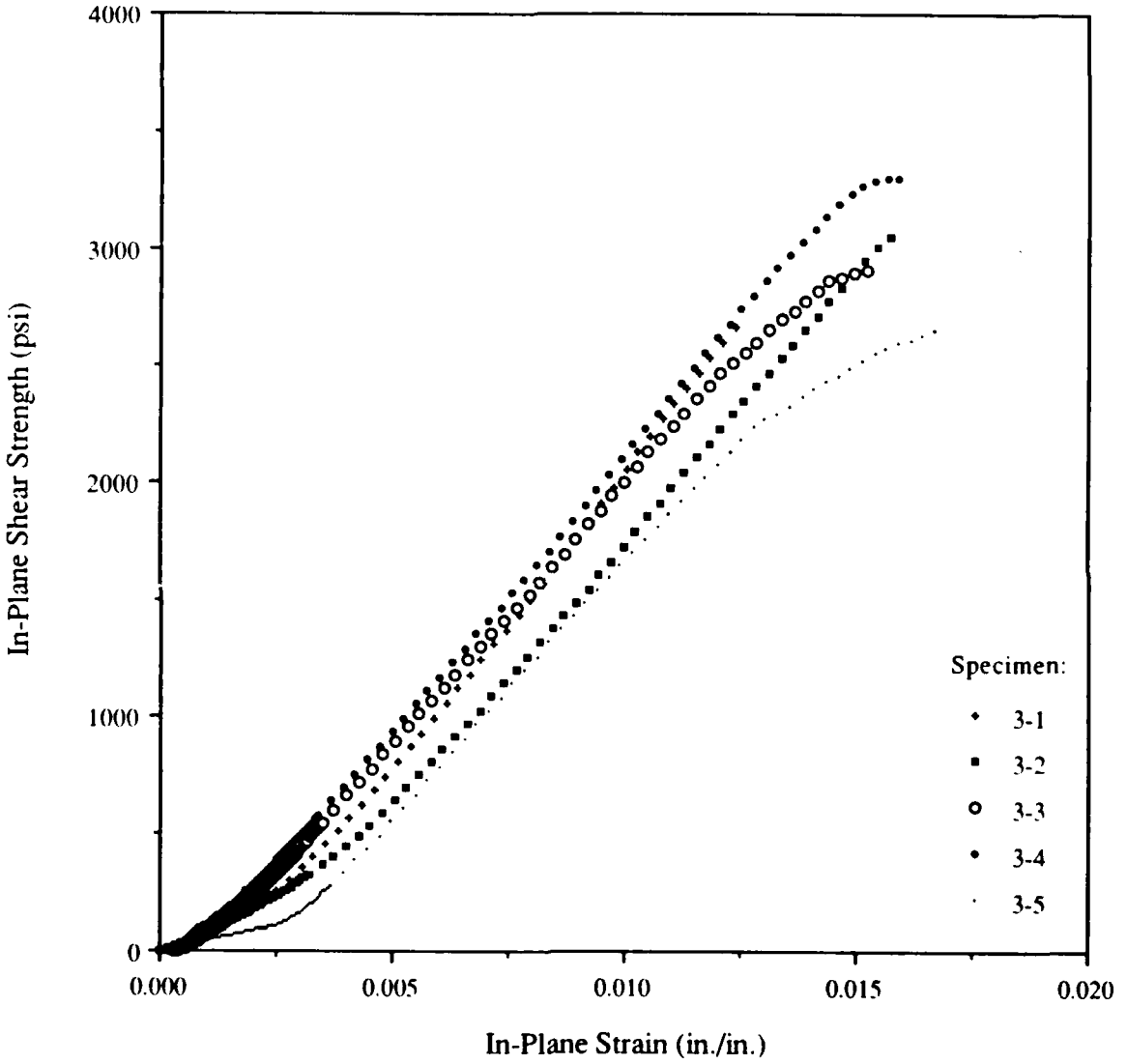

Figure D-3: In-Plane Shear Strength vs. Strain for Panel-3 Lower Face (Kevlar/DERAKANE® 510A)

Table D-10: Panel-4 In-Plane Shear Specimen Dimensions

Specimen ID	Width (in)	Length (in)
Panel 4-1	0.509	0.248
Panel 4-2	0.528	0.239
Panel 4-3	0.515	0.28
Panel 4-4	0.51	0.27
Panel 4-5	0.504	0.261

Table D-11: Panel-4 In-Plane Shear Test Data

Specimen ID	Maximum Load (lbs)	Shear Stress (psi)	Max Load Deflection (in)	Shear Strain (%)	Energy to Break (in-lbs)
Panel 4-1	421.82	3342	0.039573	1.25	8.517
Panel 4-2	412.35	3268	0.040641	1.29	7.849
Panel 4-3	525.22	3642	0.049728	1.57	12.75
Panel 4-4	444.88	3231	0.046906	1.49	9.5
Panel 4-5	353.34	2686	0.052759	1.69	10.81

Table D-12: Panel-4 In-Plane Shear Test Data Statistics

Statistic	Maximum Load (lbs)	Shear Stress (psi)	Max Load Deflection (in)	Shear Strain (%)	Energy to Break (in-lbs)
Mean	432	3234	0.045921	1.46	9.8852
SDEV	62	346	0.005710	0.19	1.95
CVAR	14.44	10.71	12.43	12.79	19.74
Minimum	353.34	2686	0.039573	1.25	7.849
Maximum	525	3642	0.052759	1.69	12.75

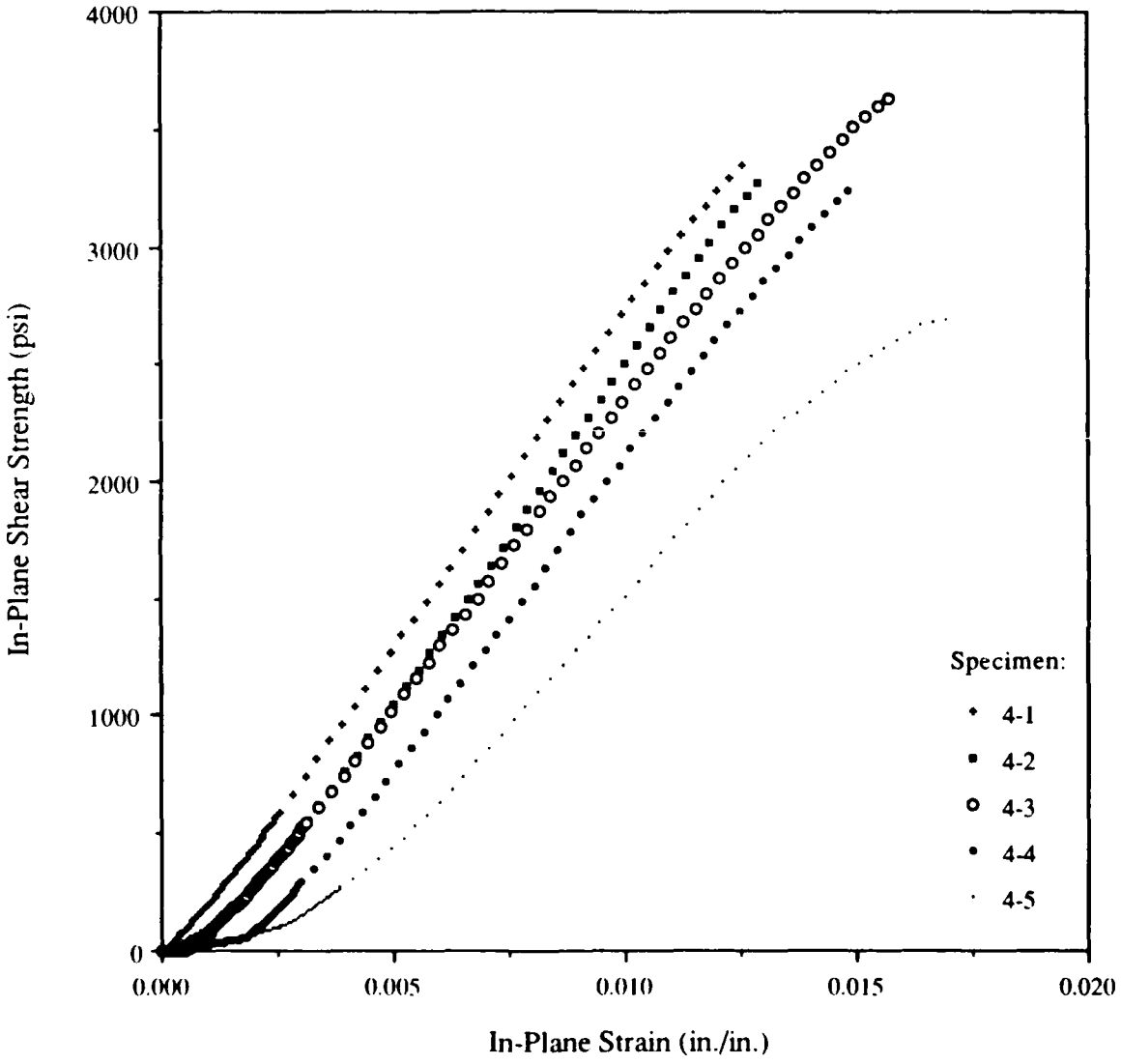

Figure D-4: In-Plane Shear Strength vs. Strain for Panel-4 Lower Face (Kevlar/DERAKANE® 510A)

Table D-13: Panel-5 In-Plane Shear Specimen Dimensions

Specimen ID	Width (in)	Length (in)
Panel 5-1	0.51	0.245
Panel 5-2	0.446	0.246
Panel 5-3	0.51	0.238
Panel 5-4	0.511	0.248
Panel 5-5	0.432	0.249

Table D-14: Panel-5 In-Plane Shear Test Data

Specimen ID	Maximum Load (lbs)	Shear Stress (psi)	Max Load Deflection (in)	Shear Strain (%)	Energy to Break (in-lbs)
Panel 5-1	383.56	3070	0.037441	1.17	6.91
Panel 5-2	301.9	2752	0.042342	1.33	5.772
Panel 5-3	337.95	2784	0.042931	1.34	6.655
Panel 5-4	333.49	2632	0.036813	1.15	5.987
Panel 5-5	264.18	2456	0.034913	1.10	4.416

Table D-15: Panel-5 In-Plane Shear Test Data Statistics

Statistic	Maximum Load (lbs)	Shear Stress (psi)	Max Load Deflection (in)	Shear Strain (%)	Energy to Break (in-lbs)
Mean	324	2739	0.038888	1.22	5.948
SDEV	44	225	0.003553	0.11	0.98
CVAR	13.71	8.23	9.13	9.01	16.40
Minimum	264.18	2456	0.034913	1.10	4.416
Maximum	384	3070	0.042931	1.34	6.91

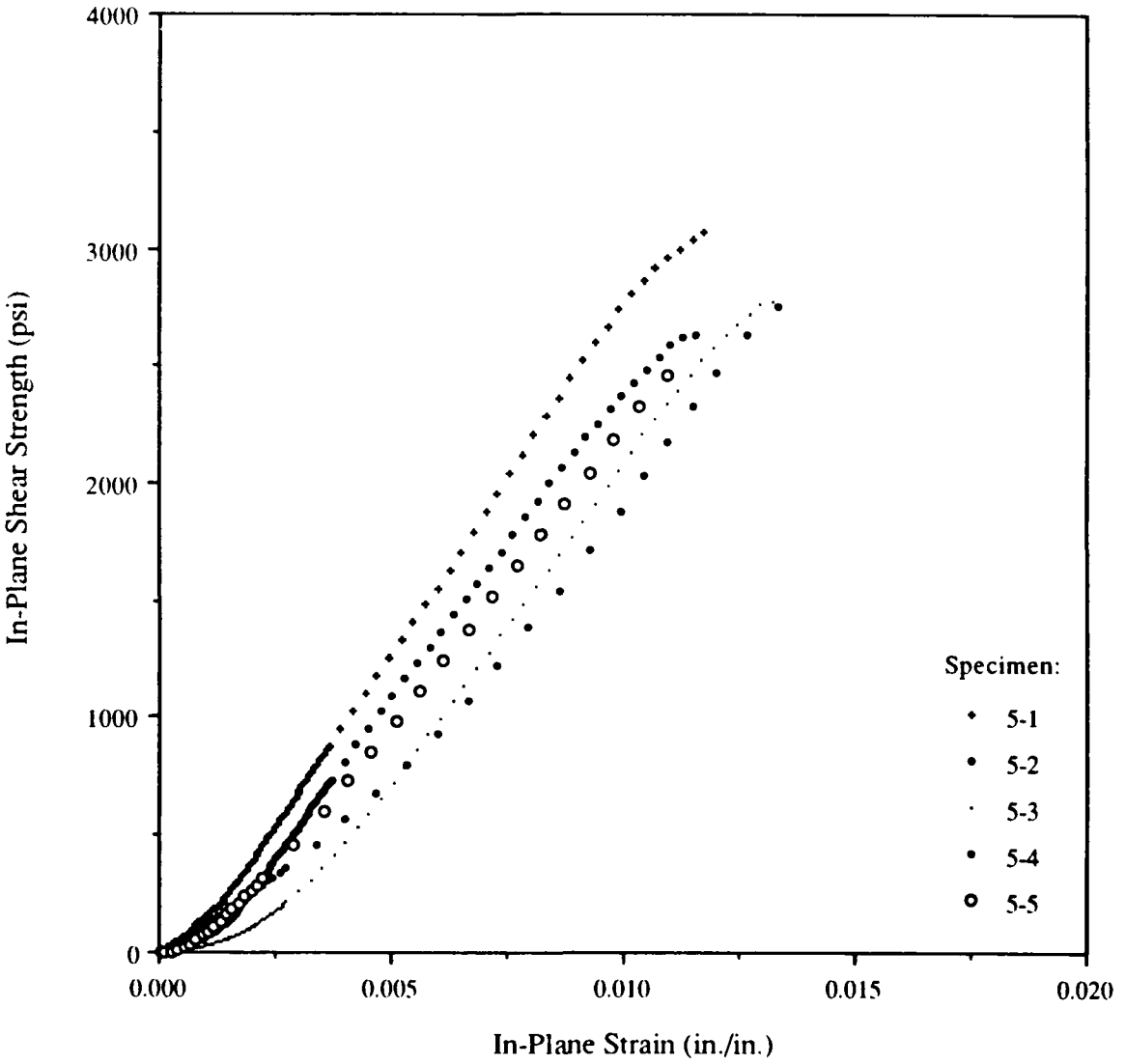

Figure D-5: In-Plane Shear Strength vs. Strain for Panel-5 Lower Face (Kevlar/DERAKANE® 8084)

Table D-16: Panel-6 In-Plane Shear Specimen Dimensions

Specimen ID	Width (in)	Length (in)
Panel 6-1	0.511	0.239
Panel 6-2	0.51	0.237
Panel 6-3	0.51	0.234
Panel 6-4	0.51	0.239
Panel 6-5	0.51	0.239

Table D-17: Panel-6 In-Plane Shear Test Data

Specimen ID	Maximum Load (lbs)	Shear Stress (psi)	Max Load Deflection (in)	Shear Strain (%)	Energy to Break (in-lbs)
Panel 6-1	349.1	2858	0.044791	1.38	7.895
Panel 6-2	352.22	2914	0.046312	1.43	9.194
Panel 6-3	386.2	3236	0.048328	1.49	9.939
Panel 6-4	383.11	3143	0.044153	1.36	9.834
Panel 6-5	395.82	3247	0.063501	1.96	13.79

Table D-18: Panel-6 In-Plane Shear Test Data Statistics

Statistic	Maximum Load (lbs)	Shear Stress (psi)	Max Load Deflection (in)	Shear Strain (%)	Energy to Break (in-lbs)
Mean	373	3080	0.049417	1.52	10.1304
SDEV	21	182	0.008036	0.25	2.20
CVAR	5.68	5.92	16.26	16.25	21.73
Minimum	349.1	2858	0.044153	1.36	7.895
Maximum	396	3247	0.063501	1.96	13.79

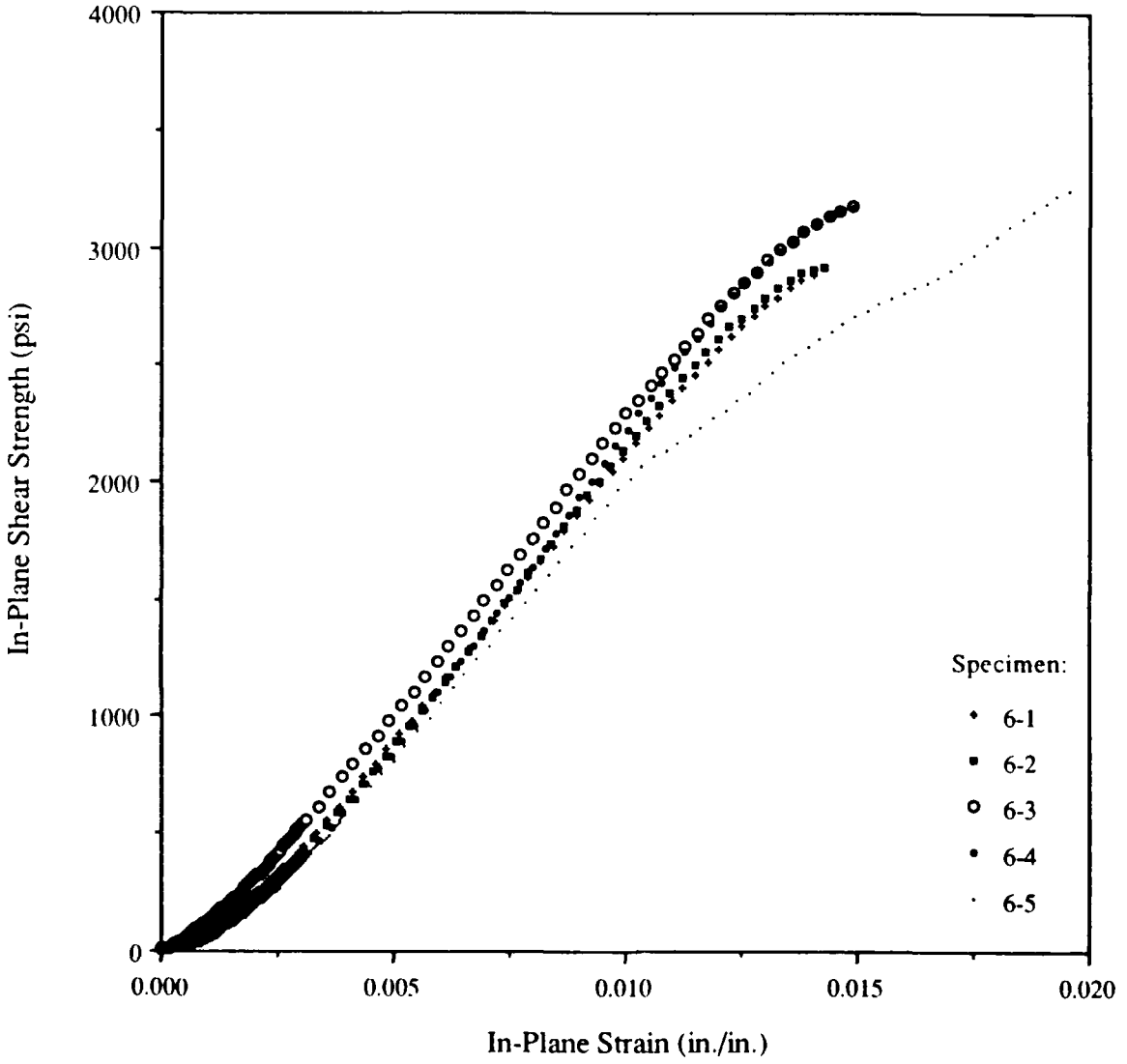

Figure D-6: In-Plane Shear Strength vs. Strain for Panel-5 Lower Face (Kevlar/DERAKANE® 8084)

APPENDIX E

PANEL STATIC PRESSURE LOADING TESTS

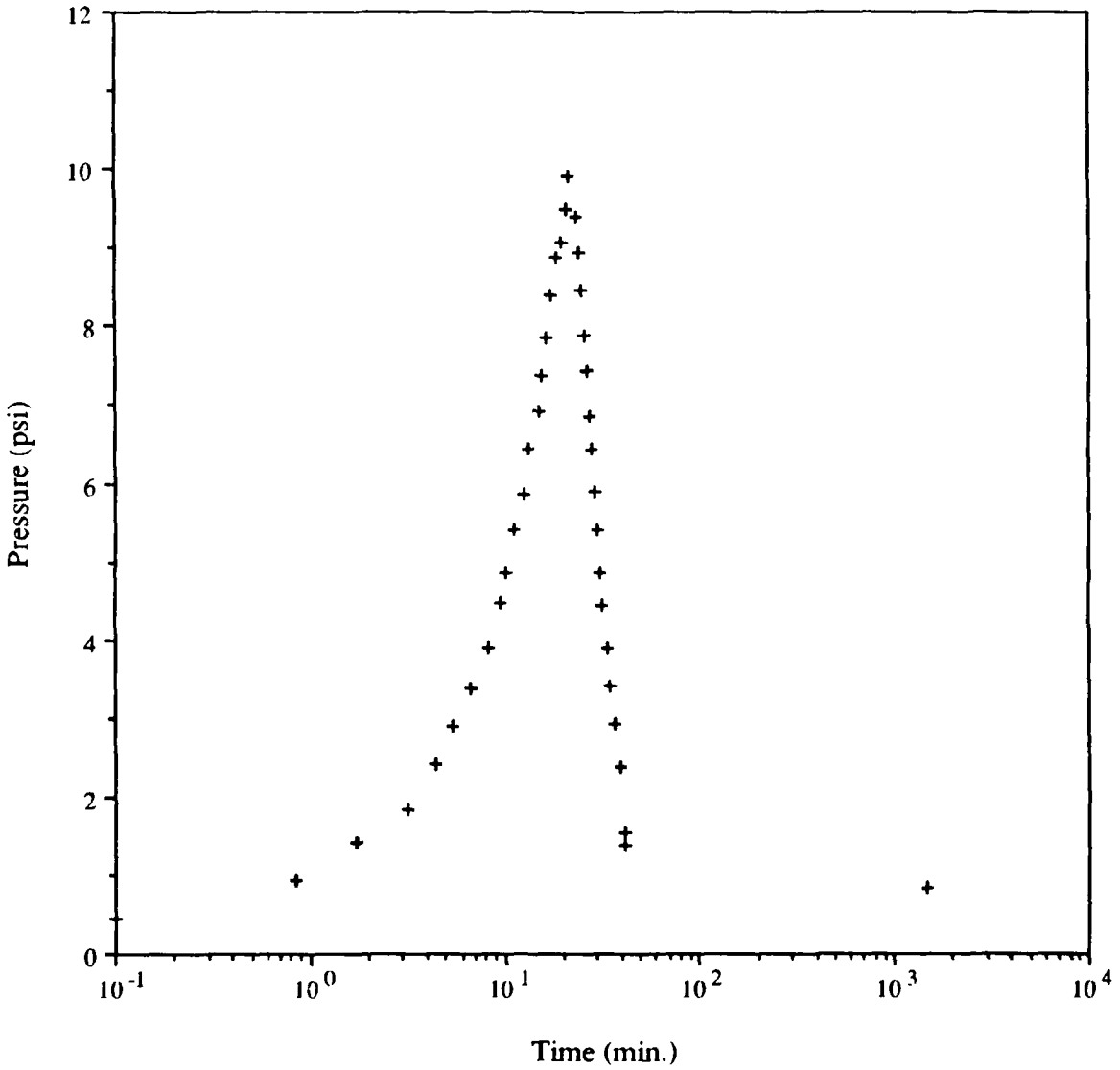

Figure E-1: Pressure vs. Time for Panel-1 Static Pressure Loading Test

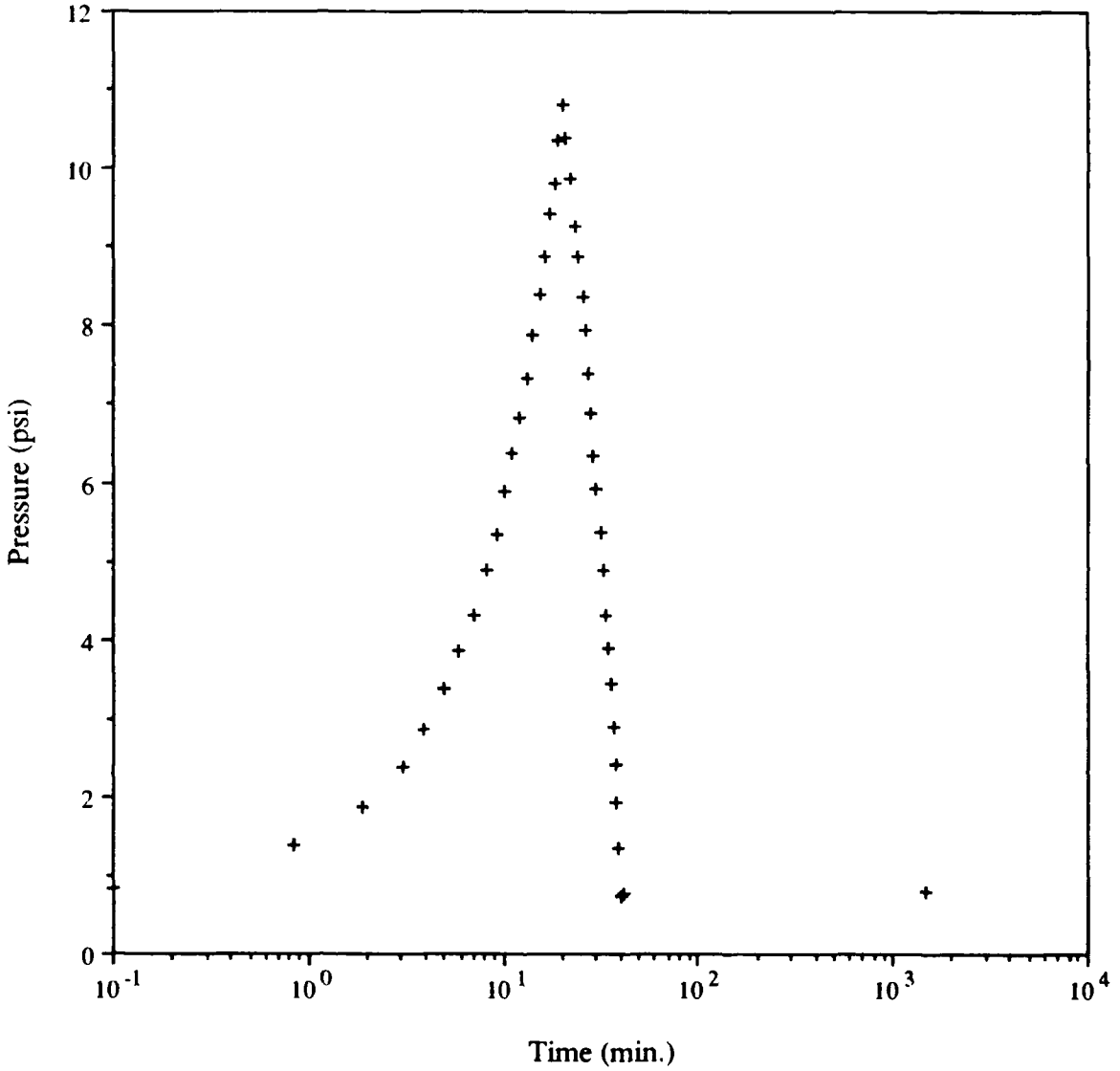

Figure E-2: Pressure vs. Time for Panel-2 Static Pressure Loading Test

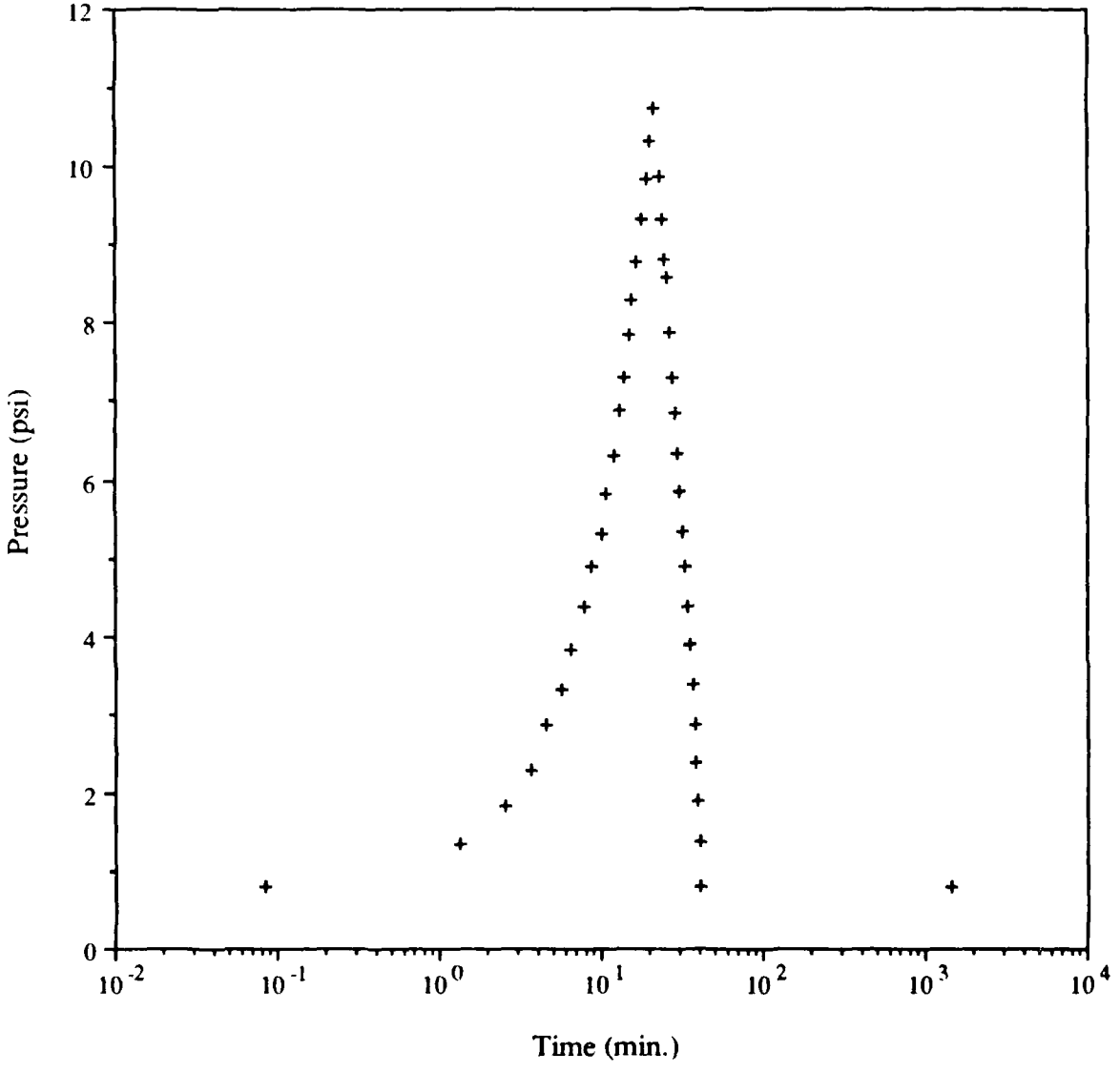

Figure E-3: Pressure vs. Time for Panel-3 Static Pressure Loading Test

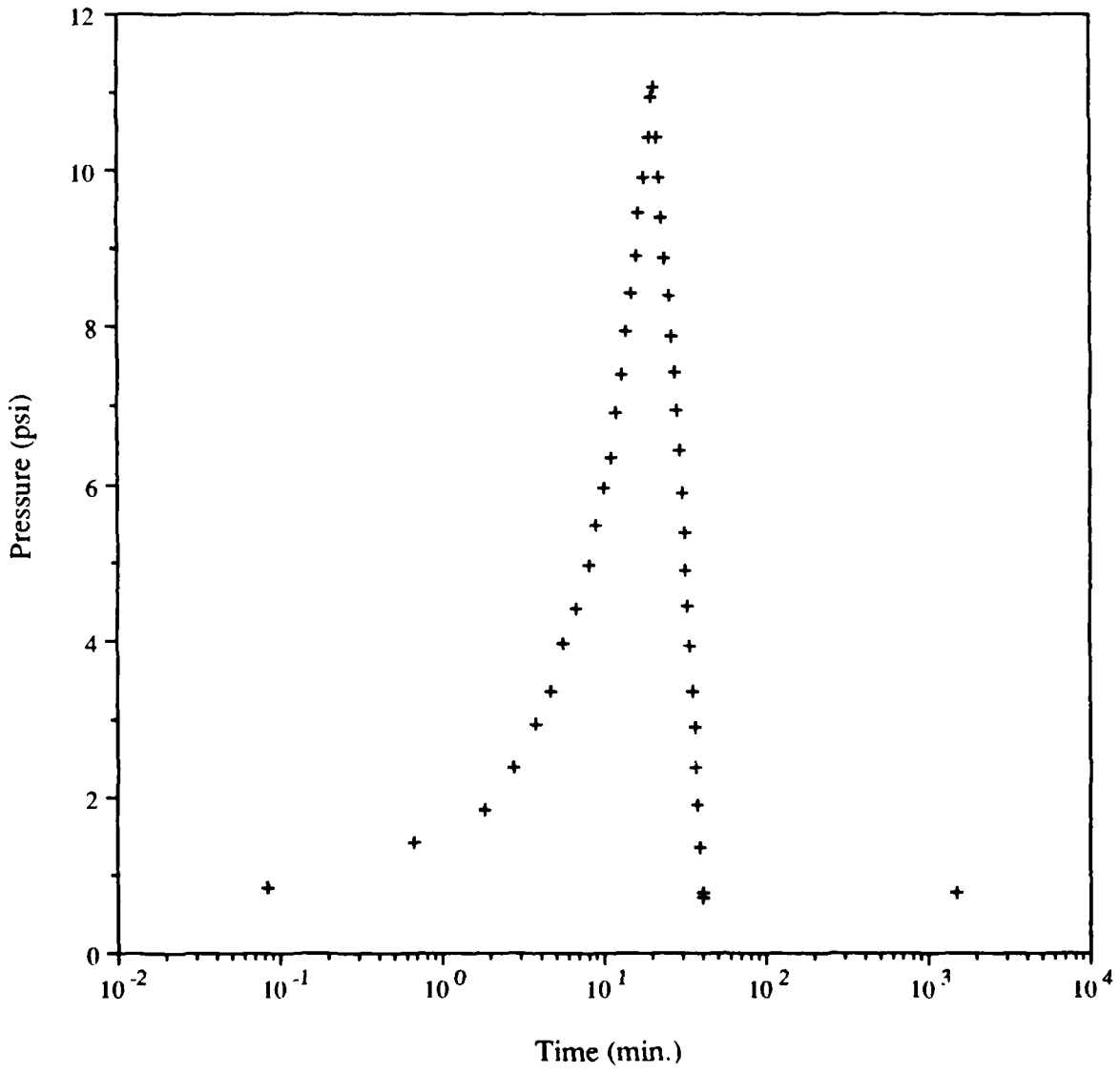

Figure E-4: Pressure vs. Time for Panel-4 Static Pressure Loading Test

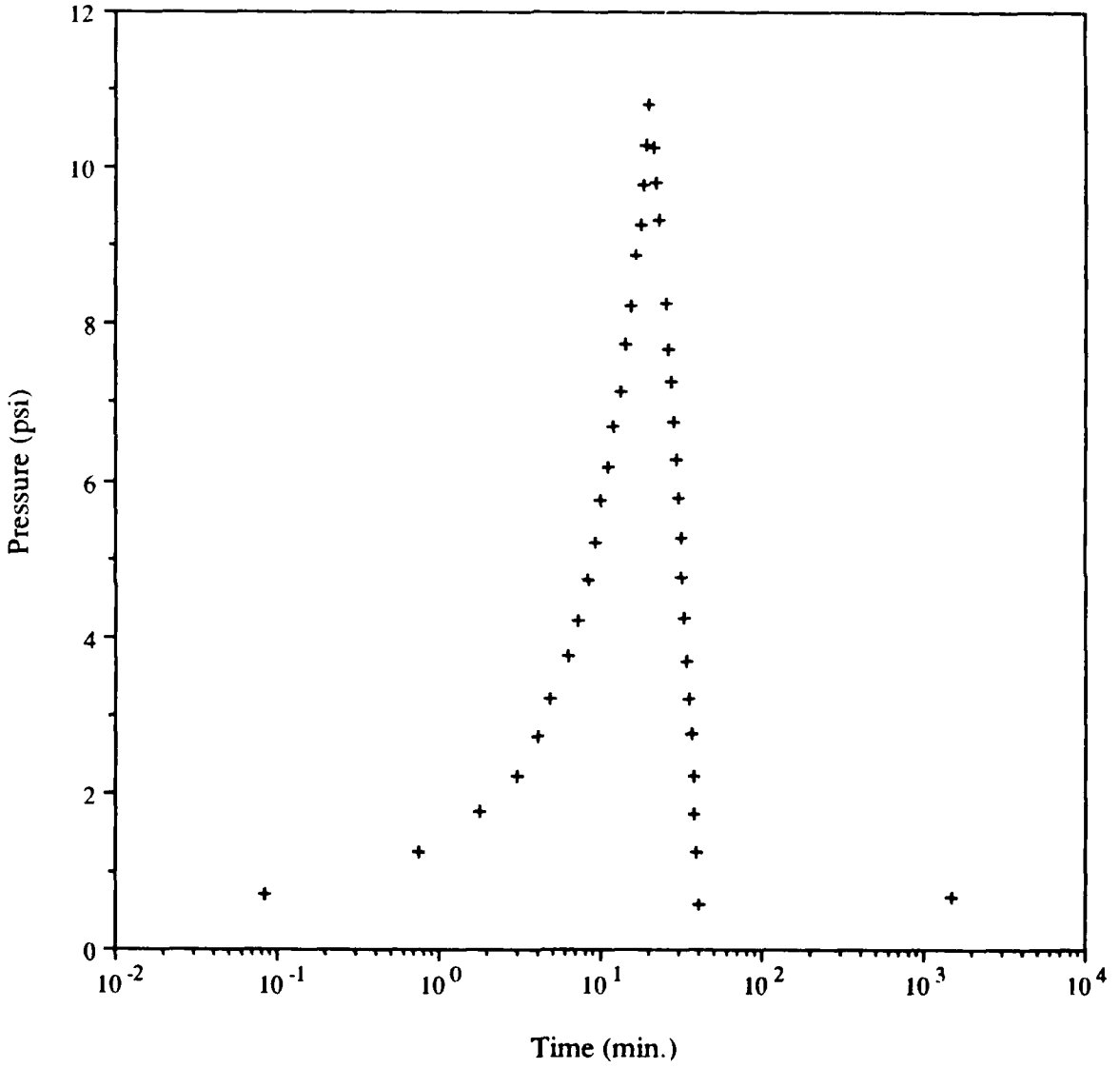

Figure E-5: Pressure vs. Time for Panel-5 Static Pressure Loading Test

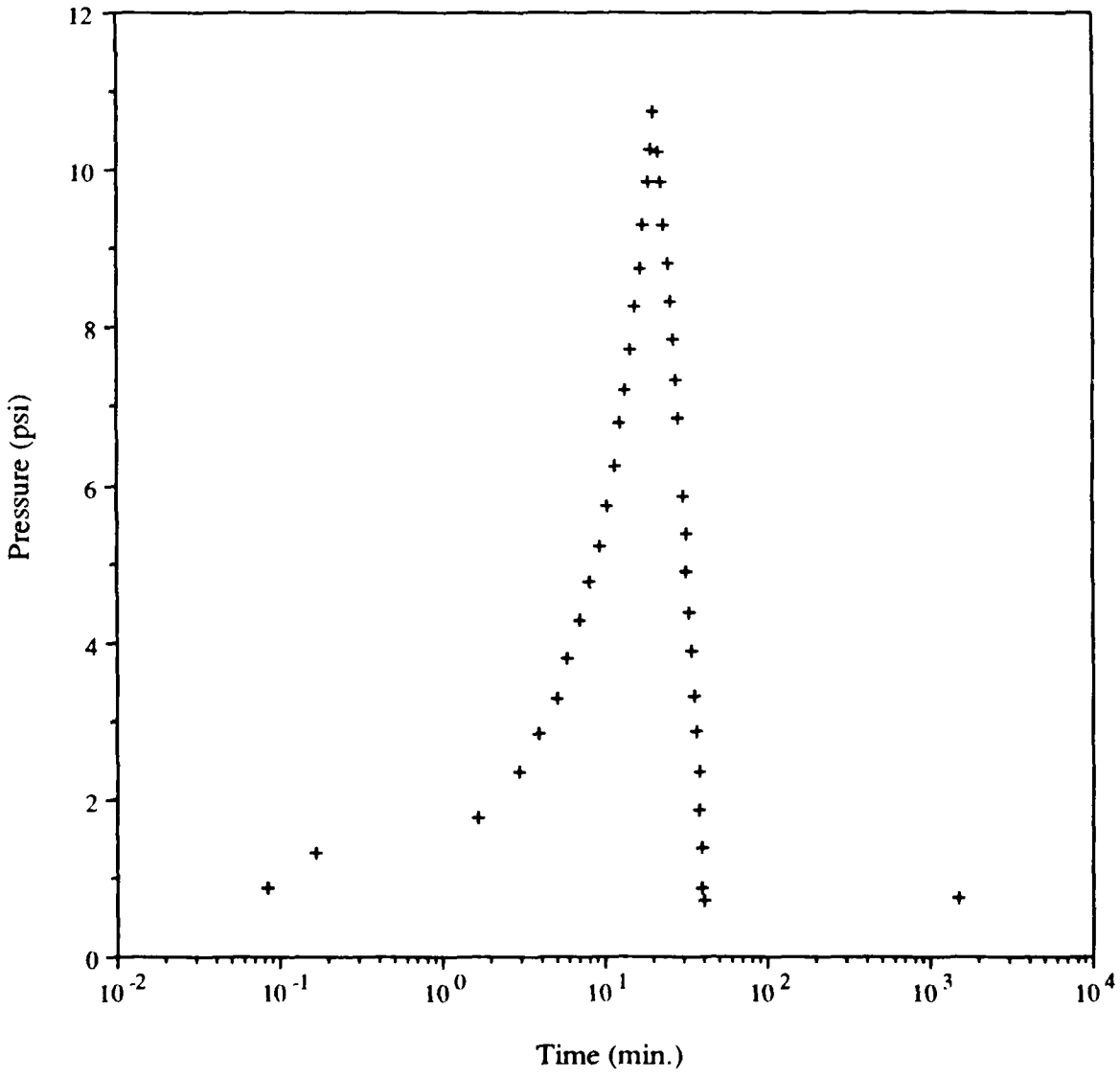

Figure E-6: Pressure vs. Time for Panel-6 Static Pressure Loading Test

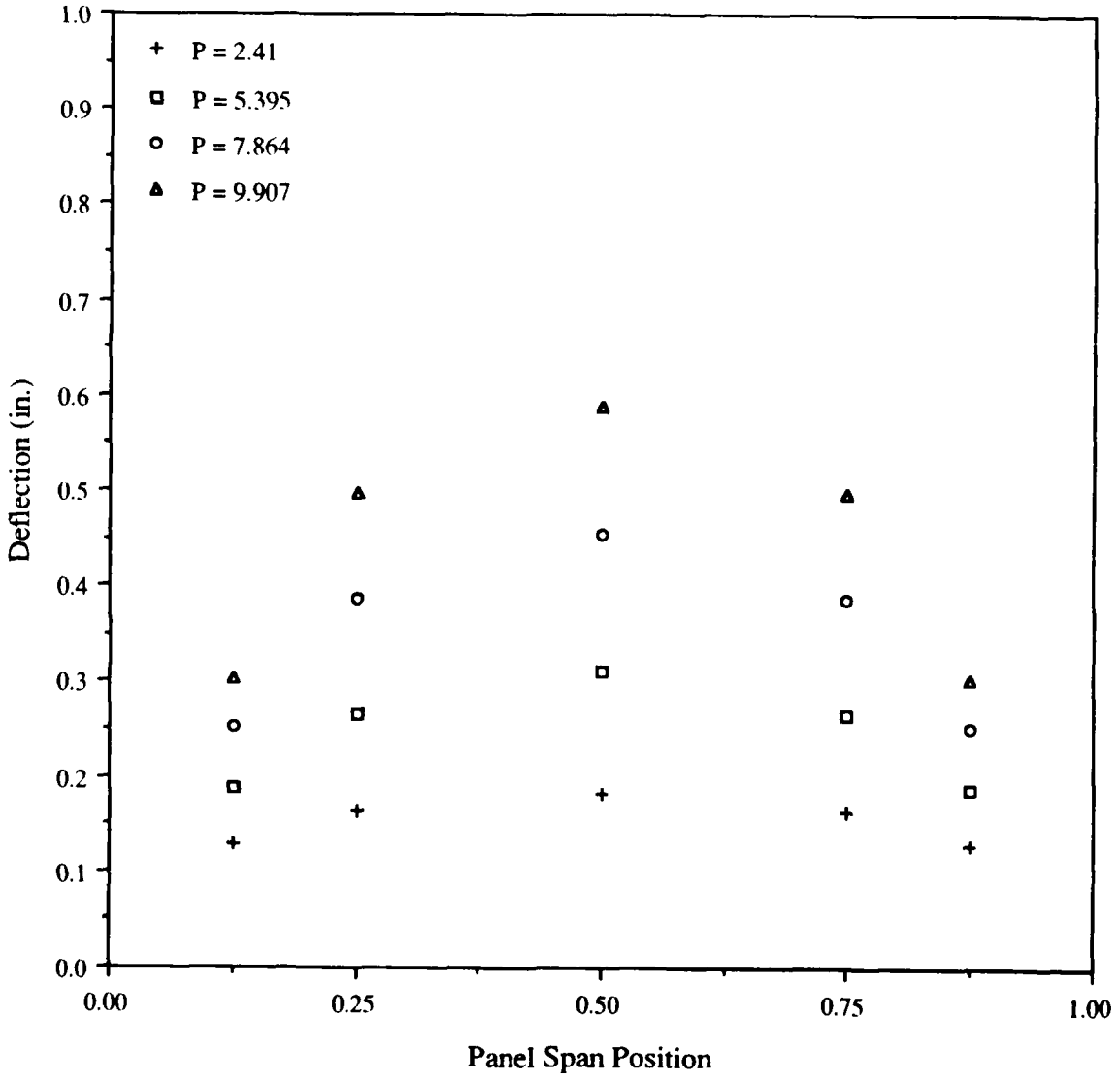

Figure E-7: Transverse Deflected Shape of Panel-1 During Load Cycle of Static Pressure Test

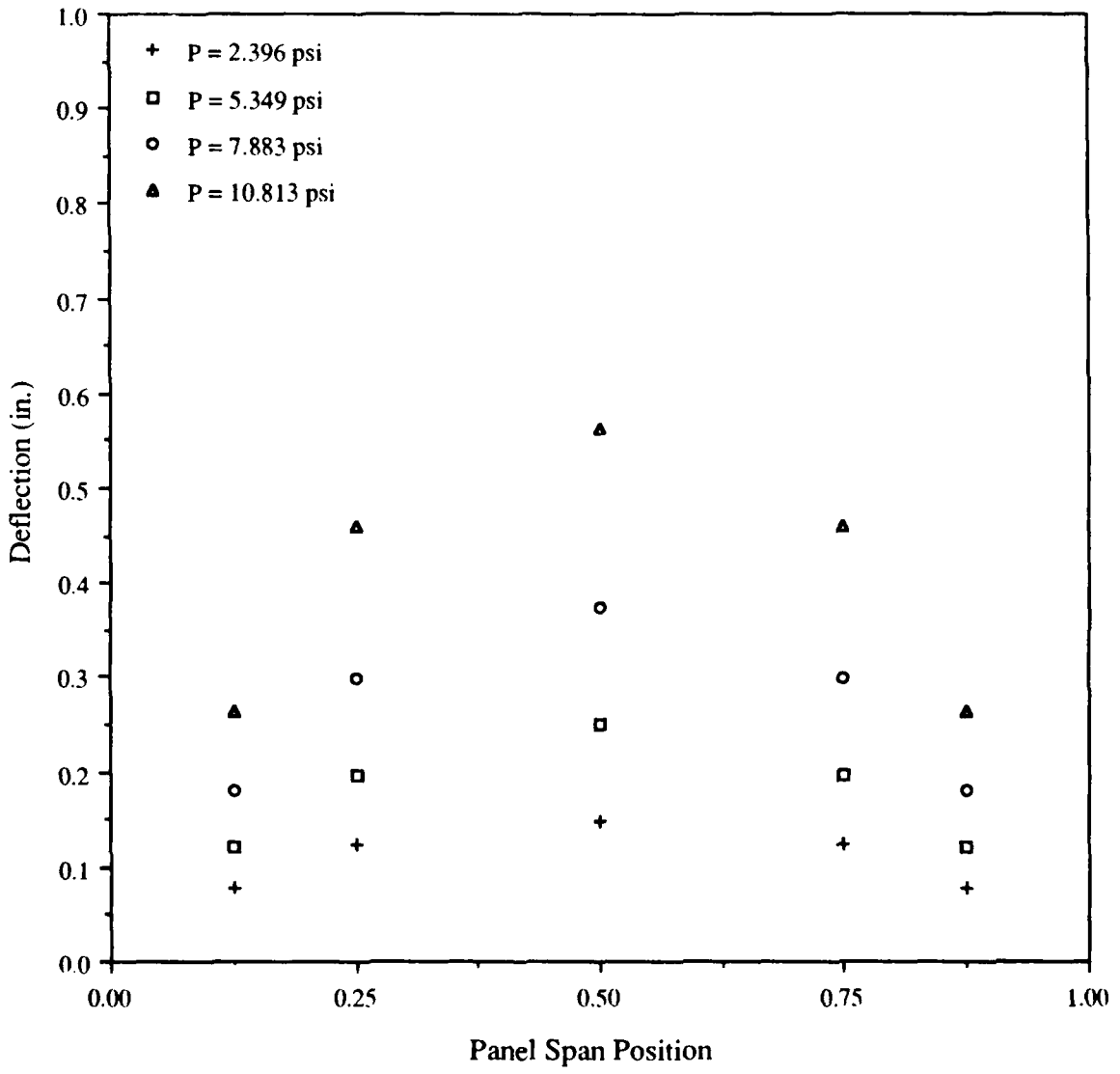

Figure E-8: Transverse Deflected Shape of Panel-2 During Load Cycle of Static Pressure Test

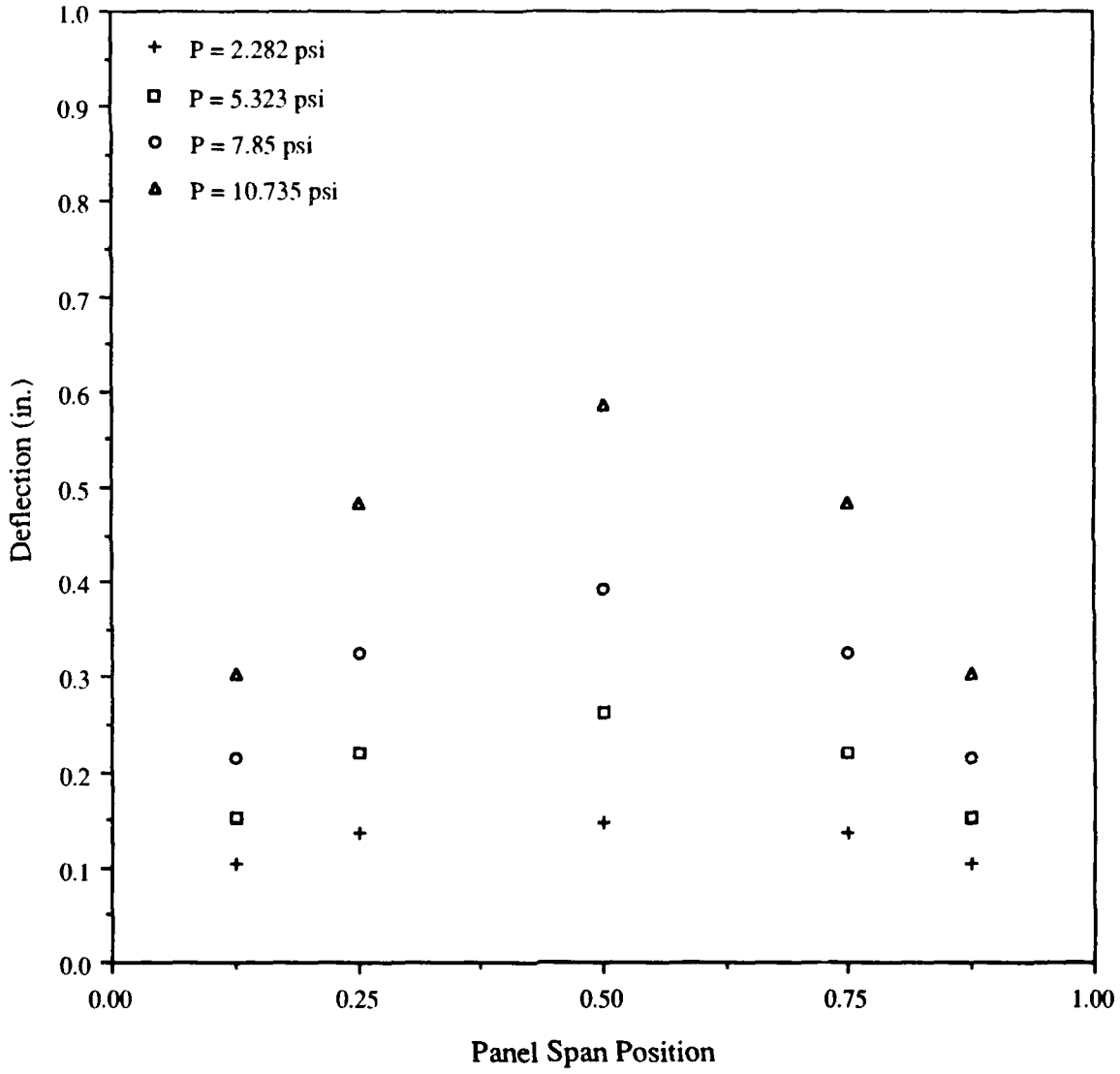

Figure E-9: Transverse Deflected Shape of Panel-3 During Load Cycle of Static Pressure Test

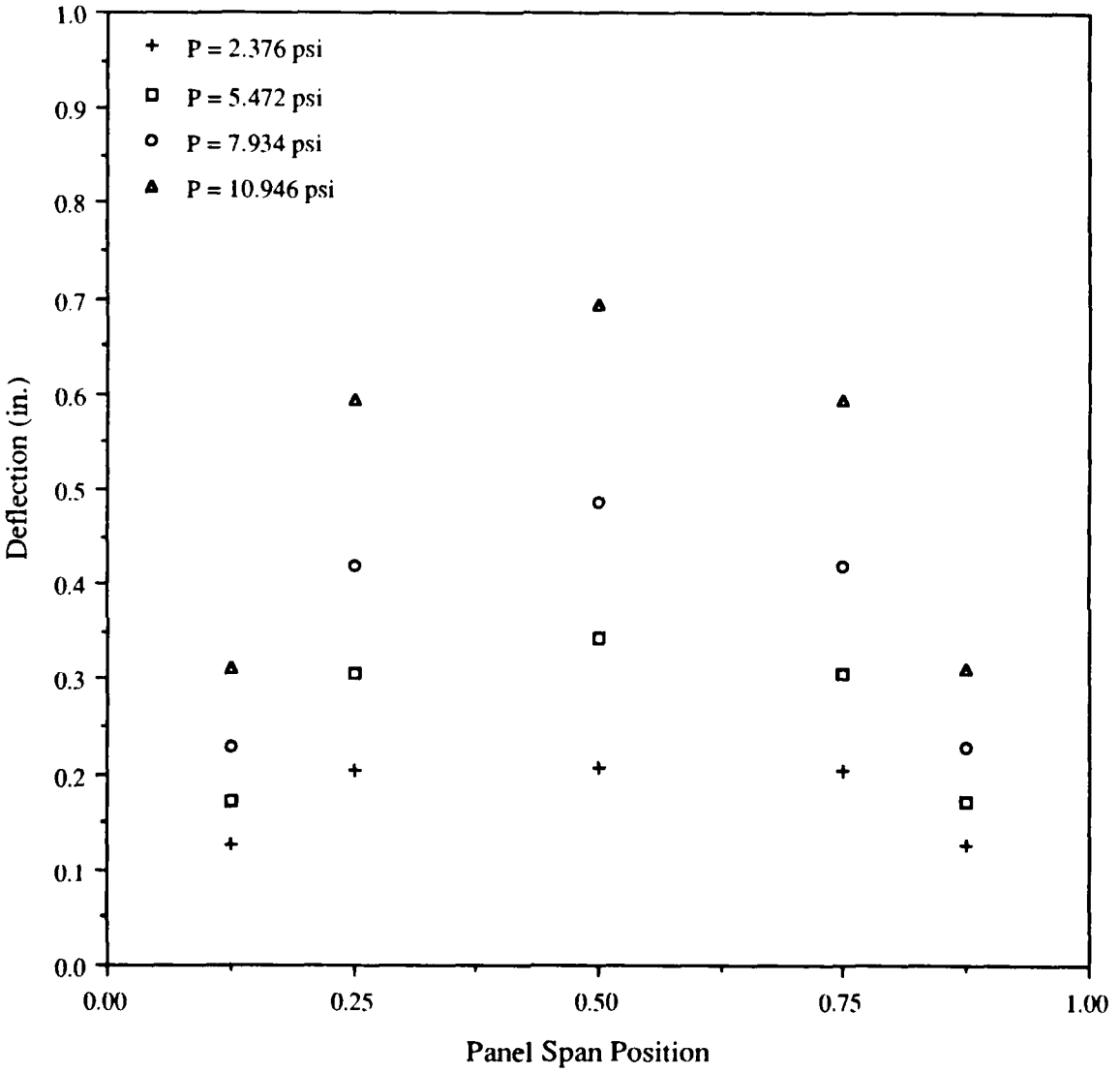

Figure E-10: Transverse Deflected Shape of Panel-4 During Load Cycle of Static Pressure Test

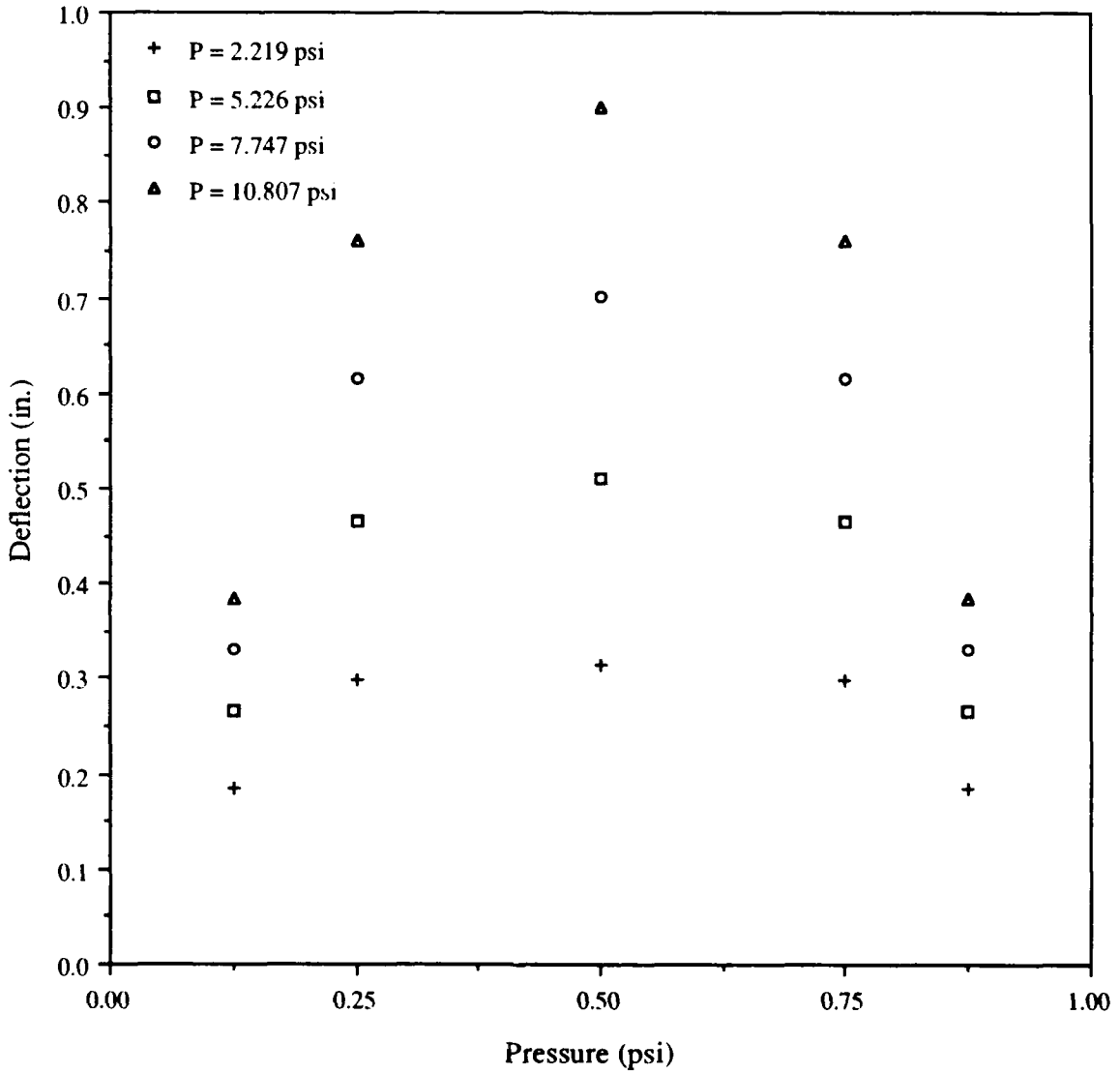

Figure E-11: Transverse Deflected Shape of Panel-5 During Load Cycle of Static Pressure Test

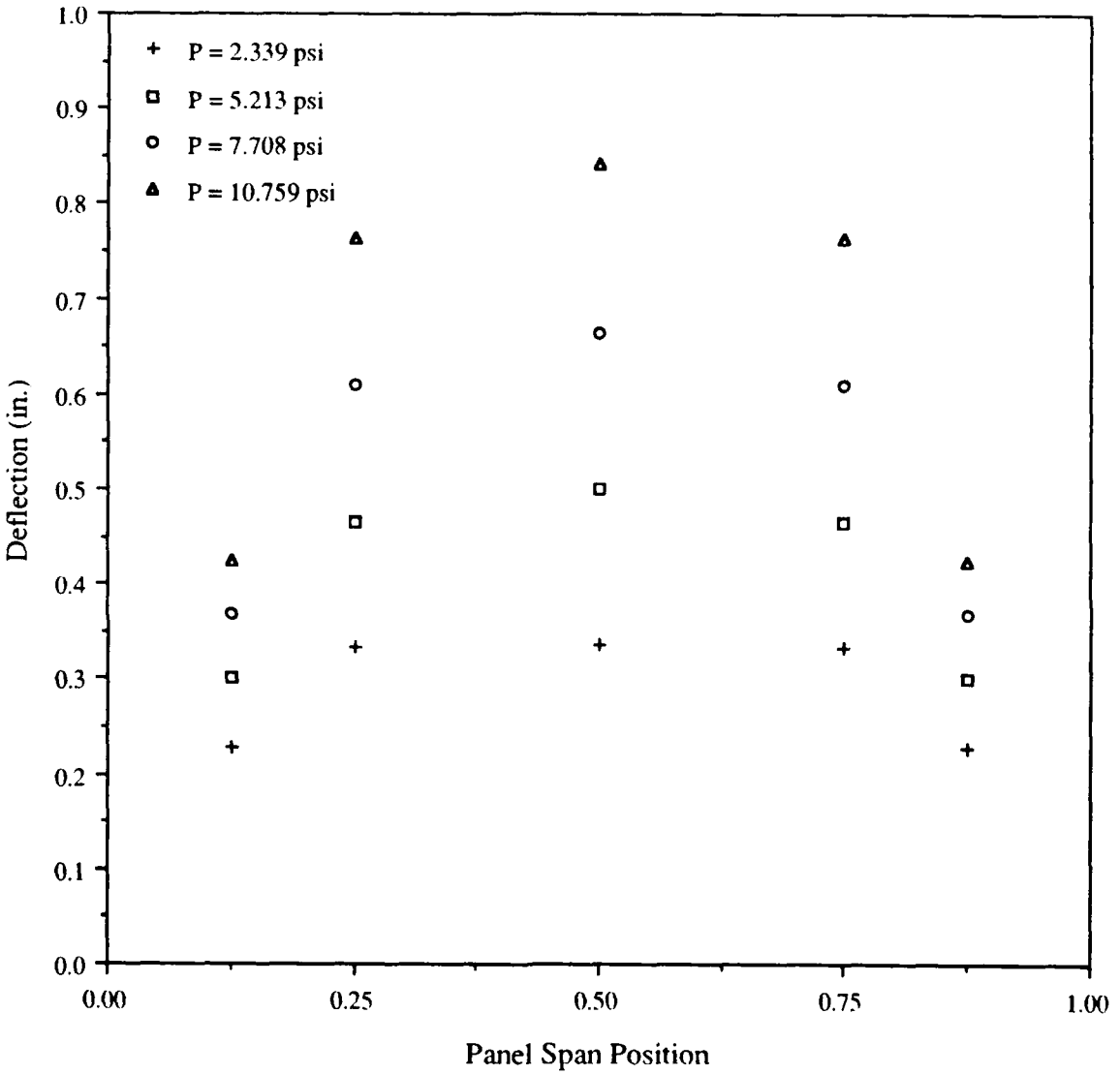

Figure E-12: Transverse Deflected Shape of Panel-6 During Load Cycle of Static Pressure Test

APPENDIX F

PANEL CYCLIC PRESSURE LOADING TESTS

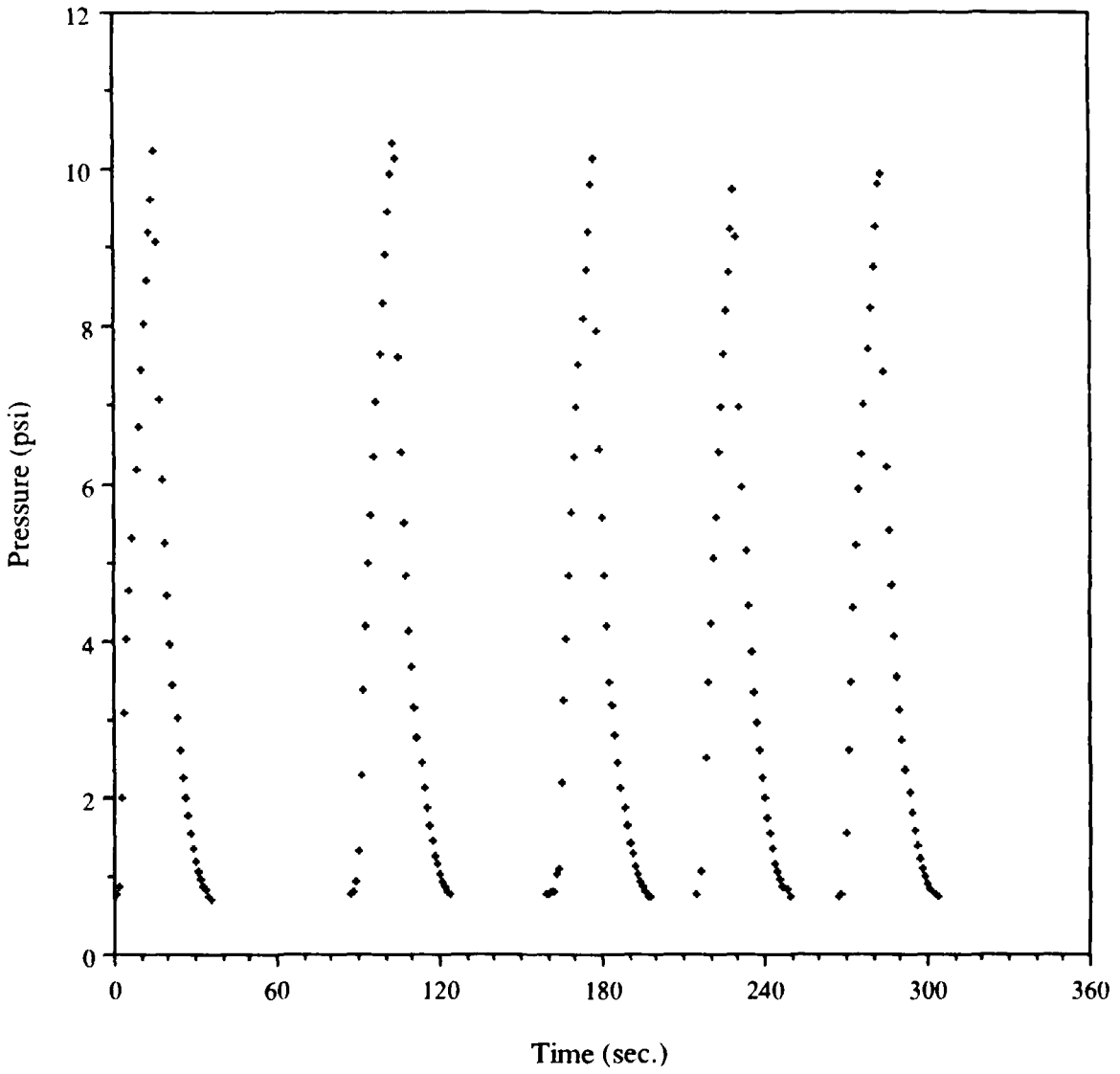

Figure F-1: Pressure vs. Time for Panel-1 Cyclic Pressure Loading Test

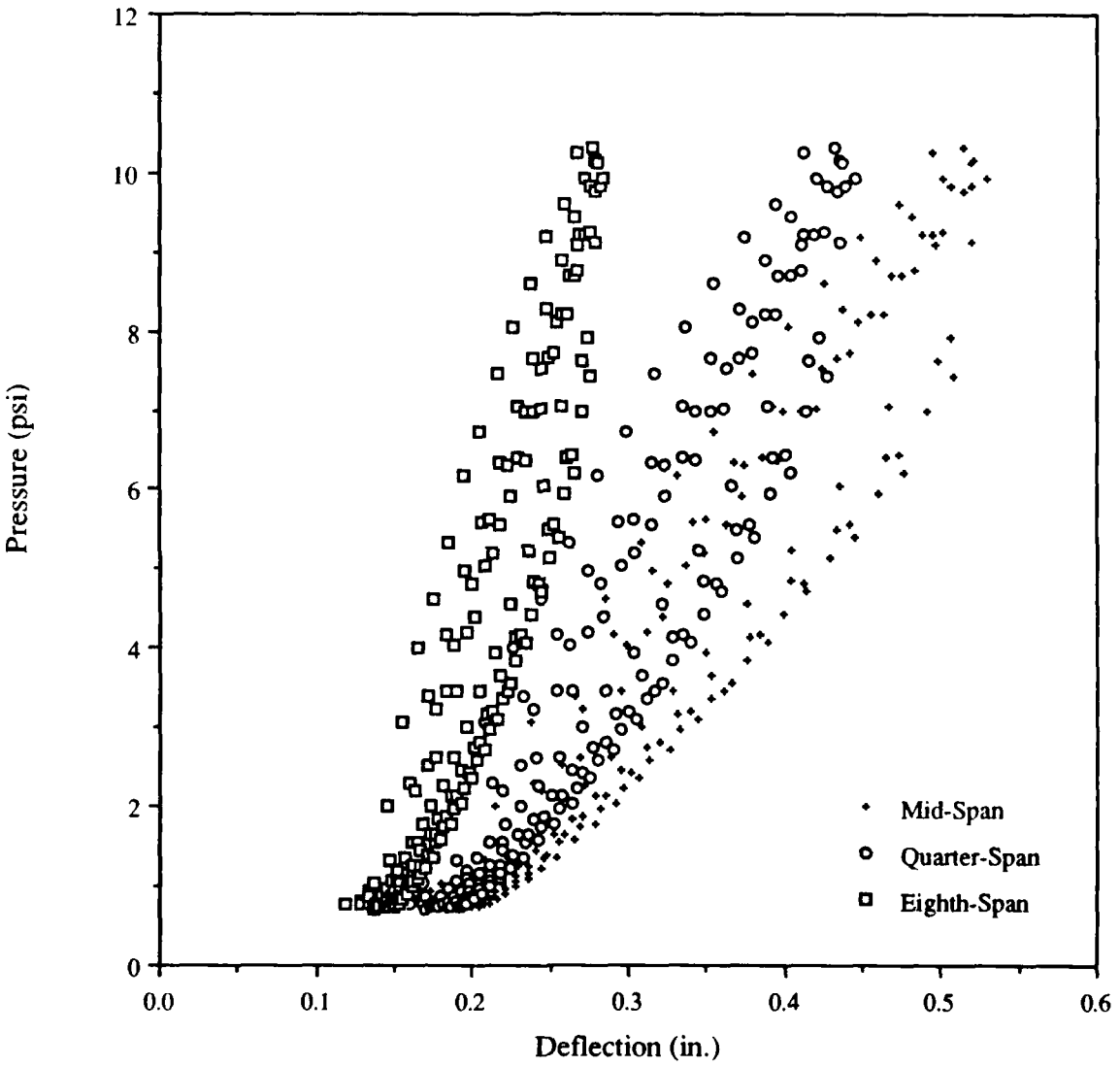

Figure F-2: Deflection Response of Panel-1 to Cyclic Pressure Loading

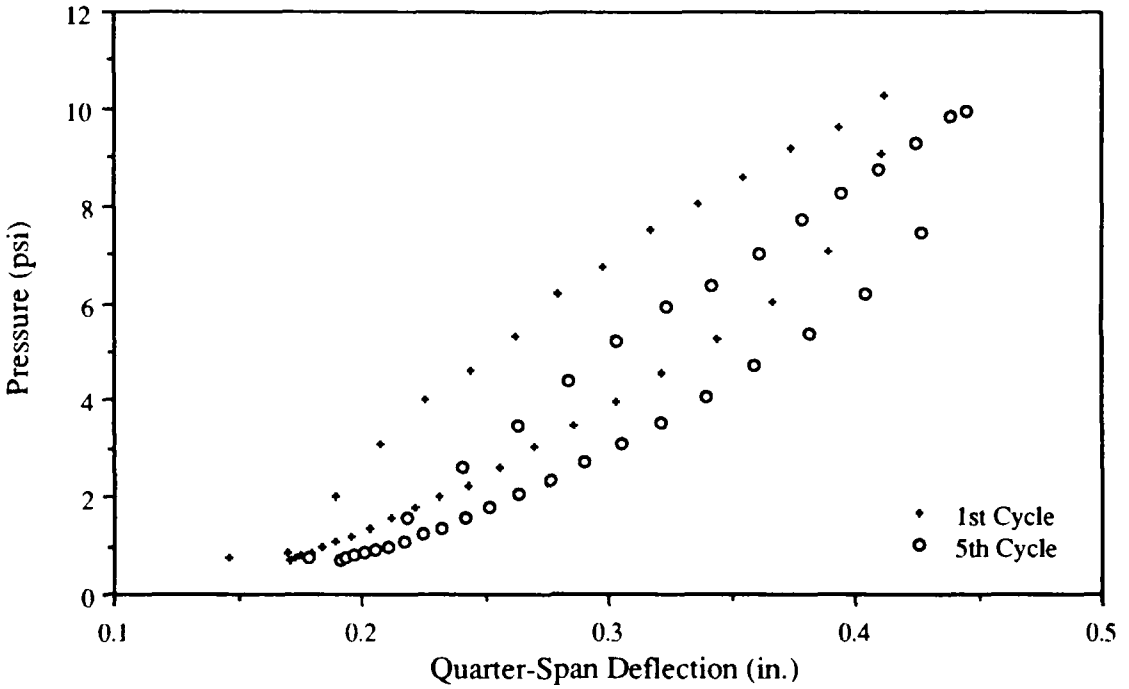

Figure F-3: Quarter-Span Deflection Response of Panel-1 to Cyclic Pressure Loading (Cycles 1 & 5)

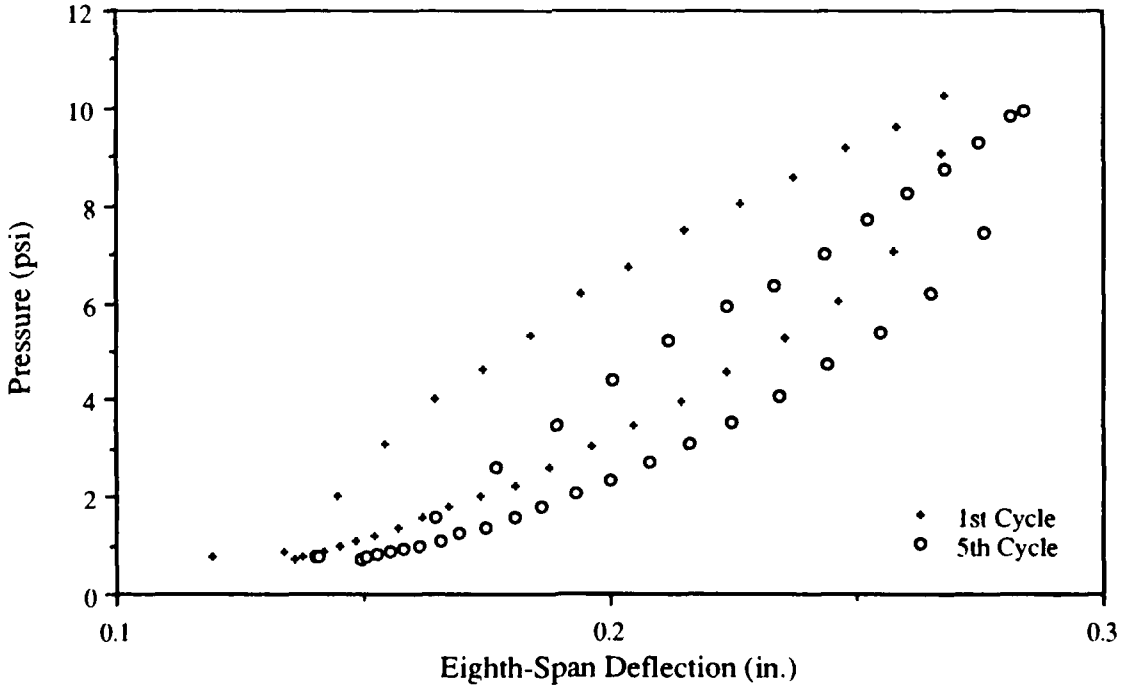

Figure F-4: Eighth-Span Deflection Response of Panel-1 to Cyclic Pressure Loading (Cycles 1 & 5)

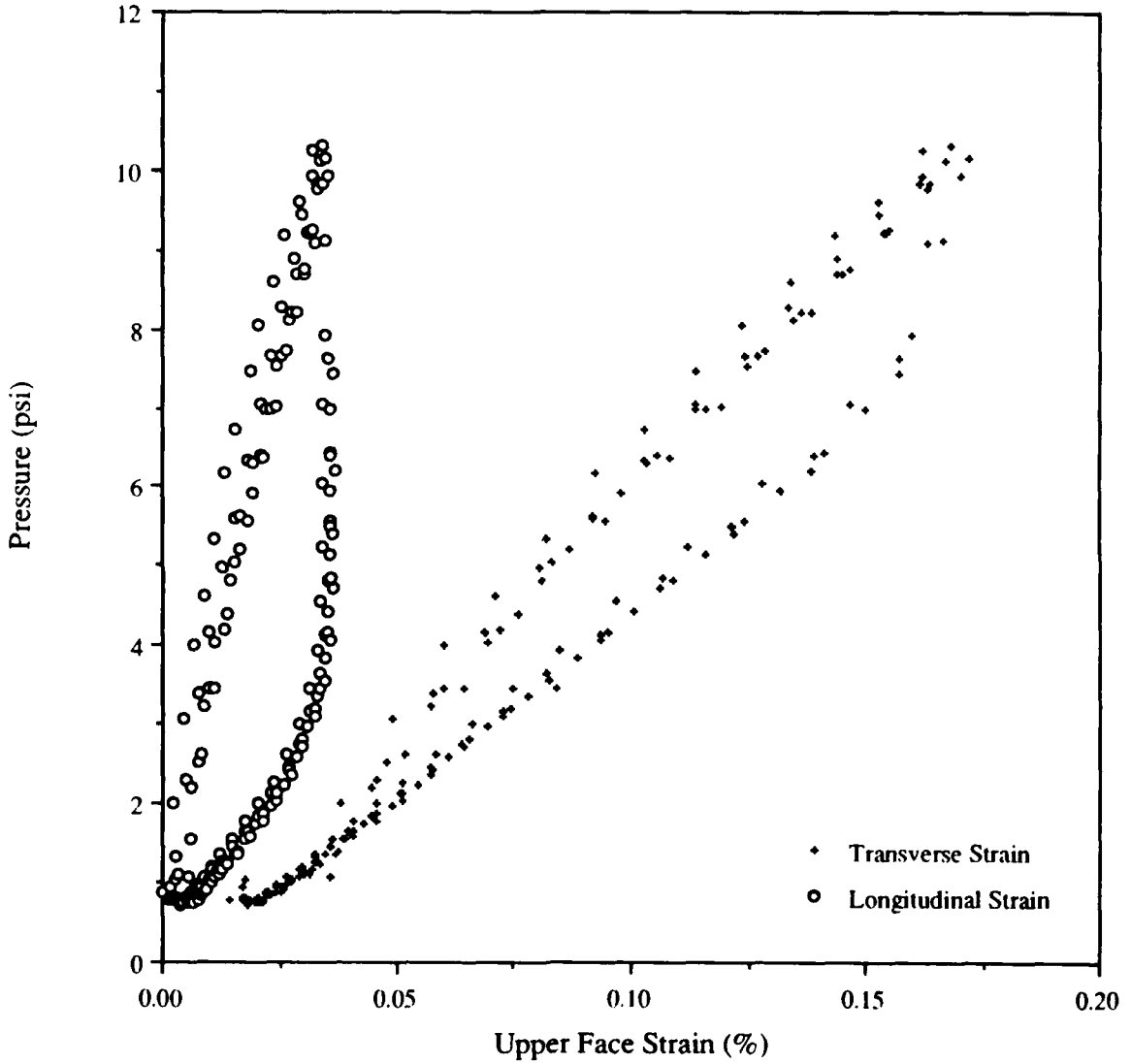

Figure F-5: Upper Face Strain Response of Panel-1 to Cyclic Pressure Loading

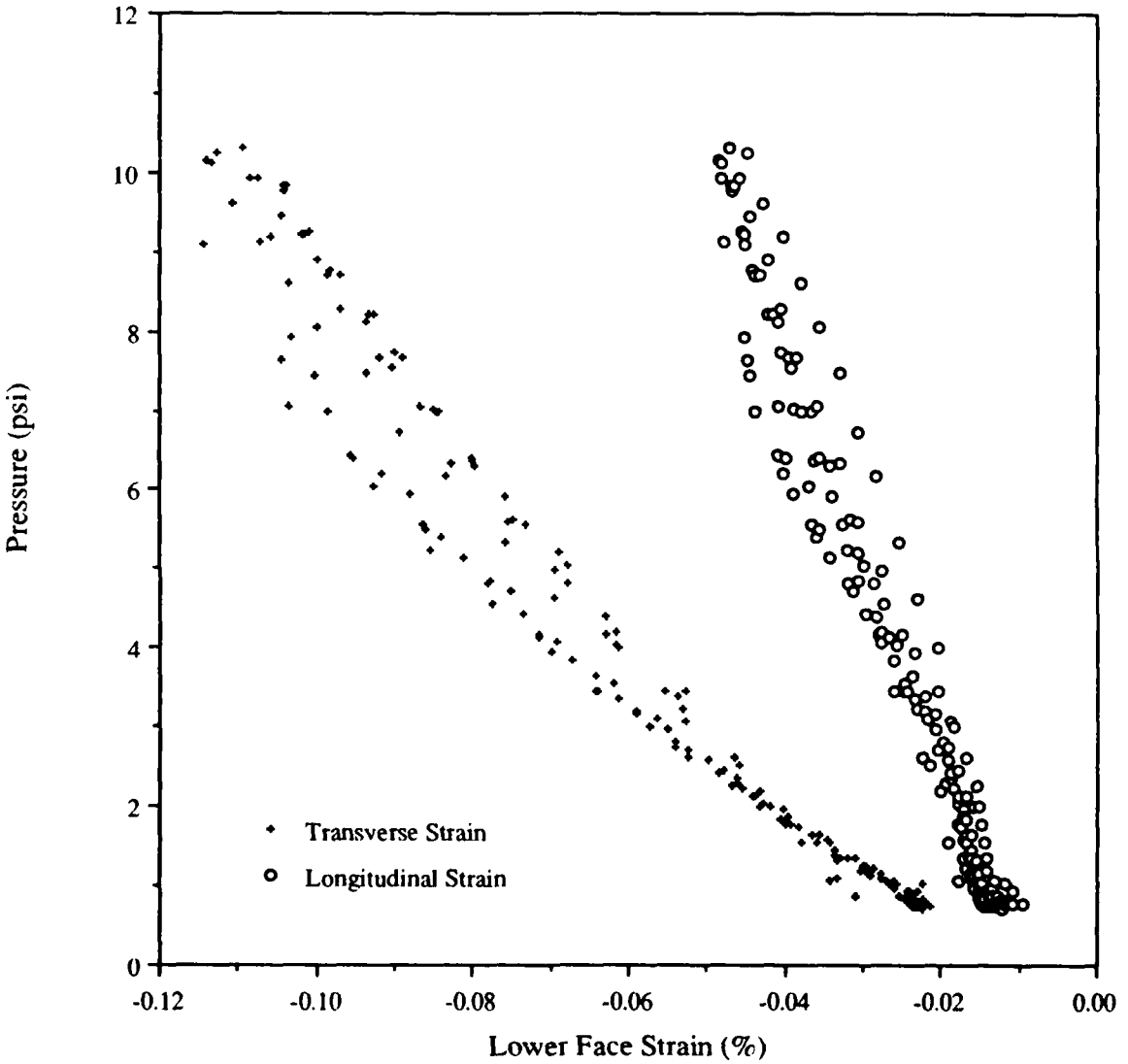

Figure F-6: Lower Face Strain Response of Panel-1 to Cyclic Pressure Loading

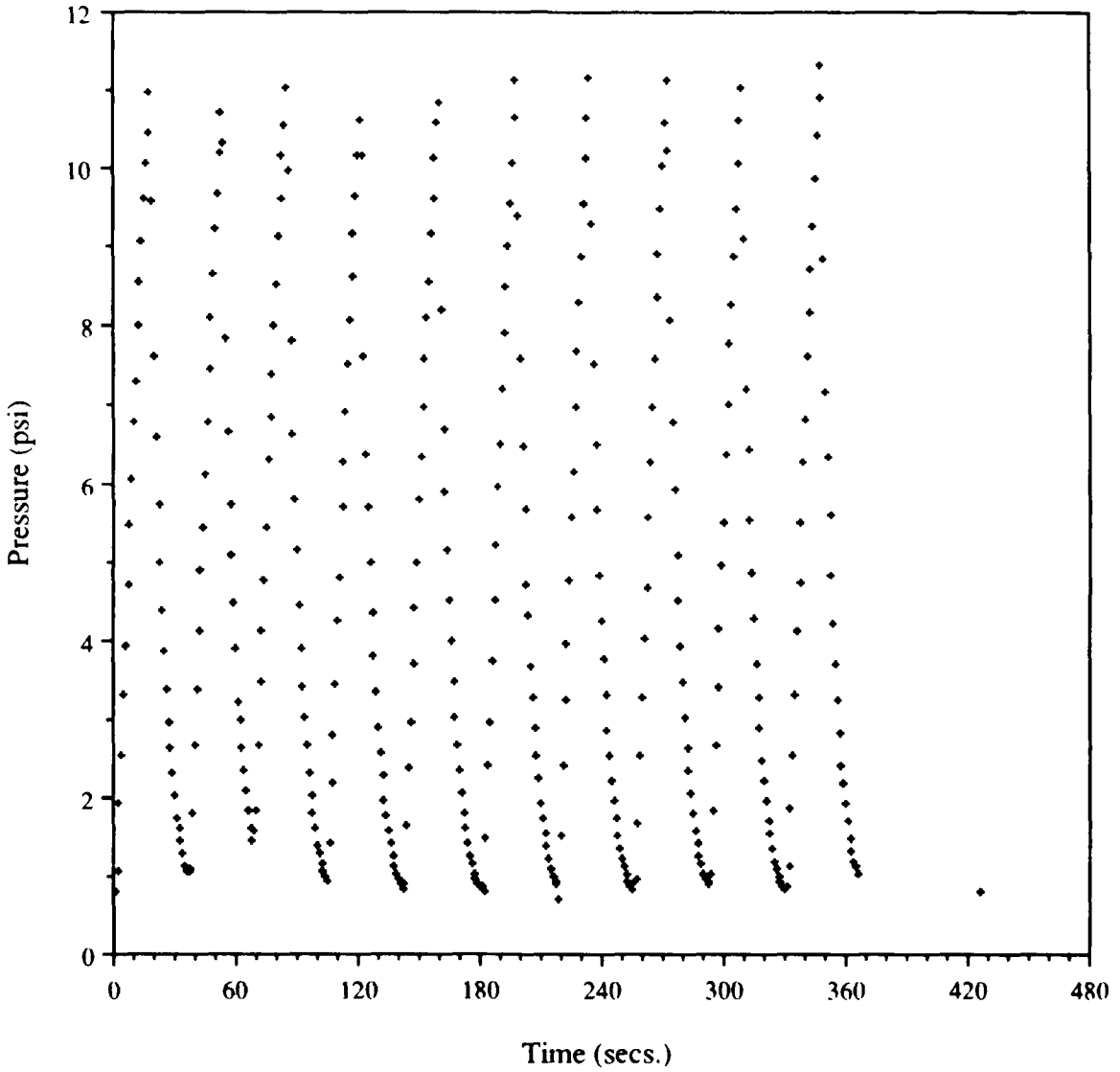

Figure F-7: Pressure vs. Time for Panel-2 Cyclic Pressure Loading Test

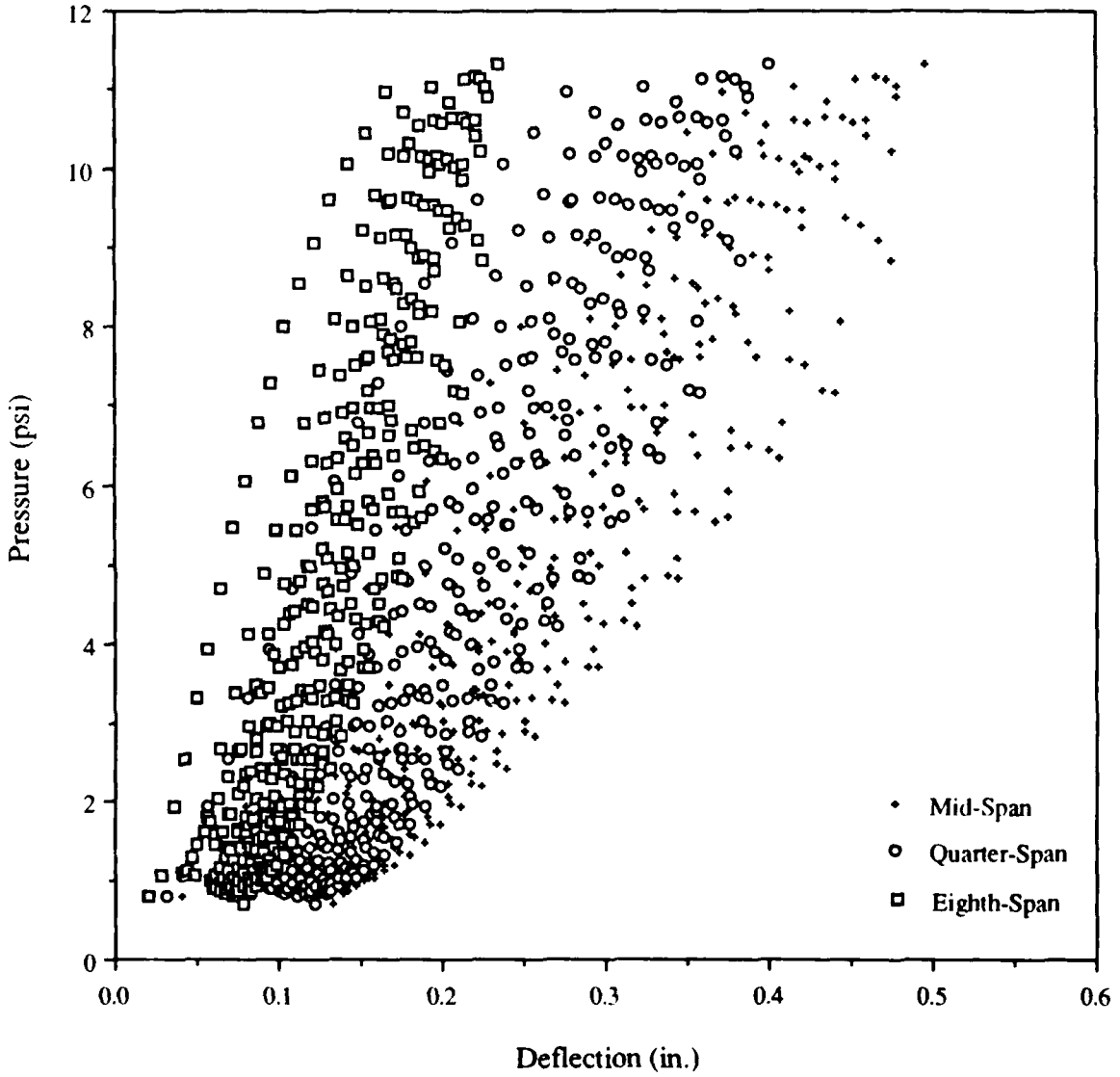

Figure F-8: Deflection Response of Panel-2 to Cyclic Pressure Loading

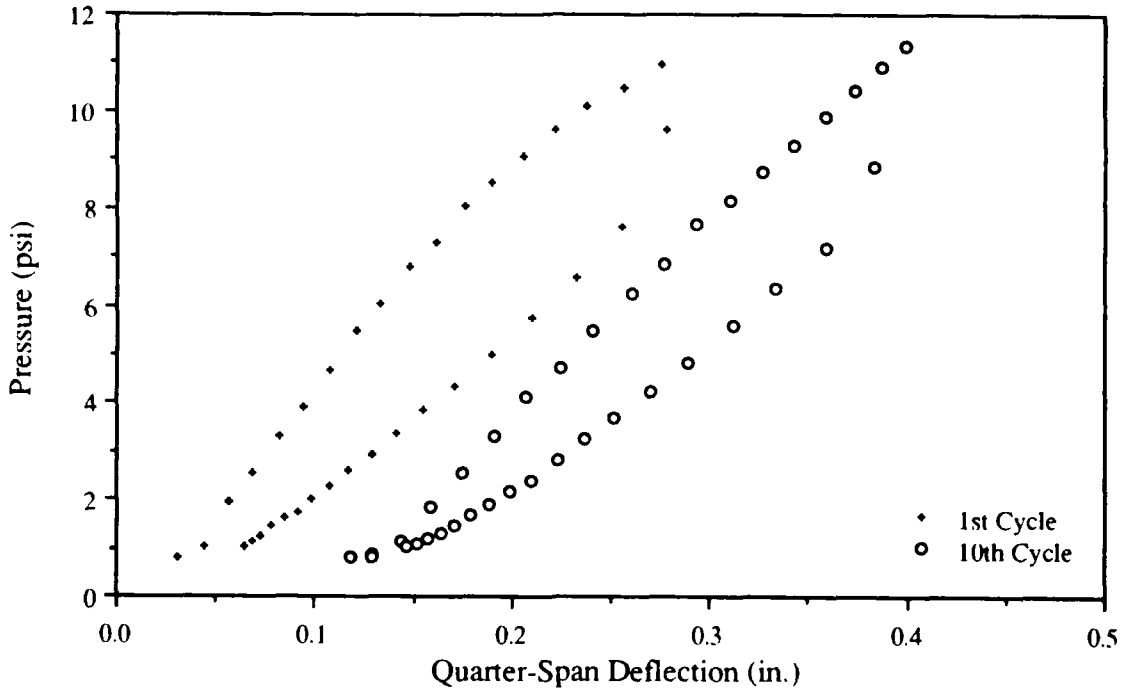

Figure F-9: Quarter-Span Deflection Response of Panel-2 to Cyclic Pressure Loading (Cycles 1 & 10)

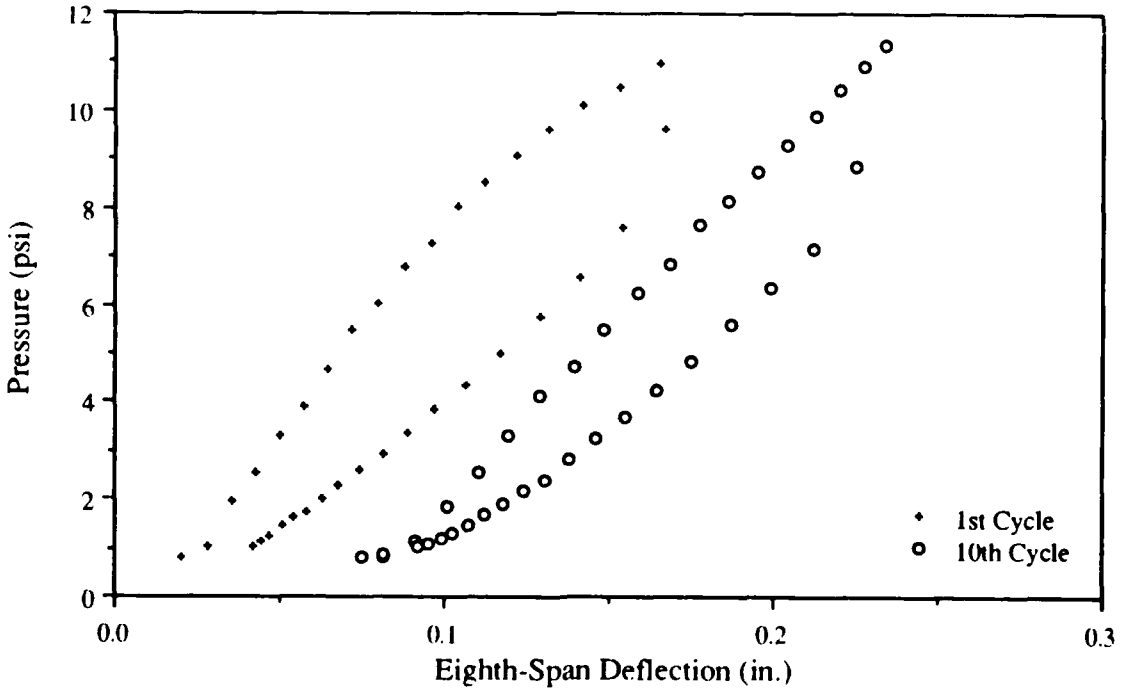

Figure F-10: Eighth-Span Deflection Response of Panel-2 to Cyclic Pressure Loading (Cycles 1 & 10)

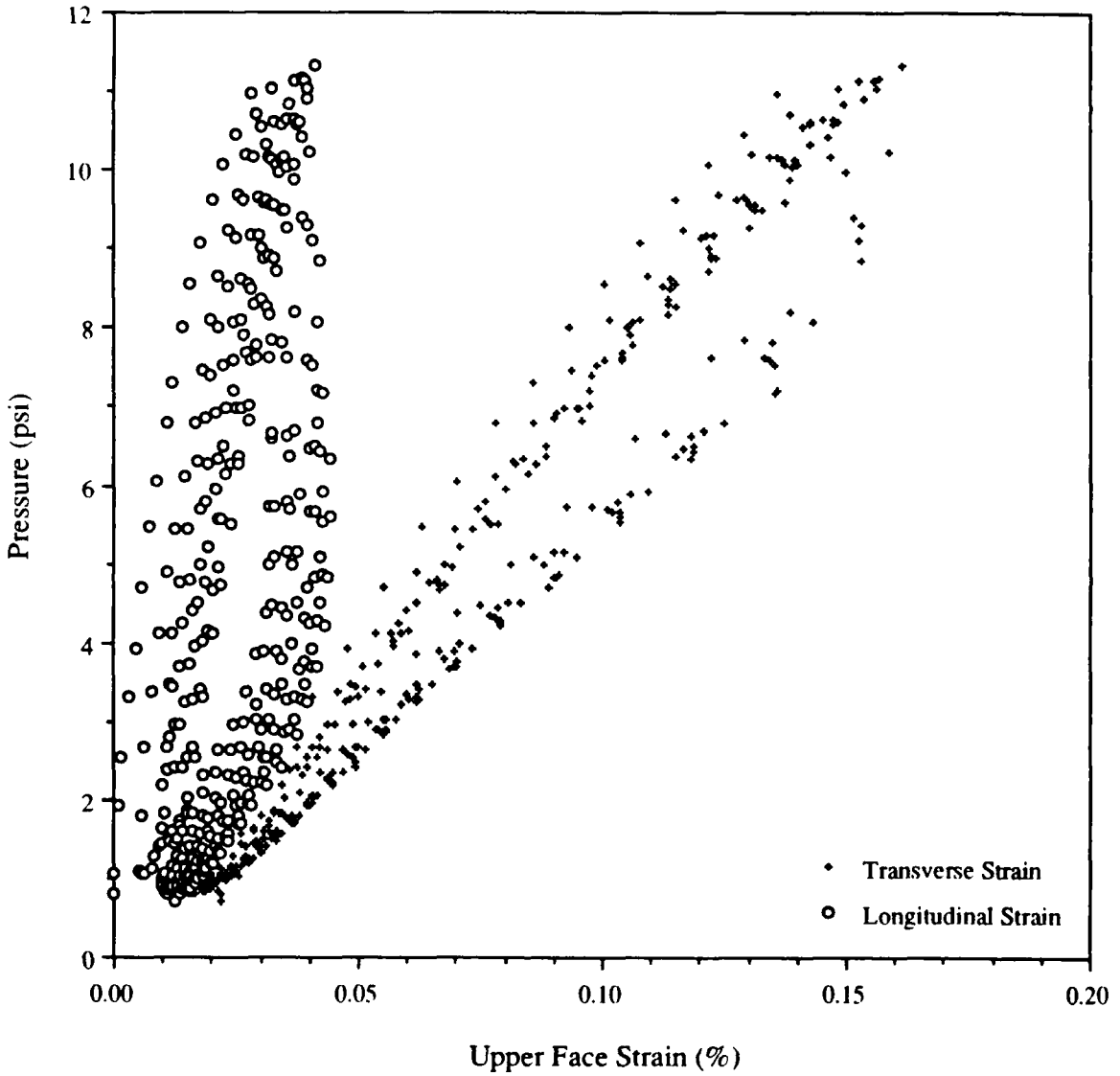

Figure F-11: Upper Face Strain Response of Panel-2 to Cyclic Pressure Loading

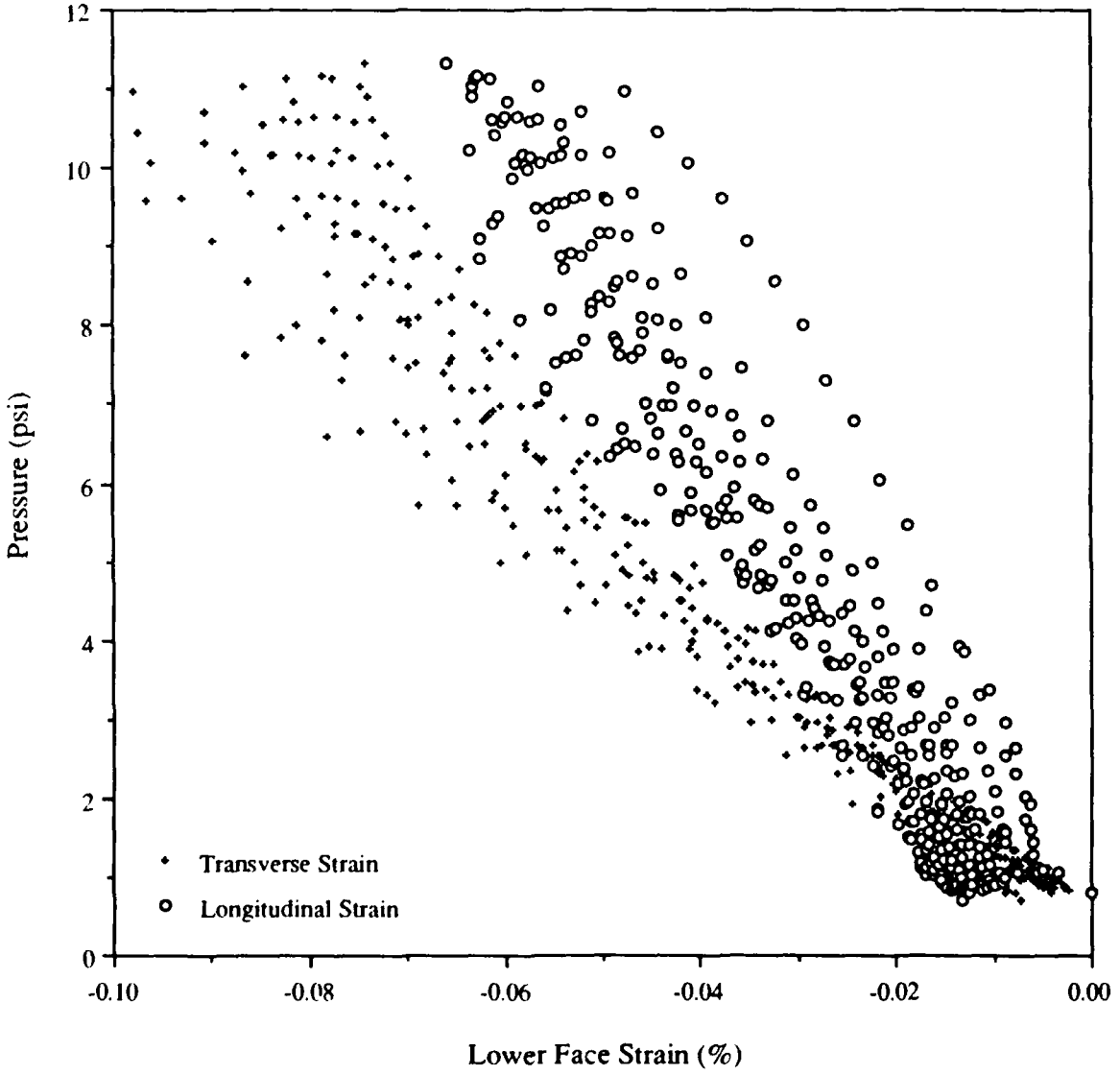

Figure F-12: Lower Face Strain Response of Panel-2 to Cyclic Pressure Loading

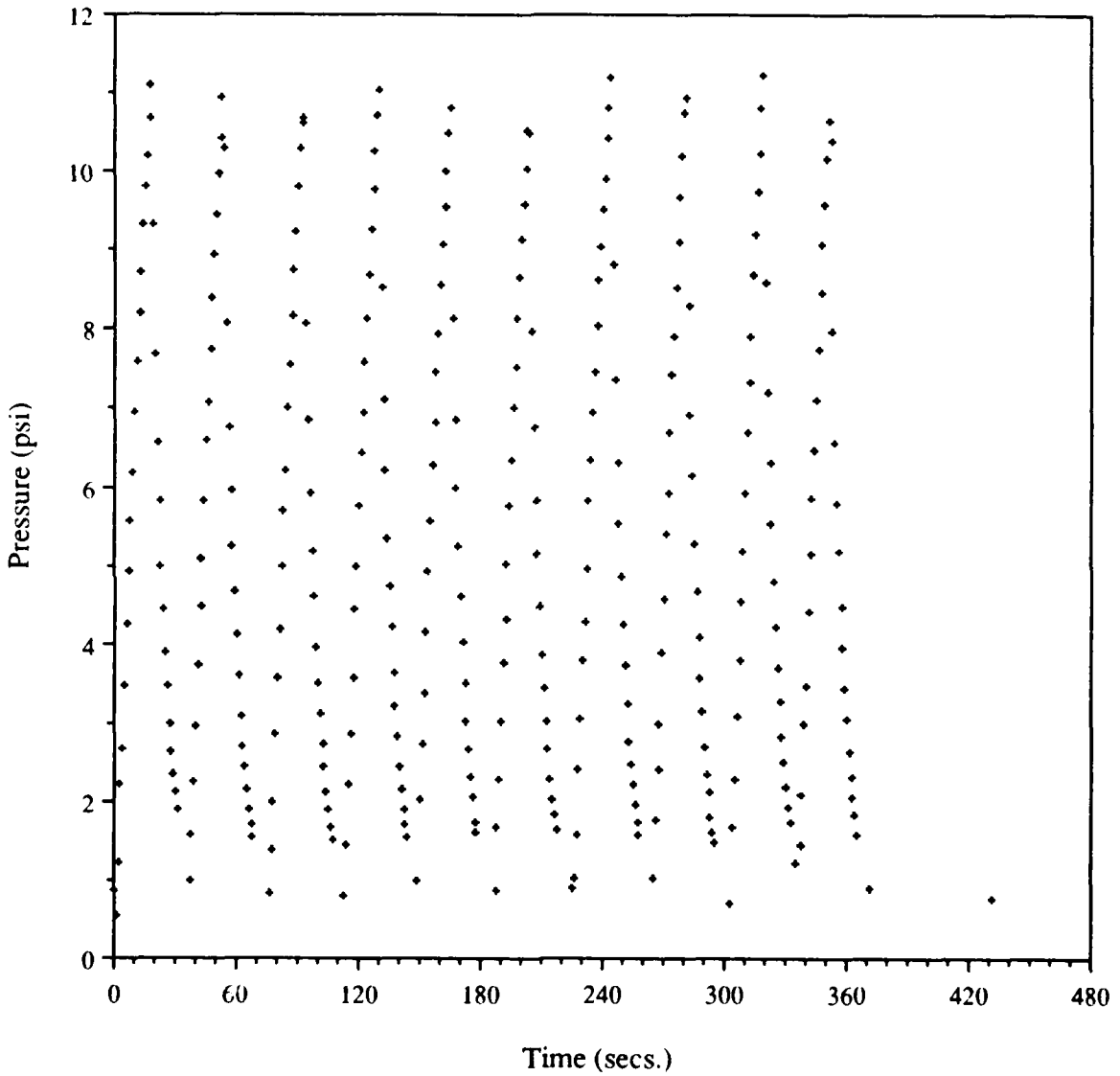

Figure F-13: Pressure vs. Time for Panel-3 Cyclic Pressure Loading Test

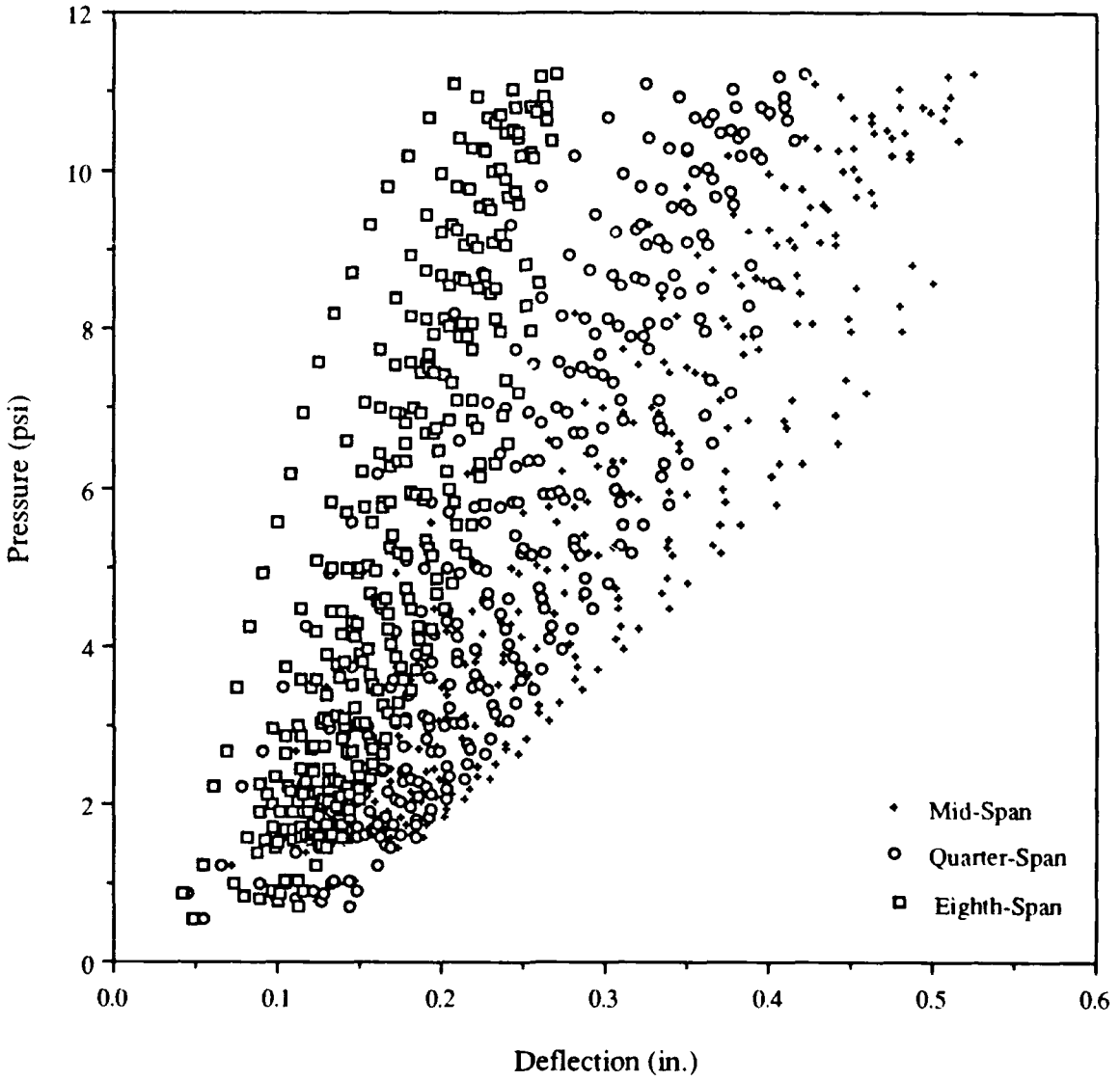

Figure F-14: Deflection Response of Panel-3 to Cyclic Pressure Loading

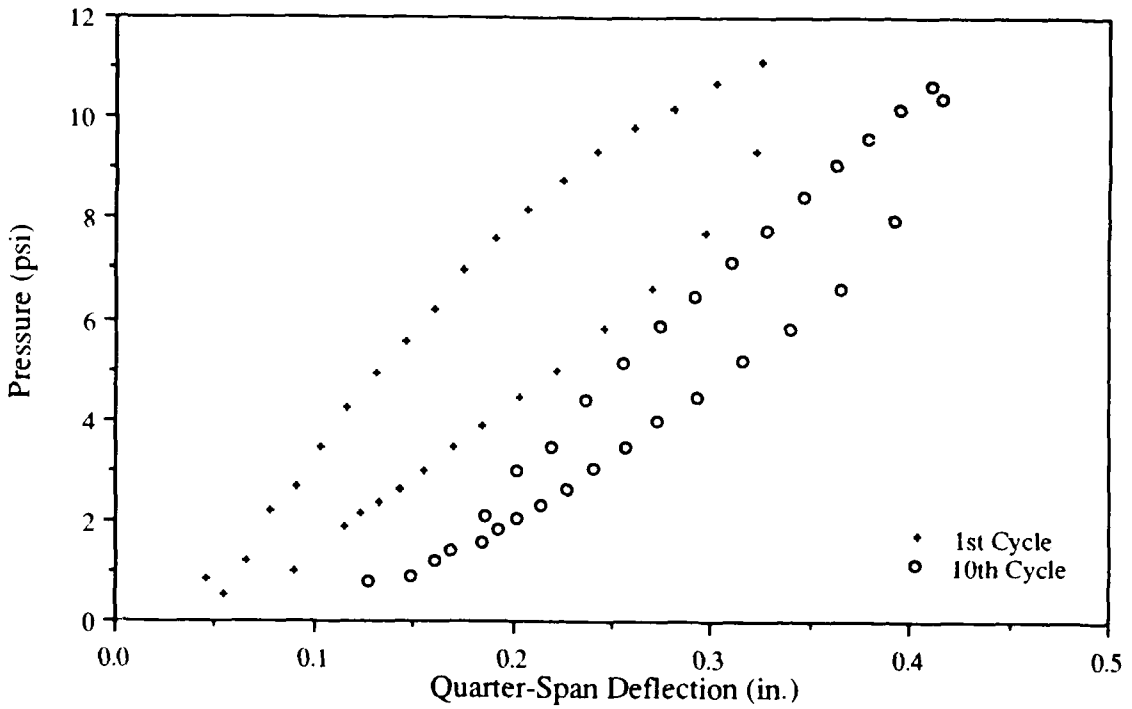

Figure F-15: Quarter-Span Deflection Response of Panel-3 to Cyclic Pressure Loading (Cycles 1 & 10)

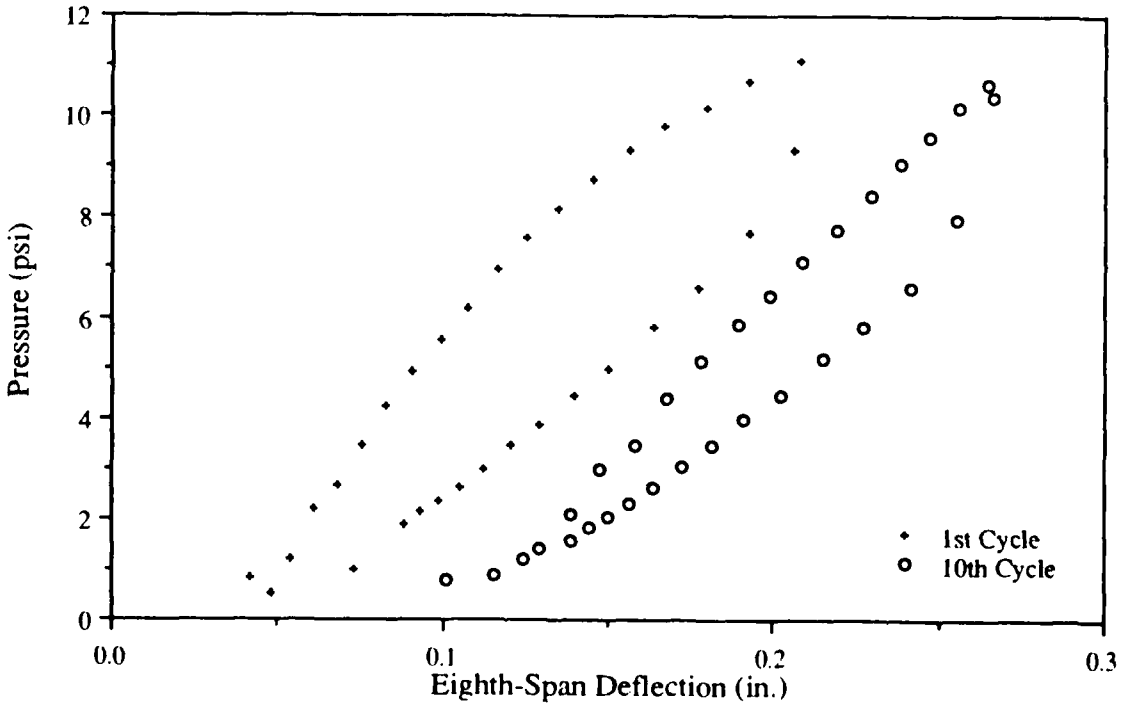

Figure F-16: Eighth-Span Deflection Response of Panel-3 to Cyclic Pressure Loading (Cycles 1 & 10)

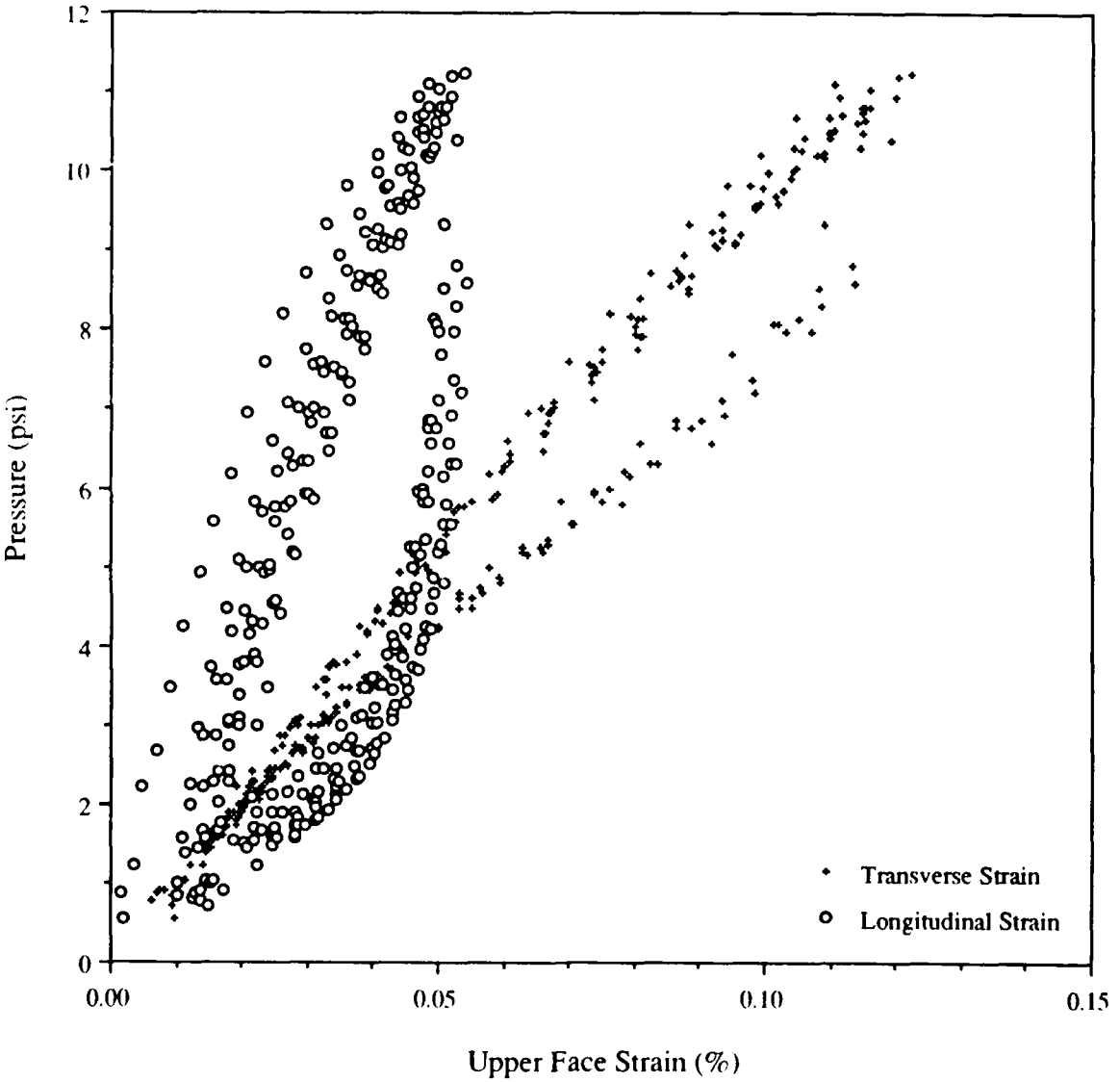

Figure F-18: Upper Face Strain Response of Panel-3 to Cyclic Pressure Loading

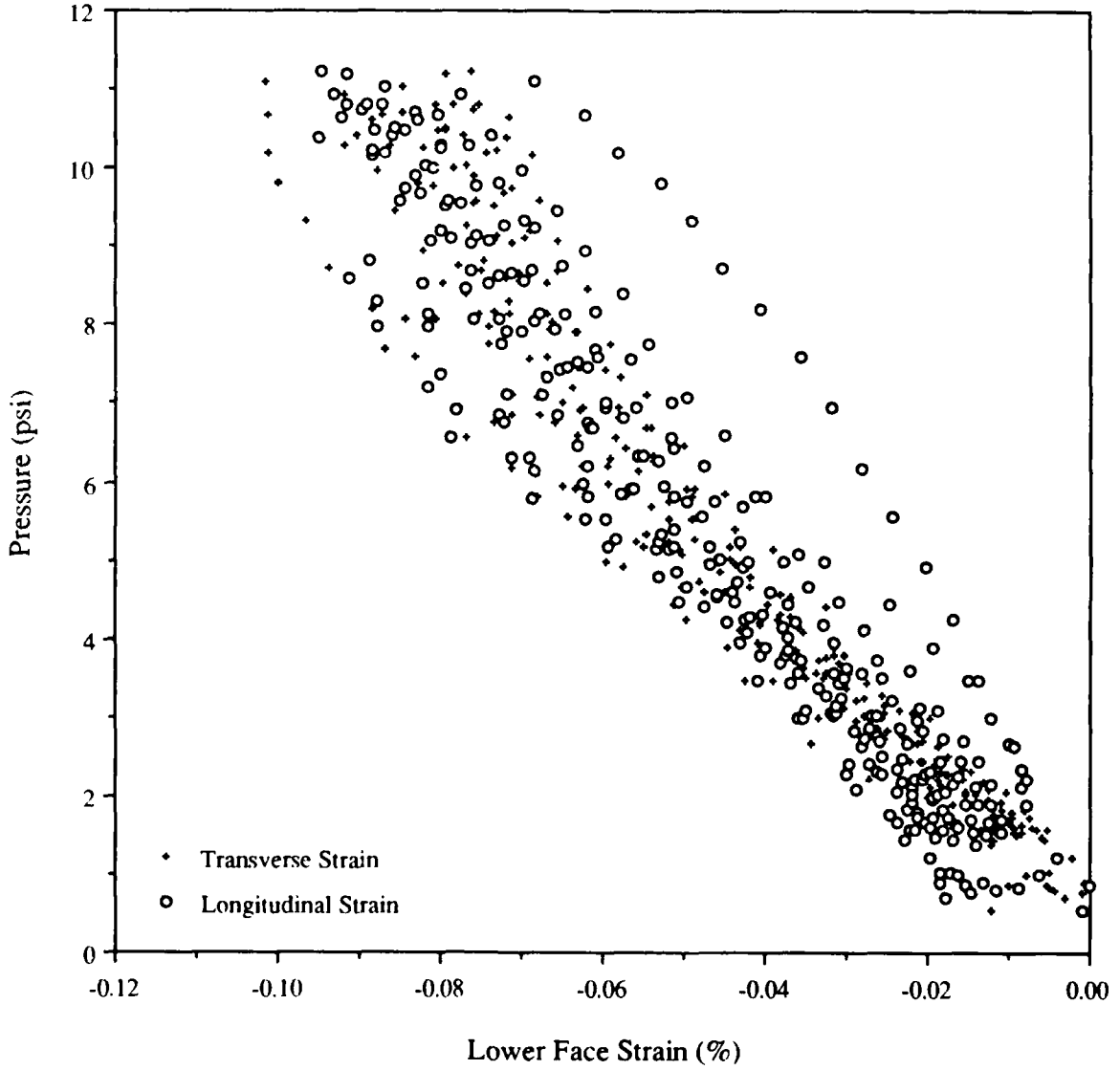

Figure F-19: Lower Face Strain Response of Panel-3 to Cyclic Pressure Loading

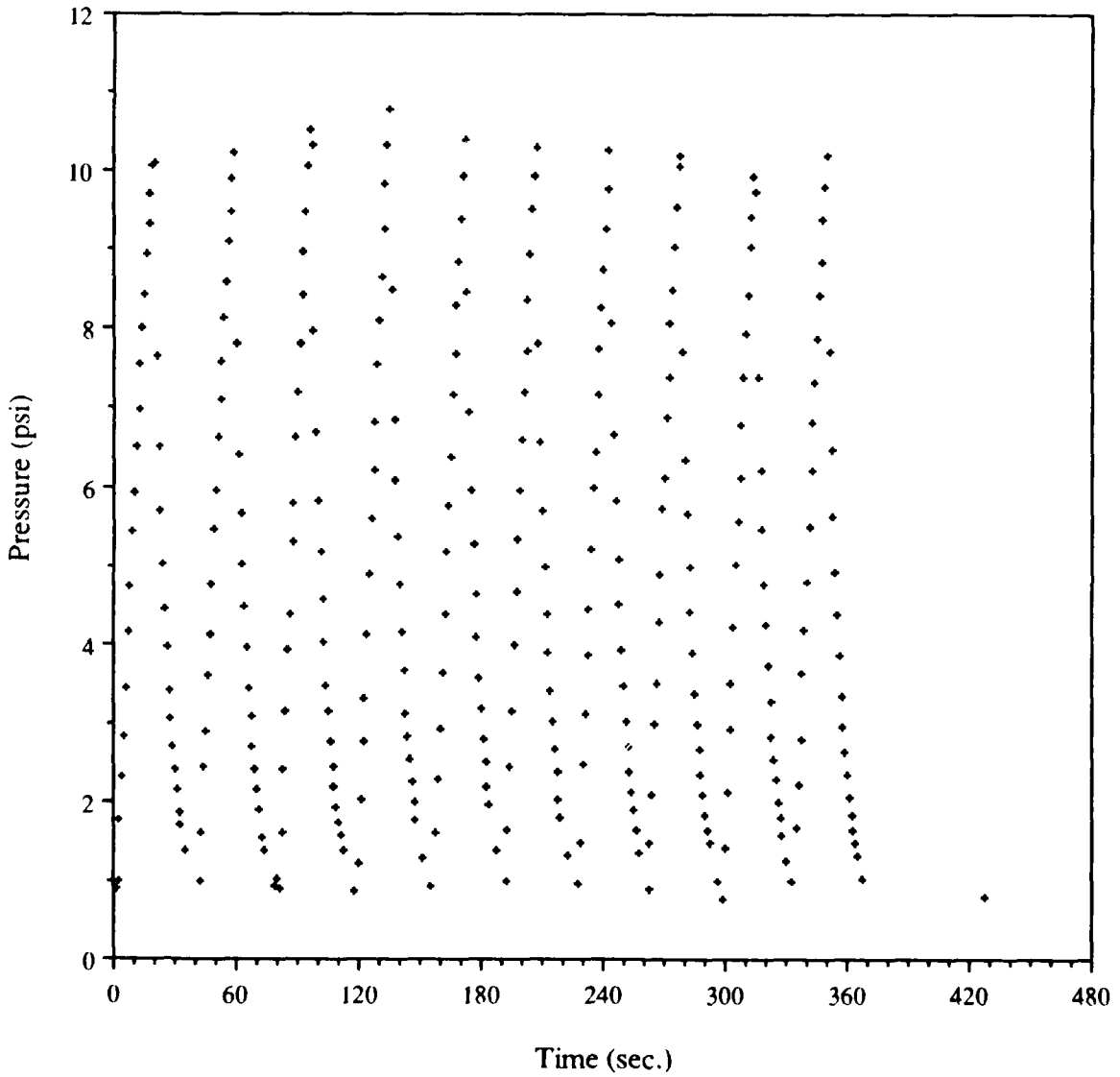

Figure F-20: Pressure vs. Time for Panel-4 Cyclic Pressure Loading

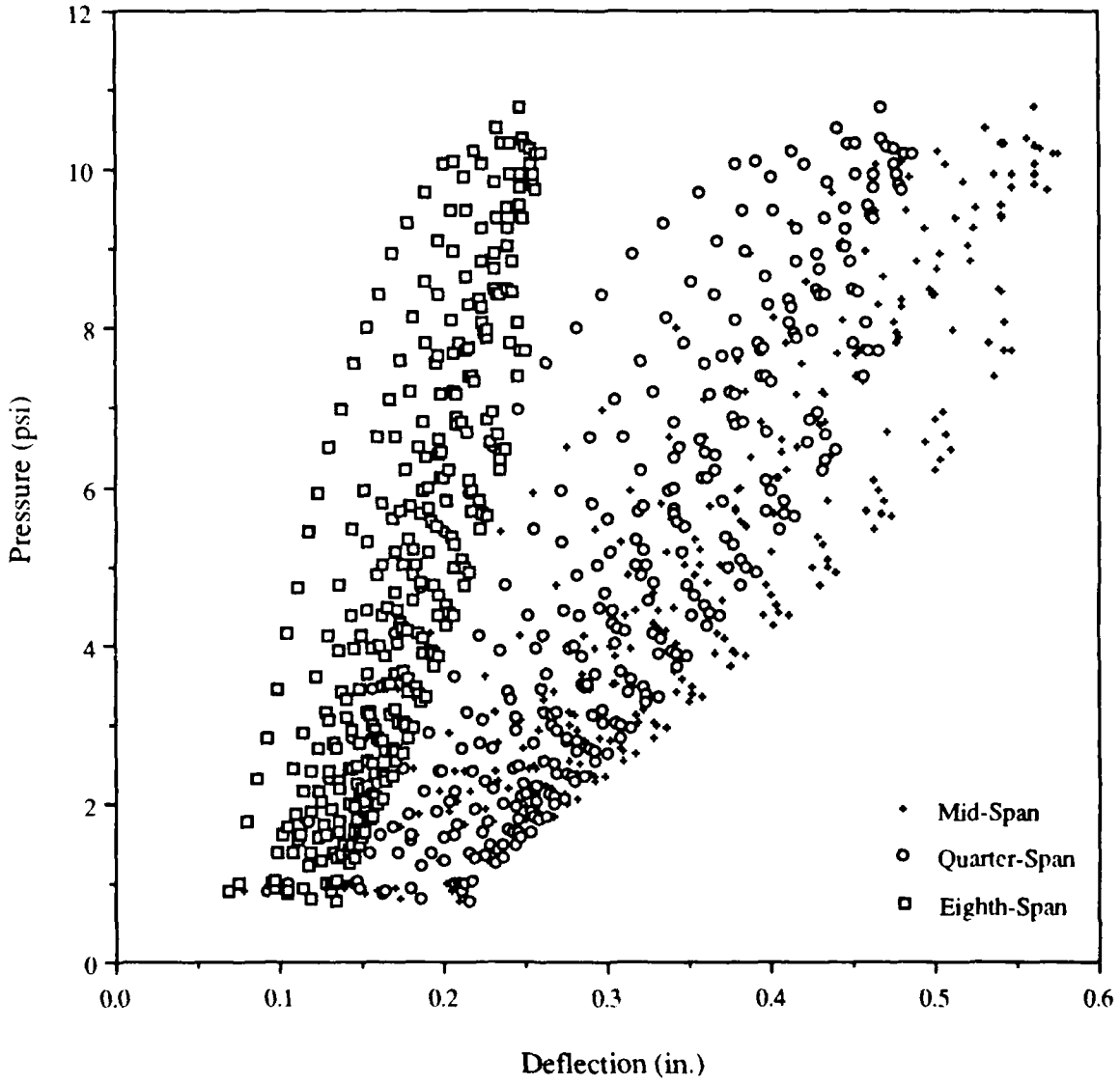

Figure F-21: Deflection Response of Panel-4 to Cyclic Pressure Loading

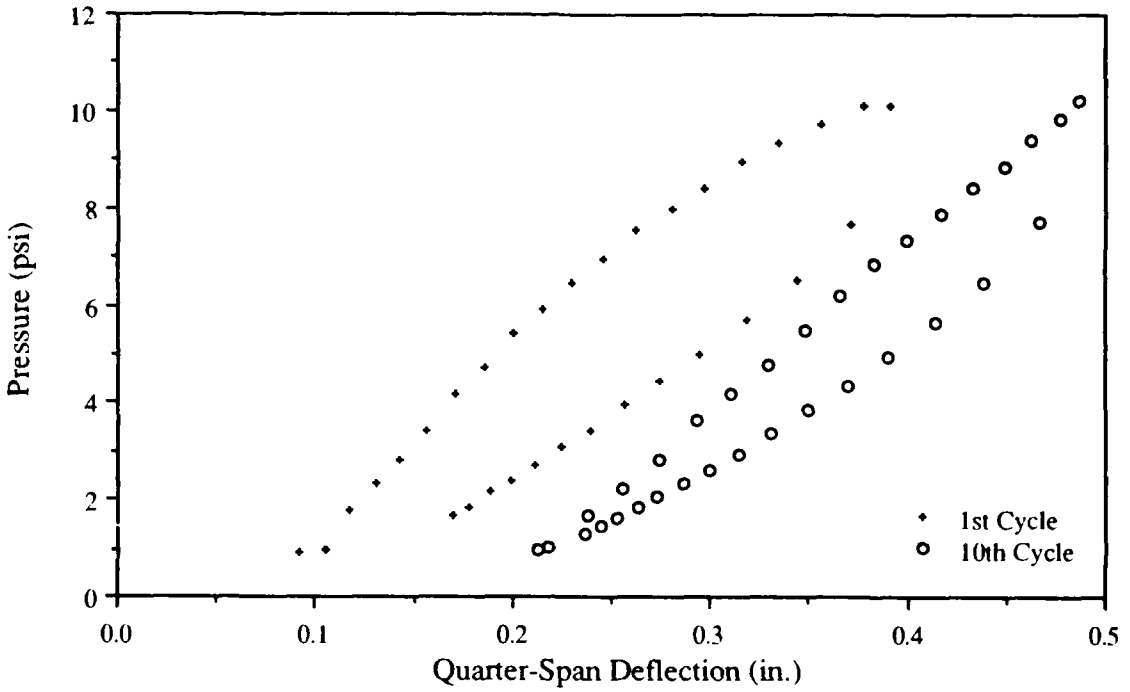

Figure F-22: Quarter-Span Deflection Response of Panel-4 to Cyclic Pressure Loading (Cycles 1 & 10)

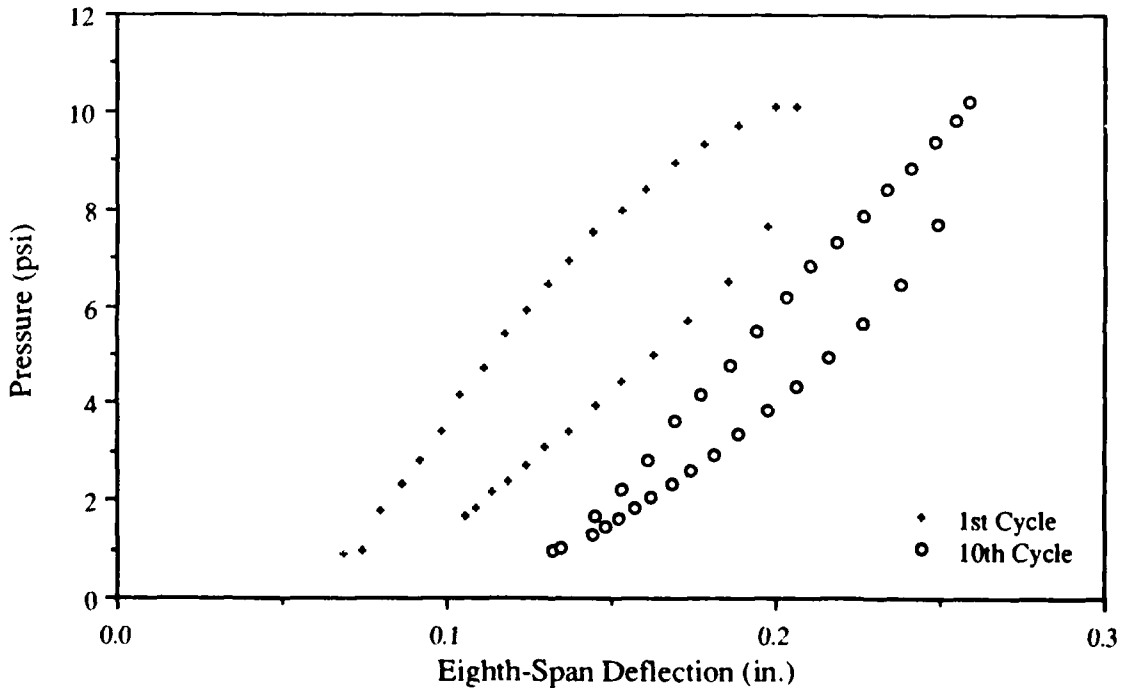

Figure F-23: Eighth-Span Deflection Response of Panel-4 to Cyclic Pressure Loading (Cycles 1 & 10)

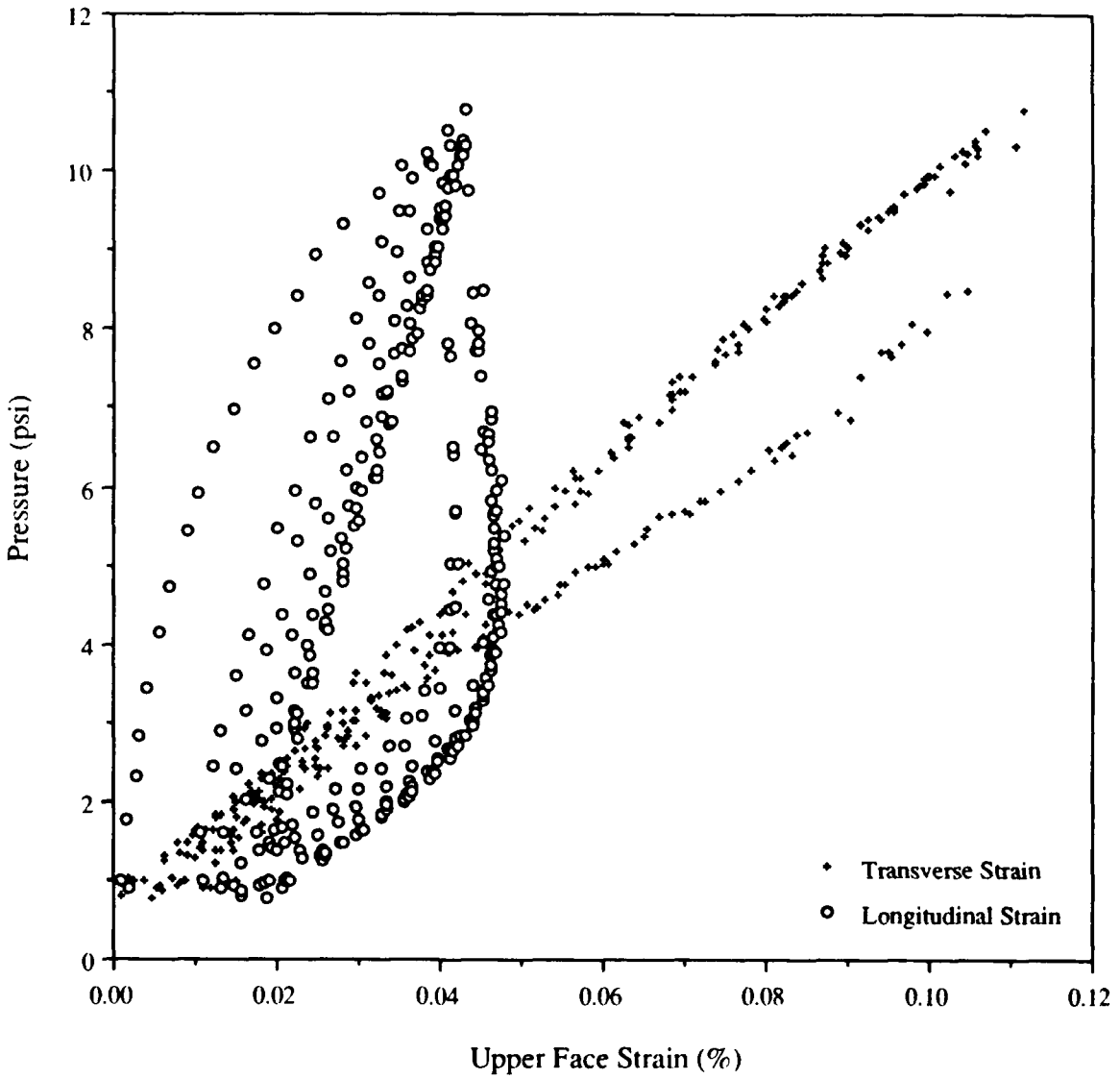

Figure F-24: Upper Face Strain Response of Panel-4 to Cyclic Pressure Loading

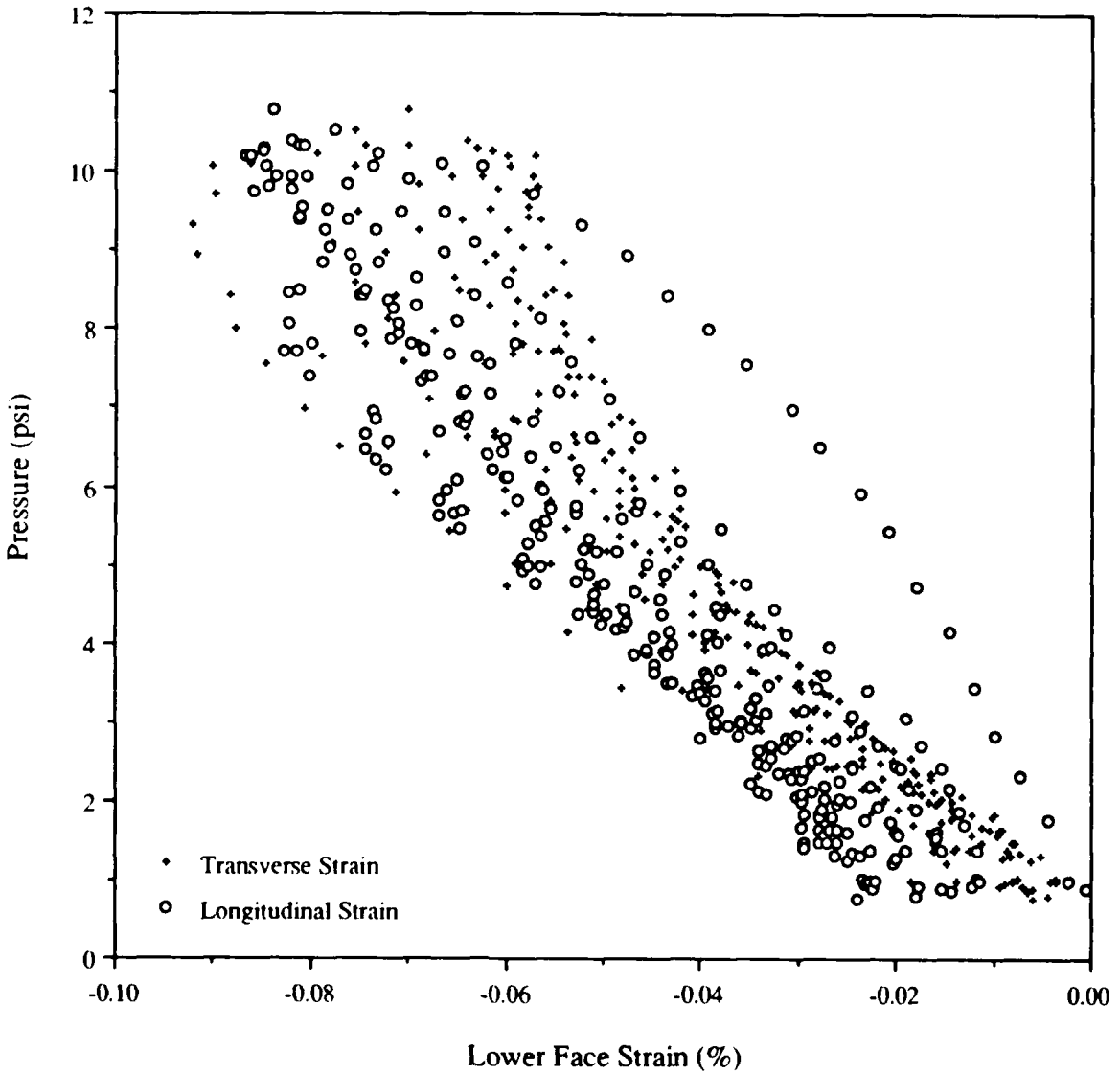

Figure F-25: Lower Face Strain Response of Panel-4 to Cyclic Pressure Loading

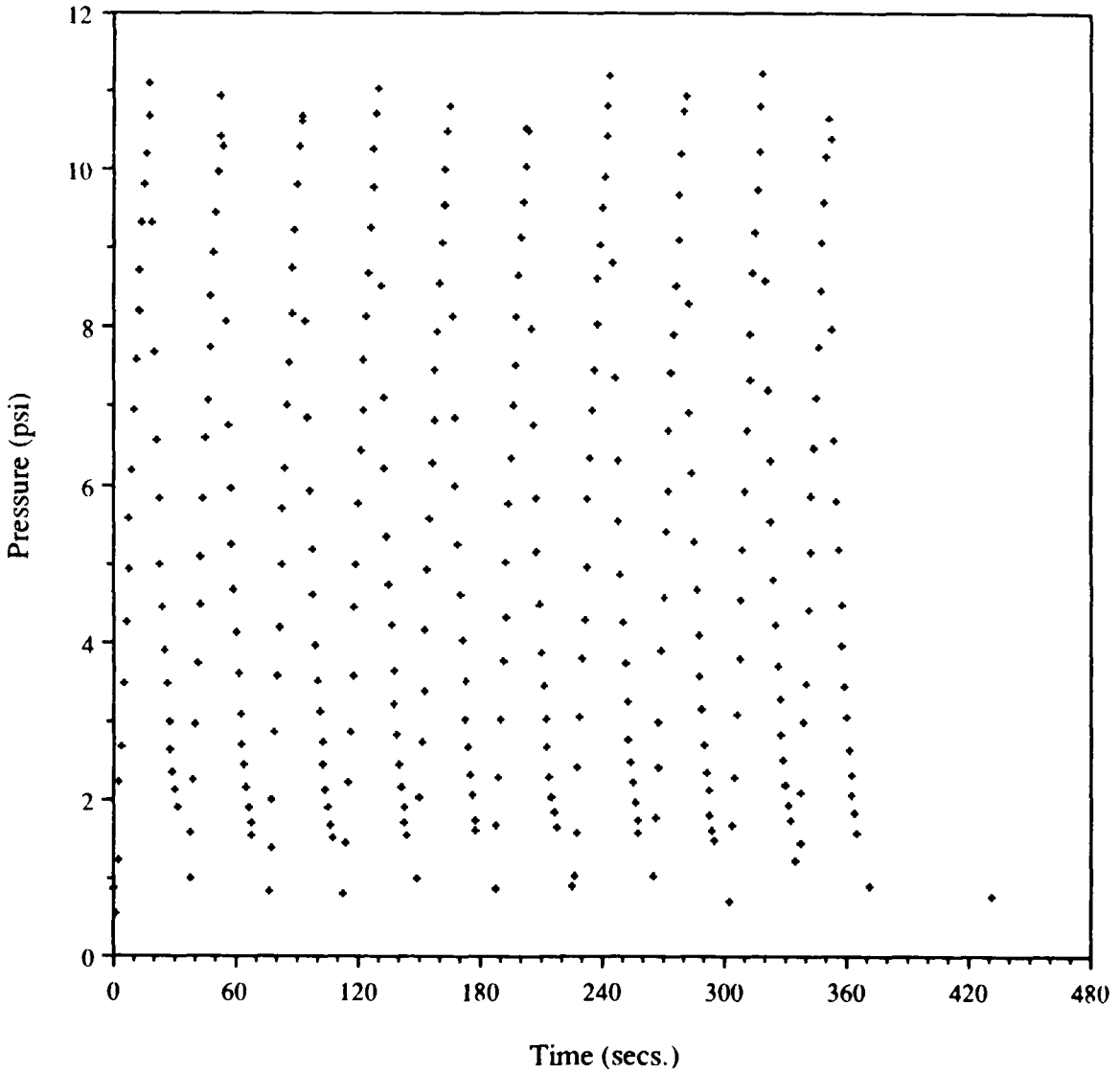

Figure F-26: Pressure vs. Time for Panel-5 Cyclic Pressure Loading

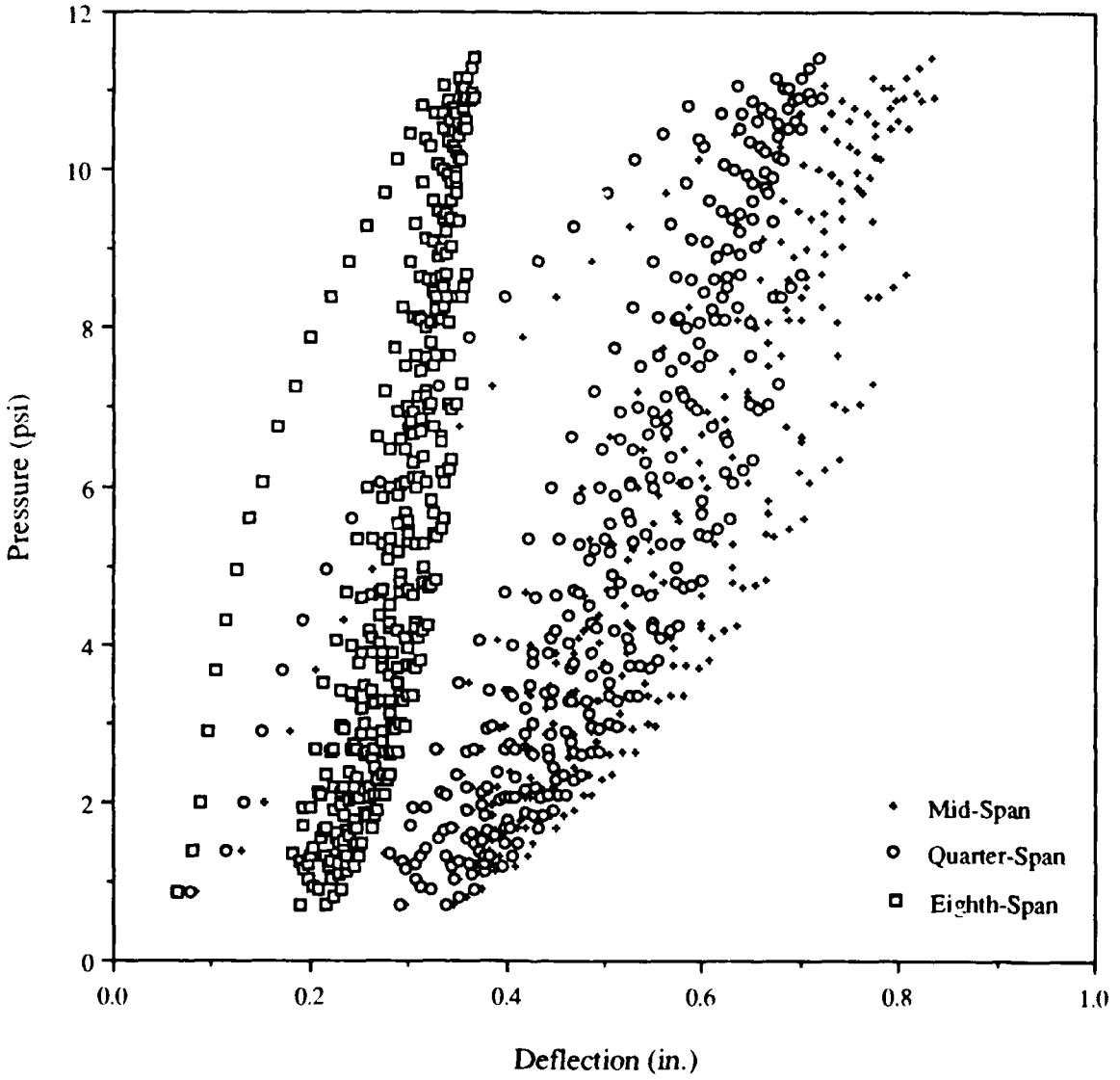

Figure F-27: Deflection Response of Panel-5 to Cyclic Pressure Loading

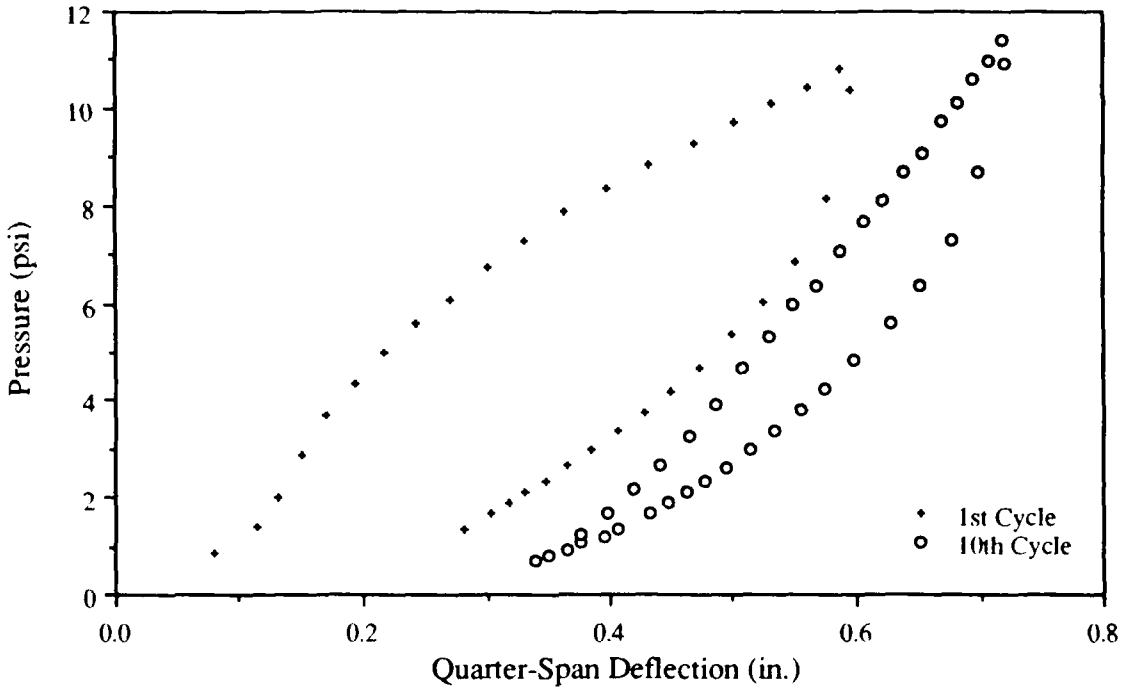

Figure F-28: Quarter-Span Deflection Response of Panel-5 to Cyclic Pressure Loading (Cycles 1 & 10)

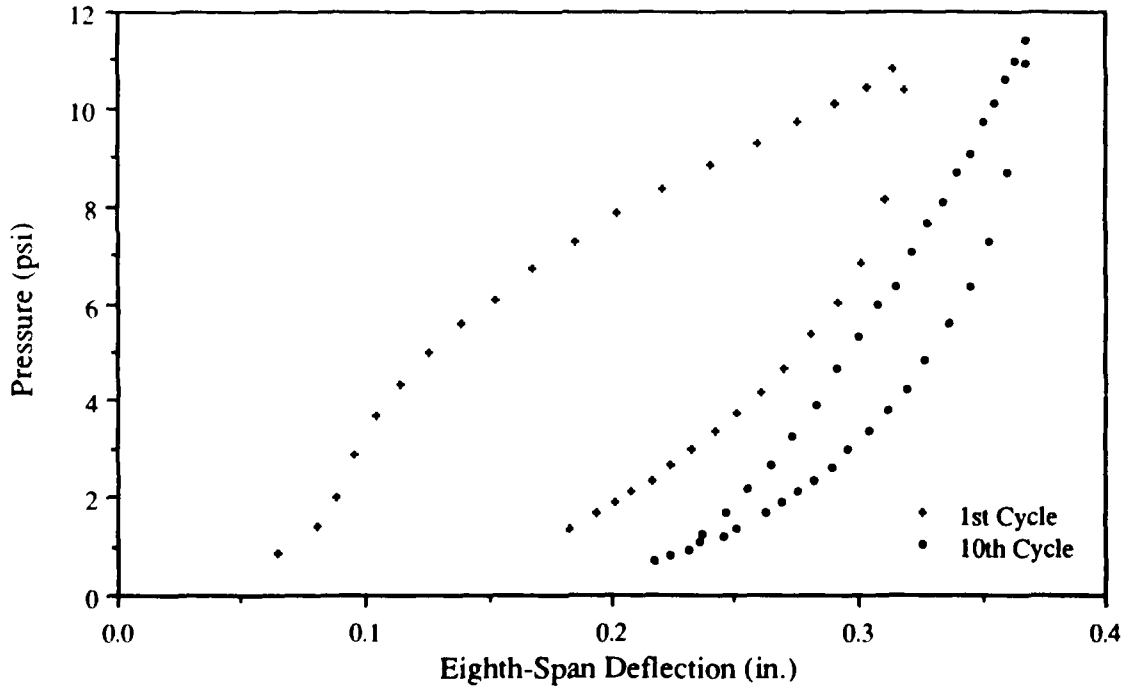

Figure F-29: Eighth-Span Deflection Response of Panel-5 to Cyclic Pressure Loading (Cycles 1 & 10)

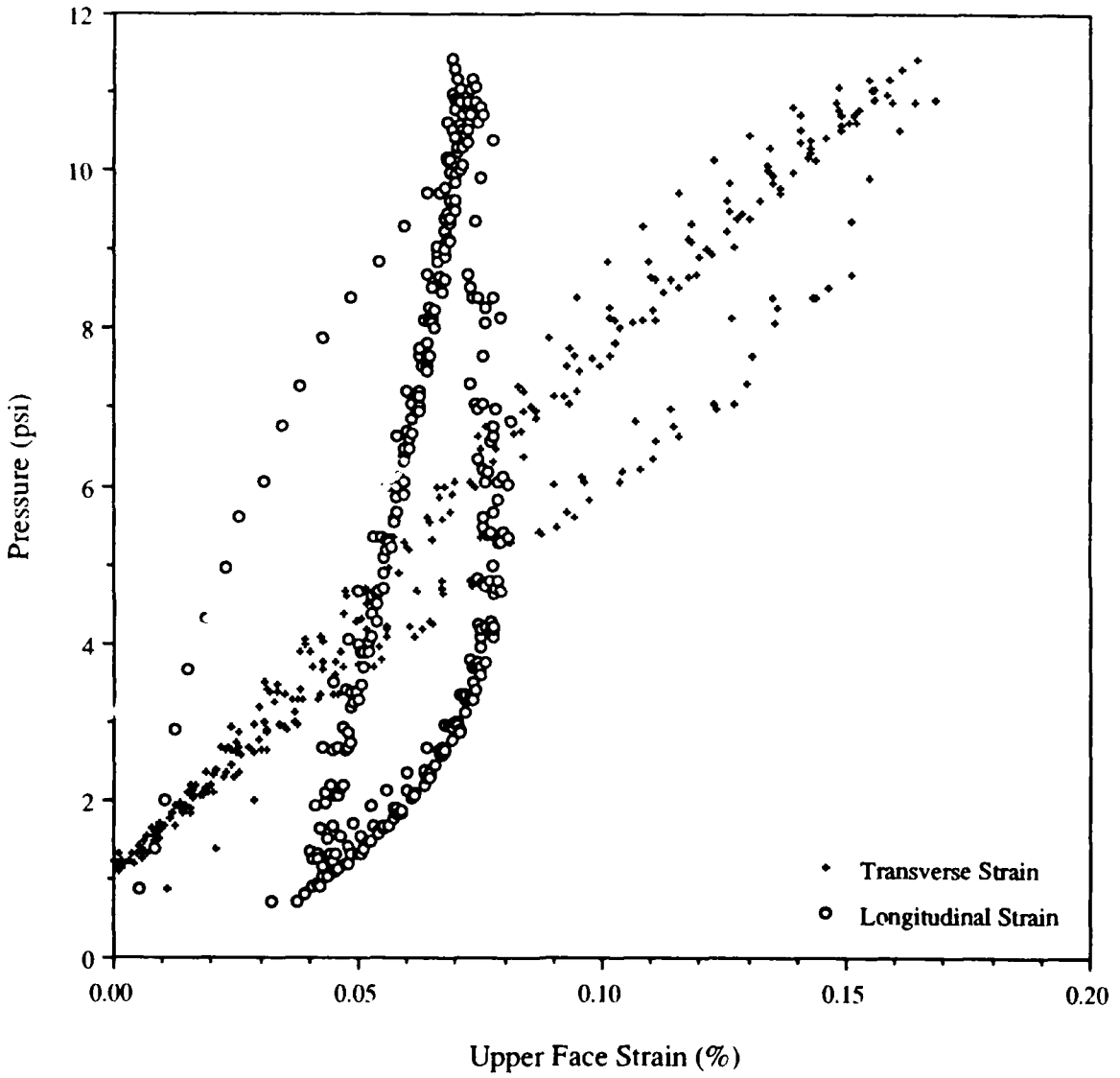

Figure F-30: Upper Face Strain Response of Panel-5 to Cyclic Pressure Loading

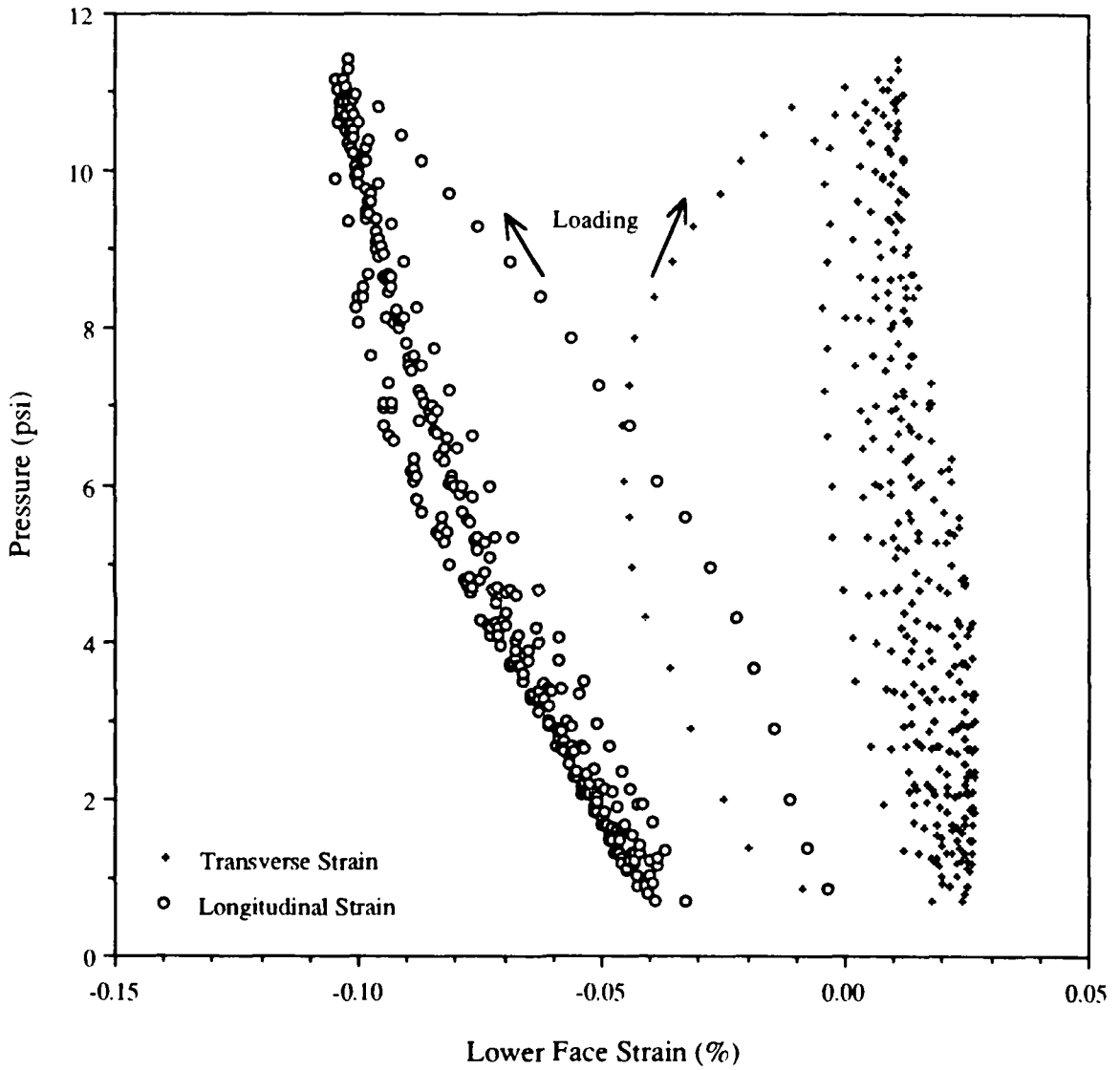

Figure F-31: Lower Face Strain Response of Panel-5 to Cyclic Pressure Loading

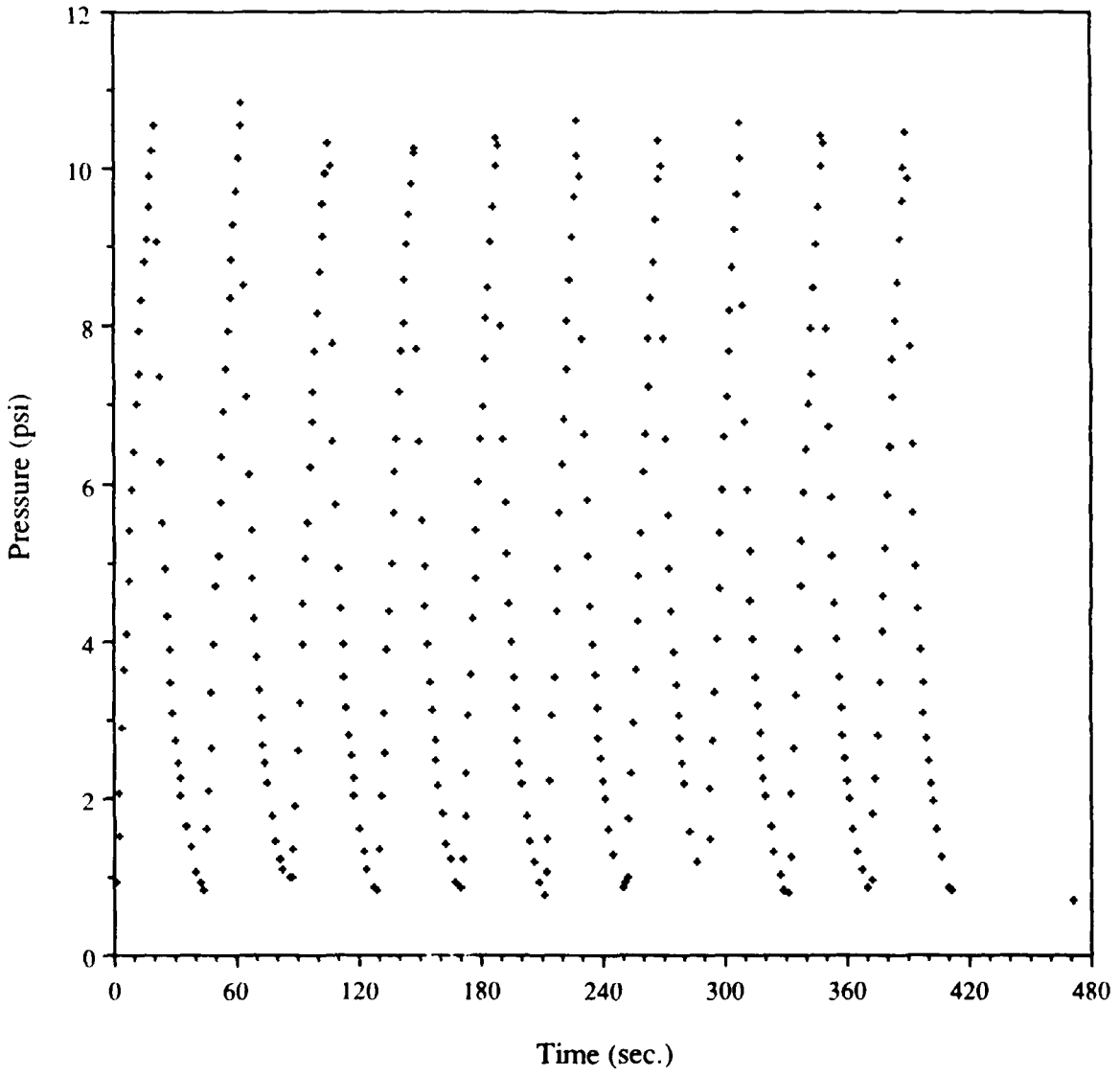

Figure F-32: Pressure vs. Time for Panel-6 Cyclic Pressure Loading

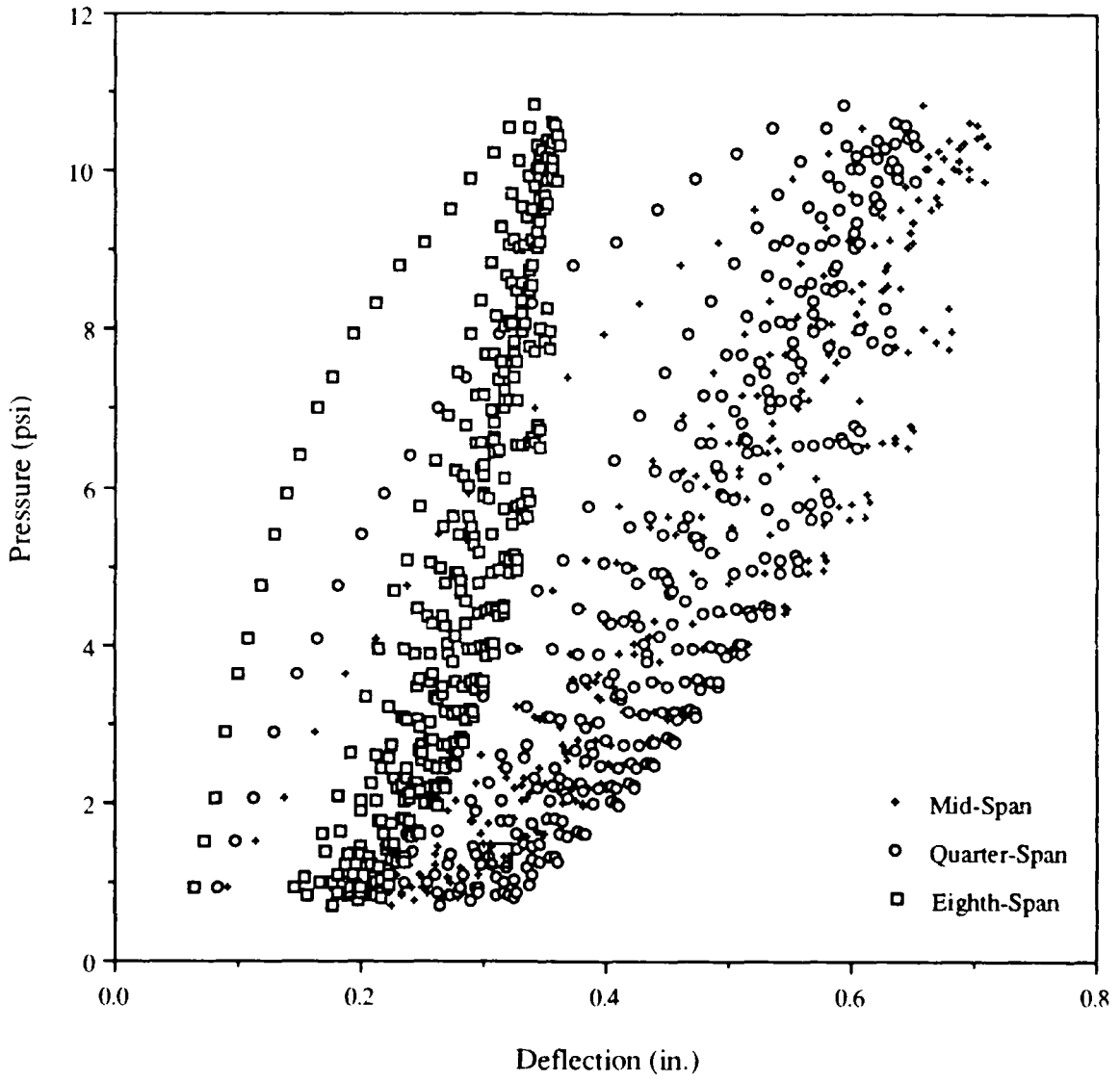

Figure F-33: Deflection Response of Panel-6 to Cyclic Pressure Loading

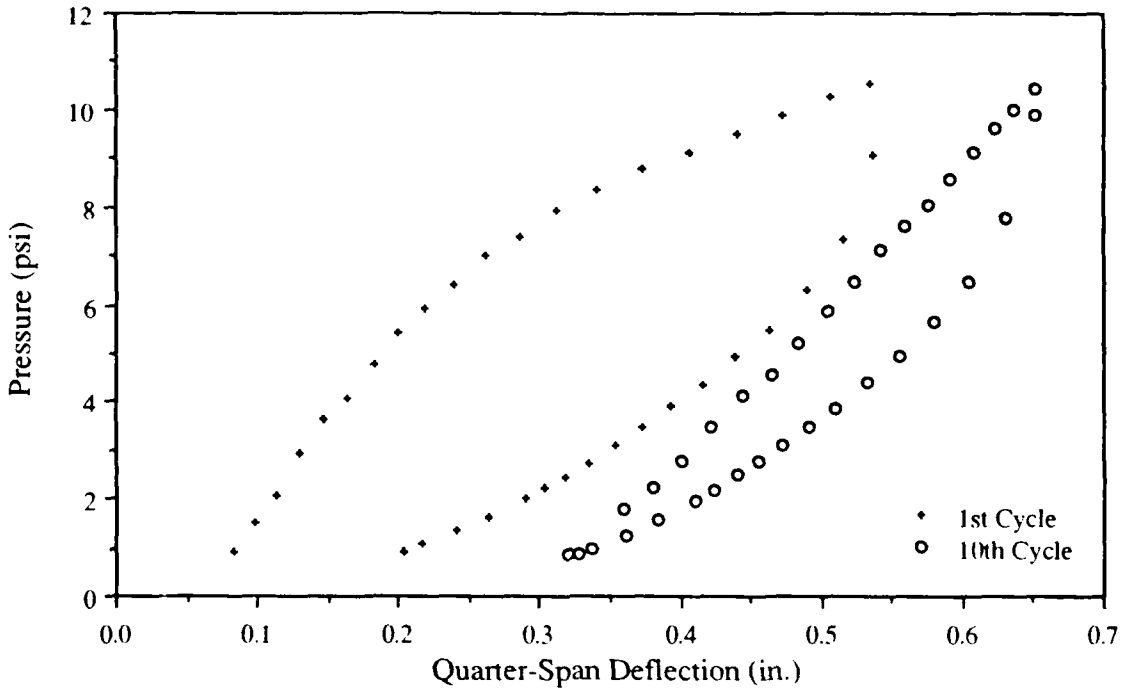

Figure F-34: Quarter-Span Deflection Response of Panel-6 to Cyclic Pressure Loading (Cycles 1 & 10)

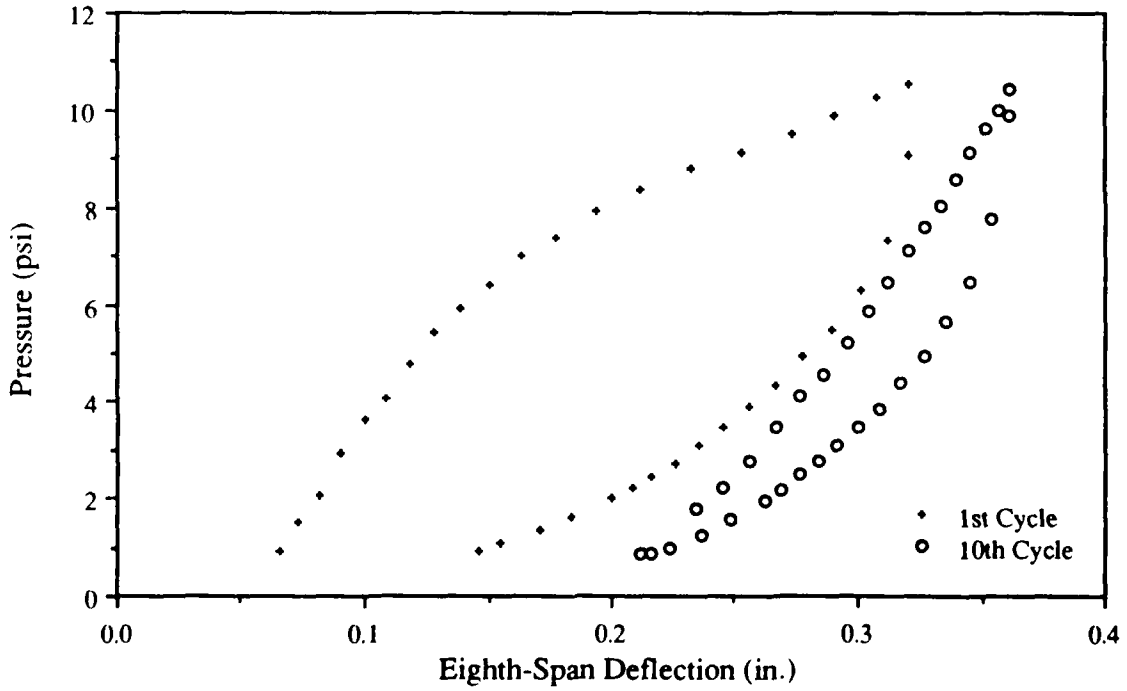

Figure F-35: Eighth-Span Deflection Response of Panel-6 to Cyclic Pressure Loading (Cycles 1 & 10)

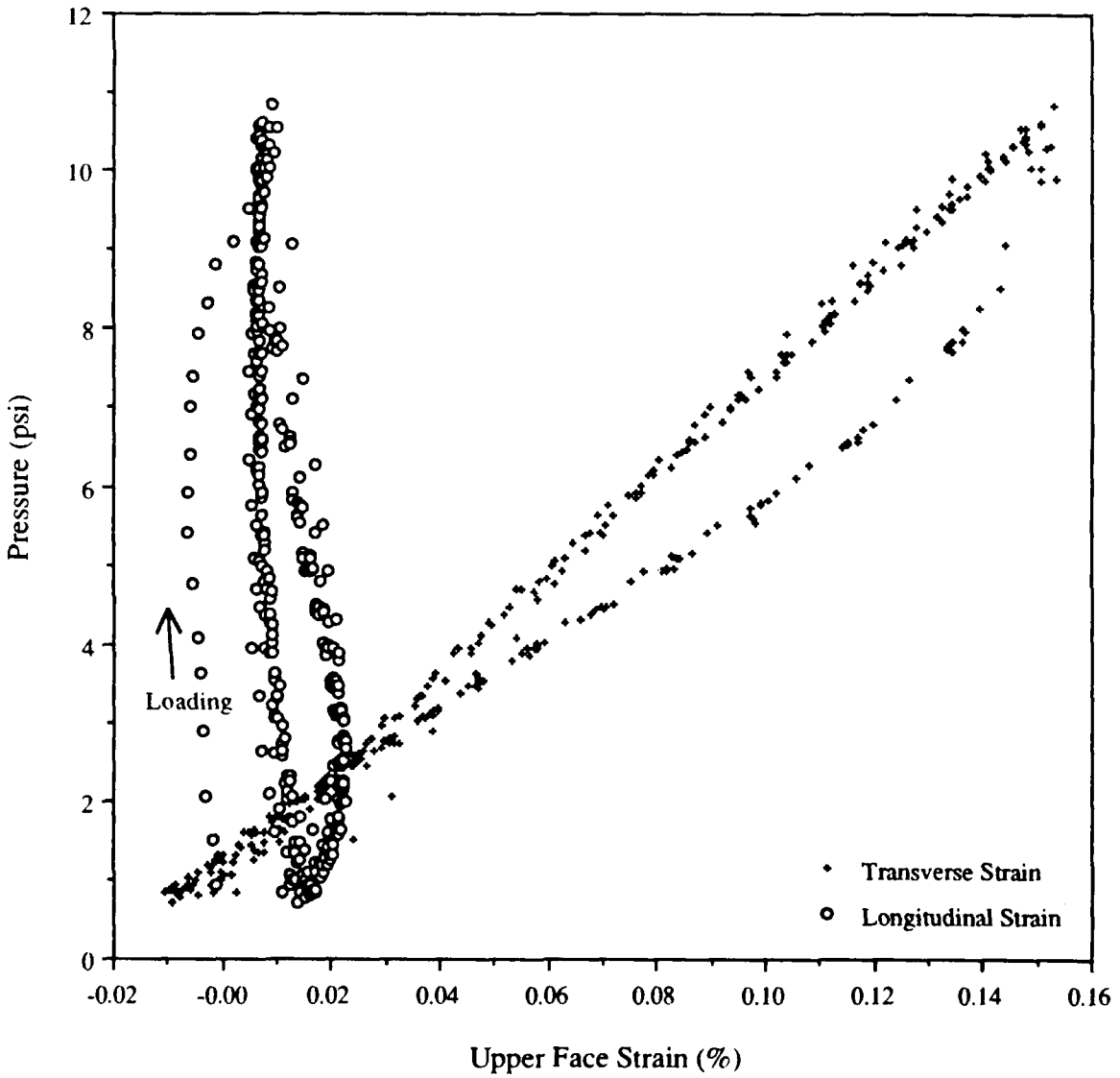

Figure F-36: Upper Face Strain Response of Panel-6 to Cyclic Pressure Loading

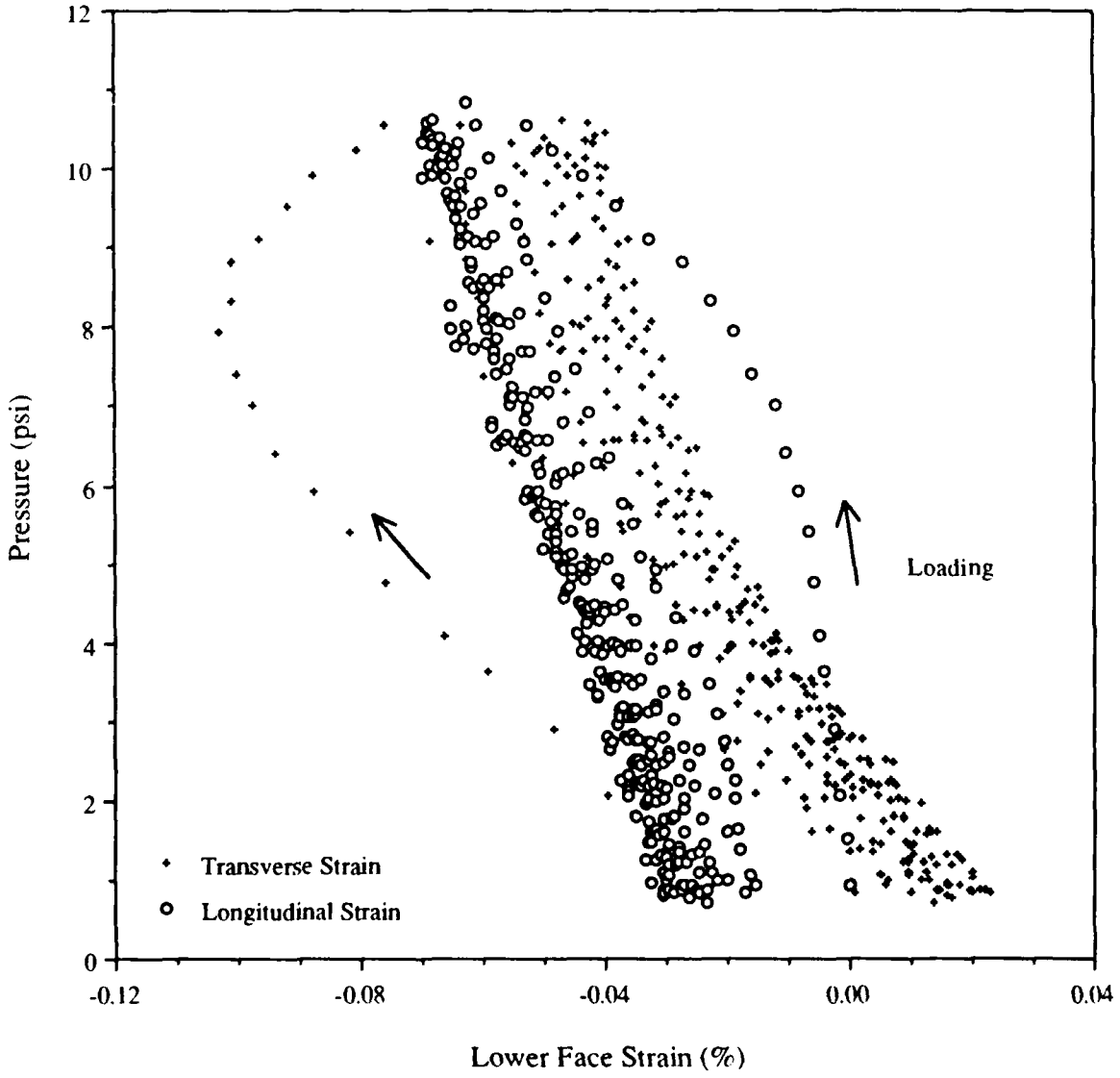

Figure F-37: Lower Face Strain Response of Panel-6 to Cyclic Pressure Loading